

Lecture Notes in Mathematics 2293

Yang-Hui He

The Calabi–Yau Landscape

From Geometry, to Physics, to Machine
Learning

Lecture Notes in Mathematics

Volume 2293

Editors-in-Chief

Jean-Michel Morel, CMLA, ENS, Cachan, France

Bernard Teissier, IMJ-PRG, Paris, France

Series Editors

Karin Baur, University of Leeds, Leeds, UK

Michel Brion, UGA, Grenoble, France

Camillo De Lellis, IAS, Princeton, NJ, USA

Alessio Figalli, ETH Zurich, Zurich, Switzerland

Annette Huber, Albert Ludwig University, Freiburg, Germany

Davar Khoshnevisan, The University of Utah, Salt Lake City, UT, USA

Ioannis Kontoyiannis, University of Cambridge, Cambridge, UK

Angela Kunoth, University of Cologne, Cologne, Germany

Ariane Mézard, IMJ-PRG, Paris, France

Mark Podolskij, University of Luxembourg, Esch-sur-Alzette, Luxembourg

Sylvia Serfaty, NYU Courant, New York, NY, USA

Gabriele Vezzosi, UniFI, Florence, Italy

Anna Wienhard, Ruprecht Karl University, Heidelberg, Germany

This series reports on new developments in all areas of mathematics and their applications - quickly, informally and at a high level. Mathematical texts analysing new developments in modelling and numerical simulation are welcome. The type of material considered for publication includes:

1. Research monographs
2. Lectures on a new field or presentations of a new angle in a classical field
3. Summer schools and intensive courses on topics of current research.

Texts which are out of print but still in demand may also be considered if they fall within these categories. The timeliness of a manuscript is sometimes more important than its form, which may be preliminary or tentative.

Titles from this series are indexed by Scopus, Web of Science, Mathematical Reviews, and zbMATH.

More information about this series at <http://www.springer.com/series/304>

Yang-Hui He

The Calabi–Yau Landscape

From Geometry, to Physics, to Machine
Learning



Springer

Yang-Hui He 

London Institute, Royal Institution of Great Britain; City, University of London; School of Physics & Chern Institute, Nankai University;
Merton College, University of Oxford
Oxford, UK

ISSN 0075-8434

Lecture Notes in Mathematics

ISBN 978-3-030-77561-2

<https://doi.org/10.1007/978-3-030-77562-9>

ISSN 1617-9692 (electronic)

ISBN 978-3-030-77562-9 (eBook)

Mathematics Subject Classification: 14-01, 14-04, 14Qxx, 14-11, 81T30, 81T33, 81T35

© Springer Nature Switzerland AG 2021

This work is subject to copyright. All rights are reserved by the Publisher, whether the whole or part of the material is concerned, specifically the rights of translation, reprinting, reuse of illustrations, recitation, broadcasting, reproduction on microfilms or in any other physical way, and transmission or information storage and retrieval, electronic adaptation, computer software, or by similar or dissimilar methodology now known or hereafter developed.

The use of general descriptive names, registered names, trademarks, service marks, etc. in this publication does not imply, even in the absence of a specific statement, that such names are exempt from the relevant protective laws and regulations and therefore free for general use.

The publisher, the authors, and the editors are safe to assume that the advice and information in this book are believed to be true and accurate at the date of publication. Neither the publisher nor the authors or the editors give a warranty, expressed or implied, with respect to the material contained herein or for any errors or omissions that may have been made. The publisher remains neutral with regard to jurisdictional claims in published maps and institutional affiliations.

This Springer imprint is published by the registered company Springer Nature Switzerland AG.

The registered company address is: Gewerbestrasse 11, 6330 Cham, Switzerland

*Catherinæ, Iacobo, & Elizabethæ,
Parentibusque suis,
pro amore Catharinae, Sanctae Alexandriae,
lacrimarum Mariae semper Virginis,
et ad Maiorem Dei Gloriam
hoc opusculum dedicat auctor . . .*

Preface

*La Géométrie, qui ne doit qu’obéir à la Physique quand elle se réunit avec elle, lui commande quelquefois (“Geometry, which should only obey Physics, when united with it sometimes commands it.” Quote from d’Alembert’s *Essay on a New Theory of Resistance of Fluids*¹).*

—Jean d’Alembert

Algebraic and differential geometry have been the *point d’appui* between pure mathematics and fundamental physics in the twentieth century. The two pillars of modern physics: (1) general relativity of the theory of gravitation and (2) the gauge theory of the Standard Model of elementary particles, are the physical realization of, respectively, (1) metrics on Riemannian manifolds and (2) connections of bundles with Lie structure. This fruitful dialogue persisted through the parallel development of these two strands of natural philosophy and was made ever more pertinent within the context of string theory, conceived to unify gravity with quantum field theory, and thereby provide an answer to Einstein’s famous dream of a Theory of Everything (ToE).

Whether string theory—with its cornerstones of supersymmetry and extra space-time dimensions yet to be verified by some ingenious experiment—is truly “the” theory of nature remains to be seen. What is indisputable is that the theory has been a muse to pure mathematics: from enumerative geometry to Moonshine, from quantum invariants to mock modular forms, etc., the discipline has provided novel, and rather unique, methods of attack for tackling a myriad of mathematical problems.

Central to string theory is the study of Calabi-Yau manifolds, serving as a beacon to such important investigations as compactification, mirror symmetry, moduli space, and duality. Since their incipience in a conjecture of E. Calabi in 1954–1957 in an esteemed tradition in geometry of relating curvature to topology, to the celebrated proof by S.-T. Yau in 1977–1978, to the prescription thereof as a large class of vacua in string theory by Candelas-Horowitz-Strominger-Witten in 1986,

¹*Essai d’une nouvelle théorie de la résistance des fluides.*

Calabi-Yau manifolds have been an inspiring protagonist in modern mathematics and theoretical physics.

There have, of course, been quite a few books already on the subject. These range from the excellent account of the master himself in *The Shape of Inner Space: String Theory and the Geometry of the Universe's Hidden Dimensions*, by S.-T. Yau and S. Nadis [363], to the now classic *The Elegant Universe*, by B. Green [167], both aimed at the general audience; from the vintage compendium *Calabi-Yau Manifolds: A Bestiary for Physicists*, by T. Hübsch [237], to the modern lecture notes *A survey of Calabi-Yau manifolds* by S.-T. Yau [362], *Calabi-Yau Manifolds and Related Geometries* by M. Gross, D. Huybrechts, and D. Joyce [171], as well as *Calabi-Yau Varieties: Arithmetic, Geometry and Physics*, by R. Laza, M. Schütt, and N. Yui (Eds. [277]), aimed at the specialist.

Why a New Book Why, then, the astute reader asks, another book on Calabi-Yau manifolds?

The primary reason is that there has been a revolution over the last score of years in science, perhaps not a paradigm shift, but certainly a transformation in style and methodology: the twenty-first century now firmly resides within the age of big data and artificial intelligence. It is therefore inevitable that mathematical physics and pure mathematics should also profit from this burgeoning enterprise. Whilst it is well-established that string theory and Calabi-Yau manifolds have been at the interface between theoretical physics and pure mathematics from the 1980s, it is less known that since around the turn of the millennium, they have also served as a bench-mark to various problems in computational mathematics as well as a passionate advocate for data mining.

Specifically, the author, as well as many other groups in string theory, enjoyed long collaborations with experts in large-scale computational projects, e.g., Macaulay2, Singular, Bertini in algebraic geometry, GAP in group theory, MAGMA or PARI/GP in number theory, and indeed the umbrella scheme of SageMath. Furthermore, even before the establishment of such online databases such as

1. “The database of L-functions, modular forms and related objects” <http://www.lmfdb.org/>
2. “The Graded Ring Database of algebraic varieties” <http://www.grdb.co.uk/>
3. “The Knot atlas” <http://katlas.org/>

which have become standard in the mathematics literature over the last two decades or so, the now-famous 473 million hypersurfaces in toric varieties from reflexive 4-polytopes and the resulting Calabi-Yau database were born from Kreuzer-Skarke in the mid-1990s. This impressive resource still remains one of the largest datasets in mathematics: <http://hep.itp.tuwien.ac.at/~kreuzer/CY/>.

Contemporaneous with these, there have emerged an increasing number of online Calabi-Yau databases of varying specialization and often of augmented sophistication in user interface, such as the “Toric Calabi-Yau Database” [345], the “Heterotic Compactification Database” [231], and the “Calabi-Yau Manifold

Explorer” [69], set up by various international collaborations of which the author has been a part, as well as “The Calabi-Yau Operator Database” [337] and elliptically fibred Calabi-Yau manifolds [131]. On a more general note, we point the reader to the ambitious and inspiring resource <https://mathdb.mathhub.info/> which attempts to link to all the various databases of pure mathematics which the various communities have been compiling. In addition, the reader is encouraged to read the enlightening transcripts of the ICM 2018 panel discussion on machine-aided proofs and databases in mathematics [102].

Why This Book It is therefore evident that a new book on Calabi-Yau manifolds, and more widely, on algebraic geometry, is very much in demand. Such a book should emphasize that the subject is not only at the intersection between mathematics and physics, but resides, in fact, at the cusp of pure and applied mathematics, theoretical physics, computer science, and data science. This book should briefly introduce the mathematical background and the physical motivation, brief because the material can be found in many textbooks. It should then delve into the heart of the matter, addressing

1. How does one explicitly construct a Calabi-Yau manifold
2. How do these constructions lead to problems in classification, ranging from the combinatorics of lattice polytopes to the representation of quivers and finite graphs
3. What databases have thus far been established
4. How to use a combination of analytic techniques and available software to compute requisite quantities, such as Hodge numbers and bundle cohomology

Throughout, algorithms and computerization will serve as the skein which threads the material, with an appreciation of their complexity and the indefatigability with which the community has utilized them to compile databases, in order to extract new mathematics and new physics. In this sense, the book will focus not on the *theory* but the *practice* of Calabi-Yau manifolds.

The Calabi-Yau Landscape and Beyond There have been many practitioners in mapping the landscape of Calabi-Yau manifolds throughout the years, exploring diverse features of interest to physicists and mathematicians alike, such as the founders S.-T. Yau in mathematics and P. Candelas in physics, as well as M. Stillman and D. Grayson in computational geometry. The author is most grateful to the fruitful collaboration with and sagacious guidance by these experts over the years.

More recently, in 2017–2018, a somewhat daring paradigm was proposed in [203, 204]. A natural question was posed: confronted with the increasingly available data on various geometric properties of Calabi-Yau varieties which took many tour de force efforts to calculate and compile, “can machine learning be applied to Calabi-Yau data, and to data in pure mathematics in general?” Indeed,

Can artificial intelligence “learn” algebraic geometry?

That is, can machine learning arrive at correct answers such as cohomology or topological invariant, *without* understanding the nuances of the key techniques of

the trade, such as Groebner bases, resolutions, or long exact sequences? What about representation theory of groups or arithmetic-geometric problems in number theory? This was shown to be mysteriously possible, in many cases with astounding accuracy. There had been some activity in the field since 2017 when [83, 203, 204, 265, 318] introduced modern data-science techniques to string theory, in applying big-data techniques to various problems in string and related mathematics by a host of independent groups. The zeistgeist of data science has thus breathed its nurturing spirit into the field of mathematical physics.

Indeed, the question can be extended to [203, 205, 209]

Can AI machine-learn mathematical structures?

Such an inquiry should be taken in tandem with, but not commensurate to, the dreams of Voevodsky [352] and the very active field of automated theorem proving (ATP) [298]. The latter has a long history in the foundation of mathematics since at least Russell and Whitehead, and attempts to formulate the axiomata of mathematics in a systematic way, before the programme took a blow from Gödel. Yet, for all practical purposes, the ATP community is thriving, to the point that Professor Kevin Buzzard thinks it is impossible not to have computers check proofs and generate new ones [66]. One could think of this direction as a “bottom-up” approach towards the AI mathematician. What we are proposing here can be thought of as a complementary “top-down” approach, where, given enough mathematically correct statements from the literature, ML extracts enough information to find new patterns and methodology.

Target Audience This book has grown out of a timely series of invited colloquia, seminars, and lectures delivered by the author in the 2017–2018 academic year, at the National Centre for Science and Technology, Taiwan; Northeastern University, Boston; Ludwig-Maximilians-Universität, Munich; Imperial College, London; L’Institut Confucius, Geneva; University of Warwick, UK; Nankai and Tianjin Universities, China; University of Plymouth, UK; Universities of Bruxelles and Leuven, Belgium; University of Nottingham, UK; Albert Einstein Institute, Potsdam; Niels Bohr Institute, Copenhagen; University of the Witwatersrand, Johannesburg; Trinity College, Dublin; Brown University, Providence; Harvard University, Boston; and University of Pennsylvania, Philadelphia. For the kind hospitality of the various hosts the author is most grateful.

One long version of the lecture slides, of which this book is a pedagogical expansion, is the lecture series given at L’Institut Confucius, Geneva, the PDFs of which are available at [206]. A short version, on the other hand, is available from the abridged lecture notes from the 2019 PIMS Summer School on Algebraic Geometry in High-Energy Physics at the University of Saskatchewan [25] and the encyclopaedia entry [208]. The audience is intended to be primarily beginning graduate students in mathematics, as well as those in mathematical and theoretical physics, all with a propensity towards computers. We will take a data-driven perspective, sprinkled with history, anecdotes, and actual code. The reader is also

referred to a recent attempt to gather the experts' voices in a collected volume on topology and physics [360].

In a sense, the list of available books mentioned earlier is aimed either at a general audience or to a more senior graduate student. The middle ground of beginning PhD students, master's students, or even advanced undergraduate students is left wanting. Students with some familiarity of Reid's undergraduate algebraic geometry [314] but not yet fully prepared for Hartshorne [194] and Griffiths-Harris [169], or with some acquaintance of Artin's introductory algebra [16] but not yet fully feathered for Fulton-Harris [147], may find it difficult to approach the subject matter of Calabi-Yau manifolds. This book is designed for them.

Disclaimer In a sense, the purpose of this book is to use Calabi-Yau databases as a playground, and explore aspects of computational algebraic geometry and data science, in the spirit of the excellent texts of Cox-Little-O'Shea [98] and Schenck [322]. This book is *not* intended to be an introductory text in string theory, nor one in algebraic geometry. It should serve as a supplement to the aforementioned host of physics and mathematics textbooks, and to entertain the beginning researcher with a glimpse of the interactions between some modern mathematics and physics, as well as an invitation to machine learning. Some undergraduate familiarity with manifolds and topology at the level of [296, 314], as well as string theory at the level of [259, 364], all excellent introductions, will more than suffice as background.

Perhaps, due to the author's constant enjoyment as an outsider, the book is intended to be some mathematics for physicists (what are some of the techniques?), some physics for mathematicians (why are physicists interested in complex algebraic geometry?), and some data science for both (what are some of the fun and modern methods in machine learning?). Throughout our promenade in the landscape, there will be a continued preference for intuition over rigour, computation over formalism, and experimentation over sophistry. It is the author's hope that we shall embark on a memorable adventure in the land of mathematics, physics, and data science, with Calabi-Yau manifolds leading as our Beatrice, and interdisciplinarity guiding as our Virgil, and we, like Dante, diligently remarking upon our journey.

Oxford, UK

Yang-Hui He

Acknowledgements

For the invaluable guidance and help of my mentors, official and unofficial, I owe eternal gratitude. Each has been a guiding light at various stages of my career: Professor Amihay Hanany, Professor Burt Ovrut, Professor Philip Candelas, Professor Dame Jessica Rawson, Professor Andre Lukas, Professor Alex Scott, Professor Shing-Tung Yau, Professor Mo-Lin Ge, and Professor Minhyong Kim. To them I raise my cup of thanksgiving.

To the host of collaborators whose friendship I have enjoyed over the years, I owe a million happy thoughts. Their camaraderie has always offered a beacon of hope even within the darkest moments of confusion. To Professor Hal Schenck, Dr Pierre-Philippe Déchant, Mrs Lorraine Hunter, Professor Tristan Hübsch, Dr Richard Eager, Dr Stephen Pietromonaco, and Dr Rémi Lodh as well as the anonymous referees of Springer, I am grateful for their careful reading and many valuable comments to the first draft. To them I raise my glass of brotherly love.

To my wife, Dr Elizabeth Hunter He, *rosa Hibernia dilectissima mea*, without whose patience and support this book would not have come into being. To my children, Katherine Kai-Lin and James Kai-Hong, without whose distractions this book would also not have come into being. To my parents, without whose love and nurturing nothing much of mine would have ever come into being.

Contents

1 Prologus Terræ Sanctæ	1
1.1 A Geometrical Tradition	3
1.1.1 A Modern Breakthrough	6
1.1.2 Preliminary Examples: 1, 2, ?...	7
1.2 $10 = 4 + 2 \times 3$: A Physical Motivation	8
1.2.1 Triadophilia	11
1.2.2 Caveat and Apology for the Title	13
1.3 Topological Rudiments	15
1.3.1 The Hodge Diamond	16
2 The Compact Landscape	19
2.1 The Quintic	20
2.1.1 Topological Quantities: Exact Sequences	22
2.1.2 Topological Quantities: Computer Algebra	24
2.2 CICY: Complete Intersection Calabi–Yau	28
2.2.1 Topological Quantities: Statistics	32
2.3 Other Datasets	34
2.3.1 Hypersurfaces in Weighted \mathbb{CP}^4	34
2.3.2 Elliptic Fibrations	36
2.4 An Explosion: The Kreuzer–Skarke Dataset	38
2.4.1 Reflexive Polytopes	38
2.4.2 CY Hypersurfaces: Gradus ad Parnassum	41
2.4.3 1, 16, 4319, 473800776	42
2.5 Cartography of the Compact Landscape	49
2.6 Epilogue: Recent Developments	50
2.7 Post Scriptum: Calabi–Yau Metrics	52
2.7.1 Numerical Metric on the Quintic	56
3 The Non-Compact Landscape	59
3.1 Another $10 = 4 + 2 \times 3$	60
3.1.1 Quiver Representations and a Geometer’s AdS/CFT	60
3.1.2 The Archetypal Example	64

3.2	Orbifolds and Quotient Singularities	66
3.2.1	McKay Correspondence	69
3.2.2	Beyond ADE	71
3.3	Toric Calabi-Yau Varieties	72
3.3.1	Cone over \mathbb{P}^2	73
3.3.2	The Conifold	77
3.3.3	Bipartite Graphs and Brane Tilings	80
3.4	Cartography of the Affine Landscape	82
3.4.1	Gorenstein Singularities	83
3.4.2	The Non-Compact Landscape	84
4	Machine-Learning the Landscape	87
4.1	A Typical Problem	89
4.1.1	WWJD	91
4.2	Rudiments of Machine-Learning	94
4.2.1	Regression and a Single Neuron	95
4.2.2	MLP: Forward Feeding Neural Networks	97
4.2.3	Convolutional Neural Networks	98
4.2.4	Some Terminology	99
4.2.5	Other Common Supervised ML Algorithms	104
4.2.6	Goodness of Fit	110
4.3	Machine-Learning Algebraic Geometry	112
4.3.1	Warm-up: Hypersurface in Weighted \mathbb{P}^4	113
4.3.2	Learning CICYs	120
4.3.3	More Success Stories in Geometry	125
4.4	Beyond Algebraic Geometry	127
4.5	Epilogue	129
5	Postscriptum	131
A	Some Rudiments of Complex Geometry	133
A.1	(Co-)Homology	133
A.2	From Real to Complex to Kähler	134
A.3	Bundles and Sequences	135
A.4	Chern Classes	138
A.5	Covariantly Constant Spinor	140
A.6	A Lightning Refresher on Toric Varieties	142
A.6.1	Digressions on Spec and All That	143
A.6.2	Example: The Conifold	144
A.6.3	From Cones to Fans	146
A.7	Dramatis Personae	147
A.8	The Kodaira Classification of Elliptic Fibrations	149
B	Gröbner Bases: The Heart of Computational Algebraic Geometry	153
B.1	An Elimination Problem	155
B.2	Hilbert Series	156

Contents	xvii
C Brane Tilings	161
C.1 Dessins d’Enfants	161
D Remembering Logistic Regression	167
E A Computational Compendium: Homage to SageMath	171
E.1 Algebraic Varieties	171
E.2 Combinatorics and Toric Varieties	173
E.3 Representation Theory	174
E.4 Number Theory and More	175
Glossary	177
References	183
Index	201

Chapter 1

Prologus Terræ Sanctæ



Cæterum ad veridicam, sicut iam polliciti sumus, Terræ Sanctæ descriptionem, stylum vertamus.

—Burchardus de Monte Sion¹

That Zeitgeist should exist in the realm of scientific inquiry is perhaps more surprising than its purported influence in the growth of civilizations. While the latter could be conceived of as the emergence of a vague concoction of cross-cultural ideas, the former requires precise concepts and objects to almost simultaneously appear, oftentimes independently and even mysteriously, within different disciplines of research. In mathematics, what initially surface as “Correspondences” in seemingly disparate sub-fields necessitates a timely arrival of hitherto unthinkable techniques for the final construction of a proof. An archetypal example of this is *Moonshine*, a list of daring conjectures by McKay–Thompson–Conway–Norton in the late 1980s, relating finite groups to modular forms, which until then lived in utterly different worlds. It so happened that Borcherds was learning quantum field theory (QFT) with conformal symmetry—yet another world—around this time, when he noted that the structure of its vertex operator algebra furnished the requisite representation, and achieved his Fields Medal winning proof of 1992. The right set of ideas was indeed “in the air”.

The involvement of physics was perhaps as surprising as the initial correspondence. But herein lies the crux of our tale. The past century has witnessed the cross-fertilization between mathematics and theoretical physics in a manner worthy of that illustrious tradition since Newton: Riemannian geometry and general relativity, operator theory and quantum mechanics, fibre bundles and gauge theory of elementary particles, etc. An impressive list of theories, such as the likes of mirror symmetry, supersymmetric indices, and Moonshine, has been the brain-children of

¹“Thus, as promised, let us now turn, to the description of the Holy Land”. Burchard of Mount Sion, from the Prologue to his *Description of the Holy Land (Prologus & Descriptio Terrae Sanctae)*, 1285).

this fruitful union. It indeed seems that QFTs with additional symmetry, specifically, conformal symmetry and supersymmetry, are the right set of ideas for physics.

The ultimate manifestation of QFTs with such rich symmetries is, without doubt, string theory. Marrying the conformal symmetries of the world-sheet with the supersymmetry of incorporated fermions, string theory materialized in the 1970–80s as an attempt to unify gravity (as described by general relativity) with quantum theory (as described by the gauge theory of the standard model (SM)) into a Theory of Everything, the holy grail of fundamental physics. The theory still remains the best candidate for a hope of reconciling the macroscopic world of stars and galaxies with the microscopic world of elementary particles of the SM, which would in turn demystify singularities such as black holes or the Big Bang.

To date, there is no experimental evidence for string theory; none at all for its cornerstones of supersymmetry and extra space-time dimensions; nor is it obvious that definitive signatures of either will be discovered in the near future. We must patiently await some ingenious experiment or some marvellous indirect observation. Why, then, string theory? While we refer the reader to the excellent response in J. Conlon’s eponymous book [92], as mathematicians and mathematical physicists our affinity to the theory are already more than justified. As mentioned above, the theory has not only made revolutionary contributions to theoretical physics in the guise of holography, QFT dualities and quantum entanglement, but furthermore, in an unexpected manner, it has been serving as a *constant muse to pure mathematics*.

Time and again, its general framework has provided unexpected insights and results to geometry, representation theory and even number theory. Hence, regardless of whether the theory will eventually become the unified Theory of Everything, its pursuit, now, in the past decades, and in the foreseeable future, is just and fitting. String theory is thus the rightful heir of that noble lineage of the interaction between geometry, algebra and physics that took a firm footing in the twentieth century; it is certainly not a fin-de-siècle fancy, but has rather conducted us, as a perspicacious mentor, into the mathematics and physics of the twenty-first century. Central to this development is the study of **Calabi–Yau varieties**, whose curvature flatness endows them with beautiful mathematical structure and physical utility, rendering them the perfect illustration of this interaction.

As we now ground ourselves into the incipience of the twenty-first century, it behoves us to contemplate whether a particular spirit permeates our time. The answer is immediate: this is the Age of Data.

From the sequencing of the human genome, to the sifting of particle jets in the LHC, to the search for exo-planets, the beginning of this century has amassed, utilized and analysed data on an unprecedented scale, due to the explosive growth and availability of computing power and artificial intelligence (AI). While it is well known that string theory has long been a Physical Beatrice to the Pure Mathematical Dante, it is perhaps less appreciated that over the past three decades it too has repeatedly provided benchmarks to computational mathematics, especially in computational algebraic geometry and combinatorial geometry.

The story, as we will shall see, goes back to the late 1980s, reaching its first climax in the mid-1990s. Interestingly, the now classic complete intersection of

Calabi–Yau (CICY) [75] and Kreuzer–Skarke (KS) [21] datasets places “big data” in pure mathematics and mathematical physics in a time ordinarily thought to predate the practice of data mining. More recently, a steadily expanding group of researchers in mathematical physics has been advocating to the physics community (q.v. [219]) the importance of interacting with Macaulay2 [163], Singular [108], Bertini [197] in algebraic geometry, GAP [338] in group theory, MAGMA [285] in number theory etc., as well as the overarching SageMath [320]. Indeed, the first sessions in theoretical high-energy physics [215] in the biannual “Society for Industrial and Applied Mathematics” (SIAM) meetings on applied algebraic geometry have emerged.

The protagonist of our chronicle is therefore engendered from the union of mathematics, physics and data science and it is this trinity that will be the theme of this book. Over the years, various fruitful collaborations between theoretical physicists, pure and applied mathematicians, and now data scientists and computer scientists, have been constructing and compiling databases of objects that may *ab initio* seem to be only of abstract mathematical interest but instead links so many diverse areas of research: Calabi–Yau manifolds constitute the exemplar of this paradigm. Thus, as much as our ethereal *Zeitgeist* being *Data*, it too should be *Interdisciplinarity*.

By now, there is a landscape of data and a plethora of analytic techniques as well as computer algorithms freely available, but lacking a comprehensive roadmap. This is our **Calabi–Yau Landscape**. There are still countless goldmines buried in this landscape, with new mathematical conjectures lying hidden (e.g., the vast majority of the manifolds obtainable from the KS dataset by triangulations have been untouched [7]) and new physics to be uncovered (e.g., the unexpected emergence of Calabi–Yau structure in the scattering of ordinary ϕ^4 QFTs [48, 49]).

Europe’s obsession with Jerusalem in the Middle Ages led to the publication of one of the very first printed maps, based on Burchardus de Monte Sion’s thirteenth century “Prologue of the Holy Land” [106]. We have thus named our prologue in homage to this early cartographical work, drawing upon the analogy that we too will be mapping out the landscape of an important terrain.

1.1 A Geometrical Tradition

Our story, as with so many in mathematics, begins with Euler, Gauß, and Riemann. The classic classification theorem of (compact, smooth, orientable) surfaces Σ (without boundary and punctures) is well known. These two-dimensional objects—smooth manifolds if you will—are topologically characterized by a single non-negative integer, the **Genus**, which counts the number of holes. This is shown in the top line of Fig. 1.1. The sphere S^2 is genus 0, the torus $T^2 \simeq S^1 \times S^1$ is genus 1, etc. We say that this integer genus distinguishes the **Topological types** of the surface.

The **Euler characteristic** (or simply, **Euler number**) χ relates topology to combinatorics: taking any convex polyhedron drawn on Σ and finding the signed

$g(\Sigma) = 0$	$g(\Sigma) = 1$	$g(\Sigma) > 1$
$\chi(\Sigma) = 2$	$\chi(\Sigma) = 0$	$\chi(\Sigma) < 0$
Spherical	Ricci-Flat: CY ₁	Hyperbolic
+ curvature	0 curvature	- curvature

Fig. 1.1 The trichotomy of Riemann surfaces Σ of genus $g(\Sigma)$, in terms of its Euler number $\chi(\Sigma) = 2 - 2g(\Sigma)$

alternating sum of the number of independent objects in each dimension, this should yield

$$\chi(\Sigma) = 2 - 2g(\Sigma) . \quad (1.1)$$

For example, on S^2 where $g = 0$, we can draw a cube, there are 8 vertices, 12 edges and 6 faces, and $8 - 12 + 6 = 2$; this should be true for any convex polyhedron, a result dating at least to Euler, which is a precursor to the index theorem. More strictly speaking, “the number of independent objects in each dimension” is given by the **Betti number** b_i that counts the number of independent algebraic cycles in dimension i , which we will later see as the rank of the i -th (co-)homology group (suitably defined). Thus,

$$\chi(\Sigma) = \sum_{i=0}^2 (-1)^i b_i , \quad b_i = \text{rk}(H_i(\Sigma)) . \quad (1.2)$$

Next, Gauß–Bonnet relates topology to differential geometry: χ should be the integral of (an appropriate) curvature R , here the Ricci curvature:

$$\chi(\Sigma) = \frac{1}{2\pi} \int_{\Sigma} R . \quad (1.3)$$

The Riemann Uniformization Theorem then gives us a wonderful trichotomy:

- $\chi(\Sigma) > 0$: spherical geometry $g(\Sigma) = 0$ where the metric is of (constant) positive curvature
- $\chi(\Sigma) = 0$: flat/torus geometry $g(\Sigma) = 1$ where the metric is Ricci-flat
- $\chi(\Sigma) < 0$: hyperbolic geometry $g(\Sigma) > 1$ where the metric is of negative curvature

In particular, every Σ admits one such constant curvature by (conformal) scaling.

We summarize the above discussion into a chain of equalities:

$$\chi(\Sigma) = 2 - 2g(\Sigma) = \frac{1}{2\pi} \int_{\Sigma} R = [c_1(\Sigma)] \cdot [\Sigma] = \sum_{i=0}^{\dim_{\mathbb{R}} \Sigma = 2} (-1)^i b^i. \quad (1.4)$$

As we proceed from left to right, the first equality is combinatorics and topology; the second relates χ to analysis and differential geometry; the third rewrites the integral as intersection (of cycles) in algebraic geometry; and the last, to homological algebra.

It is fair to say that a significant portion of modern geometry is devoted to the generalization of this beautiful story in dimension 2. This is, of course, extremely difficult; high-dimensional geometry and topology often have unpredicted properties. The Hopf Conjecture—that for a compact Riemannian manifold M of dimension $2n$, positive (sectional) curvature means positive χ and negative (sectional) curvature means $\text{Sign}(\chi) = (-1)^n$ —is one of the immediate generalizations to Fig. 1.1. For $n = 1$, we are back to the case of Σ and for $n = 2$ it has also been settled by Chern–Gauß–Bonnet, which generalizes (1.3) to $\chi(M) = \frac{1}{(2\pi)^n} \int_M \text{Pf}(\Omega)$, the integral of the Pfaffian of the curvature form Ω to the Levi-Civita connection (and for $n = 2$ reducing to $\chi = \frac{1}{128\pi^2} \int R_{abcd} R_{efgh} \epsilon^{abdf} \epsilon^{cdgh}$ for the Riemann curvature tensor R_{abcd}). However, for $n > 2$, this is still an open problem [234]!

By imposing extra symmetries problems in mathematics and physics typically become easier to manage. If arbitrary high-dimensional manifolds are difficult to tame, what about sub-classes with further structures? Indeed, for orientable surfaces such as Σ , one can impose a complex structure, much like rendering \mathbb{R}^2 into the complex plane \mathbb{C} by adding $i = \sqrt{-1}$. Thus equipped, Σ becomes a complex curve (real dimension 2 becomes complex dimension 1). In other words, 2-manifolds can be complexified to fourfolds: these are the **Riemann surfaces** Σ considered as complex curves. Note that the standard, though perhaps confusing, appellation is that (complex) curves are manifolds of real dimension 2, i.e., surfaces; likewise, a (complex) surface is a real four-dimensional manifold. In order to avoid confusion, the widely used convention is that:

- A ***n*-Manifold** refers to a manifold of real dimension n .
- A ***n*-Fold** refers to one of complex dimension n .

A cultural distinction is that differential geometers use (1) more widely and algebraic geometers (2).

In fact, Σ is furthermore Kähler, in that its local metric is the double derivative of a scalar potential function. We leave a brief recapitulation, to Appendix A, of the rudiments and notation of a successive specialization from real manifolds to complex, to Hermitian, and to Kähler geometry, as well as some key results from bundle and (co-)homology that we will use. One advantage of complexification, as we will see in the next chapter, is that we can realize the manifold as vanishing loci

of polynomials in complex projective space. In this land of (complex) *algebraic* geometry (algebraic because we are dealing with polynomials) in projective space, everything is automatically compact and Kähler.

1.1.1 A Modern Breakthrough

Within the world of Kähler geometry, there are sufficient symmetries that a powerful statement exists for all dimensions. In the mid-1950s, E. Calabi made his famous conjecture [67]:

Conjecture 1 (Calabi Conjecture) Let (M, g, ω) be a compact Kähler manifold and R a $(1, 1)$ -form such that $[R] = [c_1(M)]$. Then \exists ! Kähler metric \tilde{g} and Kähler form $\tilde{\omega}$ such that $[\omega] = [\tilde{\omega}] \in H^2(M; \mathbb{R})$ and that $R = Ric(\tilde{\omega})$, the Ricci form of $\tilde{\omega}$.

This is quite a mouthful! And indeed, it is not the purpose of this prologue, nor of this book, to delve into its subtleties. Let us first unpack the statement. As mentioned earlier for complex dimension 1, the Kähler n -fold M has a metric of the form

$$g_{\mu\bar{\nu}} = \partial\bar{\partial}K(z^\mu, \bar{z}^{\bar{\nu}}) \quad (1.5)$$

for local coordinates $z^{\mu=1, \dots, n}$, where K is a scalar function called the Kähler potential. The Kähler form is a 2-form $\omega := ig_{\mu\bar{\nu}}dz^\mu \wedge d\bar{z}^{\bar{\nu}}$ and the existence of the potential is equivalent to the closedness of ω , i.e., $d\omega = 0$. Immediately, we see why complex onefolds are Kähler: the differential of a 2-form on a two-dimensional manifold automatically vanishes.

The Chern classes $c_k(M) = c_k(T_M) \in H^{2k}(M)$, for Kähler manifolds, have an important property: the Ricci $(1, 1)$ -form, the Kähler $(1, 1)$ -form and $c_1(M)$, as real 2-forms, all reside in $H^2(M; \mathbb{R})$. The content of the conjecture is that the Chern class determines, in a unique way, the behaviour of the curvature, much like Chern–Gauß–Bonnet mentioned above. In fact, uniqueness was already shown by Calabi—it was the existence of $(\tilde{g}, \tilde{\omega})$ that remained the challenge.

Furthermore, we saw from Fig. 1.1 that the genus 1 case acts as a boundary case in the trichotomy, and this pattern of a finite number of topologies for positive curvature and zero curvature is part of a bigger conjecture that we will discuss later in this book. Here, in the Calabi Conjecture, the case when $R = 0$ (Ricci-flatness) is also obviously important, where it means that for Kähler M , unique existence of Ricci-flat Kähler metric is equivalent to the vanishing of the first Chern class $c_1(M)$. The special case of **Kähler-Einstein** manifolds, i.e., when $R = \lambda g$, where the Ricci form is proportional to the metric form for some $\lambda \in \mathbb{R}$ best illustrates the situation. Here, the natural trichotomy: $\lambda > 0$ (ample, Fano), $\lambda = 0$ (Ricci-flat) and $\lambda < 0$ (anti-ample, or general type) is the desired generalization of Fig. 1.1.

From a computational perspective, to appreciate the power of the statement, suppose we wished to go hardcore and tried to find an explicit metric in some local coordinate. Even with the help of extra properties such as Kähler, the Ricci-flat

equations are a set of complicated non-linear PDEs in the components of the metric for which there is little chance of a hope for analytic solution. We are now at liberty to only check an algebraic/topological quantity, the first Chern class, many examples of which we shall compute throughout the book, would govern the Ricci curvature. In particular, its vanishing would guarantee the uniqueness and existence of a Ricci-flat metric.

The existence part of the Calabi Conjecture was finally settled by S.-T. Yau [361], some 20 years later:

Theorem 1 (Yau) *The Calabi Conjecture holds.*

In particular, manifolds with $R = 0$ are now called **Calabi–Yau** manifolds in honour of this achievement, which uses ingenious existence methods for the solution of a Monge–Ampère PDE and for which Yau received the Fields Medal in 1982.

It should be pointed out the proof is an existence proof and to date *no explicit Ricci-flat Kähler metric has been found on any compact Calabi–Yau manifold* (beyond the trivial case of products of tori) and this remains an important open problem. Importantly, before proceeding, the reader is pointed to the survey [362], which gives a fantastic bird’s-eye-view of the historical developments and well most of the active areas of research related to Calabi–Yau manifolds.

Henceforth, we will use the acronym **CY_n** to mean a Calabi–Yau n -fold, a Ricci-flat Kähler manifold of complex dimension n .

1.1.2 Preliminary Examples: 1, 2, ? . . .

We will give many explicit examples later in the book, but for now, in order to reify the above concepts, let us present some preliminary though extremely important examples of Calabi–Yau manifolds. We saw that Riemann surfaces of real dimension 2 are complexifiable to Kähler onefolds. Indeed, the torus $T^2 \simeq (S^1)^2$ case of $g(\Sigma) = 1$ is the *only* compact, smooth, Ricci-flat, Kähler manifold of complex dimension one. That is:

Proposition 1 *A (compact, smooth) Calabi–Yau onefold is the torus T^2 as a Riemann surface/complex algebraic curve.*

We are therefore reassured that CY₁ is none other than one of the most familiar objects in mathematics. We can see this by recalling that T^2 is \mathbb{C}/L , the quotient of the complex plane by a lattice (as we remember from our first lesson in topology that identifying the opposite sides of a sheet of paper gives a doughnut), and thus a metric on T^2 can be inherited from the flat metric on the plane. Algebraically, a torus can be realized as an **elliptic curve**, the central object of geometry and number theory; there is thus a programme in understanding the arithmetic, in addition to the geometry, of Calabi–Yau manifolds [81, 277].

In complex dimension 2, the 4-torus $T^4 \simeq (S^1)^4$ is analogously Calabi–Yau. There is another called the **K3 surface** that deserves an entire treatise to itself.

Unfortunately, we do not have enough space in this book to discuss K3 surfaces and will entrust the reader to the great texts of [18, 34, 327].

So far, we have one CY₁ and two CY₂, at least topologically. However, this seemingly innocent sequence of numbers 1,2, ... of Calabi–Yau manifolds in complex dimension 1,2, ... does *not* persist. In fact, the next number in this sequence—which is perhaps the most pertinent to physics, as we shall see next—for the number of inequivalent Calabi–Yau threefolds, is already *unknown* (though it is conjectured by Yau to be finite in topological type). What we do know is that there is a vast landscape thereof and much of this book will be a status report on how much we do know of this landscape.

1.2 $10 = 4 + 2 \times 3$: A Physical Motivation

While the aforementioned advances in geometry were being made, theoretical physicists were working on the ultimate Theory of Everything. By the late 1970s, a theory of strings, born from an initial attempt to explain the mass–spin correlation of the zoo of elementary particles in the 1960s, showed great promise in unifying gravity with quantum field theory. As this book is neither on string theory nor really on algebraic geometry, but rather on the algorithms and data that emerge, the reader is referred to the canon [165], or to [316] for technical and historical accounts, and encouraged to peruse this section as quickly as possible.

As far as Calabi–Yau manifolds are concerned, the physics side of the story began in 1985, with the paper that began what is now called “**string phenomenology**” [74], a field aimed at constructing the standard model as a low-energy limit of string theory. (The gravity side is called “string cosmology” and the conjunction of the two should, in principle, encompass all that exists within the universe.) The paper immediately followed the discovery of the **Heterotic string** [164], which, being a unified theory of gravity and a QFT with a Lie algebra as large as $E_8 \times E_8$ or $SO(32)$, caused much excitement.²

The primary reason for this optimism is that the **Standard Model** gauge group $G_{SM} = SU(3) \times SU(2) \times U(1) \subset E_8$ (recall that the $SU(3)$ factor for QCD governs the dynamics of baryons and the $SU(2) \times U(1)$ factor for QED, the leptons). It has been an old question in particle physics as to why the standard model gauge group has the structure of a non-semisimple Lie group, and is such a seemingly arbitrary product of three unitary groups.

²By fusing the bosonic string (whose critical dimension is 26) with the superstring (whose critical dimension is 10) in the process of “heterosis” by assigning them to be, respectively, left and right moving modes of the string, the fact that $26 - 10 = 16$ gives 16 internal degrees of freedom to furnish a gauge symmetry. Beautifully, in 16 dimensions there are only two even self-dual integral lattices in which quantized momenta could take value, viz., the root lattices of $E_8 \times E_8$ and of $D_{16} = \mathfrak{so}(32)$.

The fact that G_{SM} is not a (semi-)simple Lie group has troubled many physicists since the early days: it would be more pleasant to place the baryons and leptons on the same footing by allowing them to be in the same representation of a larger simple gauge group. This is the motivation for the sequence in (1.6) below: starting from $SU(5)$, theories whose gauge groups are simple are called **grand unified theories** (GUTs), the most popular historically had been $SU(5)$, $SO(10)$ and E_6 , long before string theory came onto the scene in theoretical physics. Various attempts have been made to harness the following inclusion of Lie groups:

$$SU(3) \times SU(2) \times U(1) \subset SU(5) \subset SO(10) \subset E_6 \subset E_7 \subset E_8 , \quad (1.6)$$

with all the various semisimple groups to the right of G_{SM} furnishing different candidate GUT theories. Thus, a unified theory with a natural E_8 gauge group was most welcome.³ Oftentimes, we add one more $U(1)$ factor to G_{SM} , denoted as $U(1)_{B-L}$, to record the difference between baryon and lepton number, in which case

$$G'_{SM} = SU(3) \times SU(2) \times U(1) \times U(1)_{B-L} \quad (1.7)$$

and the above sequence of embeddings skips $SU(5)$.

The downside, of course, is that (standard, critical, supersymmetric) string theory lives in $\mathbb{R}^{1,9}$ and compared to our $\mathbb{R}^{1,3}$ there must be 6 extra dimensions. This remains a major challenge to the theory even today. There are two philosophies in addressing $10 = 4 + 6$: to (1) take the extra dimension to be small in the spirit of Kaluza–Klein or to (2) take them to be large in the spirit of holography. The former is called **compactification** and the latter **brane-world** and they conveniently correspond mathematically to compact and non-compact Calabi–Yau varieties, as we shall see in the first two chapters of this book.

In brief, [74] gave the conditions for which the heterotic string, when compactified, would give a supersymmetric gauge theory in $\mathbb{R}^{1,3}$ with a potentially realistic particle spectrum. Here, compactification means that the ten-dimensional background is taken to be of the form $\mathbb{R}^{1,3} \times M_6$ with $\mathbb{R}^{1,3}$ our familiar space-time and M_6 some small (Planck-scale) curled up 6-manifold, endowed with a vector bundle V at the Planck-scale too small to be currently observed directly. Specifically, with more generality, the set of conditions, known as the *Hull–Strominger System* [239, 334], for the low-energy low-dimensional theory on $\mathbb{R}^{1,3}$ to be a supersymmetric gauge theory are:

1. M_6 is complex.
2. The Hermitian metric g on M_6 and h on V satisfy:

³According to Witten, in the sense of string phenomenology, “heterotic compactification is still the best hope for the real world”.

- (a) $\partial\bar{\partial}g = i\text{Tr}F \wedge F - i\text{Tr}R \wedge R$ where F is the curvature (field strength) 2-form for h and R the curvature 2-form for g .
(b) $d^\dagger g = i(\partial - \bar{\partial}) \ln ||\Omega||$, where Ω is a holomorphic 3-form on M_6 that exists.⁴

3. F satisfies the Hermitian Yang–Mills equations

$$\omega^{ab} F_{a\bar{b}} = 0, \quad F_{ab} = F_{\bar{a}\bar{b}} = 0. \quad (1.8)$$

A sequence of arguments (cf. Appendix A.5) then leads to the fact that the simplest solution to the above conditions is that:

Proposition 2 *M_6 is Kähler, complex dimension 3, and of $SU(3)$ holonomy.*

Furthermore, one can take the vector bundle V to be simply the tangent bundle T_M . We can now refer to Berger’s famous holonomy classification [41] as to what such a manifold is.

Theorem 2 (Berger) *For M a Riemannian manifold of real dimension d that locally is not a product space nor a symmetric space, then special holonomy and manifold type obey:*

Holonomy $\mathcal{H} \subset$	Manifold type
$SO(d)$	Orientable
$U(d/2)$	Kähler
$SU(d/2)$	Calabi–Yau
$Sp(d/4)$	Hyper-Kähler
$Sp(d/4) \times Sp(1)$	Quaternionic-Kähler

Moreover, for $d = 7, 8$, there are two more possibilities, viz., G_2 and $Spin(7)$. These two, together with the $SU(d/2)$ and $Sp(d/4)$ cases, are Ricci-flat.

Thus, our internal 6-manifold M is, in fact, a Calabi–Yau threefold⁵ and our two strands of thought, in Sect. 1.1 and in the present, naturally meet. This is another golden example of a magical aspect of string theory: it consistently infringes, almost

⁴Recently, Li–Yau [281] showed that this is equivalent to ω being balanced, i.e., $d(||\Omega||g^2) = 0$.

⁵The reader might wonder how curious it is that two utterly different developments, one in mathematics, and another in physics, should both lead to Rome. Philip Candelas recounts some of the story. The paper [74] started life as two distinct manuscripts, one by Witten, and the other, by Candelas–Horowitz–Strominger, the latter began during a hike to Gibraltar reservoir, near Santa Barbara, in the fall of 1985. Both independently came to the conclusion that supersymmetry required a covariantly constant spinor and thus vanishing Ricci curvature for the internal manifold M .

It was most timely that Horowitz had been a postdoctoral researcher of Yau, and Strominger also coincided with Yau when both were at the IAS, thus a phone call to Yau settled the issue about the relation to $SU(3)$ holonomy and hence Calabi–Yau. Thus the various pieces fell, rather quickly, into place, the two manuscripts were combined, and the rest was history. In fact, it was the physicists who named these Ricci-flat Kähler manifolds as “Calabi–Yau”.

always unexpectedly rather than forcibly, upon the most profound mathematics of paramount concern, and then quickly proceeds to contribute to it.

1.2.1 Triadophilia

As seen from the above, string phenomenology aims to obtain the particle content and interactions of the standard model as a low-energy limit. In terms of the representation of G'_{SM} in (1.7), denoted as $(\mathbf{a}, \mathbf{b})_{(c,d)}$, where \mathbf{a} is a representation of $SU(3)$, \mathbf{b} , that of $SU(2)$, and (c, d) are the charges of the two Abelian $U(1)$ groups, the **Standard Model** elementary particles (all are fermions except the scalar Higgs) are as follows:

$SU(3) \times SU(2) \times U(1) \times U(1)_{B-L}$	Multiplicity	Particle
$(\mathbf{3}, \mathbf{2})_{1,1}$	3	Left-handed quark
$(\mathbf{1}, \mathbf{1})_{6,3}$	3	Left-handed anti-lepton
$(\bar{\mathbf{3}}, \mathbf{1})_{-4,-1}$	3	Left-handed anti-up
$(\bar{\mathbf{3}}, \mathbf{1})_{2,-1}$	3	Left-handed anti-down
$(\mathbf{1}, \mathbf{2})_{-3,-3}$	3	Left-handed lepton
$(\mathbf{1}, \mathbf{1})_{0,3}$	3	Left-handed anti-neutrino
$(\mathbf{1}, \mathbf{2})_{3,0}$	1	Up Higgs
$(\mathbf{1}, \mathbf{2})_{-3,0}$	1	Down Higgs

(1.9)

In addition to these are vector bosons: (1) the connection associated to the group $SU(3)$, called the gluons, of which there are 8, corresponding to the dimension of $SU(3)$, and (2) the connection associated to $SU(2) \times U(1)$, called W^\pm , Z , and the photon: a total of 4. We point out that in this book by the standard model—and indeed likewise for all ensuing gauge theories—we shall actually mean the (minimal) supersymmetric extension thereof, dubbed the **MSSM**, and to each of the fermions above there is a bosonic partner and vice versa.

Of note in the table is the number 3, signifying that the particles replicate themselves in three families, or **generations**, except for the recently discovered Higgs boson, which is only a single doublet under $SU(2)$. That there should be 3 and only 3 generations, with vastly disparate masses, is an experimental fact with confidence [343] level $\sigma = 5.3$ and has *no satisfactory theoretical explanation to date*. The possible symmetry among them, called flavour symmetry, is independent of the gauge symmetry of G'_{SM} .

Upon compactification of the E_8 heterotic string on a Calabi–Yau threefold M_6 , a low-energy supersymmetric QFT is attained. Thus, our paradigm is simply

$$\text{Geometry of } M_6 \longleftrightarrow \text{physics of } \mathbb{R}^{1,3}.$$

What a marvellous realization of Kepler’s old adage “Ubi materia, ibi geometria”!

Now, the tangent bundle T_M is of $SU(3)$ holonomy; thus E_8 is broken to E_6 since $SU(3)$ is the commutant of E_6 within E_8 . In particular, the fundamental 248-dimensional representation of E_8 branches are

$$\begin{aligned} E_8 &\rightarrow SU(3) \times E_6 \\ 248 &\rightarrow (1, 78) \oplus (3, 27) \oplus (\bar{3}, \bar{27}) \oplus (8, 1) . \end{aligned} \quad (1.10)$$

It is possible to package all of the SM particles in (1.9) into the 27 representation of E_6 , in a SUSY E_6 -GUT theory. From (1.10), this is associated with the fundamental 3 of $SU(3)$. The 27 representation is thus associated to $H^1(T_M)$ and the conjugate $\bar{27}$ to $H^1(T_M^\vee)$. Similarly, the 1 representation of E_6 is associated with the 8 of $SU(3)$, and thus to $H^1(T_M \otimes T_M^\vee)$. Thus, we have that

$$\begin{aligned} \text{generations of particles} &\sim H^1(T_M) , \\ \text{anti-generations of particles} &\sim H^1(T_M^\vee) . \end{aligned}$$

In general, even when taking an arbitrary bundle V instead of just T_M , the lesson is that

$$\begin{aligned} \text{Particle content in } \mathbb{R}^{1,3} &\longleftrightarrow \text{cohomology groups of } V, V^\vee \\ &\text{and of their exterior/tensor powers} \end{aligned}$$

The interactions, i.e., cubic Yukawa couplings in the Lagrangian, constituted by these particles (fermion–fermion–Higgs) are tri-linear maps taking the cohomology groups to \mathbb{C} ; this works out perfectly for a Calabi–Yau threefold: for example,

$$H^1(M, V) \times H^1(M, V) \times H^1(M, V) \rightarrow H^3(M, \mathcal{O}_M) \simeq \mathbb{C} . \quad (1.11)$$

An immediate *constraint* is, as mentioned above, that there be 3 net generations, meaning that

$$\left| h^1(X, T_M) - h^1(X, T_M^\vee) \right| = 3 . \quad (1.12)$$

Thus, the endeavour of finding Calabi–Yau threefolds with the property (1.12) began in 1986. We will see in the following section that the difference on the left-hand side is half of the Euler number χ .

Thus, one of the first problems posed by physicists to what Candelas calls “card-carrying” algebraic geometers was made specific:

Question 1 Are there smooth, compact, Calabi–Yau threefolds, with Euler number $\chi = \pm 6$?

This geometrical “love for threeness”, much in the same spirit as triskaidekaphobia, has been dubbed by Candelas et al. as **Triadophilia** [79]. More recently, independent of string theory or any unified theories, the question of why there might be geometrical reasons for three generations to be built into the very geometry of the standard model has been explored [220].

1.2.2 *Caveat and Apology for the Title*

As we stated at the outset, the foregoing discussions of this section were meant to be a rapid summary of how the study of Calabi–Yau manifolds first came into physics in the mid-1980s; they are neither meant to be self-contained nor complete, and chapters 12–15 of [165], Volume 2, are far more pedagogical and enlightening. More importantly, we have used the word “[Landscape](#)” rather loosely, throughout and in the title. The concept is so vast and amorphous that perhaps any focused and unambiguous usage cannot avoid being Procrustean. However, in physics, and in string theory in particular, the word has taken on a more specific meaning on which we now briefly elaborate.

The reader should not be deceived into thinking that Eqs. (1.10)–(1.12) apply universally in string theory. The number of generations of particles in (1.12), in particular, is only applicable to the so-called standard embedding of heterotic string compactification described above, as the first appearance of Calabi–Yau manifolds in physics. Today, even within the heterotic community, people are no longer searching for Calabi–Yau threefolds with Euler number⁶ ± 6 .

With the advent of string dualities in the mid-1990s, from D-branes [307] to AdS/CFT [286], from M-theory on G_2 -manifolds [20] to F-theory on fourfolds [61, 293], etc., the space of possible vacuum solutions of string theory that lead to our $3 + 1$ -dimensional world exploded to far beyond Calabi–Yau manifolds. The reader is referred to the classic textbooks [165, 308], to [35] for a modern treatment, and especially to [113, 176, 240] for those interested in phenomenology and the standard model. Since the focus of the book is to use the plethora (to which we vaguely refer as “landscape”) of Calabi–Yau manifolds as a playground for computational geometry and data science, rather than an introductory text on string theory, we will not delve into the vastness of the subject of the string landscape. For the benefit of the interested, however, we will attempt a precis of the major directions of reaching the standard model of particle physics from string theory, accentuating on where Calabi–Yau spaces appear.

⁶Serious effort, however, has been made by various groups, e.g., the UPenn-Oxford collaboration, to use stable holomorphic vector bundles V on CY_3 , whose index gives the number of particle generations. The standard embedding is the special case where V is the tangent bundle. A review of some of this direction in recent times is in [200].

CFT Constructions The context, viz., heterotic compactifications, wherein CY₃ first arose was presented above, with the emphasis on translating between the particle physics and the algebraic geometry (and for this reason we have adhered to this train of thought). However, from the point of view of the world-sheet conformal field theory (CFT), this scenario is difficult and not exactly solvable. While the 6-torus T^6 is a trivial Calabi–Yau, one could take *orbifolds* thereof, which means we take the quotient T^6/Γ , typically for a product of cyclic groups $\Gamma = \mathbb{Z}/(n\mathbb{Z}) \times \mathbb{Z}/(m\mathbb{Z}) \subset SU(3)$, and consider this to be our compactification space.

Alternatively, one could start with a solvable non-trivial two-dimensional CFT, notably minimal models with specific central charges, and tensor them together; this is the *Gepner Model*. There is a beautiful story here that the Landau–Ginzburg (LG) realization of the minimal model CFT is given by a polynomial Lagrangian governed by a (super-)potential W , which is precisely the defining hypersurface in a weighted projective space for a CY₃. This is the LG/CY Correspondence. Both these directions have led to exact MSSM particle spectrum. In fact, the sheer number of such CFT constructions, coming from the different types of lattices and orbifold groups, first gave physicists a hint of the vastness of possible string vacua, for which the word “landscape” was applied in the mid-1980s [280]. Indeed, the idea of the computational complexity of the *string landscape* was already contemplated back in [112] (q.v. [178] for recent studies).

Type II Constructions In type II superstring theory, there are D-branes, which are extended dynamical objects of spatial dimensions $-1, 1, 3, 5, 7, 9$ for type IIB and $0, 2, 4, 6, 8$ for type IIA. The most promising idea of obtaining the standard model here is to place configurations of D6-branes at angles to each other, within a CY₃ background so that the D6-branes wrap 3-cycles (elements of H_3) within the compact CY. This is the *intersecting brane-world* construction and the standard model particles are given as modes of the open string stretched between the D6-branes.

One can apply thrice T-duality (mirror symmetry) on the above to D3-brane in type IIB. In Chap. 2 of this book, we will focus specifically on D3-branes transverse to non-compact CY₃ spaces, a prototype of AdS/CFT. We will do so not because the world-volume physics therein is proficient in obtaining the standard model, nor because of the profound holographic ideas of quantum gravity that arise, but because they afford quiver realizations that illustrate the interplay between representation theory and algebraic geometry, often in a computational and algorithmic way.

F-theory and CY₄ Type IIA can be geometrized to 11-dimension M-theory, which is an S^1 -fibration over the former. Thus, intersecting brane models can be mapped to M-theory on 7-manifolds of G_2 holonomy (much like these latter manifolds can be constructed from a CY₃ M by direct product $M \times S^1$, and then quotienting by certain actions on special Lagrangian sub-manifolds of M). If we go up one more dimension, we are in 12-dimensional F-theory, which is an elliptic fibration over IIB. Here, we can compactify on CY₄ (the analogue of $10 = 4 + 2 \times 3$ is $12 = 4 + 2 \times 4$) and all the constructions in this book can be directly generalized.

In terms of standard model building, F-theory has the advantage of being purely geometric, it does not require bundle information over CY₃ as in (non-standard) heterotic compactification. Moreover, CY₄, being complex, is easier to handle than G_2 manifolds, which rests on the much more difficult mathematics of real algebraic geometry (real numbers are not algebraically closed and over them we do not have the fundamental theorem of algebra).

Flux Compactification and the Famous 10^{500} A key ingredient of a string theory is the presence of higher-form fields, i.e., multi-indexed tensors (generalizing the photon/1-index, graviton/2-index, B-field/2-index, etc.). In type II, the branes mentioned above are precisely the objects that “couple” (i.e., provide the support of region of integration of) to these form fields. Specifically, these couplings all contribute to the low-energy effective Lagrangian. This is the *flux compactification* scenario.

An archetypal situation is type IIB compactification on CY₃, but with 3-form field strengths (e.g., the NSNS H_3 and the RR F_3) contributing, and satisfying a quantization condition of their integrals over 3-cycles in the CY₃ being integers. This is a scenario that works well in producing low-energy effective theories with *moduli stabilization* (which ensures that the compact dimensions remain so under the dynamics).

The rough estimate of the possible string vacua from flux compactification proceeds as follows [50]. The typical flux (i.e., as the integer integral of the 3-forms around the 3-cycles) takes about 10 values; the typical number of 3-cycles in a compact smooth CY₃ is about 500 (we will see this estimate of the third Betti number b_3 against the actual datasets in the next chapter). Hence, there are around 10^{500} possible (flux) vacua, a number that has at the turn of the millennium very much entered into the public psyche as the “landscape”.

As one can see, this is a back-of-the-envelope assessment and says nothing about how many of such vacua even remotely resemble our observed four-dimensional universe. Some recent estimates by explicit computer scan in type II and heterotic context separately [12, 107, 155] showed that about 1 in a billion stable vacua has an exact standard model particle content. It would be interesting to see, once numerical metrics can be more efficiently computed [17, 118, 119], how correct particle masses would further reduce the possibilities.

1.3 Topological Rudiments

From the previous two sections, we have seen two parallel strands of development, in mathematics and in theoretical physics, converging on the subject of Calabi–Yau manifolds, a vast subject on which this book can only touch upon a specialized though useful portion; for such marvellous topics as mirror symmetry, enumerative geometry, etc., the reader is referred to the classics [235, 250].

For now, we nevertheless have a working definition of a (smooth, compact) Calabi–Yau n -fold; it is a manifold M of complex dimension n , which furthermore obeys one of the following *equivalent* conditions:

- Kähler with $c_1(T_M) = 0$
- Kähler (M, g, ω) with vanishing Ricci curvature $R(g, \omega) = 0$
- Kähler metric with global holonomy $\subset SU(n)$
- Kähler and admitting nowhere vanishing global holomorphic n -form $\Omega^{(n,0)}$
- Admits a covariantly constant spinor
- M is a projective manifold with (1) [Canonical bundle](#) (sheaf), the top wedge power of the cotangent bundle (sheaf),

$$K_M := \bigwedge^n T_M^\vee$$

being trivial, i.e., $K_M \simeq \mathcal{O}_M$ and (2) $H^i(M, K_M) = 0$ for all $0 < i < n$.

We remark that the global form $\Omega^{(n,0)}$ prescribes a volume form $V = \Omega \wedge \overline{\Omega}$. When $n = 3$, it can be written in terms of the Gamma matrices γ and the covariant constant spinor η (cf. [Appendix A](#)) as $\Omega^{(3,0)} = \frac{1}{3!} \Omega_{mnp} dz^m \wedge dz^n \wedge dz^p$ with $\Omega_{mnp} := \eta_-^T \gamma^{lm} \gamma^n \gamma^{pl} \eta_-$.

It is clear that in the above, the last definition is the most general. So long as M is a projective variety it is not even required that it be smooth and K_M could be a sheaf obeying the said conditions. Throughout this book, because the emphasis is on the algebraic, liberal usage of the first and last definitions will be made, and we will see how they translate to precise algebraic conditions from which we will make explicit construction of examples.

1.3.1 The Hodge Diamond

We now present the most key topological quantities of a Calabi–Yau threefold. Again, a lightning introduction of key concepts such as (co-)homology, bundles and complex geometry, in as self-contained a manner as possible, is given in [Appendix A](#). From the Hodge decomposition, Eq. [\(A.1\)](#), the Betti numbers of a Kähler n -fold M split as

$$b_k = \sum_{\substack{p,q=0 \\ p+q=k}}^n h^{p,q}(M) , \quad k = 0, \dots, 2n . \quad (1.13)$$

Now, complex conjugation (since M has at least complex structure) implies that $h^{p,q} = h^{q,p}$. Moreover, Poincaré duality implies that $h^{p,q} = h^{n-p,n-q}$. Therefore, the $(n + 1)^2$ [Hodge numbers](#) $h^{p,q}$ automatically reduces to only

$((n+1)(n+2)/2 - (n-1))/2 + (n-1)$. The clearest way to present this information is via a so-called **Hodge Diamond** (a rhombus, really).

For $n = 3$, for example, the diamond looks like

$$\begin{array}{ccccccc} & & & h^{0,0} & & & \\ & & h^{0,1} & & h^{0,1} & & \\ & h^{0,2} & & h^{1,1} & & h^{0,2} & \\ h^{0,3} & & h^{2,1} & & h^{2,1} & & h^{0,3} \\ & h^{0,2} & & h^{1,1} & & h^{0,2} & \\ & h^{0,1} & & h^{0,1} & & & \\ & & h^{0,0} & & & & \end{array} \quad (1.14)$$

Further simplifications to the diamond can be made. Because there is a unique non-vanishing holomorphic n -form, $h^{n,0} = h^{0,n} = 1$. Next, we can contract any $(p, 0)$ -form with $\bar{\Omega}$ to give a (p, n) -form, and a subsequent Poincaré duality gives a $(n-p, 0)$ -form. This thus implies that $h^{p,0} = h^{n-p,0}$.

Next, we consider some special impositions. In the case of M being compact and connected, it is standard that $b_0 = 1$. Therefore, the top and bottom tip $h^{0,0} = 1$. Moreover, from the last of the equivalent conditions of our definition of CY, $H^i(M, \mathcal{O}_M) = 0$ for $0 < i < n$. This means⁷ that $h^{1,0} = h^{0,1} = 0$.

Putting the above together, the Hodge diamond of a compact, connected, simply connected Calabi–Yau threefold becomes

$$\begin{array}{ccccc} & 1 & & b^0 & 1 \\ & 0 & 0 & b^1 & 0 \\ 0 & h^{1,1} & 0 & b^2 & h^{1,1} \\ 1 & h^{2,1} & h^{2,1} & 1 & \longrightarrow b^3 & 2 + 2h^{2,1} \\ 0 & h^{1,1} & 0 & b^4 & h^{1,1} \\ & 0 & 0 & b^5 & 0 \\ & 1 & & b^6 & 1 \end{array} \quad (1.15)$$

In other words, the Calabi–Yau threefolds of our primary concern are actually governed by only 2 degrees of freedom:

1. The **Kähler parameters**, of which there are $h^{1,1}(M)$
2. The **complex structure parameters**, of which there are $h^{2,1}(M)$

⁷Another way to see this is that for M simply connected, the first fundamental group $\pi_1(M)$ vanishes. Then, $H_1(M)$, being the Abelianization of $\pi_1(M)$, also vanishes. Hence, $h^1 = 0$.

More precisely, by Hodge decomposition $H^{p,q}(M) = H^q(M, \bigwedge^p T_M^\vee)$ (cf. (A.1)), we can express our two key Dolbeault cohomology groups as those valued in the tangent bundle T_M and its dual, T_M^\vee , the cotangent bundle:

$$H^{1,1}(M) = H^1(M, T_X^\vee), \quad H^{2,1}(M) = H^{1,2}(M) = H^2(X, T_X^\vee) \simeq H^1(X, T_X), \quad (1.16)$$

where in the last step we have used **Serre Duality** that for a vector bundle V on a compact smooth Kähler manifold M of complex dimension n , we have

$$H^i(M, V) \simeq H^{n-i}(M, V^\vee \otimes K_M), \quad (1.17)$$

and since M is Calabi–Yau, the canonical bundle $K_M \simeq \mathcal{O}_M$. This pair of non-negative⁸ integers $(h^{1,1}, h^{2,1})$, the **Hodge pair**, will play a crucial role in the ensuing.

It is well known that the Euler number of a compact smooth manifold can be expressed as an alternating sum of Betti numbers:

$$\chi(M) = \sum_{i=0}^{\dim_{\mathbb{R}}(M)} (-1)^i b^i. \quad (1.18)$$

Thus, combining with (1.13) and our shape of the Hodge diamond, we arrive at

$$\begin{aligned} \chi(M) &= 1 - 0 + h^{1,1} - (2 + 2h^{2,1}) + h^{1,1} - 0 + 1 \\ &= 2(h^{1,1} - h^{2,1}) \end{aligned} \quad (1.19)$$

for our Calabi–Yau threefold.

⁸In almost all cases, they are both positive integers. The case of $h^{2,1} = 0$ is called *rigid* because here the manifold would afford no complex deformations. The Hodge number $h^{1,1}$, on the other hand, is at least 1 because M is at least Kähler.

Chapter 2

The Compact Landscape



In the end, the search for a single, all-encompassing theory of nature amounts, in essence, to the search for the symmetry of the universe.

—Shing-Tung Yau

By now, we hope that the reader is intrigued by the richness of Calabi–Yau manifolds and thus motivated and will be impatient for explicit examples to befriend. Acquainting ourselves with a “bestiary” (in the spirit of [237]) of Calabi–Yau manifolds will indeed constitute much of the ensuing material. As the approach of this book is algebraic, we will construct all our manifolds as **Algebraic Varieties**.

The neophyte might be alarmed at the seeming sophistication of our choice, since it has become customary for the beginning student to learn the rudiments of differential geometry before algebraic geometry and thereby be familiar with charts and transition functions, *before* polynomial rings and ideals. This is perhaps ironic, since from a practical, and certainly computational, point of view, algebraic varieties are simply vanishing loci of multivariate polynomials, well known to school mathematics after an entrée to Cartesian geometry. Luckily, powerful theorems such as that of Chow [169] allow us to realize (complex analytic) manifolds as algebraic varieties and vice versa. In case the reader needs a quick introduction to polynomial rings and how ideals correspond to varieties, we give a somewhat self-contained introduction in Appendix A.6.1.

Since we are only considering complex manifolds, all our examples will be constituted by the intersection of polynomials in complex variables. Immediately, our Calabi–Yau one-folds as algebraic tori described in Proposition 1 find their incarnation: we recall from a second-term course in complex analysis that the zero locus of a cubic polynomial in two complex variables, say $(x, y) \in \mathbb{C}^2$, is a torus. Thus, a Calabi–Yau one-fold as an elliptic curve is a cubic in $\mathbb{C}[x, y]$; this is an affine variety in \mathbb{C}^2 .

While the next chapter will focus on affine varieties, in the present chapter we will exclusively consider **projective varieties**. This is for the sake of compactness, as it is well known that a projective space is attained by adding “infinity” to an affine space. Hence, affine complex coordinates $(x, y) \in \mathbb{C}^2$ are promoted to projective

coordinates $(x, y, z) \in \mathbb{C}^3$ with the extra identification that $(x, y, z) \sim \lambda(x, y, z)$ for any non-zero $\lambda \in \mathbb{C}^\times$. In other words, the elliptic curve is a cubic in \mathbb{CP}^2 with homogeneous coordinates $[x : y : z]$. We will adopt the convention in complex algebraic geometry that \mathbb{P}^n is understood to be \mathbb{CP}^n and define [Complex projective space](#) as

$$\mathbb{P}_{[z_0:z_1:\dots:z_n]}^n := \mathbb{C}_{(x_0,x_1,\dots,x_n)}^{n+1} / \sim ; \quad (x_0, x_1, \dots, x_n) \sim \lambda(x_0, x_1, \dots, x_n), \quad \lambda \in \mathbb{C}^\times. \quad (2.1)$$

We will almost exclusively work with polynomials embedded in (2.1) and some of its natural generalizations. Again, we refer the reader to Appendix A for an attempt of a self-contained initiation to all the requisite knowledge of complex algebraic geometry.

2.1 The Quintic

In the above, we constructed CY₁ as a cubic ($d = 3$) in \mathbb{P}^2 ($n = 2$), algebraically furnishing a torus into an elliptic curve.¹ Two simple numerologies should be noted:

- $1 = 2 - 1$: the dimension of the CY is 1 less than that of the ambient space since it is defined by a single polynomial; this is an example of a [hypersurface](#).
- $3 = 2 + 1$: the degree of the polynomial exceeds the dimension of the ambient projective space by 1 and is thus equal to the number of homogeneous coordinates; this we will see to be precisely the Calabi–Yau condition.

We wish to construct a Calabi–Yau ($n - 1$)-fold M realized as a [Hypersurface](#) in \mathbb{P}^n , i.e., a single homogeneous polynomial, of degree d in $n + 1$ projective coordinates. The formal way of doing this is to first write down the short exact sequence [194] (q.v. Appendix A)

$$0 \rightarrow T_M \rightarrow T_{\mathbb{P}^n}|_M \rightarrow N_{M/\mathbb{P}^n} \rightarrow 0. \quad (2.2)$$

The sequence essentially states that the tangent bundle of the ambient space $A = \mathbb{P}^n$, when restricted to the hypersurface M , breaks up into the tangent bundle T_M of M and the normal bundle N_{M/\mathbb{P}^n} as M embeds into \mathbb{P}^n . However, T_A does not quite *split* into the direct (Whitney) sum of the two, but it is a non-trivial *extension* of the two. One consequence of (2.2) is the adjunction [194] formula $K_M = (K_{\mathbb{P}^n} \otimes N_{M/\mathbb{P}^n}^\vee)|_M$ for the [Canonical bundle](#) K_M . Now, because M is defined by a single polynomial of degree d , this normal bundle is simply $\mathcal{O}_{\mathbb{P}^n}(d)|_M$.

¹Here is a wonderful quote and homage to Kronecker, from Tristan Hübsch, “Algebraic curves were created by God, algebraic surfaces by the Devil; it is then only human to create algebraic three-folds.”

We now appeal to the axioms of the (total) Chern class (cf. Definition 21 in Appendix A). First, the normalization axiom $c(\mathcal{O}_{\mathbb{P}^n}(1)) = 1 + H$ gives us the total Chern class of the tangent bundle:²

$$c(T_{\mathbb{P}^n}|_M) = (1 + H)^{n+1}, \quad (2.3)$$

where H is the hyperplane (divisor) class of $\mathbb{P}^{n-1} \hookrightarrow \mathbb{P}^n$. Next, the normal bundle, being $\mathcal{O}_{\mathbb{P}^n}(d)$, is a line bundle of degree d and has only two contributions to the total Chern class

$$c(\mathcal{O}_{\mathbb{P}^n}(d)) = c_0(\mathcal{O}_{\mathbb{P}^n}(d)) + c_1(\mathcal{O}_{\mathbb{P}^n}(d)) = 1 + dH. \quad (2.4)$$

The short exact sequence (2.2) (cf. (A.9)) implies that

$$c(T_M)c(N_{M/\mathbb{P}^n}) = c(T_{\mathbb{P}^n}|_M), \quad (2.5)$$

whence, recalling that $c_k(T_M) \in H^{2k}(M; \mathbb{R})$, we arrive at the expression for our desired Chern class for M :

$$\begin{aligned} c(T_M) &= (1 + H)^{n+1}(1 + dH)^{-1} \\ &= (1 + (n+1)H + \binom{n+1}{2}H^2 + \dots)(1 - dH + d^2H^2 - \dots) \\ &= 1 + (n+1-d)H + \left(\binom{n+1}{2} + d^2 - d(n+1) \right)H^2 + \dots \end{aligned} \quad (2.6)$$

In the above, the order H^k term is $c_k(T_M)$, so we expand only to order H^{n-1} since M is of complex dimension $n-1$ and cannot admit any Chern classes above this dimension.

Immediately, we see that $c_1(T_M) = (n+1-d)H$. Using the vanishing c_1 condition in the definition of Calabi–Yau manifolds from Sect. 1.3 (because \mathbb{P}^n is Kähler, its holomorphic subvarieties as defined by polynomials in the projective coordinates are automatically Kähler), we arrive at our suspected result.

Proposition 3 *A homogeneous degree $d = n+1$ polynomial (in the $n+1$ projective coordinates) as a hypersurface in \mathbb{P}^n defines a Calabi–Yau $(n-1)$ -fold.*

In particular, we encounter our first Calabi–Yau threefold: the degree 5 polynomial in \mathbb{P}^4 , viz., the **Quintic**, Q .

²This can itself be derived from the Euler sequence of bundles on projective space: $0 \rightarrow \mathcal{O}_{\mathbb{P}^n} \rightarrow \mathcal{O}_{\mathbb{P}^n}(1)^{\oplus(n+1)} \rightarrow T_{\mathbb{P}^n} \rightarrow 0$.

In fact, we have done more. In (2.6), setting $n = 4$ and $d = 5$, we have all the Chern classes for Q :

$$c(T_Q) = 1 + 10H^2 - 40H^3 . \quad (2.7)$$

The top Chern class, here c_3 , is the **Euler class**. Its integral over M should give the Euler number:

$$\chi(Q) = -40 \int_Q H^3 = -40 \cdot 5 = -200 , \quad (2.8)$$

where the integral of H^3 over M is a consequence of Bézout's theorem: H^3 , the intersection of 3 hyperplanes, is the class of 5 points. Another way to think of this is to pull back the integral from M to one on the ambient space A . For $\omega \in H^{n,n}(M)$ and $\mu \in H^{k,k}(A)$, where M is of codimension k in A so that the normal bundle is of rank k , we have $\int_M \omega = \int_A \mu \wedge \omega$. For our present case, $\mu = d H$.

2.1.1 Topological Quantities: Exact Sequences

We now have our favourite Calabi–Yau threefold, the quintic, of Euler number -200 . From (1.19), we immediately see that

$$h^{1,1} - h^{2,1} = -100 . \quad (2.9)$$

Obtaining each individual Hodge number, on the other hand, is an entirely different kettle of fish. This perfectly illustrates the principle of index theorems: the alternating sum is given by some topological quantity, while individual terms require more sophisticated and often computationally involved methods. Within our context, the specific index theorem is a version of Atiyah–Singer [169], stating the following theorem.

Theorem 3 (Atiyah–Singer, Hirzebruch–Riemann–Roch) *For a holomorphic vector bundle V on a smooth compact complex manifold M of complex dimension n , the alternating sum (index) in bundle-valued cohomology is given by*

$$\text{ind}(V) = \sum_{i=0}^n (-1)^i \text{rk} H^i(M, V) = \int_M \text{Ch}(V) \wedge \text{Td}(T_M) ,$$

where $\text{Ch}(V)$ is the Chern character for V and $\text{Td}(T_M)$ is the Todd class for the tangent bundle of M .

If we took the simple case of $V = T_M$ and use (A.12) and (A.14) from the Appendix, we would obtain the [Euler number](#) as a special case of the index theorem³ so that for threefolds,

$$\chi(M) = \chi(T_M) = \int_M c_3(T_M) . \quad (2.10)$$

Luckily, we do not need to do much in this very case to obtain the individual terms. First, there is only one Kähler class, which inherited from the ambient \mathbb{P}^4 —indeed, $H^2(\mathbb{P}^n; \mathbb{Z}) \cong \mathbb{Z}$ for any n , corresponding to the hyperplane class, so that $h^{1,1}(\mathbb{P}^n) = 1$ upon Hodge decomposition. Hence,

$$h^{1,1}(Q) = 1 . \quad (2.11)$$

In general, however, it must be emphasized that ambient classes *do not* descend 1-1 to projective varieties and other measures need to be taken, as we shall see.

Alternatively, we can try to obtain $h^{2,1}$. As mentioned in Sect. 1.3.1, these correspond to complex structure. What this means is the following. A generic quintic in $\mathbb{P}_{[z_0:\dots:z_4]}^4$ can be written as a sum over all possible degree 5 monomials in the 5 projective variables z_i ; each monomial has a complex coefficient. Perhaps the most familiar form of Q is

$$Q := \sum_{i=0}^4 z_i^5 - \psi \prod_{i=0}^4 z_i , \quad \psi \in \mathbb{C} , \quad (2.12)$$

consisting of the sum of the fifth powers, usually called the **Fermat form**, together with a deformation by the product, with ψ as an explicit complex parameter. The question of complex structure is then to ascertain how many such coefficients, up to variable redefinitions, there are. Again, what we shall do below is a back-of-the-envelope calculation, which *does not* work in general. Nevertheless, its simplicity is illustrative.

³In detail, we proceed as follows. Taking $V = T_M$, of rank $r = n = \dim_{\mathbb{C}} M$, we have

$$\begin{aligned} \int_M c_n(T_M) &= \sum_{i=0}^r (-1)^i \text{Ch}(\bigwedge^i T_M^\vee) \text{Td}(T_M) && \text{Borel–Serre (A.15)} \\ &= \sum_{i=0}^n (-1)^i \chi(M, \bigwedge^i T_M^\vee) && \text{Hirzebruch–Riemann–Roch, Theorem 3} \\ &= \sum_{p,q=0}^n (-1)^{p+q} \text{rk} H^q(M, \bigwedge^p T_M^\vee) && \text{definition of } \chi \text{ as index} \\ &= \sum_{i=0}^n (-1)^i h^i(M, \mathbb{C}) = \chi(M) && \text{Hodge decomposition A.1.} \end{aligned}$$

First, how many possible degree 5 monomials can be written in 5 variables? This is a standard combinatorial problem and one can quickly convince oneself that the number of degree d monomials in k variables is the so-called multiset coefficient $\binom{k+d-1}{d}$. Next, we need to subtract the reparametrizations coming from linear transformations, i.e., from $PGL(5; \mathbb{Z})$, of which there are $5^2 - 1$. Finally, we are at liberty to rescale the polynomial by an overall constant. Therefore, in all, there are

$$h^{2,1}(Q) = \binom{5+5-1}{5} - (5^2 - 1) - 1 = 126 - 24 - 1 = 101 \quad (2.13)$$

complex deformation parameters. We have therefore rather fortuitously obtained the correct values of the Hodge pair $(1, 101)$ for the quintic, and we can check that indeed their difference is -100, as is required by the Euler number in (2.9).

The proper way to perform the above computation is, as might be expected, by sequence-chasing. We once more appeal to the Euler sequence (2.2), which induces a long **Exact sequence** in cohomology (the sexy way of saying this is that the cohomological functor H^\bullet is covariant on short exact sequences):

$$\begin{aligned} 0 \rightarrow & \boxed{H^0(Q, T_Q)}^0 \rightarrow H^0(Q, T_{\mathbb{P}^4}|_Q) \rightarrow H^0(Q, N_{Q/\mathbb{P}^4}) \rightarrow \\ & \rightarrow \boxed{H^1(Q, T_Q)}^d \rightarrow H^1(Q, T_{\mathbb{P}^4}|_Q) \rightarrow H^1(Q, N_{Q/\mathbb{P}^4}) \rightarrow \\ & \rightarrow H^2(Q, T_Q) \rightarrow \dots \end{aligned} \quad (2.14)$$

In the above, we have boxed the term that we will wish to compute, viz., $H^{2,1}(Q) \simeq H^1(Q, T_Q)$. The first term $H^0(Q, T_Q) = H^{2,0}(Q)$ vanishes because Q is Calabi-Yau. The boundary map d actually has 0 rank (q.v. [237] and Eq. (6.1) of [166]), and we thus have a short exact sequence $0 \rightarrow H^0(Q, T_{\mathbb{P}^4}|_Q) \rightarrow H^0(Q, N_{Q/\mathbb{P}^4}) \rightarrow H^{2,1}(Q) \rightarrow 0$ so that

$$h^{2,1}(Q) = h^0(Q, N_Q) - h^0(Q, T_{\mathbb{P}^4}|_Q). \quad (2.15)$$

Thus, we have reduced the problem to counting global holomorphic sections. Each of the two terms can be obtained by Leray tableaux [169] (cf. summary in Appendix C.2 of [10] for the present case).

2.1.2 Topological Quantities: Computer Algebra

If a single manifold as simple as the quintic requires so extensive a set of techniques, one can only imagine how involved the generic computation in algebraic geometry is. The novice student may not appreciate how *difficult* dealing with systems of polynomials (a concept introduced at primary school) really is: the system is highly

non-linear, especially when the degrees are high. While non-linearity typically invokes the thought of transcendental functions, the field of non-linear algebra is an entire enterprise by itself.

We are fortunate that we live within the age of computers, where at least anything algorithmic such as exact or Leray sequences need not be performed by hand. The discipline of **computational algebraic geometry** is vast and it is not our place to give an introduction thereto here. The keen reader is referred to the fantastic textbook [322] for a pedagogical treatment (cf. also Appendix A.3 of [9] for a tutorial in the present context of computing bundle cohomology). Nevertheless, the key idea to the matter, viz., the **Gröbner Basis**, is so vital that we shall take an immediate foray in Appendix B.

The take-home message is a matter of nomenclature. In differential geometry, we think of a manifold in terms of local patches at the intersections of which are smooth transition functions. In algebraic geometry, we think of it as a **Variety** or the vanishing locus of a system of multivariable polynomials $\{f_i(z_k)\}$ in the coordinates $\{z_k\}$ of the ambient space, typically \mathbb{CP}^n . The fancier, purely algebraic way, of saying this is that we start with⁴ a polynomial ring $\mathbb{C}[z_k]$ and any vanishing system of polynomials therein forms an ideal.⁵ Note that we use standard notation that $\mathbb{C}[z_k]$ means the set of polynomials in the variables z_k and with coefficients in \mathbb{C} . Hence, the vanishing locus defining the manifold corresponds to ideals in $\mathbb{C}[z_k]$. This is the starting point of any code in a computer algebra system for defining a variety, as we will see now.

If the reader only wishes for a black box, much as one wishes to evaluate a complicated integral on **Mathematica** without the desire for the detailed steps, then perhaps the most intuitive software available is **Macaulay2** [163], a glimpse of whose powers we will see now. The advantages of **Macaulay2** are manifold:

- it is free (downloadable from <http://www2.macaulay2.com/Macaulay2/> and every student of algebraic geometry is encouraged to do so);
- it is included in the latest distributions of linux/MacOS/Win10 Ubuntu;
- it has been incorporated into SageMath [320] (cf. <http://doc.sagemath.org/html/en/reference/interfaces/sage/interfaces/macaulay2.html> for calling **Macaulay2** from within **SageMath**);
- the aforementioned book [322] uses it as a companion in instruction; and
- for a quick online experiment without the need to download, one could simply access it “in the cloud” at <http://web.macaulay2.com>.

Let us now redo the above Hodge computations for the **Quintic** in **Macaulay2**. All commands in **Macaulay2** are case-sensitive, and there is a convention that the first letter is in lower case and in the case of multiple words concatenated into one, and the second starts with a capital letter. First, we define the polynomial ring R in

⁴The set of polynomials in a fixed number of variables clearly forms a ring under ordinary $+$, \times .

⁵It is an **Ideal** since the vanishing locus of a system of polynomials is the same as that of the system multiplied by arbitrary polynomials.

which we work, consisting of 5 complex variables z_i . The coefficient field⁶ is here taken to be $\mathbb{Z}/1979\mathbb{Z}$ (or any other large-ish prime of one's choice); this is the case with most packages in algebraic geometry as the coefficients can grow very quickly in manipulations such as Gröbner bases, so we take them modulo some prime. One could always try a few different primes in case the variety becomes singular over particular primes of bad reduction. Thence, we define

```
R = ZZ/1979[z_0, z_1, z_2, z_3, z_4] ;
```

A shorthand for writing this is $R = \text{ZZ}/1979[z_0 \dots z_4]$. Next, we define a specific quintic polynomial ($\psi = 2$ in (2.12))

```
polyQ = z_0^5 + z_1^5 + z_2^5 + z_3^5 + z_4^5 + 2*z_0*z_1*z_2*z_3*z_4 ;
```

A shorthand for this is $\text{poly} = (\text{sum for } i \text{ from 0 to 4 list } x_i^5) + 2 * (\text{product for } i \text{ from 0 to 4 list } z_i)$;

We remark that we have chosen a particular homogeneous degree 5 polynomial for convenience. Final topological quantities should neither depend on the choice of prime for the coefficient ring nor on the particular form of the polynomial (we remember from Cartesian geometry that ellipses are simply deformed circles).

We now enter into the important step of defining the algebraic variety:

```
quintic = Proj( R/ideal(polyQ) ) ;
```

Here, we define polyQ as an ideal of the ring R and form the quotient ring $R/\langle \text{polyQ} \rangle$ first.⁷ From this quotient ring, we form the `Proj`, which is the projective version of `Spec`, the maximal spectrum (i.e., set of maximal ideals) of a ring, to which affine varieties correspond (again, `Spec`, coordinate rings, etc. are described in an introductory manner in Appendix A.6.1). Roughly, `Proj` turns quotient rings to projective algebraic varieties, furnishing the explicit map in the ring-variety correspondence [98]. In the case of multiple defining polynomials, say f_1, f_2, \dots , we can simply use `ideal({f_1, f_2, ...})`, which is the most general situation.

Thus, we have `quintic` as a projective variety. We can check⁸ its dimension using

```
dim(quintic)
```

⁶One must not confuse the coefficient ring/field with the ground ring/field: the former is where the coefficients take value and can be varied quite liberally in all our computations, and the latter is where the variables take value, which for us will always be \mathbb{C} .

⁷Indeed, unlike **Mathematica**, whose primary user is the theoretical physicist, to whom notational flexibility is more important than rigour, all the software mentioned in the preface, and **Macaulay2** in particular, are written for the mathematician, where clarity and strictness cannot be relaxed.

⁸One thing about **Macaulay2** commands is that unlike most programming languages one could in fact dispense with the brackets “(” and “)”. Therefore, commands such as `ideal polyQ` or `dim quintic` are perfectly legitimate. Dan Grayson, one of the co-founders of the project, tells me that he has spent an enormous effort to make this syntactically possible. However, to avoid confusing the reader, we will not take advantage of this liberty in this book.

which returns 3, as required. Note that without the `Proj`, the dimension would be 4 since we have not yet projectivized. Now, we can check that this quintic is smooth with the built-in command:

```
singularLocus(quintic)
```

which returns `Proj(R/1)`, meaning that the singular locus corresponds to an ideal defined by 1. This makes sense, since the zero locus of a constant polynomial is empty. In other words, there are no singular loci and our quintic is smooth. By convention, the dimension of `Proj(R/1)` is recorded as $-\infty$, as can be checked by the `dim` command. This is indeed in congruence with our conclusions from (B.3) from the Appendix, where $\psi = 2$ is a smooth point in complex structure moduli space.

Now, we move into the heart of the matter by establishing the cotangent bundle:

```
cotan = prune(cotangentSheaf(quintic));
```

First, in any computational algebraic geometry package, no assumption about smoothness is a priori made, nor is the assumption about the existence of (holomorphic) bundles. In Appendix A, we make no mention of sheaves in order to simplify the discussion. Indeed, we will make no use of sheaf theory in this book. The reader could roughly bear in mind that a sheaf is just a bundle that could change rank at sub-regions of the variety, just as a singular variety is one that could change dimension at sub-regions of the manifold. Hence, there is no command “`cotangentBundle`” in Macaulay2, but rather “`cotangentSheaf`”, which makes assumption of smoothness. Moreover, `prune` is a built-in command that simplifies the sheaf by “pruning” (a play on the word “sheaf”).

One can check that the cotangent bundle has rank 3 (as is equal to the dimension of the base manifold) simply with

```
rank(cotan)
```

Moreover, one can find the **Canonical bundle** as (the third exterior power is the wedge product \wedge^3)

```
KQ = prune(exteriorPower(3, cotan));
```

At this point, we appreciate that while the software is extremely convenient, even the state-of-the-art computers are beginning to struggle a bit: all commands so far take milliseconds to execute on a simple laptop, the exterior power, however, will take quite some time and memory and one might even need to set the prime 1979 to something smaller to enable memory allocation to store the coefficients generated in due course.

We should obtain the result `OO_quintic^1` for `KQ`, meaning that $K_Q = \mathcal{O}_Q$, the trivial structure bundle⁹ discussed in Appendix A, whereby computationally proving that Q is indeed a Calabi–Yau threefold.

⁹In computational algebraic geometry, sheafs/bundles are denoted by modules via the **sheaf-module correspondence**, a quick discussion of this was given in Appendix A.1 of [9].

Finally, we can use Hodge decomposition (A.1) to compute the requisite topological invariants:

```
H11Q = HH^1 ( cotan );
H21Q = HH^1 ( exteriorPower( 2, cotan ) );
```

In the above, HH is the sheaf-cohomology operator, and we readily obtain the results $(\mathbb{Z}/1979)^1$ and $(\mathbb{Z}/1979)^{101}$ as vectors over the base field, respectively, for H11Q and H21Q (one can use the `rank` command to obtain the numbers 1 and 101, respectively).

We conclude this section with a few lessons: (1) algebraic geometry is algorithmic. Finding geometric quantities ultimately reduces to manipulating systems of polynomials: whether one is finding a convenient basis, or computing the (co)kernels of matrices in monomials, one is lead to such systems; (2) software such as `Macaulay2` has very conveniently implemented the cruces such as finding Gröbner bases or syzygies and for simple cases are our indispensable aide; (3) sadly, computing Gröbner bases is a doubly exponential running time process, for example, an estimate on the complexity of the Buchberger algorithm has an upper bound on the degrees of the elements as $\sim (d^2/2 + d)^{2^{n-1}}$, where d is the maximal total degree of the input polynomials and n is the number of variables [126].

2.2 CICY: Complete Intersection Calabi–Yau

While we have enjoyed our promenade in the land of exact sequences and of computational geometry, the quintic—the wealth of beautiful mathematics and physics of which we had only a tiny glimpse—was less than desirable as far as (1.12) is concerned: the Euler number (2.9) of -200 is far from ± 6 , and it is not even divisible by 3.

An immediate generalization presents itself: instead of a single *hypersurface*, what about a set of polynomials in \mathbb{P}^n ? After all, any projective variety can be so realized. This turns out to be too much. The first generalization of a hypersurface is a **complete intersection**, where the codimension of the variety is equal to the number of polynomials. This is a case of the “best possible” intersection where each defining polynomial slices out one dimension. It should be emphasized that in general if one has k arbitrary polynomials intersecting in \mathbb{P}^n , it is *not* by any means guaranteed to give a variety of dimensions $n - k$.

Cyclic Manifolds How many complete intersection Calabi–Yau threefolds can be written inside \mathbb{P}^n ? Again, this is a simple combinatorial problem: partition $n + 1 =$

$$\sum_{\substack{n_i \in \mathbb{Z}_{>0} \\ i=1}}^k n_i \quad (\text{the generalization of Proposition 3}), \text{ together with } n - 3 = k \quad (\text{complete intersection condition}).$$

There are easily seen to be 5 solutions in total, of which $n = 4, k = 1, n_1 = 5$ is the quintic. By similar considerations as in Sect. 2.1, we can compute their Hodge numbers. They all have $h^{1,1} = 1$, descended from

the ambient \mathbb{P}^n . These are consequently called **cyclic** because $H^2(M; \mathbb{Z}) \cong \mathbb{Z}$, the infinite cyclic group. Adopting the notation $[n|n_1, n_2, \dots, n_k]$ to mean the complete intersection of homogeneous polynomials f_1 of degree n_1 , f_2 of degree n_2 , etc., the 5 solutions are

$$[4|5], [5|2, 4], [5|3, 3], [6|3, 2, 2] \text{ and } [7|2, 2, 2, 2]. \quad (2.16)$$

These are the quintic in \mathbb{CP}^4 , the intersection of a quadric and a quartic in \mathbb{CP}^5 , that of 2 cubics in \mathbb{CP}^5 , that of a cubic with 2 quadrics in \mathbb{CP}^6 , and that of 4 quadrics in \mathbb{CP}^7 , respectively. Again, every polynomial is considered *generic* is that the coefficients are sufficiently random so that the variety is smooth. Another thing is that algebraic geometers refer to quadratic polynomials as *quadrics*. This is due to historical reasons when quadratic surfaces (like conic sections) were called quadrics.

In fact, the first column is redundant as it is one less than the sum of the rest. By adjunction formula/Euler sequence as before, we can also compute the second Chern class (the first is, of course, 0, and the third integrates to the Euler number) as a multiple of the class H^2 for the hyperplane class $H \subset \mathbb{P}^n$ (for Q , we recall from (2.7) that this is 10). By Bézout, we can also find the volume normalization (triple intersection) $d(M) = \int_M H^3$ (for Q , we recall from (2.8) that this is 5). We summarize the data for all five in Table 2.1.

Our bestiary of Calabi–Yau threefolds has now increased from 1 to 5. Again, none has $\chi = \pm 6$, though 2 have Euler number divisible by 6. Can we proceed further? What about generalizing the ambient space to a product of projective spaces instead of a single one? This was considered by the authors of [75, 76, 151, 166] in the second lustrum of the 1980s. As with the partition problem of (2.16), this amounts to writing the configuration

$$M = \left[\begin{array}{c|cccc} n_1 & q_1^1 & q_1^2 & \dots & q_1^k \\ n_2 & q_2^1 & q_2^2 & \dots & q_2^k \\ \vdots & \vdots & \vdots & \ddots & \vdots \\ n_m & q_m^1 & q_m^2 & \dots & q_m^k \end{array} \right]_{m \times k}, \quad \sum_{r=1}^m n_r = k+3, \quad \sum_{j=1}^k q_i^j = n_i + 1 \quad \forall i = 1, \dots, m \quad (2.17)$$

Table 2.1 The 5 cyclic Calabi–Yau threefolds as complete intersections in an ambient space that is a single \mathbb{P}^n . The configuration, Hodge numbers and Euler number are given, together with the second Chern class $c_2(T_M)$, as the coefficient of H^2 for the hyperplane $H \in \mathbb{P}^n$, as well as the volume $d(M) = \int_M H^3$

A	Configuration	$\chi(M)$	$h^{1,1}(M)$	$h^{2,1}(M)$	$d(M)$	$c_2(T_M)$
\mathbb{P}^4	[4 5]	-200	1	101	5	10
\mathbb{P}^5	[5 2 4]	-176	1	89	8	7
\mathbb{P}^5	[5 3 3]	-144	1	73	9	6
\mathbb{P}^6	[6 3 2 2]	-144	1	73	12	5
\mathbb{P}^7	[7 2 2 2 2]	-128	1	65	16	4

as a set of k polynomials of multi-degree $q_j^i \in \mathbb{Z}_{\geq 0}$ in the ambient space $A = \mathbb{P}^{n_1} \times \dots \times \mathbb{P}^{n_m}$. The complete intersection condition $\dim(A) - \dim(M) = k$ translates to $\sum_{r=1}^m n_r = k + 3$ and the $c_1(T_M) = 0$ condition to $\sum_{j=1}^k q_r^j = n_i + 1$ for each $r = 1, \dots, m$. Again, the left-most column is redundant and may be omitted without ambiguity. The Calabi–Yau threefold corresponding to such a configuration as (2.17) is called by the affectionate acronym “**CICY**,” for Complete Intersection CY₃.

CICY Classifying the CICY matrices, checking redundancies and equivalences, is already a highly non-trivial task. In some sense it constituted the first emergence of (then) big data to pure mathematics and theoretical physics. Candelas and Lütken recount the fascinating tale of how this was achieved on the then CERN supercomputer, involving dot matrix printers and magnetic tapes. Likewise, Schimmrigk speaks of staring at VAX machines in Austin over long nights.

The result has persisted in two amusing forms, in the corner of Philip Candelas’ office as a rather large pile of perforated printout and in Andy Lutken’s, on a magnetic tape, should the reader even belong to the generation to know what these mean. Luckily, the data has been resurrected [10] and is now accessible at <http://www-thphys.physics.ox.ac.uk/projects/CalabiYau/cicylist/> in text and Mathematica [358] format (indeed, the webpage of André Lukas has a very useful collection of CICY and other related matter [282]). All requisite data, viz., the Hodge pair, the second Chern class and the triple intersection $d(M)$, have also been computed by Candelas et al. [75, 76], Gagnon and Ho-Kim [151], Green et al. [166], and Hubsch [237]. Hence, though we reside firmly within the Age of Data and AI, and nowadays even the most abstract branches of mathematics have enjoyed information explosion, data mining in algebraic geometry and theoretical physics dates to as early as the late 1980s. One is perhaps reminded of a popular internet meme that technically Moses was the first person to download from the Cloud onto a tablet.

The presentation of the topological data in addition to the Hodge pair requires the following. One first fixes a basis $\{J^r\}_{r=1,\dots,h^{1,1}}$ of $H^2(M, \mathbb{Z})$ so that the Kähler cone is $\mathcal{K} = \{t_r J^r | t_r \in \mathbb{R}_{>0}\}$. For the cyclic case, there is only one $J = H$. In general, J will not descend 1-1 from the m hyperplane classes of the ambient product of projective spaces, and when they do, the CICY is called *favourable*. The triple intersection form in this basis is written as

$$d_{rst} := \int_M J^r \wedge J^s \wedge J^t, \quad (2.18)$$

which can be computed by pulling back integration from the ambient product of projective space where integration is standard, viz.,

$$\int_M \bullet = \int_A \mu \wedge \bullet, \quad \mu := \bigwedge_{j=1}^K \left(\sum_{r=1}^m q_r^j J_r \right). \quad (2.19)$$

The form d_{rst} is a *completely symmetric tensor* with respect to the three indices (note that J^r is a real 2-form so that commuting them across \wedge generates 2 minus signs that cancel).

The total Chern class of a Kähler threefold can be written as

$$c(T_M) = \sum_r [c_1(T_M)]_r J^r + \sum_{r,s} [c_2(T_M)]_{rs} J^r J^s + \sum_{r,s,t} [c_3(T_M)]_{rst} J^r J^s J^t. \quad (2.20)$$

For us, $c_1 = 0$, and moreover (2.10) reads

$$\chi(M) = \sum_{r,s,t} d_{rst} [c_3(T_M)]_{rst}, \quad (2.21)$$

leaving us with c_2 as an independent set of quantities to be determined.

Compact CY₃ Data We remark that the above data is in some sense complete because of an important result of Wall [353]

Theorem 4 (Wall) *The topological type of a compact Kähler threefold is completely determined by (1) the Hodge numbers $h^{p,q}$, (2) the triple intersection number d_{rst} and (3) the first Pontrjagin class $p_1(T_M) = c_1(T_M)^2 - 2c_2(T_M)$.*

Therefore, for all the Calabi–Yau databases out there, it suffices to record the Hodge numbers, the intersection 3-tensor d and c_2 (often written as a vector in the dual basis to J^r by contracting with d , i.e., as $[c_2(T_M)]_r := \sum_{s,t} [c_2(T_M)]_{rs} d_{rst}$). This was indeed the data shown, for example, for the 5 cyclics in Table 2.1. In this sense, our Calabi–Yau threefold data is a list of integers

$\{(h^{1,1}, h^{2,1}) ; \quad [c_2]_r ; \quad d_{rst}\}, \quad r, s, t = 1, \dots, h^{1,1}.$

(2.22)

Theorem 4 should also be contrasted with the complex dimension 1 case: there, as we recall, a single integer (the genus or the Euler number) completely characterizes the topological type of a Riemann surface. In complex dimension 3, we essentially need three sets of integers. In complex dimension 2, the situation is actually quite complicated and is intimately related to the celebrated Poincaré Conjecture for 4-manifolds. At least for simply connected cases, a classical result of Milnor [291] states that the intersection form in middle cohomology suffices to classify the topology.

While we are on the subject of generalities, an important result should be borne¹⁰ in mind (q.v. e.g., [97]):

Proposition 4 *All compact smooth projective threefolds can be smoothly embedded into \mathbb{P}^7 .*

In other words, *in principle*, to classify all Calabi–Yau threefolds, we only need to systematically write all possible polynomials, degree by degree, hypersurface by hypersurface (indeed, we are by no means restricted to complete intersection—of which there is only one, as we saw in Table 2.1—there can be any number of defining polynomials). As deceptively simple as this may seem, it is evidently far too difficult a task upon further reflection.

2.2.1 Topological Quantities: Statistics

Let us return to CICYs. The configuration matrix (2.17), as might be expected, readily gives almost all the data in (2.22). One can show [237] that, with $\mu := \bigwedge_{j=1}^K \left(\sum_{r=1}^m q_r^j J_r \right)$ and with normalization $\int_{\mathbb{P}^{n_r}} J^s = \delta_{rs}$ upon integrating the ambient A as a product of projective spaces,

$$\begin{aligned} c_1^r(T_M) &= 0 \\ c_2^{rs}(T_M) &= \frac{1}{2} \left[-\delta^{rs}(n_r + 1) + \sum_{j=1}^K q_j^r q_j^s \right] \\ c_3^{rst}(T_M) &= \frac{1}{3} \left[\delta^{rst}(n_r + 1) - \sum_{j=1}^K q_j^r q_j^s q_j^t \right] \\ d_{rst} &= \int_A \mu \wedge J^r \wedge J^s \wedge J^t \\ \chi &= \sum_{r,s,t} d_{rst} c_3^{rst} = \text{Coefficient}(c_3^{rst} J_r J_s J_t \mu, \prod_{r=1}^m J_r^{n_r}) . \end{aligned} \quad (2.23)$$

¹⁰I am grateful to Mark Gross for reminding me of this. The argument uses the fact that the secant variety to a smooth threefold M is at most of complex dimension $2 \cdot 3 + 1 = 7$. Embed this into \mathbb{P}^r . If $r > 7$, then there is a point $p \in \mathbb{P}^r$ not on M , so that there is a projection π_p from p to a hyperplane H , giving us $\pi_p : M \hookrightarrow H \cong \mathbb{P}^{r-1}$. We can inductively proceed until $r = 7$. The reader is referred to Exercise IV.3.11 of [194]. The projective is needed here; for a smooth toric threefold that is not projective, q.v. [99, example 6.1.17]. I am grateful to Hal Schenck for discussions on this.

We said “almost,” because as always, it is a difficult task to find the individual Hodge numbers for which there is no shortcut, nor explicit formulae as above.

Nevertheless, the full Hodge list was computed in [166] and all the inequivalent configurations were classified in [75, 76, 151]. We summarize some key results as follows:

- There are **7890** matrices (dropping the first redundant column in (2.17)) from 1×1 (the quintic, denoted as $[5]^{1,101}_{-200}$) to a maximum of 12 rows, or a maximum of 15 columns;
- All entries $q_j^r \in [0, 5]$;
- The transpose of any CICY matrix is also a CICY;
- The 5 cyclices in Table 2.1 are the only ones with a single row, and their transposes give 4 more.
- There are 266 distinct Hodge pairs $(h^{1,1}, h^{2,1}) = (1, 65), \dots, (19, 19)$;
- There are 70 distinct Euler numbers $\chi \in [-200, 0]$ (all are non-positive and none has $|\chi| = 6$).

Recently, it was shown [51] by explicit computer check using [338] that 195 have freely acting symmetries (whereby admitting smooth quotients) with 37 different finite groups, from the simplest $\mathbb{Z}/2\mathbb{Z}$ to $(\mathbb{Z}/8\mathbb{Z}) \rtimes H_8$, of order 64.

Other famous CICYs include the Tian–Yau manifold $TY = \begin{bmatrix} 1 & 3 & 0 \\ 1 & 0 & 3 \end{bmatrix}_{-18}^{14,23}$ as well as its transpose, the Schön manifold $S = \begin{bmatrix} 1 & 1 \\ 3 & 0 \\ 0 & 3 \end{bmatrix}_0^{19,19}$, both of which have

been central in string phenomenology. It was found by Yau in the early days that TY had a freely acting $\mathbb{Z}/3\mathbb{Z}$ symmetry, so that its quotient (which is not a CICY) $[TY/(\mathbb{Z}/3\mathbb{Z})]_{-6}^{6,9}$ has $\chi = -6$. When it was found, this quotient was *the* answer to triadophilia. While it had problems with too much extra matter and a less-than-ideal E_6 GUT group, it was taken seriously as string theory’s potential solution to the universe [168].

The manifold S is also interesting; it already existed in the mathematics literature [325] as a prime example of elliptic fibration (to which we shall turn later) and a paragon of a self-mirror ($h^{1,1} = h^{2,1}$) manifold. On S , one could find a $(\mathbb{Z}/3\mathbb{Z})^2$ discrete symmetry so that the quotient is a very beautiful (again, non-CICY) self-mirror manifold of Hodge pair $(3, 3)$. In [79], a discussion of these two manifolds, their related cousins as well as quotients is presented in pedagogical detail.

It is expedient to present the distribution of the [Hodge numbers](#) over the CICY dataset. In Fig. 2.1, we show the frequency plot/histogram for $h^{1,1}$ (somewhat Gaussian), $h^{2,1}$ (somewhat Poisson) and χ , respectively, on the left. On the right of the said figure, we plot the distinct values of the Hodge pair (there are only 266 points since there is much multiplicity). As is customary, we plot twice the difference, i.e., the Euler number on the abscissa and the sum, on the ordinate. This way, mirror symmetry will be very apparent as a flip along the vertical: a mirror pair

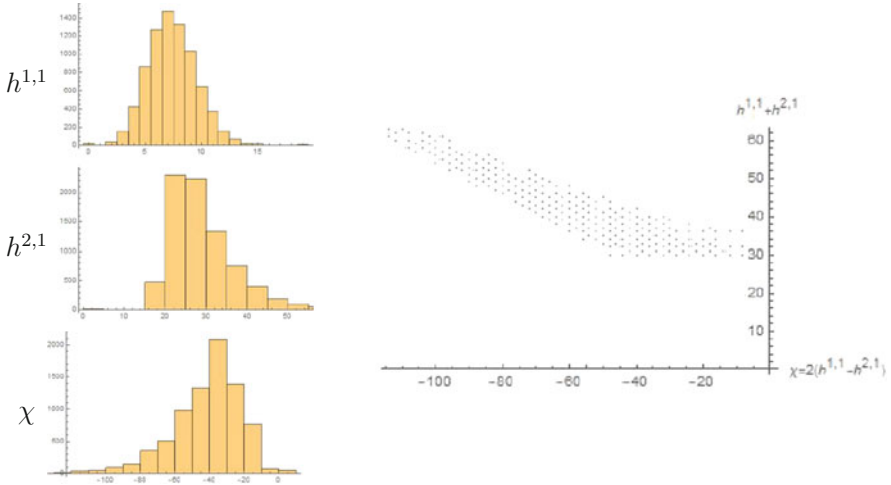


Fig. 2.1 The distribution of the Hodge numbers and the Euler numbers for CICYs; a plot of the distinct Hodge pairs, organized as $h^{1,1} + h^{2,1}$ versus the Euler number $\chi = 2(h^{1,1} - h^{2,1})$

of Calabi–Yau threefolds will be two points symmetric about the y-axis. Moreover, the line $y = |x|$ serves as a natural lower perimeter.

Note the peculiarity of the dataset: all Euler numbers are non-positive. This is a perfect case where one should be constantly vigilant when confronting data (by the standards of the 1990s, rather “big” data); eight thousand points might have led some to falsely speculate that Calabi–Yau Euler numbers cannot be positive and that mirror symmetry would not exist!

2.3 Other Datasets

Prompted by simultaneous developments in physics and mathematics, the early 1990s saw the birth of further Calabi–Yau datasets, the prominent ones of which we now present.

2.3.1 Hypersurfaces in Weighted \mathbb{CP}^4

Perhaps puzzled by the skewness in the CICY χ distribution, Philip Candelas—who, as one of the forefathers of mirror symmetry, was surely aware of this asymmetry—looked beyond CICYs with his friends. This led to a series of works shortly after the CICYs in the early 1990s [77, 78]. While CICYs generalized the quintic by extending a single \mathbb{P}^4 to a product of \mathbb{P}^n ’s, another natural extension is to consider

weights. Consider the ambient space A as *weighted* projective \mathbb{P}^4

$$A = W\mathbb{P}_{[w_0:w_1:w_2:w_3:w_4]}^4 := (\mathbb{C}^5 - \{0\}) / \sim, \quad \text{where}$$

$$(x_0, x_1, x_2, x_3, x_4) \sim (\lambda^{w_0} x_0, \lambda^{w_1} x_1, \lambda^{w_2} x_2, \lambda^{w_3} x_3, \lambda^{w_4} x_4). \quad (2.24)$$

Indeed, when all $w_i = 1$, this is simply \mathbb{P}^4 . As one might hope, a homogeneous polynomial of degree $\sum_{i=0}^4 w_i$ embedded in A as a hypersurface is Calabi–Yau.

There is a serious complication however: $W\mathbb{P}^4$ is in general singular and resolution is needed in addition to choosing a generic enough hypersurface which avoids any singularities. All this was performed in [77] and we will not delve into the details here as we shall later introduce a dataset into which these $W\mathbb{P}^4$ hypersurfaces are subsumed. Nevertheless, this dataset is very convenient in presentation—a single 5-vector of positive integers and, as we see below, is very illustrative in many respects.

In all, the authors in [77] (also independently Klemm, Schimrigk, Kreuzer–Skarke) found **7555** inequivalent Calabi–Yau threefolds as 5-vectors, giving us 2780 distinct Hodge pairs and with¹¹

$$\chi \in [-960, 960]; \quad h^{1,1}, h^{2,1} \in [1, 491]. \quad (2.25)$$

The value 960 is interesting:¹² it is in fact the largest in magnitude for χ of any Calabi–Yau threefold known to date, despite the plethora of constructions over the decades. In Fig. 2.2, we show the histograms for $h^{1,1}$, $h^{2,1}$ (somewhat Poisson) and χ (somewhat Gaussian), as well as a plot of the distinct Hodge numbers. Now, the Euler number has both positive and negative values, with most concentration on the vertical: the left–right symmetry is mirror symmetry, with apparently self-mirror manifolds dominating in number. The full list of distinct Hodge pairs can be downloaded from <http://hep.itp.tuwien.ac.at/~kreuzer/pub/misc/wp4.spec.gz> as part of the legacy database of <http://hep.itp.tuwien.ac.at/~kreuzer/CY/> upon which we shall expound in depth later in the chapter.

¹¹ Since there is some confusion in the literature in the early years about the precise expression of the Euler number in this case. It is helpful to give the correct and elegant result here, as presented in Eq (4.1) of [27]:

$$\chi = \frac{1}{d} \sum_{l,r=0}^{d-1} \sum_{\substack{0 \leq i \leq 4 \\ lq_i, q_i \in \mathbb{Z}}} \left(1 - \frac{1}{q_i} \right),$$

where $d = \sum_{i=0}^4 w_i$ is the degree of the hypersurface and $q_i = w_i/d$.

¹²I have bet a bottle of port, as it is a postprandial tradition fortified by drink in some Oxbridge colleges, against Andrew Dancer of Jesus, Oxford, in his college betting book—the volume into which we signed starting from when Napoleon matched into Prussia—that the 960 could never be exceeded. In retrospect, it was realized that the terms of the bet—neither of us being legally trained—were not entirely unambiguous: should some $|\chi| > 960$ threefold ever be found after our lifetimes, who would be there to collect or offer the prize? Richard Eager has also pointed out that the extremal manifold of Euler number -960 is the hypersurface in weighted projective space $W\mathbb{P}_{[1:12:28:42]}^4$, so that after all, 42, the answer to the meaning of life, the universe, and everything [1] is involved [109, 214].

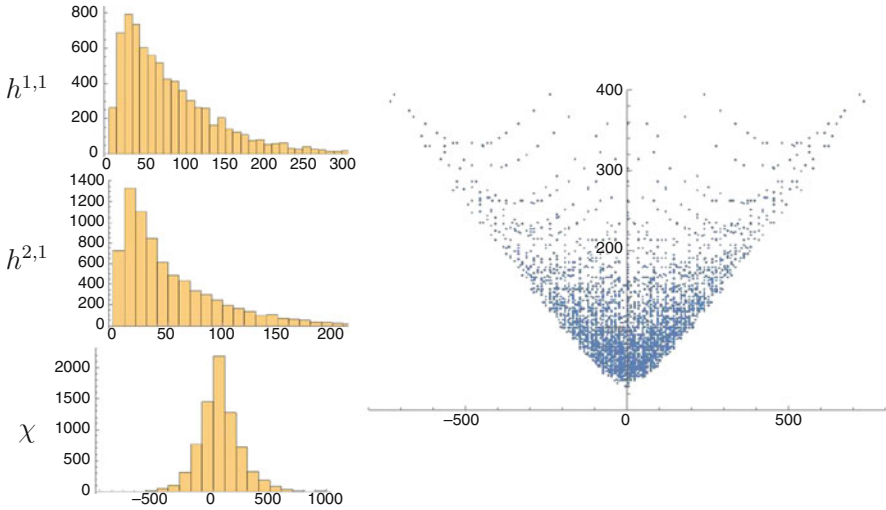


Fig. 2.2 The distribution of the [Hodge numbers](#) and the Euler numbers for hypersurfaces in $W\mathbb{P}^4$; a plot of the distinct Hodge pairs, organized as $h^{1,1} + h^{2,1}$ versus $\chi = 2(h^{1,1} - h^{2,1})$

2.3.2 Elliptic Fibrations

The 1990s saw a surge of interest in elliptic fibrations: in the mathematics because of the minimal model programme [114, 158, 170] and systematic construction of bundles over threefolds [117, 143] (generalizing Atiyah’s classical result on vector bundles over the elliptic curve [19]) and in physics because of the emergence of the so-called F-theory, which is an elliptic fibration over type IIB string theory [144, 355].

The idea of an elliptic fibration is straightforward. Recall that an elliptic curve—an algebraic realization of CY₁—is a cubic in \mathbb{P}^2 . This can be brought to Weierstraß form

$$zy^2 = 4x^3 - g_2xz^2 - g_3z^3, \quad (2.26)$$

where x , y and z are projective coordinates on \mathbb{P}^2 and g_2 and g_3 are complex parameters,¹³ which in terms of the modular parameter τ are the celebrated Eisenstein series.

Now, fibration simply means that we promote g_2 and g_3 to specific functions (sections) of chosen coordinates of a base B . Being a threefold and with fibre elliptic curves ($\dim_{\mathbb{C}} = 1$) means that the base B must be a complex surface ($\dim_{\mathbb{C}} = 2$). Thus one only needs to modify the variables so that they become sections of

¹³The version with which we are perhaps more familiar from our undergraduate days is when $z = 1$, so that we are dealing with the non-compact version embedded in $\mathbb{C}[x, y]$.

appropriate bundles over B . Specifically, it turns out taking the anti-canonical line bundle $L := K_B^{-1} = (\wedge^2 T_B^\vee)^{-1}$ of B , it suffices to take (x, y, z, g_2, g_3) as global sections of $(L^{\oplus 2}, L^{\oplus 3}, L^{\oplus 0} = \mathcal{O}_B, L^{\oplus 4}, L^{\oplus 6})$, respectively (one can check that the equation becomes homogeneous of degree 6 in terms of the sections of L). This is a fancier way of saying that we consider the fibre (2.26) itself as being a hypersurface in the weighted projective space $W\mathbb{P}_{[2:3:1]}^2$.

The situation is simplest, for instance, when the base is \mathbb{P}^2 , say with homogeneous coordinates r, s, t . We can directly write the variables as homogeneous polynomials of the specified degrees in terms of (r, s, t) , and we are back to writing the Calabi–Yau threefold as a hypersurface. The general case is more involved as one needs to find the right projective coordinates to embed K_B^{-1} so that the threefold can be written as a projective variety.

There is a common belief that most Calabi–Yau threefolds are elliptically fibered (numbers such as 80%, if not more, have been in the air), and it is still very much an active area of research to identify which CY₃s are elliptic fibrations. For CICYs, this was done in [14], and for the largest set of toric hypersurfaces (which we shall shortly address), systematic studies were carried out in [236], especially for the extremal values. Some explorations in the landscape of elliptic Calabi–Yau threefolds have been nicely summarized on Wati Taylor’s webpage at <http://ctp.lns.mit.edu/wati/data.html>.

While there is, to our knowledge, no complete database of elliptic fibration yet, there is a classification [293] of the possible bases B as well as a computation of Hodge numbers [159]. In brief, the Chern classes of the threefold can be written in terms of those of the base as [143]

$$\begin{aligned} c_1(X) &= 0, \\ c_2(X) &= c_2(B) + 11c_1(B)^2 + 12\sigma c_1(B), \\ c_3(X) &= -60c_1(B)^2. \end{aligned} \tag{2.27}$$

The base itself can only be of 4 types:

1. del Pezzo surface $dP_{r=0,1,\dots,9}$, i.e., \mathbb{P}^2 blown up at r points,¹⁴
2. Hirzebruch surface $\mathbb{F}_{r=0,\dots,12}$, i.e., \mathbb{P}^1 -bundle over \mathbb{P}^1 ;
3. Enriques surface E , i.e., a particular involution of K3 surface; and
4. blowups of \mathbb{F}_r ;

The del Pezzo and Hirzebruch surfaces are so central both to complex geometry and to today’s theoretical physics that we shall devote an appendix introducing some of their properties in A.7. Furthermore, a beautiful fact about elliptic fibrations is the classification by Kodaira of possible singularity types, for which we also leave the reader to Appendix A.8.

¹⁴The mathematician is used to $r = 0, \dots, 8$ being called del Pezzo, while the half-ample case of $r = 9$ is also considered part of the del Pezzo series. Appendix A.7 will discuss this in more detail.

2.4 An Explosion: The Kreuzer–Skarke Dataset

The mid-to-late 1990s saw the creation of what still is, by several orders of magnitude, the largest database in Calabi–Yau threefolds (about 10^{10} , as we shall soon see) or, for that matter, the largest dataset in pure mathematics.¹⁵ The idea is as before: how does one generalize \mathbb{P}^4 ? We have seen weighting and taking products as ambient spaces;¹⁶ a natural next generalization is to take A a toric variety.

Space-time certainly does not permit an introduction to this vast subject of toric varieties, and the reader is referred to the classic of [145], the modern tome of [99], or such preludes as the pertinent chapter in [235] and the brief introduction of [47, 89], as well as the tutorial in the appendix of [217] in our present context. We refer the readers to Appendix A.6 for a quick refresher on notation.

Suffice it to say here that while a (weighted) projective space of complex dimension n is \mathbb{C}^{n+1} (minus the origin), modulo the equivalence relation of the form (2.24), a toric variety of complex dimension n is \mathbb{C}^{n+k} (minus a point set obtained from the toric irrelevant ideal, which is the combinatorial Alexander dual of the so-called Stanley–Reisner ideal), modulo a set of k equivalence relations (encoded by a charge matrix). All these data can be conveniently repackaged into lattice cones and polytopes in \mathbb{R}^n and in particular the concept of reflexive polytopes, on the fundamentals of which we now conduct a lightning review.

2.4.1 Reflexive Polytopes

We begin by recalling the following definition.

Definition 1 A **Convex polytope** Δ has 2 equivalent definitions:

- (The Vertex Representation) Convex hull of set S of m points (vertices) $p_i \in \mathbb{R}^n$

$$\text{Conv}(S) = \left\{ \sum_{i=1}^m \alpha_i p_i \quad : \quad \alpha_i \geq 0, \sum_{i=1}^m \alpha_i = 1 \right\}.$$

- (The Half-hyperplane Representation): Intersection of linear inequalities (hyperplanes) $H \cdot \underline{x} \geq \underline{b}$, where \underline{b} and \underline{x} are real n -vectors and H is some $m \times n$ matrix.

¹⁵Comparable dataset includes the GAP project [338] and related atlas [96] on finite groups (about 10^7), the graded rings project [339] of algebraic varieties, especially Fano threefolds (about 10^8), the knots [340] database (about 10^6) and the L-functions and modular forms database [341] (about 10^6).

¹⁶Another intermediate is to take products of weighted projective spaces, and combining the ideas of the previous two datasets, this was performed in [255].

The extremal¹⁷ points of Δ are called vertices, extremal lines, edges, and then 2-faces, 3-faces, etc., and the $(n - 1)$ -faces of codimension 1 are called facets.

Henceforth, we focus only on *lattice* or *integral* polytopes.

Definition 2 A convex **lattice** polytope Δ_n is a convex polytope whose vertices are integral (lattice points), i.e., $p_i \in \mathbb{Z}^n$.

Often, we write subscript Δ_n to emphasize that the dimension of Δ is n , and we also often drop the adjective “convex” as it is understood to be so. In low dimension, we are very familiar with Δ_n : $n = 2$ gives lattice polygons (i.e., polygons whose vertices are given by a pair of integer Cartesian coordinates), $n = 3$ gives lattice polyhedra, etc.

Finally, in the land of lattice convex bodies, the concept of duality is central.

Definition 3 Given a lattice polytope Δ , the **Polar Dual** is the polytope

$$\Delta^\circ := \{\underline{v} \in \mathbb{R}^n \mid \underline{m} \cdot \underline{v} \geq -1 \quad \forall \underline{m} \in \Delta\}.$$

Indeed, this is a duality in the sense that $(\Delta^\circ)^\circ = \Delta$. Note that as defined, Δ° is not necessarily a lattice polytope since upon solving the inequality in the definition, the vertices of Δ° are not guaranteed to be integer but will be rational in general. However, in the special case that the polar dual is a lattice polytope, we have the following definition.

Definition 4 If Δ° is also a (convex) lattice polytope, then Δ (and also Δ° by duality) is called **reflexive**.

In the even more special case that $\Delta = \Delta^\circ$, they are called self-dual or self-reflexive.

To illustrate the above definitions, we give a pair of examples in Fig. 2.3, which we might have seen from school days. Here, Δ_2 and its polar dual Δ_2° , both lattice polygons, are given in vertex and half-plane representations. One can check the duality between them and the fact that both enjoy integer vertices.

One important observation we make is the origin is the central point. This is, in fact, a general statement (cf. [120] for a popular account).

Theorem 5 Δ is a reflexive polytope $\Leftrightarrow \Delta$ has a single interior lattice point (which can be shifted to be the origin) such that the facets of Δ are distance 1 hyperplanes from the origin.

We remark that in dimension 2, i.e., for reflexive polygons, we do not even need the second half of the condition: reflexivity for convex lattice polygons is the same as having a single interior lattice point.¹⁸ In dimension greater than 2, however, the

¹⁷That is, the intersection of Δ with a supporting hyperplane, which is a hyperplane H that has no intersection with the interior of Δ but does have intersection with Δ .

¹⁸I am grateful to Alexander Kasprzyk for pointing this out.

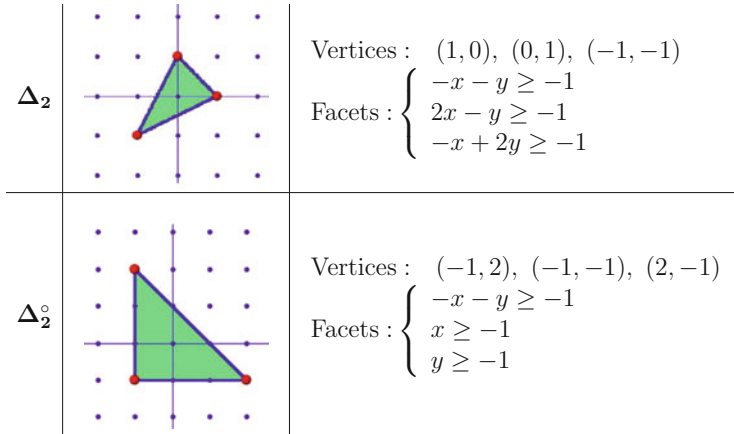


Fig. 2.3 A pair of reflexive polytopes (here, polygons), in vertex and hyperplane representations

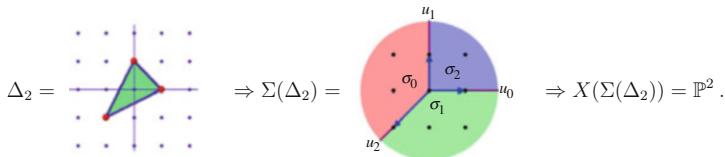


Fig. 2.4 The (reflexive) polytope giving the face fan for \mathbb{CP}^2

situation is more subtle and we need the condition that all facets are distance 1 from the single interior lattice point.

Having briefly refreshed our minds on reflexive polytopes, the key fact we now use is that they allow us to construct compact toric varieties (the reader is referred to the canonical textbooks [99, 145] as well as Appendix A.6 for a quick overview). This is done so via the so-called **Face Fan** $\Sigma(\Delta) \equiv \{\sigma = \text{pos}(F) \mid F \in \text{Faces}(\Delta)\}$, where $\text{pos}(F) \equiv \{\sum_i \lambda_i v_i \mid v_i \in F, \lambda_i \geq 0\}$. In other words, as we have a single interior point, we can subtend cones therefrom, joining the various vertices. Once we have the fan, we can obtain a compact toric variety $X(\Sigma)$. For our Δ_2 example above, we see the standard fan for \mathbb{P}^2 , as shown in Fig. 2.4. This is a nice way to think of \mathbb{P}^2 , as encoded by the lattice triangle with vertices $\{(1, 0), (0, 1), (-1, -1)\}$.

In general, a reflexive polytope Δ_n will define a compact (complex) n -fold, which is, however, not guaranteed to be smooth (for instance, in our examples in Fig. 2.4, Δ_2 is smooth, but Δ_2° is not). They are called Gorenstein Fano, in that the anti-canonical sheaf (note that we use sheaf here since the underlying variety is not guaranteed to be smooth) is ample [299]. Indeed, as with toric varieties [99], $X(\Delta)$ is smooth iff the generators of all the cones $\sigma \subset \Sigma$ are part of a \mathbb{Z} -basis (i.e., $\det(\text{gens}(\sigma)) = \pm 1$). In such a smooth case, Δ is called **regular**.

2.4.2 CY Hypersurfaces: *Gradus ad Parnassum*

Once we have a reflexive polytope Δ_n and its associated compact toric variety $X(\Delta_n)$, a beautiful construction gives us the following statement.

Theorem 6 (Batyrev–Borisov [29]) *The anti-canonical divisor in $X(\Delta_n)$ gives a smooth Calabi–Yau $(n - 1)$ -fold as a hypersurface:*

$$0 = \sum_{\underline{m} \in \Delta} C_{\underline{m}} \prod_{\rho=1}^k x_\rho^{\langle \underline{m}, \underline{v}_\rho \rangle + 1},$$

where \underline{m} (over which the sum is performed) are all the lattice points inside and on Δ , while \underline{v}_ρ are the vertices of Δ° . The coefficients $C_{\underline{m}}$ are complex numbers specifying, as for projective varieties, the complex structure.

In other words, if we have a reflexive Δ_4 , then we can easily obtain a hypersurface¹⁹ therein according to the recipe above, which is CY₃. We have not defined divisors in this book because we will not really need this concept. We can think of a divisor as a codimension 1 sub-manifold (i.e., hypersurface). In particular, the anti-canonical divisor is a hypersurface of a specific degree.

The simplest Fano (toric) fourfold is \mathbb{P}^4 (all \mathbb{P}^n are Fano because they have positive curvature), and it corresponds to a Δ_4 in exactly the same way that \mathbb{P}^2 is a toric variety in Fig. 2.4. Here, the vertices of the polytope and its polar dual are

$$\begin{aligned} \underline{m}_1 &= (-1, -1, -1, -1), & \underline{v}_1 &= (1, 0, 0, 0), \\ \underline{m}_2 &= (4, -1, -1, -1), & \underline{v}_2 &= (0, 1, 0, 0), \\ \Delta : \underline{m}_3 &= (-1, 4, -1, -1), & \Delta^\circ : \underline{v}_3 &= (0, 0, 1, 0), \\ \underline{m}_4 &= (-1, -1, 4, -1), & \underline{v}_4 &= (0, 0, 0, 1), \\ \underline{m}_5 &= (-1, -1, -1, 4), & \underline{v}_5 &= (-1, -1, -1, -1). \end{aligned} \tag{2.28}$$

We can find algorithmically (shortly we will see how this is done on the computer) all the lattice points in Δ of which there are 126 (reminiscent of (2.13)), giving us 126 monomials of degree 5 upon taking the dot product in the exponent. We have thus retrieved our favourite quintic threefold Q .

A SageMath Digression It is expedient to take a slight digression on the details of the above computation, as a means to familiarize the reader with SageMath [320]. (Luckily the software Polymake [303], like Macaulay2 and Singular, has been incorporated, and we leave a somewhat combined treatment to Appendix E.) Indeed, the Python-style environment of SageMath and its over-arching vision have rendered it an almost indispensable tool for many contemporary researchers in mathematics; the student versed therein will be very much at an advantage. Other

¹⁹If Δ_n is singular, then the corresponding hypersurface must be chosen to miss the singularities.

than downloading the freely available software from <http://www.sagemath.org/>, an extremely convenient way to run SageMath is to do so “via the cloud”, which also allows collaborations, at <https://cocalc.com/>.

We begin with defining the polytope for \mathbb{P}^4 . For convenience, we define the dual Δ° from \underline{v} in (2.28):

```
P4dual = LatticePolytope([[1,0,0,0],[0,1,0,0],[0,0,1,0],
[0,0,0,1],[-1,-1,-1,-1]]);
P4 = P4dual.polar();
```

One now checks that the vertices of Δ are indeed as given by \underline{m} in (2.28):

```
P4.vertices()
```

All lattice points on and inside Δ can now be readily found

```
pts = P4.points()
```

This returns a long list of 4-vectors, and `len(pts)` checks that indeed there are 126 of them. Moreover, we can also check polar duality that $(\Delta^\circ)^\circ = \Delta$ by `LatticePolytope(pts).polar().vertices()`, giving us back the vertices \underline{v} of Δ° .

Increasing Sophistication Returning to our question of Calabi–Yau threefolds, one would instantly ask whether there are any more than our old friend Q in \mathbb{P}^4 . Let us re-examine the 5 cyclic threefolds in (2.16), their transposes, being CICYs, are also CICY, and thus Calabi–Yau, though the ambient space A is more involved:

$$[4|5]_{-200}^{1,101}, \quad \left[\begin{array}{c|c} 1 & 2 \\ 3 & 4 \end{array} \right]_{-168}^{2,86}, \quad \left[\begin{array}{c|c} 2 & 3 \\ 2 & 3 \end{array} \right]_{-162}^{2,83}, \quad \left[\begin{array}{c|c} 2 & 3 \\ 1 & 2 \\ 1 & 2 \end{array} \right]_{-144}^{3,75}, \quad \left[\begin{array}{c|c} 1 & 2 \\ 1 & 2 \\ 1 & 2 \\ 1 & 2 \end{array} \right]_{-128}^{4,68} \quad (2.29)$$

These are all hypersurfaces in (smooth, toric) Fano fourfolds, with the ambient space being, respectively, \mathbb{P}^4 , $\mathbb{P}^1 \times \mathbb{P}^3$, $\mathbb{P}^2 \times \mathbb{P}^2$, $\mathbb{P}^2 \times \mathbb{P}^1 \times \mathbb{P}^1$ and $(\mathbb{P}^1)^4$, the polytope data for which can also be readily written down. In a way, proceeding from these 5, to the weighted projective hypersurfaces, to the hypersurfaces in Gorenstein Fano toric fourfolds, constitutes a sequential generalization and a slow climb in sophistication, a *gradus ad Parnassum*, as it were.

2.4.3 1, 16, 4319, 473800776 . . .

How many reflexive polytopes Δ_n are there? That is, how many Δ_n are there in each dimension, up to $GL(n; \mathbb{Z})$ equivalence, an equivalence up to which toric varieties are defined. For $n = 1$, there is clearly just 1, the point. For $n = 2$, this is already non-trivial and it turns out there are exactly 16, a classical result dating at least to

the early twentieth century (cf. [309] for an interesting account). For reference, we present these 16 in Fig. 2.5. The nomenclature in the figure may seem mysterious, and we shall return to that in the next chapter.

The diagram is organized so that the number of vertices increases from 3 to 6 from left to right and that of the area (the total number of lattice points) increases from 4 to 10 from bottom to top. Polar duality is reflection along the middle horizontal, on which there are 4 self-reflexive ones. We have already seen the pair (1, 16) in Fig. 2.3. Notable cases are toric del Pezzo surfaces $dP_{0,1,2,3}$ and the zeroth Hirzebruch surface \mathbb{F}_0 (cf. Appendix A.7); these are the 5 smooth Fano varieties of dimension 2. Hypersurfaces of the form in Theorem 6 give CY₁ or 16 special elliptic curves.

At $n = 3$, the number of reflexive polyhedra was already unknown to the mathematics community until our present story. Inspired by Batyrev and Borisov [29], Kreuzer and Skarke [KS] undertook the tremendous task using the computing technology of the mid-1990s to address the $n = 4$ case (which would give a class of desired Calabi–Yau threefolds) [267, 269] and, in passing, solved the $n = 3$ case as a stepping stone [268]. To confront so formidable a problem by a brute-force computer search (for which the package PALP [270], one of the first software for combinatorial geometry, was developed²⁰) indeed required the courage of physicists more than the sublimity of mathematicians.

KS found that there are 4319 Δ_3 up to $GL(3; \mathbb{Z})$, of which 18 are regular (and correspond to smooth toric Fano threefolds). Hypersurfaces of the form in Theorem 6 would give CY₂ or 4319 algebraic K3 surfaces. The *ne plus ultra* of computer work for mathematics at the turn of the millennium was the tour-de-force computation for $n = 4$, taking more than half a year on two dual Pentium III/600MHz PCs and between 10 and 30 processors on a 64 processor SGI Origin 2000 (if the younger members of the readership even know what these are) [269], giving us 473,800,652 Δ_4 up to $GL(4; \mathbb{Z})$, of which 124 are regular.

This is “big data” even by today’s standards, let alone at the turn of the century. Thus, our bestiary of Calabi–Yau threefolds grew steadily to about 10^4 between the late 1980s to the mid-1990s and suddenly exploded to 10^{10} (the actual number exceeds even this by many orders of magnitude as we shall see shortly) by the end of last decade of the twentieth century.

In summary, we have two fascinating sequences:

dimension	1	2	3	4	...	
# Reflexive Polytopes	1	16	4319	473, 800, 776	...	(2.30)
# Regular/Smooth	1	5	18	124	...	

We have no idea what the next number is for the top row, and for the bottom row, which is significantly fewer, at least a handful more have been found by exhaustive search [266], viz., $\{1, 5, 18, 124, 866, 7622, 72256, 749892, 8229721 \dots\}$. It seems

²⁰A recent update and useful manual have been provided in [52].

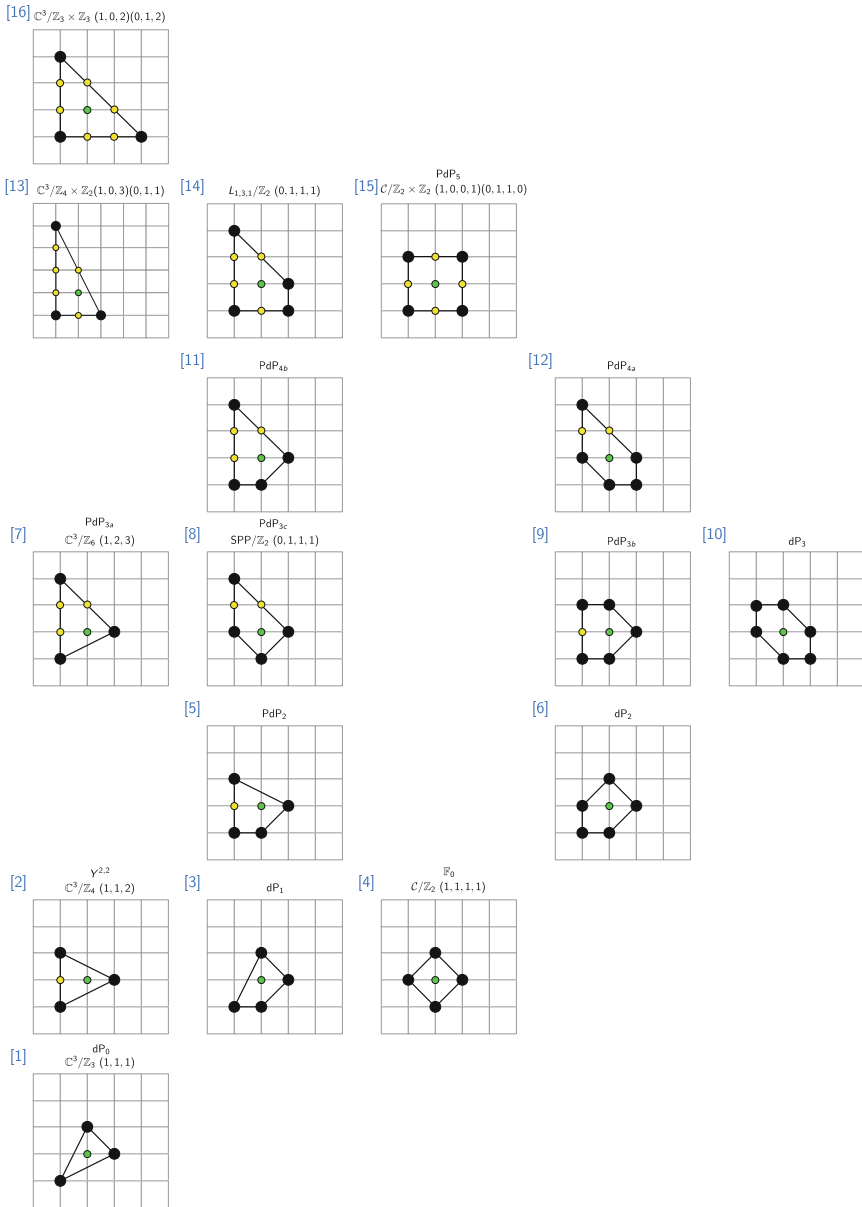


Fig. 2.5 The 16 reflexive polygons Δ_2 . The single interior point (origin) is marked in green, the vertices in black and lattice points on the facets but are not vertices in yellow. Figure taken from [185, 223]

possible that there might be a generating function for this, though so far there is no progress on this front. The reader is also referred to an excellent recent account of polytope classification and databases in [303]. In any event, the relevant data is available from KS’s Calabi–Yau page <http://hep.itp.tuwien.ac.at/~kreuzer/CY/> (the some 473 million requires about 5 Gb of storage, which is not so astronomical for today’s laptop) as well as the polytope database <https://polymake.org/polytopes/paffenholz/www/fano.html>.

Thus the status stands, partially impeded by the most untimely death of Max Kreuzer,²¹ until recently when Harald Skarke carried the torch and produced the remarkable estimate on the next number [326], a staggering $2^{2^6-4} \simeq 1.15 \times 10^{18}$ of which 185,269,499,015 are explicitly found.

Topological Data In dimension 3, we saw in (2.22) that the CY data is specified by the Hodge numbers, the second Chern class and the intersection numbers. There is a beautiful formula [28] which gives the **Hodge numbers** in terms of the polytope data

$$\begin{aligned} h^{1,1}(X) &= \ell(\Delta^\circ) - \sum_{\text{codim}\theta^\circ=1} \ell^*(\theta^\circ) + \sum_{\text{codim}\theta^\circ=2} \ell^*(\theta^\circ)\ell^*(\theta) - 5; \\ h^{1,2}(X) &= \ell(\Delta) - \sum_{\text{codim}\theta=1} \ell^*(\theta) + \sum_{\text{codim}\theta=2} \ell^*(\theta)\ell^*(\theta^\circ) - 5. \end{aligned} \quad (2.31)$$

In the above, Δ is the defining polytope for the Calabi–Yau hypersurface, Δ° , its dual; θ and θ° are the faces of specified codimension of these polytopes, respectively. Moreover, $\ell(\)$ is the number of integer points of a polytope, while $\ell^*(\)$ is the number of interior integer points. From the symmetry between the two expressions, we see immediately the following.

Corollary 1 *Polar duality $\Delta \leftrightarrow \Delta^\circ$ for the ambient toric variety is mirror symmetry for the CY₃ hypersurface.*

However, in order to compute the second Chern class and the intersection numbers, we again need to establish the sequence-chasing as in Sect. 2.14, requiring that, in particular, the ambient space be smooth. As we saw in (2.30), regular polytopes (smooth varieties) are very rare, so almost all the Δ require desingularization, which on the level of the polytope corresponds to “maximal triangulations” [267, 270] (q.v. [7] for a tutorial on how this is done using **PALP** and how to extract the Chern

²¹I have a profound respect for Max. It was not long after his visit to Oxford in 2009—a very productive and convivial period from which I still vividly remember his distinctive and infectious laughter—that Philip, Andre and I received the shocking email that his doctors gave him only a few months. During the last weeks on his deathbed as cancer rapidly took hold of him, Max emailed us regularly and our many discussions continued as normal. His several posthumous papers on the ArXiv are testimonies to his dedication to science. I am honoured and humbled that he, one of the great pioneers of Calabi–Yau data, should write his last journal paper with us [218]. *In pace requiescat.*

classes and intersection numbers). It should thus be emphasized that the actual CY hypersurfaces are much, much more than 473,800,776: even though the Hodge pair does not depend on triangulation, the Chern class c_2 and the intersection form d_{rst} do, so the topological type of the CY₃ crucially depends on different triangulations.

Unfortunately, triangulating polytopes is an exponentially expensive process. For small $h^{1,1}$ (up to 6), the full triangulations can be done on the computer while for large $h^{1,1}$ (between 240 and 491), methods were also devised to do so (q.v. Table 1 of [110] for the number of polytopes organized by $h^{1,1}$). To give an idea of the growth rate, the results from [7] on the low Kähler parameters are

$h^{1,1}$	1	2	3	4	5	6	...	
# of Polytopes	5	36	244	1197	4990	17101	...	
# of Triangulations	5	48	526	5348	57050	590085	...	
# of CY	5	39	306	2014	13635	85682	...	

(2.32)

where after triangulation, the number of unique Calabi–Yau hypersurfaces (having distinct data in the sense of (2.22)) is also checked. Note that the 5 $h^{1,1}$ cases are the 5 transposes of the cyclics as CICYs, and the ambient spaces of which are of course smooth and require no triangulation.

The motivated reader, especially when led by a curiosity induced by insomnia to befriend some Calabi–Yau threefolds—is highly encouraged to play with the interactive webpages (cf. accompanying papers [7, 161]) of Benjamin Jurke <https://benjaminjurke.com/academia-and-research/calabi-yau-explorer/> and Ross Altman <http://www.rossealtman.com/>.

Furthermore, the reader will be happy to learn that the 16 and the 4319 are built into SageMath [320] using the command `ReflexivePolytope(d, n)`, where d is the dimension and n is the n -th Δ . The 473,800,652, however, are currently too large to be built in but can be downloaded from <http://hep.itp.tuwien.ac.at/~kreuzer/CY/> in PALP format. We mention that in the KS dataset, the simplest case of \mathbb{P}^4 is given in a different but $SL(4; \mathbb{Z})$ equivalent form, with Δ given as

$$\begin{array}{ccccccccc} 4 & 5 & M:126 & 5 & N:6 & 5 & H:1,101 & [-200] \\ & & 1 & 1 & 1 & 1 & -4 \\ & & 0 & 5 & 0 & 0 & -5 \\ & & 0 & 0 & 5 & 0 & -5 \\ & & 0 & 0 & 0 & 5 & -5 \end{array}$$

Here, the first row records that the ensuing matrix for Δ° will be 4×5 and that there are 126 lattice points and 5 vertices for Δ , 6 lattice points and 5 vertices for Δ° (the one more being the origin in the interior). Consequently, the Hodge numbers are (1, 101) and $\chi = -200$ for the CY hypersurface.

A Georgia O’Keeffe Plot The KS dataset produced 30,108 distinct Hodge pairs, $\chi \in [-960, 960]$ (note that since the Hodge numbers are triangulation independent, even getting the full list of CY hypersurfaces someday when there is computing power to do all triangulations will not change this). The extremal values of ± 960 , as mentioned in the footnote of Sect. 2.3.1, are actually two hypersurfaces in weighted \mathbb{P}^4 , corresponding to the mirror pair of (11, 491) (for weights $w_i = [1 : 1 : 12 : 1 : 1]$:

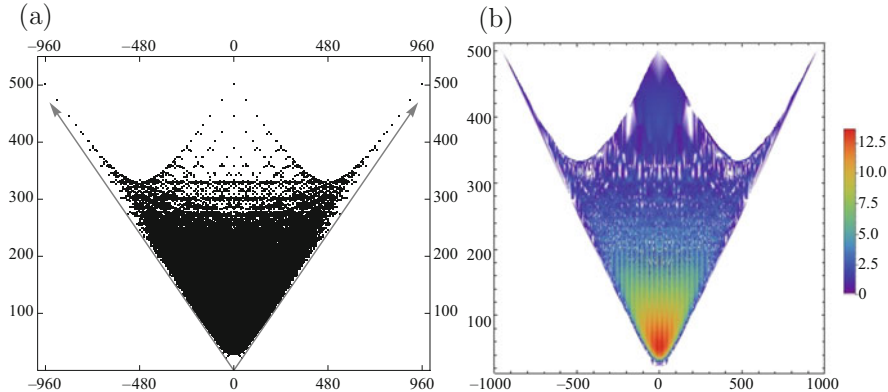


Fig. 2.6 (a) A plot of the 30,108 distinct Hodge pairs for the Kreuzer–Skarke dataset of Calabi–Yau hypersurfaces in Gorenstein Fano toric fourfolds; (b) the same but with multiplicity over the log-density of 473,800,652 over these distinct values

28 : 42]) and (491, 11) (for weights $w_i = [21 : 41 : 249 : 581 : 851]$). As always, we can plot $h^{1,1} + h^{2,1}$ versus χ , as was done in [269].

This has become one of the most iconic plots in string theory, as it is, *inter alia*, the best experimental evidence for mirror symmetry: every point has its mirror image along the vertical. We reproduce this plot in part (a) of Fig. 2.6, which is framed in Philip Candelas’ office. My only contribution—undoubtedly inspired by my 4-year-old daughter—was to colour it in [201]: in part (b) of the said figure, a heat plot of the log-density (i.e., log of the multiplicity of how many different polytopes per point of Hodge pair: we have 473,800,652 Δ_4 but only 30,108 distinct values using (2.31)) is presented. It is also curious to note that (27, 27) is the most occupied point, with a multiplicity of 910,113. The distribution of the Hodge numbers follows pseudo-Voigt/Planickian curves and is the subject of [221]. To give an idea of the sharp peak around (27, 27), we show a histogram of the number of manifolds versus the two Hodge numbers in Fig. 2.7.

There are numerous features of the plot in Fig. 2.6, most of which are still unexplained. Other than the extremals of ± 960 , why is there a boundary on top (the two bounding straight lines of funnel shape follow by definition of the plot: the Hodge numbers are non-negative), and why do they appear as parabolae? The papers of [110, 247] identify these as elliptic fibrations, while the authors in [80] find intriguing E_n (del Pezzo) structure.

Independent of the KS dataset, no Calabi–Yau from *any* construction to date has ever produced a Hodge pair above those two puzzling parabolae though there is no theoretical reason why this is so. On the other hand, at the bottom tip, there is also a paucity of manifolds, and this is also true for CY databases in general. This

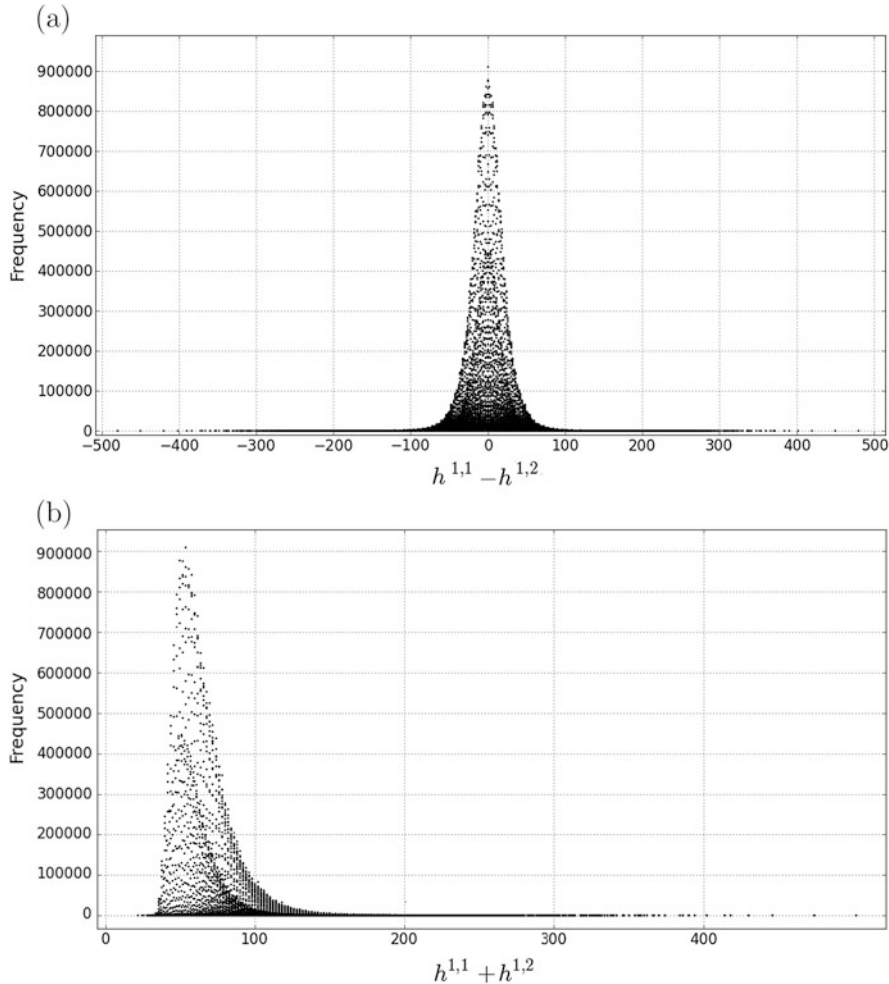


Fig. 2.7 (a) Frequency f plotted against $\frac{1}{2}\chi = (h^{1,1} - h^{1,2})$; (b) Frequency f plotted against the sum of Hodge numbers ($h^{1,1} + h^{1,2}$)

zoo of manifolds of small Hodge numbers²² is also much investigated [72, 79, 82]. Recently, there is a systematic construction [323] for (non-CI) CY in \mathbb{CP}^n which gives small Hodge numbers.

Of course, in addition to all the datasets mentioned above, the CICYs, the elliptic fibrations, the KS, etc., there have been many other constructions, such as using

²²This tip of the plot, where Hodge number is small, is what Philip [79] calls a “des res”, or a “desired residence”, in reference to newspaper advertisements from a time before the advent of social media.

Grassmannians or flag varieties as the ambient space [31] or various quotients, etc.; a good compendium is in Table 9 of [72]. Since these have not produced large or available databases online, nor are comparable in number to the KS set, we shall not address them here. Finally, we mention that shortly before Max Kreuzer's passing, he produced partial results for some 10^{10} double-hypersurfaces in toric Fano varieties coming from reflexive polyhedra in dimension 5. Amazingly, none of their Hodge pairs reside outside the bounds of Fig. 2.6.

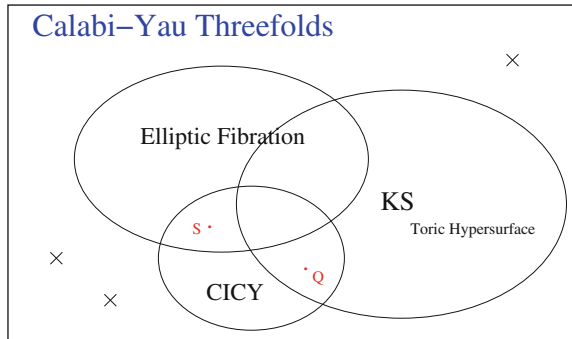
Caveat Emptor We need to warn the reader that the “explosion” in the title of this section simply refers to the vastness of the Kreuzer–Skarke dataset in contrast to the others, especially those emerging from the 1990s–2000s (even the graded rings database with its impressive list of Fano varieties [339] is not of the same order of magnitude). We will shortly see an important conjecture on the finiteness of topology types for Calabi–Yau manifolds. However, one could still have infinite families of (compact, smooth, connected) Calabi–Yau manifolds distinguished by properties more refined than mere topology, such as Gromov–Witten (GW) invariants. For instance, an ongoing programme [42] to understand the infinite possibilities of GW invariants from the so-called generalized CICYs [13], which relax the non-negativity condition in the configurations for CICYs. Likewise, the authors in [23] have recently shown an infinite family of deformations.

2.5 Cartography of the Compact Landscape

Thus we have taken a promenade through the landscape of Calabi–Yau threefolds, a contiguous development spanning a decade, from the late 1980s till the turn of the millennium. With the discovery of D-branes [307], M-theory on a G_2 manifold [20], F-theory on fourfolds [61, 144, 293], and, of course, the holographic correspondence [286] all approximately within the final lustrum of the century, coupled with the computational limits of the time, the fervour of constructing datasets of compact smooth Calabi–Yau threefolds by theoretical physicists was relatively cooled. Meanwhile, pure mathematicians interested in Calabi–Yau manifolds had too great a wealth of ideas, ranging from enumerative geometry to homological mirror symmetry, to preoccupy themselves with the tedium of data mining.

We saw above, and will shortly see, and shall see again in Chap. 4, how there has been renewed interest in the various datasets. For now, we summarize the **Landscape** of compact smooth Calabi–Yau threefolds in the Venn diagram in Fig. 2.8. The three major datasets are shown with the size of the bubbles not to scale. The crosses are supposed to signify various other constructions mentioned above. Our most familiar friends, the quintic Q and the Schoen S , are marked. With the continual growth in the number of the Calabi–Yau data, one might be led to wonder whether there might be an infinite number. While this is unsettled, there is an important conjecture of Yau [362] given as follows:

Fig. 2.8 The landscape of compact smooth Calabi–Yau threefolds



Conjecture 2 (Yau) There is a finite number of [Topological types](#) of (compact, smooth, connected) Calabi–Yau threefolds in the sense that there is a finite number of possible values to the data (2.22).

So far, this full data, viz.,

$$\{(h^{1,1}, h^{2,1}) ; [c_2] ; d_{rst}\} , \quad r, s, t = 1, \dots, h^{1,1} , \quad (2.33)$$

is really only known for the CICYs, <http://www-thphys.physics.ox.ac.uk/projects/CalabiYau/cicylist/> and, very partially, for the KS data: <http://www.rossealtman.com/>, and it would be interesting to study the statistics thereof. For known boundedness results, q.v. [357] and the Reid’s Fantasy [313]

Conjecture 2 is even expected to hold for *any dimension*, in that the topological types of the boundary case of Ricci-flatness (Calabi–Yau) are finite. In complex dimension one, we have already seen the validity of the conjecture from Fig. 1.1: the genus 1 torus is the only Ricci-flat (compact, connected, complex) onefold. Negative Ricci curvature, on the other hand, has an infinite number, viz., all $g > 1$. In complex dimension two, Ricci-flatness only comprises the topology of the 4-torus T^4 and the K3-surface, while there is an infinity of surfaces of general type, with negative curvature.

2.6 Epilogue: Recent Developments

Whereas the original triadophilia, which we recall to be the physicists’ search for smooth compact Calabi–Yau threefolds with $\chi = \pm 6$, saw its *fin-de-siècle* ebb by the aforementioned explosion of other string vacua and by the enormity of the KS data (there are more than 10^6 in the list with $\chi = \pm 6$), there has been renewed interest over the past decade in an extension of more physical importance.

Again, we emphasize that by “recent developments,” we only refer to the [Heterotic string](#) programme, which was the original one that brought Calabi–Yau manifolds into physics. As listed in Sect. 1.2.2, there are a host of ongoing

activities that study the “string landscape” and a myriad of interesting geometrical and combinatorial problems in Calabi–Yau varieties and beyond. In some sense, string theory has traded one very hard problem—the quantization of gravity—for another very hard problem—the selection of the right vacuum. Perhaps to the mathematician, the latter is even more interesting as it compels us to probe the landscape of geometric and algebraic structures.

Returning to the heterotic string, we saw that using the tangent bundle T_M in (1.8) gave, by (1.10), GUT theories with E_6 gauge group. By taking V not as T_M , but, for example, a stable $SU(4)$ or $SU(5)$ bundle, one could obtain the more interesting commutant $SU(10)$ or $SU(5)$ GUTs. This has come to be known as “non-standard” embedding and has with the developments in the theory of stable bundles on Calabi–Yau manifolds become an industry of realistic model building (cf. e.g., [116]).

One can do even better. With the incorporation of Wilson lines, i.e., representations of the fundamental group $\pi_1(M)$, should it be non-trivial, $SO(10)$ and $SU(5)$ can be further broken to the exact standard model group and instead of Hodge numbers (which are cohomologies valued in T_M , its duals and exterior powers), one computes the more general bundle-cohomologies valued in V , projected by the $\pi_1(M)$ -representations.

Question 2 In summary, the mathematical problem of general heterotic string compactification becomes:

- Find a smooth, compact Calabi–Yau threefold M with non-trivial fundamental group $\Gamma = \pi_1(M)$. This is usually done by finding an “upstairs” CY threefold \tilde{M} with a freely acting discrete symmetry Γ so that “downstairs” $M \cong \tilde{M}/\Gamma$;
- Find a stable holomorphic $SU(4)$ or $SU(5)$ vector bundle V with index ± 3 on M (cf. Theorem 3);
- Compute the cohomology groups $H^*(M, \wedge^i V)$ which must match the table in (1.9). This done by constructing \tilde{V} (of index $\pm 3|\Gamma|$) on \tilde{M} equivariant under Γ and computing the equivariant cohomologies $H^*(\tilde{M}, \wedge^i \tilde{V})^\Gamma$ together with the projection of a chosen representation of Γ .

This is a rich and interesting story in algebraic geometry and in physics, and we apologize that a subject deserving an entire book by itself (a feeble attempt was made in [200] as a quick introduction) has been relegated to an epilogue. However, venturing into the landscape of the extra data of bundles over Calabi–Yau manifolds is incompatible with the limitations of space and energy.

The problem, due to its physical significance, galvanized Burt Ovrut²³ into launching an ongoing programme by teaming up with card-carrying geometers Ron Donagi and Tony Pantev at UPenn during the early years of the millennium. It was supported by one of the earliest inter-disciplinary grants for algebraic geometry/theoretical physics by the USNSF [115], a collaboration at whose fruiting

²³The relentlessness with which Burt pursues this ultimate Triadophilia—of not only 3 generations but also the exact spectrum and precise properties of the standard model—is truly inspiring. I deeply appreciate the guidance he has given me over the years.

stages I was fortunate to join. The first answer to the above question, called the “Penn Model”, was found in [53], built on a particular bundle of extension type on a quotient of the Schoen manifold, by tuning parameters in constituent line bundles in the exact sequence and exploiting the double elliptic fibration structure of S .

Again, with the advances in computer algebra, the above problem can be algorithmized [9] over the various datasets (CICYs [10], elliptic fibration [149] and some preliminary cases of the KS set [217, 218]), with a few more exact solutions produced [55], before a tour-de-force scan over Whitney sums of line-bundles within the regions of stability inside the Kähler cone was performed over the CICY list [12]. Over an impressive consortium of some 10^{10} candidates which would have made KS proud, the authors in [12] found about 200 exact solutions to the problem, whereby giving 200 possibilities of (heterotic) string compactifications on smooth compact Calabi–Yau threefolds endowed with (poly-)stable holomorphic vector bundles whose cohomologies give the *exact* charged matter content of the MSSM.²⁴

It is interesting that this 1 in a billion factor of reduction is very much in line with independent model-building results from type II strings on branes [155]. Recently it has been suggested that even within the CICY list alone, there might be 10^{23} bundles²⁵ giving the exact standard model matter content [95]. Indeed, the string landscape is far more vast [179] than the initial quick estimates of 10^{500} [249]. The statistics of string vacua is very much an active field [121] and one could, as with fields of cosmogony or exo-planets, take either the anthropocentric view that there is a fundamental selection rule rendering our universe “special” or the more existentialist one that we are simply a stochastic point in a multitude of universes.

2.7 Post Scriptum: Calabi–Yau Metrics

We have now taken a long stroll in the garden of Calabi–Yau manifolds, one of whose key definitions is its Ricci-flat metric, without a single mention of the metric. This, as mentioned from the outset, is not due to negligence but to the fact (and challenge!) that no analytic Ricci-flat Kähler metric has ever been found on a compact Calabi–Yau n -fold (other than the trivial case of tori $T^{2n} \simeq \mathbb{C}^n / \Lambda$ for some lattice Λ where the flat metric on \mathbb{C}^n is inherited from the discrete quotient). One could try to pull-back the Fubini–Study metric on \mathbb{P}^4 onto the quintic as a natural course of action but would find the resulting metric to be positively curved in some patches and analytically finding a Ricci-flat metric globally has so far defied every attempt.

²⁴As always with these constructions, the uncharged matter corresponds to $H^*(M, V \otimes V^\vee)$, which give scalar moduli in the field theory.

²⁵Tristan Hübsch very charmingly calls it “a mole of models” and we almost entitled the paper as such.

Once we dispense with “compactness”, analytic metrics can indeed be found, as we will see in the next chapter. As a postscriptum to this chapter, let us see some important directions in at least numerically computing the Calabi–Yau metric. It will also serve to put on a concrete footing some of the terminology introduced in the previous and present chapters, as well as Appendix A, such as Kähler and volume forms. There are two main approaches to this: the so-called Donaldson algorithm [11, 17, 54, 118, 119, 123] and the functional method [227, 228]. As the focus on this book is on the algebraic and algorithmic, we will only give a brief exposition of the former.

Let X be a smooth, compact Calabi–Yau threefold, a compatible Hermitian metric $g_{a\bar{b}}$, with its associated Kähler form $\omega = ig_{a\bar{b}}dz^a \wedge d\bar{z}^{\bar{b}}$ and a nowhere-vanishing complex (volume) three-form Ω . The Calabi–Yau condition is then

$$d\omega = 0(\text{Kähler}), \quad \Omega \stackrel{!}{\neq} 0, d\Omega = 0(\text{Ricci-flat}). \quad (2.34)$$

Let x^a , $a = 1, 2, 3$ be the three complex coordinates on X . Since $g_{a\bar{b}}$ is Hermitian, the pure holomorphic and anti-holomorphic components of the metric must vanish. Only the mixed components survive, which are given as the mixed partial derivatives of a single real scalar function, the Kähler potential K :

$$g_{ab}(x, \bar{x}) = g_{\bar{a}\bar{b}}(x, \bar{x}) = 0, \quad g_{a\bar{b}}(x, \bar{x}) = \partial_a \partial_{\bar{b}} K(x, \bar{x}). \quad (2.35)$$

The Kähler form derived from the Kähler potential is

$$\omega = \frac{i}{2} \sum_{a, \bar{b}=1}^3 g_{a\bar{b}}(x, \bar{x}) dx^a \wedge d\bar{x}^{\bar{b}} = \frac{i}{2} \partial \bar{\partial} K(x, \bar{x}), \quad (2.36)$$

where ∂ and $\bar{\partial}$ are the Dolbeault operators (so that in terms of the ordinary differential $d = \partial + \bar{\partial}$ and $\partial^2 = \bar{\partial}^2 = 0$).

Recall that K is only *locally* defined—globally one needs to glue together the local patches by finding appropriate transition functions f (Kähler transformations) so that

$$K(x, \bar{x}) \sim K(x, \bar{x}) + f(x) + \bar{f}(\bar{x}). \quad (2.37)$$

Since X is Kähler, the Ricci tensor is given by

$$R_{a\bar{b}} = \partial_a \partial_{\bar{b}} \ln \det g_{a\bar{b}}. \quad (2.38)$$

In practice, finding a Ricci-flat Kähler metric on X reduces to finding the corresponding Kähler potential as a real function of x and \bar{x} . Yau’s celebrated proof [361] of the Calabi conjecture [67] guarantees that this Calabi–Yau metric is unique in each Kähler class.

The general idea of Donaldson's algorithm [118] is to approximate the Kähler potential of the Ricci-flat metric using a finite basis of degree- k polynomials $\{s_\alpha\}$ on X , akin to a Fourier series representation. This “algebraic” Kähler potential is parametrized by a Hermitian matrix $h^{\alpha\bar{\beta}}$ with constant entries. Different choices of $h^{\alpha\bar{\beta}}$ correspond to different metrics within the same Kähler class. One then iteratively adjusts the entries of $h^{\alpha\bar{\beta}}$ to find the “best” (in the sense of a *balanced* metric at degree k which we define shortly) degree- k approximation to the unique Ricci-flat metric. As one increases k , the balanced metric becomes closer to Ricci-flat at the cost of exponentially increasing the size (and thus sadly increasing computational complexity) of the polynomial basis $\{s_\alpha\}$ and the matrix $h^{\alpha\bar{\beta}}$. Specifically, we perform the following:

1. Let the degree k be a fixed positive integer and denote by $\{s_\alpha\}$ a basis of global sections of $\mathcal{O}_X(k)$ (q.v. Appendix A):

$$H^0(X, \mathcal{O}_X(k)) = \text{span}\{s_\alpha\}, \quad \alpha = 1, \dots, N_k. \quad (2.39)$$

In other words, we choose an N_k -dimensional basis of degree- k holomorphic polynomials $s_\alpha(x)$ on X . The values of N_k grow factorially with k .

2. Make an ansatz for the Kähler potential of the form

$$K(x, \bar{x}) = \frac{1}{k\pi} \ln \sum_{\alpha, \bar{\beta}=1}^{N_k} h^{\alpha\bar{\beta}} s_\alpha(x) \bar{s}_{\bar{\beta}}(\bar{x}), \quad (2.40)$$

where $h^{\alpha\bar{\beta}}$ is some invertible Hermitian matrix. We see that without the mixing by the matrix h , the shape of K is that of the potential of the standard Fubini-Study metric on \mathbb{CP}^n .

3. The pairing $h^{\alpha\bar{\beta}} s_\alpha \bar{s}_{\bar{\beta}}$ defines a natural inner product on the space of global sections, so that h gives a metric on $\mathcal{O}_X(k)$. Consider the Hermitian matrix

$$H_{\alpha\bar{\beta}} \equiv \frac{N_k}{\text{Vol}_{\text{CY}}} \int_X d\text{Vol}_{\text{CY}} \frac{s_\alpha \bar{s}_{\bar{\beta}}}{h^{\gamma\bar{\delta}} s_\gamma \bar{s}_{\bar{\delta}}}, \quad (2.41)$$

where Vol_{CY} is the integrated volume measure of X :

$$d\text{Vol}_{\text{CY}} = \Omega \wedge \overline{\Omega}. \quad (2.42)$$

In general, $h^{\alpha\bar{\beta}}$ and $H_{\alpha\bar{\beta}}$ will be unrelated. However, if they are inverses of each other

$$h^{\alpha\bar{\beta}} = (H_{\alpha\bar{\beta}})^{-1}, \quad (2.43)$$

the metric on $\mathcal{O}_X(k)$ given by $h^{\alpha\bar{\beta}}$ is said to be **balanced**. This balanced metric then defines a metric $g_{a\bar{b}}^{(k)}$ on X via the Kähler potential (2.40). We also refer to this metric on X as balanced.

4. Donaldson's theorem then states that for each $k \geq 1$, a balanced metric exists and is *unique*. Moreover, as $k \rightarrow \infty$, the sequence of metrics $g_{a\bar{b}}^{(k)} = \partial_a \partial_{\bar{b}} K$ converges to the unique Ricci-flat Kähler (Calabi–Yau) metric on X .
5. In principle, for each k , one could solve (2.43) for the $h^{\alpha\bar{\beta}}$ that gives the balanced metric using (2.41) as an integral equation. However, due to the highly non-linear nature of the equation, an analytic solution is not possible. Fortunately, for each integer k , one can solve for $h^{\alpha\bar{\beta}}$ iteratively as follows:

- (a) Define Donaldson's “ T -operator” as

$$T: h_{(n)}^{\alpha\bar{\beta}} \mapsto T(h_{(n)})_{\alpha\bar{\beta}} = \frac{N_k}{\text{Vol}_{\text{CY}}} \int_X d\text{Vol}_{\text{CY}} \frac{s_\alpha \bar{s}_{\bar{\beta}}}{h_{(n)}^{\gamma\bar{\delta}} s_\gamma \bar{s}_{\bar{\delta}}}. \quad (2.44)$$

- (b) Let $h_{(0)}^{\alpha\bar{\beta}}$ be an initial invertible Hermitian matrix.
- (c) Then, starting with $h_{(0)}^{\alpha\bar{\beta}}$, the sequence

$$h_{(n+1)} = [T(h_{(n)})]^{-1} \quad (2.45)$$

converges to the desired balanced metric $h^{\alpha\bar{\beta}}$ as $n \rightarrow \infty$.

The convergence is very fast in practice, with only a few iterations ($\lesssim 10$) necessary to give a good approximation to the balanced metric.

6. There are several measures of convergence one could use; a standard one is defined as follows. Consider the top-form ω^3 defined by the Kähler form. Since X is a Calabi–Yau threefold with $\Omega \wedge \bar{\Omega}$ the unique (up to scaling) non-vanishing $(3, 3)$ -form, these two must be proportional, i.e., $\omega \wedge \omega \wedge \omega \propto \Omega \wedge \bar{\Omega}$. Thus, the ratio of these two top-forms, compared to the ratio of their respective integrals, must be equal:

$$\frac{\text{Vol}_K := \int_X \omega^3}{\text{Vol}_{\text{CY}} := \int_X \Omega \wedge \bar{\Omega}} \quad \Rightarrow \quad \frac{\omega^3}{\text{Vol}_K} = \frac{\Omega \wedge \bar{\Omega}}{\text{Vol}_{\text{CY}}}. \quad (2.46)$$

In other words, the quantity

$$\sigma_k \equiv \frac{1}{\text{Vol}_{\text{CY}}} \int_X d\text{Vol}_{\text{CY}} \left| 1 - \frac{\omega_k^3 / \text{Vol}_K}{\Omega \wedge \bar{\Omega} / \text{Vol}_{\text{CY}}} \right| \quad (2.47)$$

is 0 if and only if ω_k converges to the Ricci-flat Kähler (CY) metric, as we increase the degree k .

2.7.1 Numerical Metric on the Quintic

As always, we default to the quintic CY₃ to illustrate the details. Take the Fermat Quintic \mathcal{Q} from (2.12) with the parameter $\psi = 0$:

$$\mathcal{Q} := \left\{ \sum_{i=0}^4 z_i^5 = 0 \right\} \subset \mathbb{P}^4. \quad (2.48)$$

Fixing a positive integer k , $\{s_\alpha\}$ can be chosen to be monomials of degree k on \mathcal{Q} . On \mathbb{P}^n , finding all monomials of degree k is a standard problem in combinatorics and amounts to choosing k elements from $n+k-1$. Since the ambient space is \mathbb{P}^4 , there are $\binom{5+k-1}{k}$ ways of doing so. Explicitly, for the first few values of k , the monomial bases are (the arguments here are a direct generalization of (2.13))

k	N_k	$\{s_\alpha\}$
1	5	$z_i = 0, \dots, 4$
2	15	$z_i z_j, 0 \leq i \leq j \leq 4$
3	35	$z_i z_j z_k, 0 \leq i \leq j \leq k \leq 4$
4	70	$z_i z_j z_k z_\ell, 0 \leq i \leq j \leq k \leq \ell \leq 4$

(2.49)

On \mathcal{Q} we need to impose the defining quintic equation (2.48) when we encounter variables of powers greater than or equal to 5. For example, we can choose to replace $z_0^5 \rightarrow -\sum_{i=1}^4 z_i^5$. This amounts to a reduction in the number of independent monomials of degree $k \geq 5$. In general, we have that

$$N_k = \begin{cases} \binom{5+k-1}{k}, & 0 < k \leq 4 \\ \binom{5+k-1}{k} - \binom{k-1}{k-5}, & k \geq 5 \end{cases} \quad (2.50)$$

Since the metric is a local quantity, we need to focus on particular affine patches of \mathcal{Q} . Suppose we are in the $z_0 = 1$ patch. We can eliminate one of the remaining four coordinates, say, $z_1 = (-1 - z_2^5 - \dots - z_4^5)^{1/5}$, so that the good local coordinates are (z_2, z_3, z_4) , which we then set to be x^α . The holomorphic volume form is then

$$\Omega = \int_Q \frac{dz_1 \wedge dz_2 \wedge dz_3 \wedge dz_4}{1 + z_1^5 + z_2^5 + z_3^5 + z_4^5} = \frac{dz_2 \wedge dz_3 \wedge dz_4}{5z_1^4}, \quad (2.51)$$

where the (Griffith) residue theorem [169] is applied in the last equality upon integrating out z_1 .

In general, we

1. work in the affine patch defined by z_I for some $I = 0, \dots, 4$. For numerical stability, z_I should have the largest norm of the z_i .²⁶
2. eliminate one of the four remaining variables $z_{J \neq I}$ by solving for z_J using the defining equation of Q . The remaining three variables then constitute the “good coordinates” of the patch on Q —we denote these by x^a for $a = 1, 2, 3$. For numerical stability (cf. §3.4.2 of [123]), we eliminate the variable for which $|\partial Q/\partial z_J|$ is the largest. In practice, we need to be careful about sampling random points on a manifold, with a weight measure; details can be found in [54, 123] (see Appendix A of [17] for a summary; we will return to the issue of metrics and machine-learning [15, 17, 124] in the last chapter).
3. We can now evaluate elements of the monomial basis $\{s_\alpha\}$ at each point p_M and obtain the T -operator. Choosing some initial invertible Hermitian matrix $h^{\alpha\bar{\beta}}$, we numerically perform the integration in (2.44) with respect to the weight measure of points.
4. Set the new $h^{\alpha\bar{\beta}}$ to be $(T_{\alpha\bar{\beta}})^{-1}$ and iterate. The algorithm is insensitive to the initial choice of $h^{\alpha\bar{\beta}}$, and in practice fewer than 10 iterations are needed to converge to the balanced metric. The actual computation for the metric $g_{ab}^{(k)}$ is as follows:
 - (a) From $h^{\alpha\bar{\beta}}$, we obtain the Kähler form in terms of the coordinates (z_0, \dots, z_4) of the “ambient” affine patch (with, for example, $z_0 = 1$) on \mathbb{P}^4 :

$$K(z, \bar{z}) = \frac{1}{k\pi} \ln \sum_{\alpha, \bar{\beta}=1}^{N_k} h^{\alpha\bar{\beta}} s_\alpha(z) \bar{s}_{\bar{\beta}}(\bar{z}) \Rightarrow \tilde{g}_{i\bar{j}}(z, \bar{z}) = \partial_i \partial_{\bar{j}} K. \quad (2.52)$$

- (a) We pull back this metric via the immersion of the Fermat quintic polynomial to find the metric g_{ab} on Q . Suppose, without loss of generality, that we are in the patch $z_0 = 1$ and the good coordinates on Q are $x_a = (z_2, z_3, z_4)$ with z_1 to be eliminated via

$$z_1^5 = -1 - \sum_{i=2}^4 z_i^5 \Rightarrow \frac{\partial z_1}{\partial z_i} = -\frac{z_i^4}{z_1^4} \quad i = 2, 3, 4. \quad (2.53)$$

The other situations of different I and J are simply permutations of the following discussion. As the metric is a tensor, the pullback is given simply by multiplying with Jacobian $J^i{}_a$. Explicitly, the Jacobian is $J^i{}_a = \frac{\partial z_i}{\partial x_a} =$

$$\frac{\partial z_i}{\partial z_k=0,\dots,4} = \begin{pmatrix} 0 & -z_2^4/z_1^4 & 1 & 0 & 0 \\ 0 & -z_3^4/z_1^4 & 0 & 1 & 0 \\ 0 & -z_4^4/z_1^4 & 0 & 0 & 1 \end{pmatrix}.$$

²⁶In other words, if one works in homogeneous coordinates, we take z_I to be the coordinate with the largest norm and then divide the other coordinates by z_I .

(c) Finally, using the metric $g_{a\bar{b}}$ on Q , the Kähler form is

$$\omega = \frac{i}{2} \sum_{a,\bar{b}}^3 g_{a\bar{b}}(x, \bar{x}) dx^a \wedge d\bar{x}^{\bar{b}}. \quad (2.54)$$

5. The error measure σ in (2.47) can also be obtained by numerical integration. In Fig. 2.9 we show the relevant quantities. We sample 500K random points on Q for the Donaldson algorithm to obtain the measure σ . This is shown in part (a) for $k = 1, \dots, 12$. In part (b), we keep track of the time taken on Mathematica on an ordinary laptop and see that the exponential growth of complexity (q.v.[17], courtesy of A. Ashmore for re-computing and re-drawing the figure).

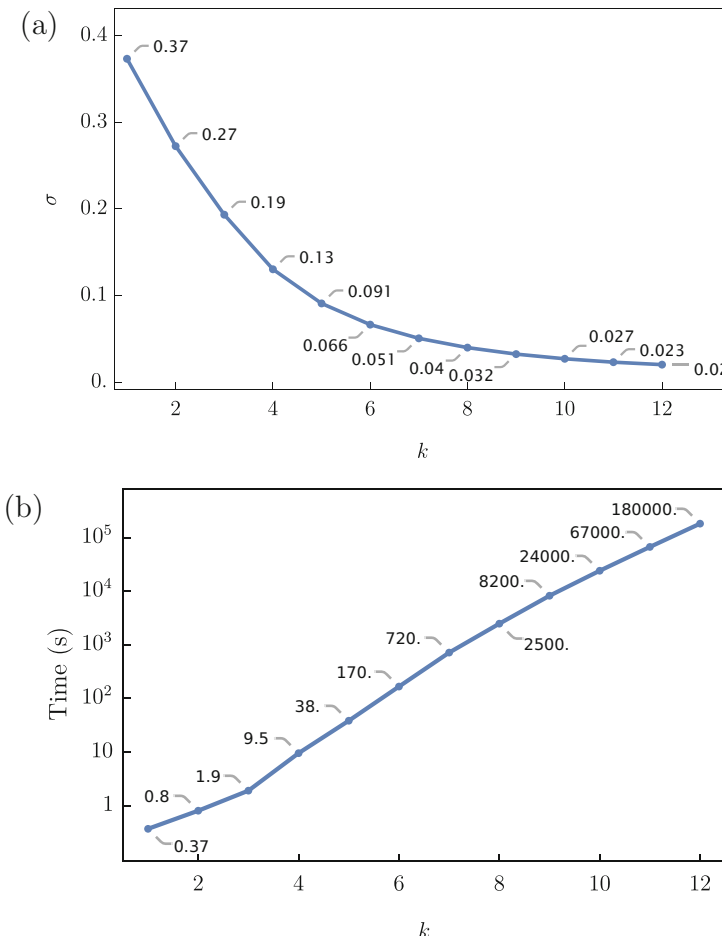


Fig. 2.9 (a) The convergence of the σ measure for the quintic as we increase k ; (b) Time taken in seconds of the computation for the numerical metric on a log scale

Chapter 3

The Non-Compact Landscape



At the end of the lecture, an arcane dialogue took place between the speaker [Calabi] and some members of the audience, Ambrose and Singer if I remember correctly. There followed a period of tense silence. Professor Struik broke the ice. He raised his hand and said: ‘Give us something to take home!’ Calabi obliged, and in the next five minutes he explained in beautiful simple terms the gist of his lecture. Everybody filed out with a feeling of satisfaction.

—Gian-Carlo Rota, *Ten Lessons I wish I had given*

Relaxing the condition of compactness usually grants us liberty, as for instance in the familiar setting of Liouville’s theorem on bounded entire functions. In other words, one could think of local models of Calabi-Yau manifolds when one works on some affine patch. In this sense, in the following we will use the words “**non-compact**”, “**affine**”, and “**local**” inter-changeably.

What is the simplest non-compact Calabi-Yau n -fold? Clearly, it is just \mathbb{C}^n , which is not only Ricci flat, but completely flat. Therefore, as the quintic was the *point d’appui* in the previous chapter, \mathbb{C}^3 will be so for our present one. In particular, $\mathbb{C}^3 \simeq \mathbb{R}^6$ is a cone over the round sphere S^5 (just like the more familiar case of \mathbb{R}^3 being a cone over S^2) in that its flat metric¹ can be written as

$$ds^2(\mathbb{C}^3) = dr^2 + r^2 ds^2(S^5), \quad (3.1)$$

¹In the few times I met Calabi when I was a postdoc at the University of Pennsylvania he struck me as a gentleman of the Old School. I remember when Serge Lang came to give a colloquium (in his 70s) and in his typically flamboyant style turned to Calabi in the middle of his talk when he came to a certain manifold—having repeatedly cross-examined various members of the audience throughout the lecture, and even jokingly told a poor chap to get out when he could not provide a correct answer—“You, Calabi! is it Ricci flat!?” Eugenio calmly answered with his usual charm and diplomacy, “Sorry, I am afraid I was asleep.”

where r is the radial coordinate of the cone with $r = 0$ being at the origin. One might be misled into thinking that this is all too trivial but we will soon see a richness in both the mathematics and the physics.

3.1 Another $\mathbf{10} = \mathbf{4} + \mathbf{2} \times \mathbf{3}$

While local Calabi-Yau manifolds enjoy a wealth of usefulness in many contexts, in parallel to Sect. 1.2 from the Prologue, we take the point of view of their rôle in building the standard model from string theory. The interest in non-compactness began with the late Joe Polchinski's discovery of Dirichlet branes, or **D-branes** as dynamical objects in string theory [307]. In a nutshell, a D p -brane is, by convention, a $(p + 1)$ -dimensional space-time object (one of whose dimension is time) whose world-volume supports a $(p + 1)$ form so that a charge can be obtained by integration. One can see the form as the connection of a $U(1)$ -bundle on the D p -brane. For a stack of N D-branes (i.e., N of them placed in parallel and with separation taken to the zero limit), the gauge group is “enhanced” from $U(1)^N$ to $U(N)$. This is all we will need from the vast theory of D-branes.

Thus the importance which a D3-brane plays is that its world-volume is $3 + 1$ dimensional, and, for our *local* purposes, is $\mathbb{R}^{1,3}$ which gives us a *brane-world*² scenario [312]. The 6 directions perpendicular to a stack of N D3-branes will again be Calabi-Yau, albeit non-compact. In this set-up, in contrast to the *compactification* scenario of the previous chapter, the (supersymmetric) standard model lives on the $\mathbb{R}^{1,3}$ of the D3-brane, interacting with the transverse or bulk dimensions only via gravity.

It should be pointed out that phenomenologically viable theories from brane constructions need to satisfy global consistency conditions; for these, the type IIA intersection brane mentioned in Sect. 1.2.2 are much more conducive to model building. In this chapter, we will take the mirror consideration of IIB D3-branes at singularities, for several reasons. First, in line with the theme of this book, they better illustrate singular and non-compact Calabi-Yau varieties and their resolutions. Second, they were the original archetypes for the gauge-gravity holographic correspondence (aspects of which we will shortly attempt an explanation to the pure mathematician). Finally, they offer an interesting forum for some beautiful dialogue between physics, geometry and representation theory.

3.1.1 Quiver Representations and a Geometer’s AdS/CFT

While the setup of the D-brane’s correspondence between gravity in the bulk and gauge theory on the world-volume goes under the rubric of **holography** or

²The curvature of the brane and back-reactions with the background metric, for our algebro-geometric purposes, will be neglected throughout.

AdS/CFT, the challenge of capturing the interest of an algebraic geometer is the one which we will embrace here. Once we phrase at least some of the subject purely in term of the mathematics, we will then see that there too is a plethora of combinatorial data.

In order to venture into this landscape of non-compact Calabi-Yau spaces, we need a few preliminary concepts from representation theory.

Definition 5 A **quiver** $\mathcal{Q} = (\mathcal{Q}_0, \mathcal{Q}_1, W)$ is a finite directed graph with the set of vertices \mathcal{Q}_0 and arrows \mathcal{Q}_1 , the cardinalities of which are N_0 and N_1 respectively:

- \mathcal{Q} is equipped with a *representation*, meaning that we attach vector spaces $V_i \simeq \mathbb{C}^{n_i}$ to each node for some positive integer n_i , whence each arrow $(X_{ij} \in \mathcal{Q}_1) \in \text{hom}(V_i, V_j)$ can be considered as an $n_j \times n_i$ matrix; we allow self-adjoining arrows, $\phi_i = X_{ii}$, as well as cycles which are closed loops $X_{i_1 i_2} X_{i_2 i_3} \dots X_{i_k i_1}$ formed by the arrows.
- \mathcal{Q} is also furnished by *relations*; this is imposed by the **superpotential** W which is a polynomial in all the arrows, treated as formal matrix variables:

$$W = \sum_{k=1}^{N_2} c_k \text{Tr}(\prod X_{ij}) \dots \text{Tr}(\prod X_{i'j'}) \quad (3.2)$$

summed over possible cycles with coefficients $c_k \in \mathbb{C}$. The formal polynomial relations amongst the arrows are determined by the vanishing of the Jacobian $\partial_{X_{ij}} W$. We denote the number of monomial terms in W by N_2 .

The term quiver was coined by Gabriel [150] because its nodes, like the holster for the weapon, are holders for arrows.

Indeed, even the pure mathematics community is using the term “superpotential”, which originates in supersymmetric gauge theories and string theory.³ The allowance for loops and cycles significantly complicates the representation theory of \mathcal{Q} but is necessary for the physics. The integers N_0 , N_1 and N_2 will play an interesting combinatorial rôle for a wide class (almost all which we will consider)

³There is an underlying 4-dimensional supersymmetric gauge theory, whose action, in $\mathcal{N} = 1$ superspace is

$$S = \int d^4x \left[\int d^2\theta d^2\bar{\theta} \Phi_i^\dagger e^V \Phi_i + \left(\frac{1}{4g^2} \int d^2\theta \text{Tr} \mathcal{W}_\alpha \mathcal{W}^\alpha + \int d^2\theta W(\Phi) + \text{c.c.} \right) \right],$$

where V is the vector multiplet and Φ , the hypermultiplet. The effective potential in terms of the scalars is

$$V(\phi_i, \bar{\phi}_i) = \sum_i \left| \frac{\partial W}{\partial \phi_i} \right|^2 + \frac{g^2}{4} \left(\sum_i q_i |\phi_i|^2 \right)^2$$

whose vanishing is precisely the vacuum defined by the D- and F-terms being 0.

of quivers. To the above quiver data, one associates a 4-dimensional supersymmetric gauge theory with gauge group $\mathcal{G} = \prod_{i=1}^{N_0} U(n_i)$ via the dictionary:

Node i:	Factor $U(n_i)$ in \mathcal{G}
Arrow $i \rightarrow j$:	A so-called bi-fundamental field X_{ij} transforming as $(\square, \bar{\square})$ of $U(N_i) \times U(N_j)$
Loop $i \rightarrow i$:	A so-called adjoint field $\varphi_i = X_{ii}$ of $U(N_i)$
Cycle $i_1 \rightarrow i_1 \rightarrow \dots i_k \rightarrow i_1$:	Gauge Invariant Operator (GIO) created by concatenating along a path, via matrix multiplication and finishing with an overall trace: $\text{Tr}(X_{i_1 i_2} X_{i_2 i_3} \dots X_{i_k i_1})$; a term such as $\text{Tr}(\prod X_{ij})$ is called a Single-trace GIO while products thereof $\text{Tr}(\prod X_{ij}) \dots \text{Tr}(\prod X_{i'j'})$ are Multi-trace GIO
2-Cycle $X_{ij} X_{jk}$:	Mass term
Superpotential (3.2):	Superpotential in the Lagrangian with couplings c_i ; the set of polynomials $\{\partial_{X_{ij}} W\}$ are the F-Terms .

The list of labels $\vec{n} = (n_1, n_2, \dots, n_{N_0})$ is called the *dimension vector* and for the simplest case when all $n_i = 1$, the arrows are just complex numbers and the quantum field theory has gauge group $U(1)^{N_0}$. Finally, recall:

Definition 6 The *incidence matrix* of \mathcal{Q} is an $N_0 \times N_1$ integer matrix $d_{i\alpha}$ where $i = 1, \dots, N_0$ indexes the nodes and $\alpha = 1, \dots, N_1$, the arrows, such that each arrow $i \rightarrow j$ gives a new column in $d_{i\alpha}$, with -1 at row i and $+1$ at row j , and 0 otherwise.

Then $\sum_{\alpha} d_{j\alpha} |X_{ij}|^2 - \zeta_i$ are known as **D-terms**, where $\zeta_i \in \mathbb{C}$ are so-called Fayet-Iliopoulos (FI) parameters.⁴ Note that unlike the F-terms, these are non-holomorphic, as they involve the complex conjugates of X_{ij} .

Of course, D-terms and F-terms have a long history in supersymmetric gauge theories and possess many subtle quantum field theoretical properties. Continuing with the theme of the book being accessible to a general mathematically inclined readership, we will use no more than the following (rough) definition:

D-term \sim the incidence matrix $d_{j\alpha}$ of the quiver \mathcal{Q} ;

F-term \sim the partial derivatives (Jacobian variety) of a formal polynomial

$$W(X_{ij}) \text{ (the superpotential) in the arrows } X_{ij} . \quad (3.3)$$

⁴In general, one assigns charges q_{α} to the fields and sums over $q_{\alpha} |X_{i\alpha}|^2$ but for our present purposes of $U(1)^{N_0}$ theories, the incidence matrix serves to encode the charges. Moreover, the FI-parametres exist only for the $U(1)$ gauge group factors.

What does all of this have to do with geometry? There is a key object in geometric representation theory,⁵ coming from a quiver [256, 297].

Definition 7 The representation variety $\mathcal{M}(\mathcal{Q})$ is the GIT quotient of the representations $Rep(\mathcal{Q}) = \bigoplus_{i,j} \text{hom}(\mathbb{C}^{n_i}, \mathbb{C}^{n_j})$, with relations from W , quotiented by the complexified group $\mathcal{G}_{\mathbb{C}} = \prod_i GL_{n_i}(\mathbb{C})$

$$\mathcal{M}(\mathcal{Q}) = \text{Spec} \mathbb{C}[Rep(\mathcal{Q}) / \langle \partial_{X_{ij}} W \rangle]^{\mathcal{G}_{\mathbb{C}}} \simeq \langle \partial_{X_{ij}} W \rangle // \mathcal{G}_{\mathbb{C}},$$

where Spec is the maximal spectrum of the quotient ring.

From the point of view of geometric representation theory, $\mathcal{M}(\mathcal{Q})$ can be construed as the centre of the path algebra of \mathcal{Q} .

As with many objects in mathematics, there is the *formal* definition and there is the *working* definition. The above formal definition will mean absolutely nothing to the beginning student, nor will we digress too far here to delve into all the terms such as GIT (geometric invariant theory), the double slash notation, the vector space Rep , etc. The one thing on which we have spent some time is “Spec”, since its usage appears in several places in the book; this, together with some other elements of algebraic geometry, is summarized in Appendix A (especially Sect. A.6.1).

What the above theorem computationally means, roughly, is just the following:

$$\mathcal{M}(\mathcal{Q}) \simeq \text{set of minimal cycles in } \mathcal{Q}/\text{F-term relations}. \quad (3.4)$$

In other words, we (1) find the (Eulerian) minimal cycles in the quiver; (2) for each we can perform successive matrix multiplication (since each arrow is a matrix), and (3) finish off with matrix trace. The result is a list of (very big) polynomials, one for each minimal cycle; each is a polynomial in all the component variables of the arrow matrices. If there are no F-terms (i.e., no superpotential), then finding the relations (maximal Spec) amongst these polynomials will give the defining equation of $\mathcal{M}(\mathcal{Q})$. If there are non-trivial F-terms, then we need to find the relations, up to these F-terms. We will illustrate this with many examples, illustrating the algorithm in Proposition 5.

In physics, $\mathcal{M}(\mathcal{Q})$ is called the **vacuum moduli space (VMS)** of the gauge theory⁶ because solving for the F-terms and D-terms amounts to finding the space

⁵Strictly speaking a *quiver variety* in the sense of [297] is a more general and decorated (in the sense of extra data) notion, and $\mathcal{M}(\mathcal{Q})$ really ought to be called the King variety, after [256]. I had suggested this to fellow numerologist Alastair King but he, in his humility, insisted that it be called the representation variety.

⁶To be more precise, \mathcal{M} here defined is the mesonic, Higgs branch of the moduli space because the gauge invariants are built by taking traces. We could contract with other invariant tensors, for instance, contracting with Levi-Civita symbols to obtain the GIOs would give the baryonic moduli space. The Jacobian variety $\langle \partial_{X_{ij}} W \rangle$ is itself also interesting and the equations $\partial_{X_{ij}} W = 0$, which are collectively the F-terms, gives the so-called *master space* [136, 300].

of solutions which the vacuum expectation values of the scalars parametrize the supersymmetric vacuum.

The rest of this chapter is concerned with:

Question 3 When is the representation variety $\mathcal{M}(\mathcal{Q})$ an affine variety that is (local) Calabi-Yau M ? In particular, what is the relation between \mathcal{Q} and M when $\dim_{\mathbb{C}}(M) = 3$?

The skeptical reader may wonder why we have chosen to present varieties in this seemingly convoluted way through representation of quivers. Other than the fact that it is the central way to understand it in physics, we are assured by the universality of quiver moduli space [37, 233, 238, 252, 256, 315], in that *any* variety can be obtained by a suitably chosen quiver with superpotential.⁷ In other words, we can always find some \mathcal{Q} and W so that the VMS $\mathcal{M}(\mathcal{Q})$ is the desired variety.

3.1.2 The Archetypal Example

We have certainly bombarded the reader with volley of definitions and abstractions. It is illustrative to take a look at a simple example, which will help to anchor us. Let us take the “clover” quiver with a specific cubic superpotential:

$$W = \text{Tr}(XYZ - XZY), \quad (3.5)$$

In the above, there is a single node labelled N . Thus, our 3 arrows X, Y, Z are $N \times N$ matrices. The F-terms are obtained from the partials of W with respect to the variables X, Y, Z : one note about taking a derivative by a matrix variable is that within the trace, we can cyclically permute the variables by properties of matrix trace, so that we can move the variable to be differentiated to the last position (this matrix derivative is sometimes called the cyclic derivative). Performing this we obtain $\partial_X W = YZ - ZY$, $\partial_Y W = ZX - XZ$ and $\partial_Z W = XY - YX$. On the other hand $\text{Tr}(X), \text{Tr}(Y), \text{Tr}(Z)$ are clearly the 3 minimal generators for the GIOs. Hence,

$$\mathcal{M}(\mathcal{Q}) \simeq \text{Spec}(\mathbb{C}[\text{Tr}(X), \text{Tr}(Y), \text{Tr}(Z)] / \langle [X, Y], [Y, Z], [X, Z] \rangle). \quad (3.6)$$

⁷The formal way to state this is,

Theorem 7 *Given any scheme \mathcal{M} , there exists a quiver \mathcal{Q} and an ideal \mathcal{J} in the path-algebra $k\mathcal{Q}$ over the ground field k whose moduli space of all indecomposable $k\mathcal{Q}/\mathcal{J}$ -modules (and even with dimension vector $(1, 1, \dots, 1)$), is isomorphic to \mathcal{M} .*

Again, we relegate this important theorem to a footnote because the technicalities therein will intimidate the neophyte.

While the space may look rather complicated, the case of $N = 1$ should be immediately clear to us. Here, X, Y, Z are just complex numbers and the F-terms provide no extra relations. Hence, $\mathcal{M}(\mathcal{Q})$ is parametrized freely by 3 complex variables, i.e.,

$$\mathcal{M}(\mathcal{Q}_{N=1}) = \text{Spec } \mathbb{C}[X, Y, Z] = \mathbb{C}^3, \quad (3.7)$$

and we have retrieved our simplest non-compact Calabi-Yau 3-fold. In general, one can check (though the defining equations become quite involved) that $\mathcal{M}(\mathcal{Q}_{N \geq 1}) \simeq (\mathbb{C}^3)^N / \mathfrak{S}_N$, the N -th symmetric product of \mathbb{C}^3 , i.e., the direct product of N copies of \mathbb{C}^3 , quotiented by the action of the symmetric group by permutations.

The strategy used above to compute $\mathcal{M}(\mathcal{Q})$ explicitly is generally applicable [62] (formalized in [284] and algorithmized in [290]) to obtaining $\mathcal{M}(\mathcal{Q})$:

Proposition 5 *The VMS $\mathcal{M}(\mathcal{Q})$ is realized as an affine algebraic variety by the following algorithm*

1. Let GIO_{min} be the set of minimal (Eulerian) cycles in \mathcal{Q} , i.e., $\Phi_{r=1,\dots,k}$, each of which is a polynomial in X_{ij} and k , the total number of such cycles;
2. Consider the ring map⁸ from the quotient ring by the Jacobian ideal by Φ_r as

$$\mathbb{C}[X_{ij}] / \langle \partial W \rangle \xrightarrow{\theta} \mathbb{C}[\phi_r];$$

3. \mathcal{M} is the image of this map, as an affine variety in \mathbb{C}^k .

In the above example for $N = 1$, we have $\Phi : \mathbb{C}[X, Y, Z] \rightarrow \mathbb{C}^3$. Later we will study more involved examples.

Though the above exercise may seem trivial, there is highly non-trivial mathematics and physics involved. The quiver with superpotential given in (3.5) is called the **$\mathcal{N} = 4$ super-Yang-Mills** theory in $(3+1)$ -dimensions. It is the unique conformal, supersymmetric, quantum field theory with maximal supersymmetry in 4-dimensions, and on it countless articles and books have been written. The insight of [286] was that it is precisely the world-volume theory on the D3-brane and there is a “holographic” duality between this gauge theory and the gravity in the bulk Calabi-Yau. More precisely, the D3-branes furnish an asymptotic metric of $AdS_5 \times S^5$ the information of the full string theory on which is holographically projected onto the world-volume gauge theory. The anti-de Sitter space (AdS) and the world-volume conformal field theory (CFT) is what engendered the name “AdS/CFT”. This S^5 factor is none other than the S^5 in (3.1). We will return to this point later in the chapter.

⁸As coordinate rings the map should go in the reverse direction so that as varieties the map goes as indicated, but we beg the readers’ indulgence so that it is clear that the *image* is an affine variety in \mathbb{C}^k .

Maldacena's duality is a set of precise statements on relating correlation functions and partition functions, in a particular limit of large N . Our algebraic geometer's AdS/CFT, that $\mathcal{M}(Q) \simeq \mathbb{C}^3 = \text{Cone}(S^5)$, already remarkable, is only a tip of the iceberg of correspondences. But since this is a book on Calabi-Yau varieties and not on QFTs, we will content ourselves with playing on this oasis of a tip.

The point is that because the position of the brane is specified by a point in the transverse non-compact Calabi-Yau space M , the physical moduli, given by the vacuum expectation values (VEVs) of the scalar fields of the world-volume gauge theory, parametrize M by furnishing its coordinates. Now, the gauge theory on the brane is encoded by a quiver with representation variety $\mathcal{M}(Q) = VMS$. Therefore, tautologically, by construction,

$$M \simeq \mathcal{M}(Q) = VMS. \quad (3.8)$$

Therefore, string theory provides a natural answer to Question 3.

3.2 Orbifolds and Quotient Singularities

So far, our non-compact landscape consists of a single point, \mathbb{C}^3 . What is the next natural candidate? Since we are working locally, we are at liberty to allow certain singularities. There is a class of generalizations of manifolds which are called V-manifolds [321], now better known as **Orbifolds**. These are perfectly adapted to our present needs.

Briefly, one considers the action of a discrete, finite group $G \curvearrowright \mathbb{C}^n$ with a fixed locus, usually taken to be just a point, the origin, and forms the quotient: the very fact there is a fixed locus means that the quotient is not smooth, quite contrary to what one is used to. Indeed, in our discussion of projective spaces and toric varieties in the previous chapter, we remove the origin (Stanley-Reisner ideal) before the quotient so as to avoid singularities.

In order to preserve Calabi-Yau-ness, we must at least work within $SU(n)$ holonomy, i.e., we should only consider orbifolds of the form

$$\mathcal{M} \simeq \mathbb{C}^n/G, \quad G \text{ discrete, finite, subgroup of } SU(n). \quad (3.9)$$

It turns out that this condition is not sufficient for \mathcal{M} to be local Calabi-Yau, but is a necessary starting point.

In dimension⁹ $n = 1$, we essentially have only \mathbb{C} quotiented by a cyclic group so that the result is a pizza wedge but with the origin singular.

⁹In *real* dimension 1, there is only $\mathbb{R}/(\mathbb{Z}/2\mathbb{Z})$, which is just a half-line with the point at the origin a singular point, coming from the real axis folded over.

In dimension $n = 2$, we are considering \mathbb{C}^2 quotiented by discrete, finite, subgroups of $SU(2)$, whose classification goes back (at least) to Klein [264]

Group	Name	Size	
$A_n \simeq \mathbb{Z}/(n+1)\mathbb{Z}$	Cyclic	$n+1$	
D_n	Binary Dihedral	$4n$	
E_6	Binary Tetrahedral	24	
E_7	Binary Octahedral (Cube)	48	
E_8	Binary Icosahedral (Dodecahedron)	120	

(3.10)

For reference, we give all the explicit 2×2 generators for the groups in (B.10) in the Appendix.

To see this, we recall that $SU(2)$ is the lift of $SO(3)$ by its centre $\mathbb{Z}/2\mathbb{Z}$, so we only need the regular symmetries in $SO(3)$, which are the two infinite families of the symmetries of the regular n -gon: the cyclic group of size n and dihedral groups of size $2n$; as well as the symmetries of the 5 Platonic solids: the tetrahedron T , the cube C , the octahedron O , the dodecahedron D and the icosahedron I . However, $C-O$ and $D-I$ are graph dual to each other and share the same symmetry so we only have the 3 exceptional symmetry groups, viz., the alternating group \mathfrak{A}_4 of size 12, the permutation group \mathfrak{S}_4 of size 24, as well as \mathfrak{A}_5 of size 60. Now all these groups need to be lifted to $SU(2)$, and become their binary counterparts, except the cyclic case which is Abelian whereby affording no lift. The fact that we have named the groups **ADE** is a whole story by itself to which we will devote the next subsection.

Geometrically, $\mathbb{C}^2/(G \subset SU(2))$ should correspond to an interesting set of surface singularities. To write their affine equations as hypersurfaces in \mathbb{C}^3 is simple enough: one only needs to write down the list of generators of invariants under the group action (by a classical theorem of Hilbert-Noether, the ring of invariants is finitely generated) and find the defining relation amongst them. This is a traditional problem in *polynomial invariant theory* and the textbook [335] offers a great account from a computational/Gröbner basis perspective (q.v. Appendix B.2).

The Ordinary Double Point Let us illustrate the above discussions with the simple case of $A_1 = \mathbb{Z}/2\mathbb{Z}$. Let the coordinates of \mathbb{C}^2 be u, v and let $A_1 \curvearrowright \mathbb{C}^2$ by $(u, v) \rightarrow (-u, -v)$. Note that as a matrix group, the generator is $\begin{pmatrix} -1 & 0 \\ 0 & -1 \end{pmatrix}$ and we have to make sure that the generators, and hence all group elements, are unitary and have determinant 1, so as to guarantee the group is properly a subgroup of $SU(2)$.

Clearly, the basic invariants are $x = u^2$, $y = v^2$ and $z = uv$; in the sense that any other invariant of A_1 is a polynomial in these 3. There is a single relation amongst the invariants, viz., $xy = z^2$, so we can write the equation defining \mathbb{C}^2/A_1 , embedding into \mathbb{C}^3 with coordinates (x, y, z) as

$$\mathbb{C}^2/A_1 : \quad \{xy = z^2\} \subset \mathbb{C}[x, y, z]. \quad (3.11)$$

This is perhaps the most well-known algebraic singularity and is known as the *ordinary double point*.

Doing the same for all the groups in (3.10) gives the list of well-known du Val singularities [125], and as with A_1 , one can readily check that the affine equations of these as hypersurfaces $F(x, y, z)$ in \mathbb{C}^3 are:

$$\begin{aligned} A_n &: xy + z^n = 0 \\ D_n &: x^2 + y^2z + z^{n-1} = 0 \\ E_6 &: x^2 + y^3 + z^4 = 0 \\ E_7 &: x^2 + y^3 + yz^3 = 0 \\ E_8 &: x^2 + y^3 + z^5 = 0. \end{aligned} \tag{3.12}$$

One checks, by solving simultaneously for $F = \partial_x F = \partial_y F = \partial_z F = 0$, that the origin $(x, y, z) = (0, 0, 0)$ is a solution, meaning that it is a singular point.

Desingularization As with all singularities, the standard procedure is to smoothen¹⁰ (also called desingularize, or resolve) it. In performing resolution of a singularity M to a smooth variety \widehat{M} , one compares the [Canonical bundle](#) $K_{\widehat{M}}$ of \widehat{M} with the canonical sheaf (we have to say sheaf here since M is singular) K_M

$$K_{\widehat{M}} = f^*(K_M) + D \tag{3.13}$$

where $f : \widehat{M} \rightarrow M$ is the *resolution map* and the “extra” divisor D is called the *discrepancy*. Now M , being local Calabi-Yau, has $K_M = \mathcal{O}_M$, and if the discrepancy is 0 and $K_{\widehat{M}} = \mathcal{O}_{\widehat{M}}$ would mean that \widehat{M} is Calabi-Yau. Such a resolution has a cute name:

Definition 8 When the discrepancy divisor $D = 0$ and the canonical sheaf naturally pulls back as $K_{\widehat{M}} = f^*(K_M)$, the resolution $f : \widehat{M} \rightarrow M$ is called *crepant*.

That is, we have dropped the “dis” in “discrepant”, as a bit of word-play in English. It is these resolutions that we need for our Calabi-Yau purposes.

The list (3.12) is exhaustive in that we have (cf. [60, 329]):

Theorem 8 *The elements of the list (3.12) admit crepant resolutions to smooth K3 surfaces and vice versa, and they are all (up to analytic isomorphism) the local models for K3 surfaces.*

¹⁰We do not have the space in this book to enter into the extensive subject of singularity resolution in mathematics, nor the physical interpretation in terms D-branes. We mention here that there are 2 standard ways of “resolving” a singularity: (1) desingularization by deformation; and (2) blowup. For Kähler spaces, as is the case with everything in this book, (1) is a complex structure deformation and (2) is a Kähler structure/metric deformation.

Deformation is easy to see. For example, $xy + z^n = 0$ is singular at $(0, 0, 0)$ as discussed. Thus, we deform the origin by considering the variety $xy + z^n = \epsilon$. Blow-up, on the other hand, is introduced in Appendix A.7, where we replace the origin by a \mathbb{CP}^1 . The desingularization discussed here is done by blow-up and the extra divisor D , for $xy + z^n = 0$, is the class of the \mathbb{CP}^1 .

The situation is even better; explicit metrics are known for many of these [272]. For the A_n series it is the celebrated Eguchi-Hanson metric [128]. In fact, for A_1 which we discussed above, the double point, the quotient \mathbb{C}^2/A_1 is the total space of the cotangent bundle over S^2 , and the Ricci flat metric for it was one of the very first to be constructed [128].

3.2.1 McKay Correspondence

The specialness of the ADE list is remarkable from many approaches in mathematics and this meta-pattern [152] appears in so many mysterious and inter-connected ways that it has inspired an entire discipline of *ADE-ology* [70, 213]. A highlight of this is the [McKay Correspondence](#), a brief exposition on which we cannot resist but giving here.

Take our discrete finite subgroup $G \subset SU(2)$, it has a defining 2 complex-dimensional representation **2**, which for the non-Abelian cases is irreducible and for the Abelian A_n -series, is the direct sum of 2 (conjugate) one-dimensional representations. John McKay¹¹ performed an experiment: tensor **2** with all the irreducible representations (irreps) r_i of G , decompose this into irreps as

$$\mathbf{2} \otimes \mathbf{r}_i = \bigoplus_j a_{ij}^2 \mathbf{r}_j \quad (3.14)$$

and note the multiplicities $a_{ij}^2 \in \mathbb{Z}_{\geq 0}$. He subsequently noticed that [289] if one were to interpret a_{ij} as the **adjacency matrix** of a finite graph, they are precisely the Dynkin diagrams of the affine ADE Lie algebras, as shown in Table 3.1.

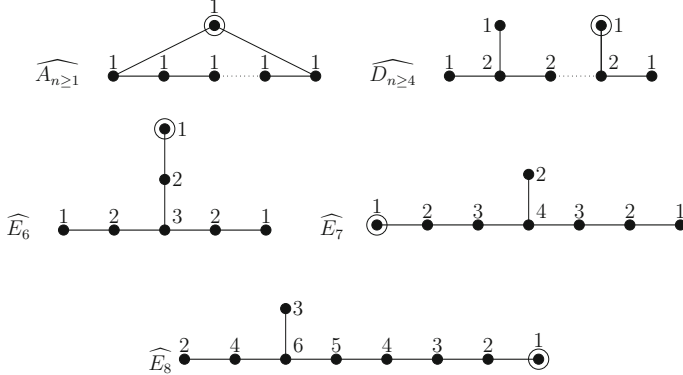
Just to briefly recall some rudiments to clarify this amazing fact, we have:

Definition 9 For a finite directed graph with n nodes, the **adjacency matrix** a_{ij} is an $n \times n$ matrix of non-negative integers whose (i, j) -th entry counts the number of arrows from node i to node j .

In the Dynkin diagram case, each line is understood to represent a bi-directional pair of arrows $i \leftrightarrow j$. Next, an affine Lie algebra is an infinite dimensional extension of the ordinary Lie algebra whose Dynkin diagram has one more “affine” node which we circle in the figure. Finally, of the complete set of semi-simple Lie algebras, the ADE ones are the *simply-laced*, i.e., there are no double or triple bonds, so that all simple roots are at 60 or 90 degrees from each other.

¹¹John’s super-human ability to notice patterns from unthinkably disparate branches of mathematics, whereby giving profound new insight, is legendary. Yet of all his correspondences, he seems most proud of the ADE one.

Table 3.1 The extended (affine) ADE diagrams, with integer labels being the Coxeter numbers. The affine nodes are circled explicitly; without this node, the diagram is the Dynkin diagram of the ordinary ADE Lie algebra



McKay Quiver for $\mathbb{Z}/(2\mathbb{Z})$

It is expedient to illustrate how to obtain the McKay quiver from (3.14) for a simple case. Take, for example, our ordinary double point in (3.11), which geometrically is the orbifold \mathbb{C}^2/A_1 where $A_1 = \mathbb{Z}/(2\mathbb{Z})$, the cyclic group of order 2 acting on the complex coordinates (u, v) of \mathbb{C}^2 by inversion: $(u, v) \rightarrow (-u, -v)$. The defining (fundamental) representation of this $\mathbb{Z}/(2\mathbb{Z})$ is thus the negative of the identity matrix $-\mathbb{I}_{2 \times 2}$. The group itself has only 2 elements, which we can denote as $\{1, -1\}$. The irreducible representations of A_1 are, since it is Abelian, all 1-dimensional. There are two of them: (1) the trivial representation **1** where all group elements are mapped to the identity (every finite group has this representation); and (2) the representation **1'** where the 2 elements are switched. Subsequently, we have 2 nodes of the McKay quiver, which can be labelled **1** and **1'**.

The fundamental **2** in this case is a direct sum **1' \oplus 1'**, since we have both coordinates being negated (a non- $SU(2)$ action $(u, v) \rightarrow (u, -v)$, for example, would correspond to **1' \oplus 1'**). Of all the ADE groups, only A-type has this split because it is Abelian; for the others **2** is a faithful, indecomposable, 2-dimensional defining representation. Thus, (3.14) reads

$$\begin{aligned} (\mathbf{1}' \oplus \mathbf{1}') \otimes \mathbf{1} &= \mathbf{1}' \oplus \mathbf{1}' \\ (\mathbf{1}' \oplus \mathbf{1}') \otimes \mathbf{1}' &= \mathbf{1} \oplus \mathbf{1}. \end{aligned} \tag{3.15}$$

Thus, for the node **1**, there are two arrows to node **1'**; likewise, for the node **1'**, there are two arrows to node **1**. Letting the pairs of bi-directional arrows be represented by a single line, the quiver looks like the Oxygen molecule $\bullet - \bullet$. This is the Dynkin diagram for affine A_1 . In general, for $A_n = \mathbb{Z}/((n+1)\mathbb{Z})$, one gets a necklace of $n+1$ beads, which is the Dynkin diagram for affine A_n .

The remarkable observation of McKay in the late 1970s is that if we did this for all the discrete subgroups of $SU(2)$, the corresponding quivers are precisely the Dynkin diagrams of the (extended) ADE Lie algebras. These are shown in Table 3.1. The computational way to obtain the quivers from the decomposition is to use the character inversion formula in (3.17) (q.v., [182] for a detailed exposition).

As is typical of correspondences from John McKay, the above is remarkable in that it relates two seemingly unrelated fields; Lie algebras and finite groups. To this we can add geometry. It turns out that in the resolution of the singularities in (3.12), one performs blow-ups and the exceptional curves are \mathbb{P}^1 's whose intersection matrix is precisely a_{ij} [329]. Thus, we have returned to our initial discussion about the moduli space of quivers:

Proposition 6 *The representation variety $\mathcal{M}(\mathcal{Q})$ for the affine Dynkin diagrams considered as quivers (the superpotentials are fixed and can be found in e.g. [246]) are the affine hypersurfaces in (3.12), which are local Calabi-Yau 2-folds, i.e., K3 surfaces.*

This beautiful web of relations quickly found its place in string theory [122, 153, 246, 276], with the word “quiver” introduced into physics by [122] and the general method of computation set out in [276] and algorithmized in [182]. Recall our example of \mathbb{C}^3 . It can be thought of as an orbifold of \mathbb{C}^3 with the trivial group $G = \mathbb{I}$ and this gave us $\mathcal{N} = 4$ super-Yang-Mills theory in 4 dimensions. The discrete subgroups of $SU(2)$, then, furnish orbifolds of the form $\mathbb{C} \times (\mathbb{C}^2/G)$ and these will give McKay quivers (each node also with an added self-adjoining loop due to the \mathbb{C} factor) which correspond to a special class of $\mathcal{N} = 2$ supersymmetric QFTs in 4 dimensions.

3.2.2 Beyond ADE

And so we can generalize. A discrete subgroup G of $SU(3)$ would give an orbifold of the form $\mathbb{C}^3/(G \subset SU(3))$. Luckily, crepant resolutions also exist for these and they are indeed locally Calabi-Yau 3-folds [157, 244]. However, unlike the $n = 2$ case where the crepant solution to K3 surfaces is unique, the $n = 3$ case exists but is not unique and the resolutions are related to each other by flop transitions.

The $SU(3)$ subgroups were first classified at the turn of the twentieth century when matrix groups were still known as collineation groups [46]. Again, the classification scheme follows the dichotomy: (1) infinite-families, and (2) finite exceptional cases. In addition to the obvious cases of the $SU(2)$ subgroups which embed non-transitively (with a block-matrix structure) as well as the Abelian case of $\mathbb{Z}/p\mathbb{Z} \times \mathbb{Z}/q\mathbb{Z}$, the extra $SU(3)$ groups are

Infinite Series	$\Delta(3n^2), \Delta(6n^2)$	
Exceptionals	$\Sigma_{36 \times 3}, \Sigma_{60 \times 3}, \Sigma_{168 \times 3}, \Sigma_{216 \times 3}, \Sigma_{360 \times 3}$	(3.16)

The two infinite families Δ of size $3n^2$ and $6n^2$ are certain non-Abelian extensions of $A_n \times A_n$ and the sizes of the 5 exceptionals (the analogue of the symmetries of the Platonic solids) are marked as subscripts.

Using GAP [338], the representations for all these groups were worked out in [182] and using the orthonormality of finite group characters, one can invert the generalization of (3.14) (with a chosen defining representation \mathbf{R} of G) as

$$\mathbf{R} \otimes \mathbf{r}_i = \bigoplus_j a_{ij}^{\mathbf{R}} \mathbf{r}_j \quad \Rightarrow \quad a_{ij}^{\mathbf{R}} = \frac{1}{|G|} \sum_{\gamma=1}^r r_{\gamma} \chi_{\gamma}^{\mathbf{R}} \chi_{\gamma}^{(i)} \overline{\chi_{\gamma}^{(j)}} \quad (3.17)$$

where $\chi_{\gamma}^{(i)}$ are the entries in the finite character table of G , with (i) indexing the irreps/rows and γ the conjugacy classes/columns; the number of irreps and number of conjugacy classes are both equal to a positive integer r and r_{γ} is the size of the γ -th conjugacy class.

Using this, the analogues of the McKay ADE quivers were drawn (cf. Fig. 5 in cit. ibid.). In physics, they correspond to $\mathcal{N} = 1$ super-conformal field theories in 4-dimensions. In mathematics, they are quivers whose $\mathcal{M}(Q)$ are non-compact Calabi-Yau 3-folds.

Our non-compact landscape has therefore grown from a single example of \mathbb{C}^3 to an infinite number. On the physics side, there is a long programme to try to seriously construct the standard model from branes at singularities [3–5, 22, 40, 87, 140, 155, 258, 312, 348, 350].

To close the discussion on orbifolds, for $n > 3$ in (3.9), the situation is much more complicated. Very little is known about which groups admit crepant resolution to Calabi-Yau manifolds. Nevertheless, the $n = 4$ case has also been classified in [46] and the McKay quivers for these, studied in [183].

3.3 Toric Calabi-Yau Varieties

As with the compact case, the combinatorics of toric geometry gives us the most fruitful method of construction. The geometer need not be alarmed by the title of this subsection: while there are no compact Calabi-Yau manifolds which are toric (in fact they do not even admit any continuous isometries), the fact that we are only concerned with non-compact Calabi-Yau manifolds in this chapter salvages the situation [99] (cf. [47] for a more immediate treatment). Since we are dealing with a local, affine variety, the **Toric variety** is described by a single cone. We again refer to Appendix A.6 for notation and a rapid discussion on such cones.

The vanishing of the first Chern class translates to the fact that the end-points of the generators of the cone are co-hyperplanar. That is, an affine toric variety of complex dimension n is defined by a rational polyhedral cone in \mathbb{R}^n , but for an affine Calabi-Yau manifold, the end-points lie on a hyperplane and therefore a lattice $(n - 1)$ -polyhedron suffices to encode it. In summary,

Theorem 9 An affine (local) toric Calabi-Yau 3-fold M is represented by a toric diagram \mathcal{D} that is a convex lattice polygon, defined up to $GL(2; \mathbb{Z})$. In particular, this gives an infinite number of toric Calabi-Yau 3-folds.

Now, \mathbb{C}^n is the prototypical example of an affine toric variety, so let us illustrate the above theorem with our familiar \mathbb{C}^3 . The cone for \mathbb{C}^3 has 3 generators, viz., the standard basis of \mathbb{R}^3 , which are clearly coplanar. Therefore, the toric diagram for \mathbb{C}^3 can simply be taken, after $GL(2; \mathbb{Z})$, to be the lattice triangle: $\{(0, 0); (0, 1); (1, 0)\}$.

Next, it should be noted that the Abelian orbifolds to which we alluded earlier are all toric varieties, though the non-Abelian ones are not. Specifically, letting the coordinates of \mathbb{C}^3 be (x, y, z) , the 2 generators of $\mathbb{Z}/p\mathbb{Z} \times \mathbb{Z}/q\mathbb{Z}$ with $p, q \in \mathbb{Z}_+$ can be chosen as

$$(x, y, z) \rightarrow (x, \omega_p y, \omega_q^{-1} z), \quad (x, y, z) \rightarrow (\omega_q x, \omega_q^{-1} y, z) \quad (3.18)$$

to ensure that the group embeds into $SU(3)$, where ω_p and ω_q are the primitive p -th and q -th roots of unity respectively. In particular, \mathbb{C}^3 itself and $\mathbb{C}^3/(\mathbb{Z}/r\mathbb{Z})$ for $r \in \mathbb{Z}_{\geq 2}$ are all toric varieties (the $\mathbb{C}^3/(\mathbb{Z}/2\mathbb{Z})$ case is actually just $\mathbb{C} \times \mathbb{C}^2/(\mathbb{Z}/2\mathbb{Z})$ since there will always be one coordinate fixed). The toric diagram for this Abelian orbifold is the lattice right-angle triangle whose legs (cathethi) are of length p and q . Consequently, by choosing large enough p and q , any toric diagram is a sub-diagram of that of the Abelian orbifold.

3.3.1 Cone over \mathbb{P}^2

We return to our Question 3 of relating the quiver and the Calabi-Yau 3-fold, which in the toric context translates to

Question 4 What quiver with superpotential \mathcal{Q} has as its representation variety (VMS) $\mathcal{M}(\mathcal{Q})$ an affine toric Calabi-Yau 3-fold with toric diagram \mathcal{D} (a lattice convex polygon)?

So far, we know the clover quiver (3.5) corresponds to \mathbb{C}^3 , or

$$\mathcal{D} = \{(0, 0); (0, 1); (1, 0)\}, \quad (3.19)$$

the (minimal) lattice triangle. Also, we know that lattice triangle with legs (p, q) corresponds to the McKay quiver for $\mathbb{Z}/p\mathbb{Z} \times \mathbb{Z}/q\mathbb{Z}$, which turns out to be the clover repeated pq times, with all nodes tri-valent. In physics, this is known as a *brane-box model* [188]. As an illustration, in Fig. 3.1, we draw the toric diagram for $\mathbb{C}^3/(\mathbb{Z}/3\mathbb{Z}) \times (\mathbb{Z}/3\mathbb{Z})$, as well as how the cones over \mathbb{P}^2 to which we now turn, as well as over its toric blow-ups (the toric del Pezzo surfaces).

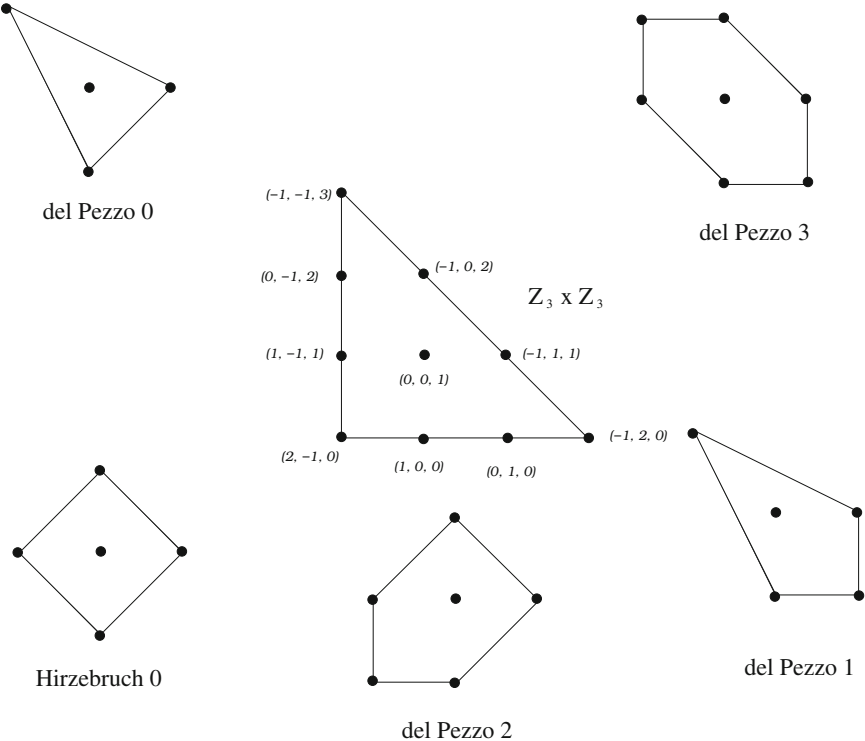


Fig. 3.1 The toric diagram of $\mathbb{C}^3/(\mathbb{Z}/3\mathbb{Z}) \times (\mathbb{Z}/3\mathbb{Z})$ as an affine cone; the coordinates of the vertices are just one choice, any $SL(3; \mathbb{Z})$ transformation is equivalent. The subdiagrams are the cones over the toric del Pezzo surfaces which are partial resolutions of $\mathbb{C}^3/(\mathbb{Z}/3\mathbb{Z}) \times (\mathbb{Z}/3\mathbb{Z})$

It is expedient to illustrate all of this with a simple but important example. Consider the action on \mathbb{C}^3 by a $\mathbb{Z}/(3\mathbb{Z})$ action

$$(x, y, z) \longrightarrow (\omega_3 x, \omega_3 y, \omega_3 z), \quad \omega_3^3 = 1. \quad (3.20)$$

This is an $SU(3)$ action since the matrix $\text{Diag}(\omega_3, \omega_3, \omega_3)$ is special unitary. There are 3 irreps for the Abelian group $\mathbb{Z}/(3\mathbb{Z})$, all of dimension one, $\mathbf{1}$, $\mathbf{1}_{\omega_3}$, and $\mathbf{1}_{\omega_3^2}$ and the action corresponds to a 3-dimensional reducible representation $R_3 = \mathbf{1}_{\omega_3}^{\oplus 3}$. The quiver can then be obtained from the analogue of (3.14), viz.,

$$R_3 \otimes \mathbf{r}_i = \bigoplus_j a_{ij} \mathbf{r}_j \quad \Rightarrow \quad \text{Adjacency Matrix: } a_{ij} = \begin{pmatrix} 0 & 3 & 0 \\ 0 & 0 & 3 \\ 3 & 0 & 0 \end{pmatrix}, \quad (3.21)$$

which says there are 9 arrows and 3 nodes with triplets going in a cycle. We label the nodes from 1 to 3 and let $X_{ij}^{\alpha=1,2,3}$ denote the triplet of arrow from node i to j . The superpotential W can also be found by projection on the clover using [276] and we have the quiver data

$$W = \sum_{\alpha,\beta,\gamma=1}^3 \epsilon_{\alpha\beta\gamma} X_{12}^{(\alpha)} X_{23}^{(\beta)} X_{31}^{(\gamma)}, \quad (3.22)$$

with arrows $X_{12}^{(\alpha)}$, $X_{23}^{(\beta)}$, $X_{31}^{(\gamma)}$ and the completely antisymmetric Levi-Civita symbol $\epsilon_{\alpha\beta\gamma}$. Note that the dimension vector is $(1, 1, 1)$ and the $(1, 2, 3)$ are just index labels for the nodes.

Now, let us check that $\mathcal{M}(\mathcal{Q})$ is as promised. In order to do so, we apply Proposition 5 and to make everything crystal clear, we will again resort to Macaulay2 [163] for our illustration.¹² We begin by ordering the variables as

$$(X_{12}^1, X_{12}^2, X_{12}^3, X_{23}^1, X_{23}^2, X_{23}^3, X_{31}^1, X_{31}^2, X_{31}^3) \rightarrow (X_1, X_2, \dots, X_9) \quad (3.23)$$

and define the ring of the 9 arrow variables

$$\text{R}=ZZ/101[X_1..X_9];$$

Next, there are clearly $3^3 = 27$ GIOs (minimal loops) $X_{12}^\alpha X_{12}^\beta X_{12}^\gamma$, which we index as y_1, y_2, \dots, y_{27} (recall that 101 is just a prime of convenient choice):

$$\begin{aligned} S &= ZZ/101[y_1..y_{27}]; \\ \text{gios} &= \{ \\ &\quad X_1*X_4*X_7, X_1*X_4*X_8, X_1*X_4*X_9, \\ &\quad X_1*X_5*X_7, X_1*X_5*X_8, X_1*X_5*X_9, \\ &\quad X_1*X_6*X_7, X_1*X_6*X_8, X_1*X_6*X_9, \\ &\quad X_2*X_4*X_7, X_2*X_4*X_8, X_2*X_4*X_9, \\ &\quad X_2*X_5*X_7, X_2*X_5*X_8, X_2*X_5*X_9, \\ &\quad X_2*X_6*X_7, X_2*X_6*X_8, X_2*X_6*X_9, \\ &\quad X_3*X_4*X_7, X_3*X_4*X_8, X_3*X_4*X_9, \\ &\quad X_3*X_5*X_7, X_3*X_5*X_8, X_3*X_5*X_9, \\ &\quad X_3*X_6*X_7, X_3*X_6*X_8, X_3*X_6*X_9 \} ; \end{aligned}$$

The superpotential expands to a six-term cubic

$$W = X_{23}^1 X_{31}^2 X_{12}^3 - X_{23}^1 X_{31}^3 X_{12}^2 + X_{23}^3 X_{31}^1 X_{12}^2 + X_{23}^2 X_{31}^3 X_{12}^1 - X_{23}^3 X_{31}^2 X_{12}^1 - X_{12}^3 X_{23}^2 X_{31}^1. \quad (3.24)$$

¹²The map θ is actually a projection, and one can compactify the whole algorithm in one fell swoop using elimination, as is detailed in §2.1 of [198]. However, for illustrative purposes we will use the ring map presented in the text here.

Using our relabelling and taking the partial derivatives with respect to all 9 variables, we have the Jacobian ideal in R

$$\text{jac} = \{ -x_{\{6\}} * x_{\{8\}} + x_{\{5\}} * x_{\{9\}}, \quad x_{\{6\}} * x_{\{7\}} - x_{\{4\}} * x_{\{9\}}, \\ -x_{\{5\}} * x_{\{7\}} + x_{\{4\}} * x_{\{8\}}, \quad x_{\{3\}} * x_{\{8\}} - x_{\{2\}} * x_{\{9\}}, \\ -x_{\{3\}} * x_{\{7\}} + x_{\{1\}} * x_{\{9\}}, \quad x_{\{2\}} * x_{\{7\}} - x_{\{1\}} * x_{\{8\}}, \\ -x_{\{3\}} * x_{\{5\}} + x_{\{2\}} * x_{\{6\}}, \quad x_{\{3\}} * x_{\{4\}} - x_{\{1\}} * x_{\{6\}}, \\ -x_{\{2\}} * x_{\{4\}} + x_{\{1\}} * x_{\{5\}} \};$$

We are now ready to perform the map θ :

$$M = \ker(\text{map}(R/\text{jac}, S, \text{gios}));$$

Note that we use the kernel rather than the image in Macaulay2 since, as we mentioned in the footnote to Proposition 5, the map between varieties is in the opposite direction from that between coordinate rings. As an ideal in S , M is the affine variety $\mathcal{M}(\mathcal{Q})$. First, $\dim(M)$ returns 3, which is good. Next, we can see, using

$$\text{minimalPresentation}(M)$$

what it actually is. This minimal presentation strips off trivial linear relations and reduces the the number of variables in S . In all, only 10 variables are left and V is realized as the (non-complete) intersection of 27 quadrics in \mathbb{C}^{10} , which the astute algebraic geometer would recognize. There is a standard Veronese embedding of $v : \mathbb{P}^2 \hookrightarrow \mathbb{P}^9$ of degree 3

$$v : \mathbb{P}^2 \hookrightarrow \mathbb{P}^9 \tag{3.25}$$

$$; [z_0 : z_1 : z_2] \longrightarrow [z_0^3 : z_0^2 z_1 : z_0 z_1^2 : z_1^3 : z_0^2 z_2 : z_0 z_1 z_2 : z_1^2 z_2 : z_0 z_2^2 : z_1 z_2^2, z_2^3],$$

since there are exactly 10 degree 3 monomials in 3 variables. In fact, these are precisely the 10 generators of the ring of invariants under the action of the $G = \mathbb{Z}/3\mathbb{Z}$ in (3.20) and there are 27 quadratic relations amongst them (the 27 quadrics returned from the minimal presentation).

Rephrasing all this in the affine language $M = \text{Spec}\mathbb{C}[x, y, z]^G$ is the spectrum of the G -invariant polynomial ring. That is, $M \simeq \mathbb{C}^3/(\mathbb{Z}/3\mathbb{Z})$, the orbifold we desired. Furthermore, the cubics furnish the degree 3 sections of a line bundle over \mathbb{P}^2 , and thence, the orbifold is

$$\mathbb{C}^3/(\mathbb{Z}/3\mathbb{Z}) = \text{Cone}(\mathbb{P}^2) \simeq \text{Tot}(\mathcal{O}_{\mathbb{P}^2}(-3)), \tag{3.26}$$

the total space of the anti-canonical bundle over \mathbb{P}^2 . We can intuitively think of this as the negative curvature of the cone cancelling the positive curvature of \mathbb{P}^2 , giving a zero-curvature space which is Calabi-Yau.

Finally, as an Abelian orbifold, M is toric, and the toric diagram can be retrieved readily. The 10 exponents of the invariant cubics from (3.25) are $\{(3, 0, 0), (2, 1, 0), (1, 2, 0), (0, 3, 0), (2, 0, 1), (1, 1, 1), (0, 2, 1), (1, 0, 2), (0, 1, 2), (0, 0, 3)\}$

(one can check that as vectors they are co-planar since each triple sums to 3). The dual cone σ^\vee to the cone σ spanned by these 10 vectors can be readily found, again using SageMath [320], as was done in the digression in Sect. 2.4.2:

```
sigma = Cone([
    [3, 0, 0], [2, 1, 0], [1, 2, 0], [0, 3, 0], [2, 0, 1],
    [1, 1, 1], [0, 2, 1], [1, 0, 2], [0, 1, 2], [0, 0, 3]]);
```

and then `sigma.dual().rays()` returns $\{(1, 0, 0), (0, 1, 0), (0, 0, 1)\}$, which is the toric diagram: its endpoints are coplanar—by appropriate $GL(2; \mathbb{Z})$ we can make the toric diagram as $\mathcal{D} = \{(1, 0), (0, 1), (-1, -1)\}$. Viewed from the plane on which the respective endpoints are coplanar, σ and σ^\vee are simply Δ_2 and Δ_2° in Fig. 2.3 respectively, or, the top and bottom of Fig. 2.5.

3.3.2 The Conifold

If the toric diagram \mathcal{D} for \mathbb{C}^3 is the minimal lattice triangle $\{(0, 0), (1, 0), (0, 1)\}$, then one might wonder to what space—call it \mathcal{C} —the next simplest case of $\mathcal{D} = \{(0, 0), (1, 0), (0, 1), (1, 1)\}$, the minimal square, might correspond. The non-triangular shape already precludes the possibility of it being an orbifold of \mathbb{C}^3 and we seem to have the beginning of another interesting family of toric Calabi-Yau 3-folds (simply enlarging the square indeed gives orbifolds of \mathcal{C}).

The defining equation of \mathcal{C} can be readily found through toric methods, as in the previous subsection. We first restore the third coordinate of the toric cone, say by adding height one for the z direction, i.e.,

$$\mathcal{D} = \{(0, 0, 1), (1, 0, 1), (0, 1, 1), (1, 1, 1)\}; \quad (3.27)$$

there are of course many $GL(3; \mathbb{Z})$ -equivalent ways of doing this. Next, we treat these vectors as exponents of monomials in the 3 variables $\{x, y, z\}$, giving us the monomials $\{u, v, s, t\} := \{z, xz, yz, xyz\}$ which satisfy the single quadric relation

$$\{ut = vs\} \subset \mathbb{C}[u, v, s, t], \quad (3.28)$$

In summary, this hypersurface in \mathbb{C}^4 , with $(0, 0, 0, 0)$ as its singular point, is an affine, toric, Calabi-Yau 3-fold, called the **Conifold** in the physics literature. In the mathematics literature, it is just called a quadric hypersurface in \mathbb{C}^4 , the 3-dimensional version of the ordinary double point in (3.11).

Topologically, the conifold is the total space of the cotangent bundle over S^2 (as a local K3 surface), this is the total space of the cotangent bundle over S^3 . The metric (the 3-complex-dimensional analogue of Eguchi-Hanson [128]), was found in [73]. It is also a conical metric in the sense that the Calabi-Yau metric can be put in the form of (3.1), but now the base, instead of being S^5 , is a 5-manifold known rather esoterically as $T^{1,1}$ [73]. For a summary table of some of the most studied toric

Calabi-Yau 3-folds and their toric diagrams, see p9 of [202]. Further pedagogical material on toric Calabi-Yau 3-folds, quivers and related physics and mathematics can also be found in cit. ibid.

The conifold is one of the central objects in the mathematics and physics of mirror symmetry and geometric transitions and deserves a monograph by itself. Sadly, due to spacetime constraints as well as the theme of this book, we shall only make two remarks.

Geometric Transitions We can explicitly find the conifold—and indeed any of the affine varieties in this chapter—inside the compact ones from the previous chapter. This justifies the name “local” to which we alluded at the beginning of the chapter. For instance, \mathcal{C} can be a local singularity of our familiar quintic Q from Sect. 2.1. Suppose a particular quintic (in the moduli space of complex structures, which we recall to be possible choices of monomials) looked like

$$\overline{Y} := \{z_3g(z_0, \dots, z_4) + z_4h(z_0, \dots, z_4) = 0\} \subset \mathbb{P}_{[z_0:\dots:z_4]}^4, \quad (3.29)$$

where g and h are homogeneous quartic polynomials in the projective coordinates. Unlike the generic quintic, or the Fermat quintic, \overline{Y} is singular, with its singular locus given as

$$\text{Sing}(\overline{Y}) = \{z_3 = z_4 = g(z_0, \dots, z_4) = h(z_0, \dots, z_4) = 0\} \quad (3.30)$$

which consists of $4^2 = 16$ points (nodes), being the intersection of two quartics in the 3 remaining homogeneous variables. These nodes can be

1. Resolved to Y by blow-up;
2. Smoothed to \tilde{Y} by adding generic quintic monomials.

From Y to \tilde{Y} is a geometric transition of the conifold type. In relation to Conjecture 2, it is believed by an optimism known as **Reid’s Fantasy** (after Miles Reid), that all Calabi-Yau 3-folds can be related to each other by versions of such geometric transitions.

Sasaki-Einstein Manifolds The other emblematic aspect of the conifold is its conical form of the metric, analogous to \mathbb{C}^3 in (3.1). This important property is one of a class of manifolds known as *Sasaki-Einstein*. In general, suppose we have a Kähler n -fold M with Kähler form ω which is a cone over a $(2n - 1)$ -dimensional real manifold X . The metric takes the form

$$ds^2(M) = dr^2 + r^2 ds^2(X), \quad (3.31)$$

with $r \in \mathbb{R}_{\geq 0}$ the radial coordinate for the cone where $r = 0$ is the tip. The base $(2n - 1)$ -manifold is called Sasakian when M is Kähler. If in addition M is Calabi-Yau, then X is called Sasaki-Einstein.

The Kähler form ω can be written, for η a global one-form on X , as $\omega = -\frac{1}{2}d(r^2\eta) = \frac{1}{2}i\partial\bar{\partial}r^2$. Moreover, X has a Killing vector field R called the **Reeb vector**, defined, for the complex structure \mathcal{I} on M , as $R := \mathcal{I}(r\frac{\partial}{\partial r})$.

Now, when M is furthermore toric Calabi-Yau, meaning that we have an integrable torus action \mathbb{T}^n which leaves ω invariant, everything becomes even more explicit and the metric can be elegantly written down [148]. Taking $\partial/\partial\phi_i$ to be the generators of the torus action, with ϕ_i to be the angular coordinates, allows for the introduction of symplectic coordinates y_i defined as $y_i := -\frac{1}{2}\langle r^2\eta, \frac{\partial}{\partial\phi_i} \rangle$, with $\langle \cdot, \cdot \rangle$ the usual bilinear pairing between forms and vector fields.

Subsequently, the Kähler form and the metric become, in these symplectic coordinates

$$\omega = dy_i \wedge d\phi_i, \quad ds^2 = G_{ij}dy_i dy_j + G^{ij}d\phi_i d\phi_j, \quad (3.32)$$

where G^{ij} is the inverse of $G_{ij} := \partial_i \partial_j G$ for some symplectic potential G determined from the complex structure as $\mathcal{I} = \begin{bmatrix} 0 & -G^{ij} \\ G_{ij} & 0 \end{bmatrix}$. There is a long programme to understand the geometry of Sasaki-Einstein cones in relation to the world-sheet conformal field theory, generating such beautiful results as the equivalence of the minimization of the volume of the base X and the maximization of certain central charge in the field theory [65, 127, 174, 223, 287].

Now, with non-compact manifolds, it is difficult to have a canonical notion of Hodge numbers and other such topological quantities. Thus, while we have an infinite number of data points, it is hard to have a succinct analogue of the Hodge-pair plot of Fig. 2.6. With a compact Sasaki-Einstein base, however, one *does* have an ordinary sense of Euler and Betti numbers. The statistical studies of these, versus the normalized volumes for toric Calabi-Yau 3- and 4-folds coming from reflexive polytopes (cf. the 16 polygons of Fig. 2.5 and the analogous 4319 polyhedra) were initiated in [223].

The Conifold Quiver Returning to our question of quiver representations; what (\mathcal{Q}, W) has \mathcal{C} as its moduli space? This problem was solved by [263] in one of the earliest examples of AdS/CFT beyond \mathbb{C}^3 . The required data is a 2-noded quiver (with dimension vector (N, N)), with 4 arrows ($A_{1,2}$ and $B_{1,2}$, which are bi-fundamentals under $SU(N) \times SU(N)$) and 2-term quartic superpotential (upon expanding out the antisymmetric symbol ϵ):

Quiver diagram:

```

    graph LR
      A(( )) -->|A_{1,2}| B(( ))
      B -->|B_{1,2}| A
      A -->|A_{1,2}| B
      B -->|B_{1,2}| A
  
```

	$SU(N)$	$SU(N)$
$A_{i=1,2}$	□	□
$B_{j=1,2}$	□	□

$$W = \text{Tr}(\sum_{i,j,k,l=1,2} \epsilon_{il}\epsilon_{jk} A_i B_j A_l B_k)$$

$$= \text{Tr}(A_1 B_1 A_2 B_2 - A_1 B_2 A_2 B_1).$$
(3.33)

One can check the VMS quite simply in this case. Taking $N = 1$, we again have $W = 0$ so no further quotients by the Jacobian ideal are needed. There are 4 minimal loops: $u = A_1 B_1$, $t = A_2 B_2$, $v = A_1 B_2$ and $s = A_2 B_1$, and they satisfy the one equation, the hypersurface in (3.28), as required for the defining quadric of \mathcal{C} . Taking $N > 1$ would have given us the symmetric product $\mathcal{C}^N / \mathfrak{S}_N$.

3.3.3 Bipartite Graphs and Brane Tilings

Having gained some confidence with examples, one might wonder whether there exists, on returning to the original Question 3 of this chapter, an algorithm for translating between the quiver data and the Calabi-Yau data. For orbifolds, we saw that we needed the character table of the finite group and then happily used McKay's method. Surely, the rich combinatorics of toric varieties should facilitate this translation. Indeed, the method was given in [292] and algorithmized in [134], wherein the direction $\mathcal{Q} \rightarrow \mathcal{D}$, from the quiver (with superpotential) data to the toric diagram, was called, rather unimaginatively, the *forward algorithm*, and the direction $\mathcal{D} \rightarrow \mathcal{Q}$, the *inverse algorithm*.

The forward algorithm is more or less by direct computation, using a toric version of what was done in Sect. 3.3.1. The inverse algorithm uses the facts that (1) every toric diagram is a sub-diagram of that of $\mathbb{C}^3 / (\mathbb{Z}/p\mathbb{Z} \times \mathbb{Z}/q\mathbb{Z})$ for sufficiently large p, q , meaning that geometrically every affine toric Calabi-Yau 3-fold is a partial resolution of the said orbifold (corresponding to node deletion in its toric diagram); (2) the quiver for the orbifold is known and it is simply the generalized McKay quiver with superpotential; and (3) the desired quiver can be obtained by deletion of the nodes which corresponds to removal of arrows (Higgsing in the field theory).

This inverse algorithm of “geometrical engineering” (a whimsical but very appropriate term first coined in [251]) the quiver/physics from the given Calabi-Yau geometry turns out too computationally expensive, with the bottle-neck being finding the dual cone for a given convex lattice polyhedral cone, which is exponential in complexity. The break-through came in the mid-2000s when it was realized [139, 184] that a seemingly frivolous relation for the quiver \mathcal{Q} is actually of deep physical and mathematical origin and consequence: whenever $\mathcal{M}(\mathcal{Q})$ is toric, it was noted that

$$N_0 - N_1 + N_2 = 0 \tag{3.34}$$

for N_0 , the number of nodes, N_1 , the number of arrows, and N_2 , the number of monomial terms in the superpotential. In our running examples, for \mathbb{C}^3 , this is $1 - 3 + 2 = 0$, for \mathcal{C} , this is $2 - 4 + 2 = 0$, for $\text{Cone}(\mathbb{P}^2)$, this is $3 - 9 + 6 = 0$.

Over the years, the *School of Hanany* pursued the mapping between toric Calabi-Yau manifolds and quiver representations relentlessly. In brief, (3.34) is the Euler relation for a torus, and the quiver data (and superpotential) can be re-packaged into a bipartite tiling (called **brane tiling** or **dimer model**) of the doubly-periodic

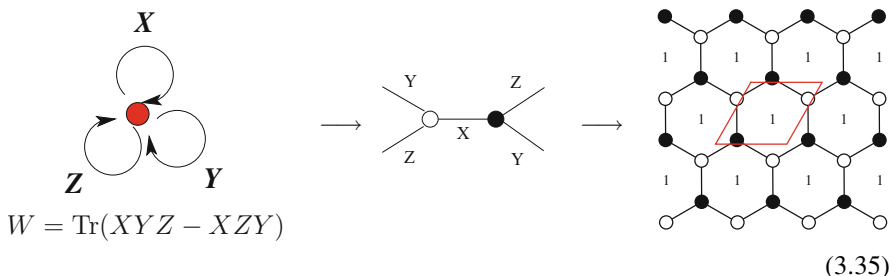
plane. This bipartite-ness is profound and involves a plethora of subjects ranging from scattering amplitudes, to dessins d'enfants, to cluster mutation, etc. [137, 138, 141, 175, 191, 229, 347].

The bipartite tiling perspective on quiver representations and Calabi-Yau moduli spaces has grown into a vast field in itself [100, 135, 185–187, 189, 190, 192], on which there are excellent introductory monographs [58, 253, 359], a short invitation by means of a conference report [202], and an upcoming book [59]. Again, with an apology we refer the curious reader to these references as well as two bird's-eye-view summary diagrams in Appendix C.

For now we will only summarize the method of translating between the quiver data and the bipartite graph data:

1. Consider a monomial term in W , if it comes with a plus (respectively minus) sign, draw a black (respectively white) node (the choice of colour is, of course, purely by convention), write all the variables in the monomial clockwise (respectively counter-clockwise) as edges around the node;
2. Connect all the black/white nodes by these edges. Because W has the property (this comes from the fact that the VMS is a toric variety, corresponding to a so-called *binomial ideal*, q.v., Appendix A.6) that each variable appears exactly twice with opposite sign, we end up with a bipartite graph \mathcal{B} ;
3. The condition (3.34) dictates that \mathcal{B} is a bipartite graph on T^2 , or, equivalently, a tiling of the doubly periodic plane;
4. Each node in \mathcal{B} is a term in W and thus a GIO, and edge is perpendicular to an arrow in \mathcal{Q}_1 obeying orientation and each face in \mathcal{Q} corresponds to a node in \mathcal{Q}_0 ; in other words, \mathcal{B} is a dual graph of \mathcal{Q} ;
5. In particular, being the dual, \mathcal{B} has $N_2/2$ pairs of black/white nodes, N_1 edges and N_0 inequivalent (polygonal) faces.

Note that while the quiver has two pieces of information the adjacency matrix and the superpotential, the tiling encodes both in one. We illustrate the above procedure with our archetypal example of \mathbb{C}^3 :



We have marked the fundamental domain of T^2 with the red parallelogram; therein, there is 1 pair of black-white nodes, each of valency 3, corresponding respectively to the $+XYZ$ and $-XZY$ terms in W . The edges together give the honeycomb tiling of the doubly periodic plane, with a single inequivalent face which is a hexagon marked “1”.

The set of relations in (3.35) is only a corner of an intricate web of correspondence which we summarize in Fig. C.1 in Appendix C. For further reference, the situation for our other favourite example, the conifold \mathcal{C} , is shown in Fig. C.2 in the said appendix.

These explorations by physicists have generated sufficient interest in the mathematics community that teams of “card-carrying” algebraic geometers and representation theorists [32, 36, 44, 45, 104, 154, 242, 273, 294, 336, 351] have formalized the statement into

Theorem 10 *Let \mathcal{Q} be a quiver with superpotential, which is graph dual to a bipartite graph drawn on T^2 according to the steps above. Then the (coherent component of, i.e., the top dimensional irreducible piece of) the moduli space $\mathcal{M}(\mathcal{Q})$ is an affine toric Calabi-Yau 3-fold.*

A systematic probe of this toric landscape was initiated in [103] and updated using the latest algorithms and computer power in [142], marching upwards in incremental area of the toric diagram \mathcal{D} .

We remark, therefore, that we have an infinite number of affine toric Calabi-Yau 3-folds, coming from (1) a lattice convex polygon \mathcal{D} as a toric diagram; or (2) a bipartite graph \mathcal{B} on T^2 as a quiver with superpotential. Mapping between these two sets is intricate. It is generally believed that set (2) surjects onto set (1) and the orbit of quivers \mathcal{Q} or dimers \mathcal{B} mapping to the same \mathcal{D} are related to each other by cluster mutation (known as Seiberg duality in the field theory). As mentioned, we leave the full details this toric-bipartite story to the wonderful reviews of [253, 359], the upcoming book [59], or, for the impatient, the terse report in [202].

3.4 Cartography of the Affine Landscape

We have taken our stroll in the landscape of non-compact, or affine, Calabi-Yau 3-folds, through the eyes of quiver representations, which *ab initio* may seem convoluted but turns out to luxuriate in an extraordinary wealth of mathematics and physics. Indeed, the relaxation of compactness gave us not only explicit Ricci-flat metrics but also many infinite families of manifolds, exemplified by orbifolds and toric varieties.

Let us part with one last small but fascinating family, the del Pezzo surfaces, which we have encountered in many different circumstances (cf. Appendix A.7). These Fano surfaces are all of positive curvature, so a complex cone over them (think of these projective varieties simply affinized) with the tip at the origin, can be judiciously chosen to make the cone Calabi-Yau. Computationally, we can “affinize” any compact projective variety M to a non-compact one \hat{M} rather easily by promoting the homogeneous coordinates of the projective space into which M embeds to affine coordinates, i.e.,

$$M \subset \mathbb{P}_{[z_0:z_1:\dots:z_n]}^n \longrightarrow \hat{M} \subset \mathbb{C}_{(z_0,z_1,\dots,z_n)}^{n+1}. \quad (3.36)$$

In this sense, \hat{M} is a complex cone over M (not to be confused with the real cone which we discussed throughout the chapter for Sasaki-Einstein manifolds) with the origin of \mathbb{C}^{n+1} as the tip.

In general, in this affinization M and \hat{M} cannot both be Calabi-Yau, one compact, and the other non-compact. This is our case here, M is a Fano surface and \hat{M} is the affine Calabi-Yau 3-fold. We already saw this in Sect. 3.3.1 with the cone over \mathbb{P}^0 , which we recall is the first of the del Pezzo family (including Hirzebruch zero). In this sense $Tot(\mathcal{O}_{\mathbb{P}^2}(-3))$ is a wonderful affine Calabi-Yau 3-fold, it is an orbifold, it is toric, and it is a del Pezzo cone.

Adhering to the notation of the Appendix, we can write dP_0 for \mathbb{P}^2 . It turns out that $dP_{0,1,2,3}$ and $\mathbb{F}_0 = \mathbb{P}^1 \times \mathbb{P}^1$ are all toric, with their toric diagrams being number 1, 3, 6, 10 and 4 respectively in Fig. 2.5. The higher ones with more blow-up points, $dP_{4,5,6,7,8}$ are not toric varieties, though their associated quivers were found in [356] using exceptional collections of sheafs. As a historical note, the Calabi-Yau metrics for these del Pezzo cones—undoubtedly part of the tradition of the Italian School of algebraic geometry—were found by Calabi himself shortly after Yau’s proof.

3.4.1 Gorenstein Singularities

Before closing, we make a brief remark about the singular nature of our manifolds. In this chapter, except for \mathbb{C}^3 , all the affine Calabi-Yau varieties are singular (at least) at the origin. We saw in Sect. 3.2 that orbifolds are by construction so. Algebraic singularities in geometry is a complicated business and much effort has been devoted to their smoothing or resolutions.

The class of singularities of concern to us is called **Gorenstein**, which is a rather tamable situation. The formal definition of Gorenstein-ness is intimidating and will take us too far into the inner sanctum of commutative algebra. Roughly, a Gorenstein singularity is one outside of which there exists a global holomorphic form, or, from a sheaf-theoretical point of view, the affine scheme is Gorenstein if its canonical sheaf is a line bundle (of degree 0). In other words, Gorenstein-ness is local Calabi-Yau-ness.

Luckily, there is an explicit computation that checks this crucial condition [332]:

Theorem 11 (R. Stanley) *The numerator of the Hilbert series of a graded Cohen-Macaulay domain R is palindromic iff R is Gorenstein.*

Recalling the basics of Hilbert series from Appendix B.2, we can see this theorem in action. We will not need the details of Cohen-Macaulay domains in this book; suffice it to say that many coordinate rings of complex varieties have this property. The Hilbert series for \mathbb{C}^3 is just $1/(1-t)^3$ from (B.5), the numerator is 1 and is trivially palindromic. For the conifold \mathcal{C} , it is $\frac{(1-t^2)}{(1-t)^4}$ (coming from 4 generators obeying a single quadratic relation) and the numerator upon cancellation is $1+t$, which is palindromic.

The Hilbert series for $\mathbb{C}^3/(\mathbb{Z}/3\mathbb{Z})$, using (B.8), is $\frac{1+7t+t^2}{(1-t)^3}$ and the numerator is palindromic: the coefficients of the lowest and highest term are both 1. In fact, for dP_n , the Hilbert series is $\frac{1+(7-n)t+t^2}{(1-t)^3}$ [39]. We have included all the Hilbert series (Molien series) for the discrete finite ADE subgroups of $SU(2)$ in (B.10) in the appendix.

In general, once we have some affine variety M , we can use the Gröbner basis methods detailed in the appendix to find the Hilbert series, and need only check the palindromy of the numerator to see whether M is “local Calabi-Yau”.

3.4.2 The Non-Compact Landscape

As we reach the end of our exposition, it is expedient to recall the vista of the non-compact Calabi-Yau 3-folds, in analogy to the Venn diagram in Fig. 2.8 of Sect. 2.5. We show the [Landscape](#) of non-compact Calabi-Yau 3-folds in Fig. 3.2. As in the compact case, the Venn diagram is only topologically relevant and the size of the bubbles is not significant. Several bubbles are meant to capture an infinite number of spaces.

The analogue of the simplest starting point quintic Q is here \mathbb{C}^3 , from which we have Abelian orbifolds of the form $\mathbb{C}^3/(\mathbb{Z}/p\mathbb{Z} \times \mathbb{Z}/q\mathbb{Z})$ for any $p, q \in \mathbb{Z}_{\geq 1}$, of which there is already an infinite number. Next, we have orbifolds of \mathbb{C}^3 by discrete finite subgroups of $SU(3)$ of which, in addition to the ADE subgroups of $SU(2)$, there are two infinite families, the delta-series, as well as a number of exceptionals.

The Abelian orbifold $\mathbb{C}^3/(\mathbb{Z}/3\mathbb{Z})$ is the cone (total space of the anticanonical bundle) over $dP_0 = \mathbb{P}^2$, the first member of the very special family of del Pezzo surfaces. It is also a toric variety, as are all Abelian orbifolds. This toric family is again infinite in number: any convex lattice polygon is the toric diagram of an

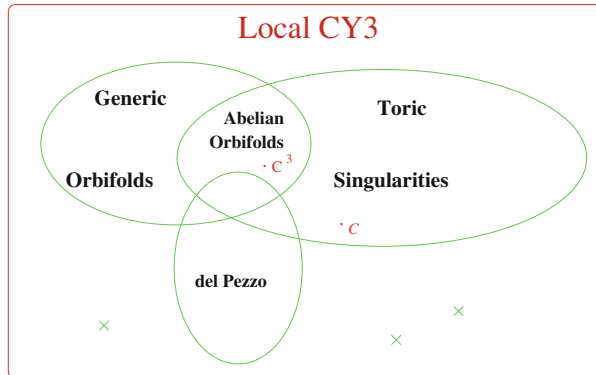


Fig. 3.2 The landscape of non-compact, affine, local Calabi-Yau 3-folds

affine, toric Calabi-Yau 3-fold. The prototypical example in this toric class is \mathcal{C} , the conifold, or the quadric hypersurface in \mathbb{C}^4 .

Of course, unlike local K3 surfaces, whose algebraic models can *only* be the ADE singularities, local Calabi-Yau 3-folds have no known complete characterization, the families chosen in the above Venn diagram are those which have been intensely studied, by mathematicians and physicists alike, and in particular, realized as the moduli space of quiver representations. The crosses outside the bubbles denote the plethora of other local Calabi-Yau models on which, though most certainly infinite in number, there has not been too intense an investigation.

Nunc Dimitis With our tantalizing pair of plots of the Calabi-Yau landscape in Figs. 2.8 and 3.2, let us pause here. We have taken a promenade in the land of CY₃, mindful of the intricate interplay between the mathematics and the physics, emboldened by the plenitude of data and results, and inspired by the glimpses of the as yet inexplicable.

We have devoted a duo of chapters on cartography; first on the compact and second on the non-compact, gaining familiarity with the terrain of CICYs, KS hypersurfaces, orbifolds, del Pezzo cones, lattice polytopes, etc. The landscape of Calabi-Yau manifolds will certainly continue to provoke further exploration, especially with the advance of ever new mathematics, physics and computing.

Assured by the abundance of data and the increasing computing power to calculate requisite quantities, we are perhaps simultaneously daunted by the complexities involved in the analysis, in the algorithmic sense of “complexity”. In the ensuing chapter, we shall speculate as to what might be done when confronted with the staggering mountains of the Calabi-Yau landscape.

Chapter 4

Machine-Learning the Landscape



*Die Physik ist für die Physiker eigentlich viel zu schwer.*¹

—David Hilbert

And so we have taken our excursion into the landscape of compact and non-compact Calabi–Yau manifolds, and like the keen geologist, soiled our hands with fascinating samples for scrutiny and experimentation, rather than like the artist, whose primary concern is with an impression of the magnificent vista. Thus prepared, we enter the last chapter, where with the plenitude of data collected, we can speculate upon its treatment. We mentioned at the very outset of the preface that a *Zeitgeist*, cultural and intellectual, seems to be curiously present, which breathes its *spiritus movens* onto scientific progress. Indeed, were we to examine our Scientific Age, it is without doubt that the omnipresence of data is what propels much research: from exoplanets, to the human genome, to the outpouring of particle jets at CERN.

It is natural, therefore, to ask whether the most cutting-edge techniques from Data Science can be applied to the landscape of Calabi–Yau manifolds, to algebraic geometry, and indeed, to mathematical physics and pure mathematics in general. This idea of machine-learning (ML) the Calabi–Yau landscape, and thence to mathematical structures² was initiated in [203, 204]. It was fortuitous that in 2017, the year that Sophia became the first non-human citizen, four independent

¹This is a famous quote from Hilbert at the turn of the twentieth century, that “physics has become much too difficult for physicists,” meaning that physicists and mathematicians must work together to tackle the key problems of fundamental physics. Indeed, the twentieth century took this advice and the foundational questions in physics were inextricably linked to the deepest mathematics. Perhaps, starting from the twenty-first century, data science and computer algorithms will become an integral part of mathematical physics and pure mathematics.

²For a quick summary and some speculations about the AI mathematician, q.v. [66, 205]. Indeed, the field is growing so rapidly that even as I am editing the final versions of the draft, papers in the intersection of ML and physics/mathematics are appearing each week. In our present context, two attempted rapid literature reviews, directly to the physicist and the mathematician, respectively, are presented in [209].

collaborations [83, 203, 204, 265, 318] brought machine-learning to string theory. It is interesting to note that the first annual “Strings” conference began in the 1980s, from which offshoots of “String Phenomenology” and “String Mathematics” emerged in the early 2000s and in 2017/8, began the new series of “String Data”. The reader is also referred to the “String-Data Cooperation” on Github, inaugurated by Sven Krippendorf et al. in Munich [333], which should grow to a marvellous repository of the data which we have discussed so far and of much more beyond.³

Of course, in this respect, the mathematical physics community is rather behind the experimental, where the constant influx of data had long propelled the field into machine-learning techniques. For instance, the first AI-HENP (high energy and nuclear physics) seminar at CERN dates back to 1990 (interestingly around the same time as the establishment of the CICY data), and by 2010 the trigger system for particle detection already had machine-learning algorithms built in [84]. By now, we hope the reader is convinced that there is a vast landscape of **mathematical data**, mostly compiled in the last decade or so, ranging from algebraic geometry, to representation theory, to number theory, etc.; the first two parts of this book have been using the Calabi–Yau data as a playground to illustrate various ideas in geometry and physics.

The initial investigations of 2017 have since been taken to various industrious and profitable ventures by many authors. In the string context, these have included explorations in the cosmological landscape [283], F-theory groups and matter [43, 354], heterotic orbifold landscape [295], reinforcement learning of vacua from branes [180], genetic algorithms on flux vacua [91], standard model data mining and statistical predictions [107, 177, 275, 304, 305], symmetries [271], and CFT properties [86], etc. In the stringy-geometry direction in particular, these have ranged from machine-learning CICYs [63, 64, 129, 130, 212], triangulations of the Kreuzer–Skarke dataset [8], bundle cohomology [57, 94, 262], distinguishing elliptic fibrations [211], classifying CYs [173], CY numerical metrics [17], or even to the linguistic structure of ArXiv mathematical physics sections [222], etc.

Remarkably, there have been daring proposals that quantum field theoretical structures, be it AdS/CFT [195, 196], renormalization group flow [260], or QFT itself [181], are guises of neural networks. In parallel, in the computational mathematical community, ML techniques have recently been applied to efficiently finding S-pairs in Gröbner bases [306] and in computation in toric varieties [328].

In the context of the structure of mathematics, there has been a programme on how different branches of mathematics respond to machine-learning [205]. One could imagine that number theory, especially unknown patterns in primes, would be the most resilient. This seems indeed to be the case, and we will discuss some of the experiments towards the end of the chapter. Since 2017, preliminary explorations, in addition to the algebro-geometric ones above, have included machine-learning representation theory [210] (surprisingly, simple finite groups

³The reader is also referred to an exciting and relatively new field of topological data analysis [302], which has recently been applied to the landscape [88, 90].

seem to be distinguishable from non-simple ones by looking only at the Cayley table), knot invariants [245], cluster mutation in quiver theory [24], combinatorics of graphs [216] (where possession of Euler or Hamilton cycles, or graph Laplacian spectra, seem to be learnable from classifying the adjacency matrix), to number theory (the Birch–Swinnerton-Dyer Conjecture [6] and the Sato–Tate Conjecture [226] in arithmetic geometry), etc.

In this final chapter, we shall let our imagination take the reins and be no longer like the meticulous naturalists, but rather the fearless frontiersmen and roam freely in the landscape which we had charted in the previous chapters. We will attempt to introduce some rudiments of machine-learning to the students in mathematics and theoretical physics communities who are also interested in explorations in data. In keeping with the theme of this book, we will focus on Calabi–Yau data as a playground; we have used it as a kindergarten to learn some physics and some mathematics; now, we will use it to learn some modern data science. Recently, there is an excellent monograph on introduction to data science to the theoretical physicist [319], and the reader should refer to it for a self-contained and technical introduction.

4.1 A Typical Problem

First, let us motivate the reader with the problem at hand. Reviewing the previous two chapters, we are encouraged by the ever-growing database of geometries,⁴ mostly freely available online, as well as the computer software, especially the open-source **SageMath** umbrella [320], designed to calculate many of the requisite quantities.

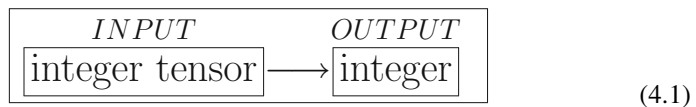
Much of these data have been the brain-child of the marriage between physicists and mathematicians, especially incarnated by applications of computational algebraic geometry, numerical algebraic geometry and combinatorial geometry to problems which arise from the classification in the physics and recast into a finite, algorithmic problem in the mathematics. In principle, as far as addressing problems such as searching for the right bundle cohomology to give the Standard Model—which we recall was what inspired the field of Calabi–Yau data from the late 1980s—is concerned, one could scan through configurations, find large clusters of computers⁵ and crunch away.

⁴In this book, we have only focused on Calabi–Yau threefolds for concreteness; there are many other datasets which have been established, ranging from the closely related bundles over CY threefolds, generalization of CICYs, etc., to diverse subjects as the ATLAS of finite groups, etc., as mentioned in the Preface.

⁵I remember a wonderful quote from Dan Freedman’s lectures when I was a PhD student at MIT, on addressing a difficult calculation; he, with his usual dry sense of humour, said, “this is a problem perfectly adapted to large parallel clusters of graduate students.”

However, we have repeatedly alluded to the fact, even when demonstrating the powers of the likes of `Macaulay2` [163] and `SageMath` [320] in the foregoing discussions, that most of the core algorithms are exponential in running time and in memory usage. This is the case for establishing Gröbner bases (due to getting all pairs of S-polynomials), for finding dual cones (due to finding all subsets of facets to check perpendicularity), for triangulation of polytopes (due to collecting all subsets of lattice points on the polytope), etc., which are the crux of the computational methods. Even parallelizable computations in numerical algebraic geometry [197, 290] suffer from the need to find a large number of paths in homotopy continuation.

Confronted with this limitation, it would be helpful to step back and re-examine the desired result [203, 204]. One finds that regardless of the origin and the intent, the typical problem in computational algebraic geometry is one of the form



We see this in all the cases presented hitherto (note that where the output is a list of integers, we can just focus on one at a time, conforming to the paradigm of (4.1)), e.g.,

- Computing the Hodge number of a CICY.

Input: an integer matrix whose row size ranges from 1 to 12, column size, from 1 to 15, and whose entries are from 0 to 5;
Output: a non-negative integer $h^{2,1}$ or a positive integer $h^{1,1}$.
- Computing the cohomologies of a line bundle L over a CICY M .

Input: the CICY configuration matrix as above, plus a vector of the integer (negative also allowed) degrees of L ;
Output: a list of non-negative integers, the rank $h^*(M, L)$ of the cohomology of L .
- Computing the Hodge numbers and Chern classes of a KS Calabi–Yau threefold.

Input: an integer polytope, specified either by a list of integer 4-vectors or by the coefficients of the hyperplane inequalities defining the polytope;
Output: integers $(h^{1,1}, h^{2,1})$, integer coefficients of c_2 (expanded into the basis of Kähler classes).
- Computing the triple intersection numbers of a hypersurface in weighted projective \mathbb{P}^4 .

Input: a 5-vector of co-prime positive integers;
Output: a list (totally symmetric 3-tensor) of non-negative integers.
- Computing the quiver from given affine toric Calabi–Yau threefold.

- Input:** the list of integer vertices of a convex lattice polygon, the toric diagram \mathcal{D} ;
- Output:** the integer adjacency matrix of the quiver as well as the list of non-negative integer exponents of the monomial terms to include in the superpotential.
- Computing the number of cluster mutation/Seiberg dual phases of a quiver (whose moduli space of representations, the VMS, is toric Calabi–Yau threefold).
- Input:** the Kasteleyn adjacency matrix of the bipartite graph (brane-tiling) on the doubly periodic plane;
- Output:** a positive integer.

The list goes on and on. Such computations are also typical in standard model building in string theory. This is because, due to the lack of analytic metrics of any kind on compact CYs, most calculations are, at this stage, interpretations of integer topological invariants like Hodge numbers or ranks of bundle cohomologies, as particle numbers or charges. We will, however, mention a little on numerical metrics towards the end of this chapter.

4.1.1 WWJD

As we enter the Age of Data Science and Artificial Intelligence (AI), one cannot resist asking how one might address problems of the type presented at the end of the previous section, without recourse to traditional methods, which are known to be computationally expensive. Indeed, WWJD? **What Would JPython/Jupyter Do?**

The joke is perhaps so esoteric that it might be lost on most. First, JPython, or its successor, Jython, is the implementation of the Python Programming language [310] for the JAVA platform, and Jupyter [248] is an open-source project whose core language consists of Julia, Python and R, whose interface is where Python and SageMath [320] are usually run.

According to card-carrying computer scientists and data scientists, these are the platforms of their preference, and Python, together with C++, the programming languages of choice, one higher and one slightly lower level. Second, in some circles, especially among Evangelical Christians, many wear T-shirts with the acronym WWJD, or “What Would Jesus Do”, as a constant reminder of how to lead one’s life.

So, what would one versed in Python do? Let us make an analogy. Suppose we are given the handwritten digits

$$1 \ 2 \ 3 \ 4 \ 5 \ 6 \ 7 \ 8 \ 9 \ 0 \quad (4.2)$$

and we wish to let the computer recognize them. The input is an image, which is nothing but a $m \times n$ matrix (indexing the pixels in a two-dimensional grid) each

entry of which is a 3-vector of a real value between 0 and 1, denoting the percentage of RGB values. Or, if we only wish to keep black-white (greyscale) information as is sufficient for this case, each entry is then a real number between 0 and 1. In fact, it is even sufficient to only keep the information of whether each pixel is occupied so that the input is an $m \times n$ matrix of 0s and 1s. The output is an integer from 0 to 9. In the computer science literature, this is called a *10-channel output*.

As mathematicians or theoretical physicists, what might instinctively come to mind in order to solve this problem is to exploit geometry and find, say, a clever Morse function so we scan the input matrix row-wise and column-wise and detect the critical points; these points will be different because the topologies of the digits are all different. Or, perhaps, one could compute the persistent homology, as it has become fashionable of late, of the pixels as a point cloud of data. The downside to all of these is that (1) the computation is very expensive, and (2) there is too much variation: how I write the digits will differ substantially (though not overwhelmingly) from how you would write them. Upon reflection, this is rather like the situation of our concern: the computation, such as Gröbner bases, is too expensive and the input has some variation in configuration, e.g., CICY matrices are defined only up to permutations and splitting-equivalence, or a polytope is only defined up to $GL(n; \mathbb{Z})$.

How does your smartphone, or, indeed, Google, treat (4.2)? With today's access to data, one can readily proceed to repositories wherein there is a plenitude of writing samples. For example, the NIST (National Institute of Standards) database [342] has some 10^6 actual samples, classified in the form

$$\left\{ \begin{array}{l} 4 \rightarrow 4, \quad 6 \rightarrow 6, \quad 6 \rightarrow 6, \quad 1 \rightarrow 1, \quad 0 \rightarrow 0, \quad 6 \rightarrow 6, \quad 4 \rightarrow 4, \\ 0 \rightarrow 0, \quad 3 \rightarrow 3, \quad 2 \rightarrow 2, \quad 3 \rightarrow 3, \quad 8 \rightarrow 8, \quad 7 \rightarrow 7, \quad 0 \rightarrow 0, \\ 2 \rightarrow 2, \quad 9 \rightarrow 9, \quad 1 \rightarrow 1, \quad 5 \rightarrow 5, \quad 9 \rightarrow 9, \quad 4 \rightarrow 4, \quad 8 \rightarrow 8 \end{array} \right\} \quad (4.3)$$

from which we see large (and in some sense also small) variation in hand-writing.

Returning to the earlier point of representation of pixelated images, one example of the number 3, for instance, would be

The diagram shows a handwritten digit '3' enclosed in a white box on the left, followed by a right-pointing arrow. To the right of the arrow is a large 16x16 matrix with binary values (0s and 1s). The matrix is enclosed in a large curly brace on the right, and another right-pointing arrow is at the end of the brace, followed by the label '(4.4)'.

A few technical remarks here. In the NIST database, the digits are given in 28×28 pixel grayscales. So each pixel, of the 28^2 pixels, is represented by a real number from 0 to 1 (with 1 meaning white and 0, black) in order to designate the level of grey. This could be useful in that when people write, how the strokes taper off and become lighter differs from digit to digit; thus the level of greyscale is an extra feature in the input. For simplicity, we have made the image purely black and white, whereby representing the digit by a binary 28×28 matrix (one can literally see this in the matrix of 1s and 0s above). An ML algorithm would then have to be able to tell that this matrix corresponds to the number 3.

What the likes of smartphones perform is the following four-step procedure:

1. Acquire data: The collection of known cases (input → output), such as (4.3), is commonly called **training data**.
2. Machine-Learn: This is the core algorithm which is slowly dominating all fields of human endeavour, from patient diagnoses, to LHC particle data analysis, to speech and hand-writing recognition, etc. This chapter will be devoted to an invitation to this subject for mathematicians and theoretical physicists;⁶
3. Validate: Once the machine/AI has “learnt” the training data, we can take a set of so-called **validation data**, which, importantly, the machine has *not* seen before. This is in the same format as the training data, with given input and output. Thus we can see how the machine performs by checking the predicted output with the actual output.
4. Predict: If the validation is well-behaved, then the machine-learning is successful and we can use it to predict new output on input heretofore unseen.

We now move to a rapid introduction to machine-learning, and the reader is referred to the canonical textbooks in [230]. Furthermore, there have been several introductory monographs, tailored for the mathematician and the physicist [232], which are also excellent resources. Of course, the entire field of machine-learning has been around for decades and has been an indispensable tool in many areas of science. The famous discovery of the Higgs boson, for instance, could not have been made, without machine-learning the patterns of particle jets. Back in the early days, the human eye had to disentangle hundreds of trajectories in cloud chambers. The amount of data now clearly precludes this possibility.

The explosion in the last decade or so of machine-learning is due to an important advancement in hardware: the gaming industry has brought about the proliferation of graphic processing units (GPUs) in addition to the standard CPU, even to the personal computer. Each GPU is a processor specialized in tensor transformations. Essentially, every personal device now has become somewhat like a super-computer

⁶Indeed, for this audience which is versed in the elements of differential and algebraic geometry and/or quantum field theory and general relativity, the tools in the subject of machine-learning should present no conceptual challenge. This is part of the appeal of the field, it is remarkably simple but extraordinarily powerful and universally applicable, so powerful, in fact, that there is still much which seems almost magical and awaits statements of formal theorems and rigorous proofs.

with thousands of parallel cores. This ready availability of the mini-super-computer has thus given a new incarnation to machine-learning whose algorithms have existed for decades but have been seriously hindered by the limitations of computing power.

Theoretical physics has been no exception in taking advantage of this explosion of technology [279]. The novelty of [203, 204] is the proposal that the machine-learning paradigm can, too, be applied to fields of pure mathematics such as algebraic geometry.

4.2 Rudiments of Machine-Learning

Again, we refer the reader to [232, 319] for marvellous introductions to ML and data science for the mathematician and the physicist. There are canonical references in [230], as well as a more recent and comprehensive introduction [156]. In this book, we will largely focus on supervised ML because of the structure of the mathematical data and the type of problem we wish to study. But first, let us comment on some generalities, especially some of the jargon necessary for the entrance into any subject.

Definition 10 A **point cloud** is a collection of data points, represented, typically, in \mathbb{R}^n .

The first step in data science is representation of the data, which itself is an art. The point cloud is a standard way of collecting the features into vectors in Euclidean space (the \mathbb{R}^n is commonly called the “feature space”), with flat metric.⁷ For example, the matrix in (4.4) could be seen as a point in \mathbb{R}^{28^2} by flattening and concatenating the rows/columns. Of course, and this is especially the case with image processing, one might wish to retain the matrix structure of the input, in which case we will be working with $\mathbb{R}^{28} \otimes \mathbb{R}^{28}$. Much of ML is concerned with extracting information from the point cloud. Typically, n is very large (many features), and it is not immediately clear how to proceed; this has been called the “curse of dimensionality”.

The data points can come with a label or not. The label could be a categorical value where some subsets of the data are assigned one of the discrete categories in a classification. It could also be a continuous value, in which case we have a map from $\mathbb{R}^n \rightarrow \mathbb{R}$. When we have unlabeled data and we wish to find patterns, this goes under the general rubric of **unsupervised ML**. There are sophisticated methods such as clustering analysis, or autoencoder, etc. In this book, due to the type of problems thus far discussed, we will actually only focus on **supervised ML**, where we have *labeled data*, and we shall “train” and “validate”. The labels, as we

⁷Recently, there have been works by none other than Prof. Yau himself in studying the “manifold” nature of data [278]. It has been a particular honour to get him interested in the ML mathematical structures programme [226].

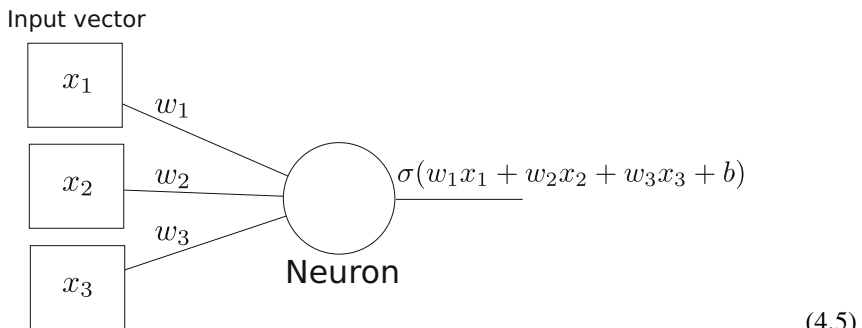
will see, come from the results of often-intensive computation, such as topological invariants of varieties, or properties of groups, or arithmetic of elliptic curves, etc. In this context, the representation of the data point is the “input” while the label is the “output”.

4.2.1 Regression and a Single Neuron

The steps outlined above in addressing (4.3) should remind the reader of first-year undergraduate statistics: it is what one does in **regression**. As a refresher, we leave a concrete example of logistic regression to Appendix D. In fact, supervised ML is but a massive generalization of regression in some sense. In this spirit, we begin with:

Definition 11 A **neuron** or **Perceptron** is a function $f(\sum_I w_I x_I + b)$ which is preferably but not necessarily analytic, whose argument is x_I , a tensor for some multi-index I and whose range is typically in $[0, 1] \subset \mathbb{R}$. The parameters w_I are called weights and b , the bias or off-set.

The multi-index is so that if the input is a vector, we have a single index, if it is a matrix, then I is a pair of indices, etc. We will loosely call w_I a weight vector because it has a single multi-index. The range is usually in $[0, 1]$ in order to imitate the “activation” of an animal neuron, which “fires” or not according to stimuli. Schematically, the perceptron looks like (for vector input x_I , and sigmoid function, for example)



The bias b is included to offset the resulting weighted sum so as to stay in the *active region*. To be more explicit, consider the sigmoid activation function. If we have a large input vector, without a bias, applying a sigmoid activation function will tend to map the output to 1 due to the large number of entries in the sum, which may not be the correct response we expect from the neuron. We could just decrease the weights, but training the neuron can stagnate without a bias due to the vanishing gradient near $f(x) = 1$ and 0.

Thus, standard choices of f are the following:

$$\text{Logistic Sigmoid} \quad (1 + e^{-x})^{-1}$$

$$\text{Hyperbolic tangent} \quad \tanh(x) = \frac{e^x + e^{-x}}{e^x - e^{-x}}$$

Softplus $\log(1 + e^x)$, a “softened” version of **ReLU** (Rectified Linear Unit):
 $\max(0, x)$

$$\text{Parametric ReLU} \quad R(x) = \begin{cases} x, & x \geq 0 \\ \alpha x, & x < 0 \end{cases}$$

$$\text{Softmax} \quad x_i \rightarrow \frac{e^{x_i}}{\sum_i e^{x_i}}$$

$$\text{Maxout} \quad x_i \rightarrow \max_i x_i$$

$$\text{Identity} \quad x_i \rightarrow x_i$$

Note that to all these shapes of f , weights and biases are added, so the last case of the “identity” activation really means an arbitrary affine transformation $x_i \rightarrow w_{ij}x_j + b_i$.

What is astounding is that this idea of imitating the neuron in order to facilitate computation dates as far back as 1957, at the very dawn of computers [317]: Cadmium Sulphide photo-voltaic cells the size of a wall were linked up and stimulated in order to learn/produce pixelated images. The nomenclature “perceptron”, with its charming “-tron” ending probably gives away its 1950–60s origin.

With the neuron, the “training” proceeds as follows:

- The **training data**: $D = \{(x_I^{(j)}, d^{(j)})\}$ with input x_I and *known* output $d^{(j)}$ where j indexes over the number of data points;
- Find an appropriate **Loss Function** (sometimes called the cost-function) whose minimization optimizes the parameters w_i and b . We can define $\widehat{d^{(j)}} := f(\sum_I w_I x_I^{(j)} + b)$, as a “fitted value”. Then, typically, if $d^{(j)}$ is a continuous variable, we use the sum-squared-error (the standard deviation):

$$SD := \sum_j (\widehat{d^{(j)}} - d^{(j)})^2, \quad (4.6)$$

if $d^{(j)}$ is a discrete (categorical) variable, especially in a binary classification where $d^{(j)} = 0, 1$, we use the cross entropy:

$$CE := -\frac{1}{|D|} \sum_j d^{(j)} \log \widehat{d^{(j)}} + (1 - d^{(j)}) \log(1 - \widehat{d^{(j)}}). \quad (4.7)$$

Minimizing these with respect to the weights and biases fixes them;

- The neuron is now “trained” and we can validate against *unseen* data.

Of course, this is precisely (non-linear) regression for model function f . We remark that this, and most of the ensuing discussions, are **supervised ML**, in the sense that there are distinct pairs of inputs and outputs. The machine is “supervised”, as

it were, to associate specific inputs with outputs. Again, the reader is referred to Appendix D for details of a calculation.

4.2.2 MLP: Forward Feeding Neural Networks

Next, we can generalize the neuron to:

Definition 12 A collection of neurons is known as a **layer** where the weight vector w_I is promoted to a weight matrix. We denote the output of the i -th neuron in this layer as f_i such that

$$f_i := f\left(\sum_I W_{iI}x_I + b_i\right).$$

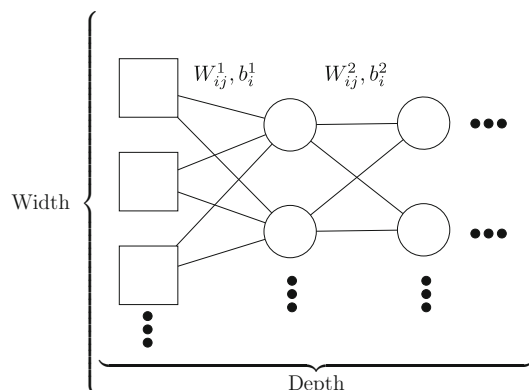
We can certainly string a sequence of layers in the next generalization by extending to several layers:

Definition 13 A **multi-layer perceptron (MLP)** is a sequence of layers where the output of the previous layers is the input to the next layer, applying a different weight matrix and bias vector as we propagate through. All internal layers between the input and output layers are referred to as *hidden layers*. Denoting the output of the i -th neuron in the n -th layer as f_i^n , with $f_I^0 = x_I$ as the input vector,

$$f_i^n = f(W_{ij}^n f_j^{n-1} + b_i^n).$$

Schematically, the MLP looks like Fig. 4.1, where the left-most layer is the *input layer*, the right-most, the *output layer* and everything in between, *hidden layers*. The MLP is the simplest type of a **neural network**, consisting of only forward-propagating layers, as one goes from left to right sequentially in the layers as

Fig. 4.1 Schematic of a forward feeding neural network (multi-layer perceptron). Each node is a neuron, with appropriate activation function with its own weights W and biases b



indicated in Fig. 4.1. In general, a neural network is any finite directed graph of neurons and could consist of backward as well as forward propagation, even cycles in the graph are perfectly allowed. What we therefore have is a **network** of neurons, called a neural network ([Neural Network](#)).

If there are many hidden layers, the neural network is usually called *deep* and the subsequent machine-learning is referred to as **Deep Learning**. The number of neurons/nodes for a layer is called the **width**. We should point out that the words “perceptron” and “MLP” have since fallen out of fashion; today, we simply refer to them, respectively, as “neuron”/“node”, and (multi-layer) “forward feeding NN”.

The “magic” of the NN stems from the historical notion of *connectivism* [156], where computational power is expected to emerge from complexity and inter-connectivity of graphs. To this effect we do have a powerful theorem, which basically shows that one can approximate any input-output (think of the Laurent series being able to approximate any analytic function). There are various ways to phrase this universality; we take the following pair of statements:

Theorem 12 (Universal Approximation Theorem) *We have the following approximations by feed-forward NNs:*

Arbitrary Width *For every continuous function $f : \mathbb{R}^d \rightarrow \mathbb{R}^D$, every compact subset $K \subset \mathbb{R}^d$, and every $\epsilon > 0$, there exists [101] a continuous function $f_\epsilon : \mathbb{R}^d \rightarrow \mathbb{R}^D$ such that $f_\epsilon = W_2(\sigma(W_1))$, where σ is a fixed continuous function, $W_{1,2}$ affine transformations and composition appropriately defined, so that $\sup_{x \in K} |f(x) - f_\epsilon(x)| < \epsilon$.*

Arbitrary Depth *Consider a feed-forward NN with n input neurons, m output neuron and an arbitrary number of hidden layers each with $n + m + 2$ neurons, such that every hidden neuron has activation function φ and every output neuron has the identity activation function.⁸ Then, given any vector-valued function f from a compact subset $K \subset \mathbb{R}^m$, and any $\epsilon > 0$, one can [254] find an F , a NN of the above type, so that $|F(x) - f(x)| < \epsilon$ for all $x \in K$.*

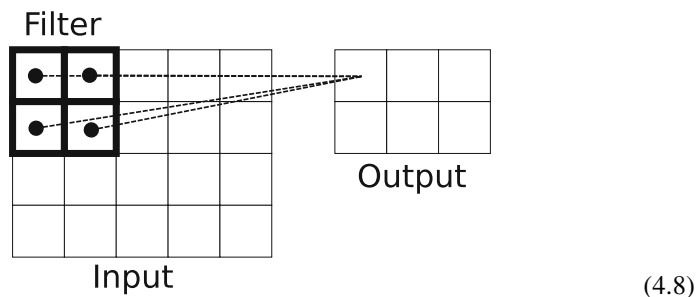
4.2.3 Convolutional Neural Networks

The MLP is one commonly used NN. For image/tensor processing, another widely used one is the *Convolutional neural network* (CNN) which is an alternative type of network that thrives when inputs contain translational or rotational invariance, whereby making them particularly useful for image recognition. We point out that for CNNs, it is important to retain the tensor structure of the input. For example, an $n \times n$ matrix input such as (4.4) is *not* to be flattened into a data point in \mathbb{R}^{n^2} . The neighbouring pixels to a pixel play an important role.

⁸Here $\varphi : \mathbb{R} \rightarrow \mathbb{R}$ is any non-affine continuous function which is continuously differentiable at least at one point and with non-zero derivative at that point.

Like a fully connected, feed-forward layer, convolution layers use a set of neurons which pass a weighted sum through an activation function. However, neurons in convolution layers do not receive a weighted sum from all the neurons in the previous layer. Instead, a *kernel* (not to be confused with the kernel of matrix; this is more of a kernel in the sense of a discrete transform) restricts the contributing neurons.

To be more explicit, consider a two-dimensional input (matrix). A *kernel* will be a grid sized $n \times n$ which convolves across the input matrix, taking the smaller matrix the grid is covering as the input for a neuron in the convolution layer, as exemplified by the following which is a size 2×2 kernel:



The output generated by convolving the kernel across the input matrix and feeding the weighted sums through activations is called a feature map. Importantly, the weights connecting the two layers must be the same, regardless of where the kernel is located. Thus it is as though the kernel window is scanning the input matrix for smaller features which are translationally invariant. For instance, when the kernel window moves one unit to the right, the connected neuron in the output layer will be the centre square in the top row.

In the running examples of the handwritten digit recognition problem, the network may learn to associate rounded edges with a zero. What these features are in reality relies on the weights learned during training. A single convolution layer will usually use several feature maps to generate the input for the next layer.

Of the multitude of NNs in existence, in this book we will only make use of MLPs and CNNs, and with fairly small depth and width. Suffice it to mention in passing that there are recurrence NNs (RNNs) which excel at series prediction, Boltzmann machines which specialize in stochastic decision making, autoencoders which find good lower dimensional representation of the input data, etc.

4.2.4 Some Terminology

It is expedient to summarize, at this point, some of the standard terms used in the ML community. The vastness of the literature and the stylistic differences in

phrasing from mathematics/physics texts may often intimidate the amateur;⁹ here, let us gather, at one glance, a small descriptive lexicon (not in an alphabetical order, but in an attempted narrative).

Architecture: The choice of layers and activation functions which determine a NN is called its architecture. The choice of this, of course, can significantly change the performance.

Backward Propagation (Chain Rule): In the actual optimization of the loss function, be it (4.6) or (4.7), or otherwise, the standard numerical method (going back at least to Cauchy) is **gradient descent** (or often called the method of *steepest descent*). We recall this as follows:

Proposition 7 *To find the (local) minimum \vec{x}^* of a differentiable function $f(\vec{x}) : \mathbb{R}^n \rightarrow \mathbb{R}$, the iteration ($n = 1, 2, \dots, \eta > 0$)*

$$\vec{x}_{n+1} := \vec{x}_n - \eta \nabla f(\vec{x}_n)$$

ensures that $f(\vec{x}_{n+1}) \leq f(\vec{x}_n)$.

The step-size parameter η is commonly called the **Learning Rate**.

In a multi-layer NN one might be overwhelmed by how many gradient descents to perform, since each node in each layer could come with its own optimization, constituting hundreds to thousands of activation functions and even more parameters. Luckily, we are saved by the chain rule. This gives us the flexibility to adjust the weights and biases of a neural network when training, in a consistent manner. It is called *back propagation* in the ML literature and, though a simple corollary of the chain rule, achieves parameter adjustments by optimizing the loss function. It is so named as adjustments are first made to the last layer and then successive layers, moving backwards through the hidden layers.

To illustrate, consider a neural network with M layers and a mean squared error loss function, as in the standard deviation in (4.6),

$$E := \frac{1}{N} \sum_{train}^N \left(\vec{\sigma}^M - \vec{t} \right)^2, \quad (4.9)$$

where N is the number of training entries to which we sum and \mathbf{t} , the expected output for a given entry. Taking derivatives, shifts in the last weight matrix become

$$\frac{\partial E}{\partial W_{ij}^M} = \frac{2}{N} \sum_{train} (\sigma_i^M - t_i) \sigma_i'^M \sigma_j^{M-1}. \quad (4.10)$$

⁹Having myself suffered as an amateur to ML, at least let my pains be not in vain.

Likewise, working backwards, shifts in the second to last weight matrix:

$$\frac{\partial E}{\partial W_{ij}^{M-1}} = \frac{2}{N} \sum_{train} \sum_u (\sigma_u^M - t_u) \sigma_u'^M W_{ui}^M \sigma_i'^{M-1} \sigma_j^{M-2}. \quad (4.11)$$

Defining $\Delta_i^M := (\sigma_i^M - t_i) \sigma_i'^M$ and $\Delta_i^m := \sum_u \Delta_u^{m+1} W_{ui}^{m+1} \sigma_i'^m$, we can write by induction, for an arbitrary layer m ,

$$\frac{\partial E}{\partial W_{ij}^m} = \frac{2}{N} \sum_{train} \Delta_i^m \sigma_j^{m-1}, \quad \frac{\partial E}{\partial b_i^m} = \frac{2}{N} \sum_{train} \Delta_i^m. \quad (4.12)$$

By utilizing our neural network's final output and the expected output, we can calculate the Δ s successively, starting from the last layer and working backwards. We shift the weight values in the direction the gradient is descending to minimize the error function. Thus shifts are given by

$$\Delta W_{i,j}^m = -\eta \frac{\partial E}{\partial W_{ij}^m}, \quad \Delta b_i^m = -\eta \frac{\partial E}{\partial b_i^m}, \quad (4.13)$$

where η is the learning rate. Care must be taken when choosing the learning rate. A rate too small leads to slow convergence and the possibility of becoming trapped in a local minimum. A rate too large leads to fluctuations in errors and poor convergence as the steps taken in parameter space are too large, effectively jumping over minima.

Note that parameter shifts are dependent on the gradient of the activation function. For activation functions such as sigmoid or tanh, this then drives the output of a neuron to its minimal or maximal value, as parameter shifts become increasingly small due to the vanishing gradient. This is advantageous in an output layer where we may want to use binary classification. However, if neurons in hidden layers are driven to their min/max too early in training, it can effectively make them useless as their weights will not shift with any further training. This is known as the *flat spot problem* and is why the ReLU activation function has become increasingly popular. Moreover, there is a version of the universality theorem [193] which essentially states that ReLUs are already good enough:

Theorem 13 (ReLU Universal Approximation) *For any Lebesgue-integral function $f : \mathbb{R}^n \rightarrow \mathbb{R}$ and any $\epsilon > 0$, there exists a fully connected ReLU NN F with width of all layers less than $n + 4$ such that $\int_{\mathbb{R}^n} |f(x) - F(x)| dx < \epsilon$.*

Over-fitting: In any statistical model, it is important that one does not over-fit, i.e., to allow for so many parameters in the model so as to render any dataset to be able to be fitted to any desired model; this must be avoided as the model might do extremely well for a training set and be completely useless for prediction. In regression, as shown in the example in Appendix D, a chosen function may not have too many parameters, but a NN could have tens of thousands of parameters, so it is important to check, especially in light of the Universal Approximation Theorems, that the NN could actually predict something meaningful.

For the neural network, *over-fitting* occurs during training when accuracy against the training dataset continues to grow, but accuracy against unseen data stops improving. The network is not learning general features of the data any more and the complexity of the net architecture has more computing potential than required. The opposite problem is *under-fitting*, using too small a network which is incapable of learning data to high accuracy.

An obvious solution to over-fitting is *early stopping*, cutting the training short once accuracy against unseen data ceases to improve. However, we also wish to delay over-fitting such that this accuracy is as large as possible after stopping.

A common solution is called *Dropout*, which is a technique where neurons in a given layer have a probability of being switched off during one training round. This forces neurons to learn more general features about the dataset and can decrease over-fitting [331]. In practice, one adds a *dropout layer* to an NN which removes, at random, nodes from the previous layer.

Cross-Validation: Another important way to avoid over-fitting, as we had already discussed, is that the ML algorithm be trained and validated on complementary datasets: a labeled dataset \mathcal{D} is split disjointly into $\mathcal{T} \sqcup \mathcal{C}$, the training and validation sets. In order to obtain statistical error, one often performs *n-fold* cross-validation, where \mathcal{D} is split into n disjoint subsets. Training is then performed on $n - 1$ of these chosen at random, and validated on the remaining 1. This is repeated n times to gather standard deviation on the performance.

Goodness of Fit: The performance of a validation can be measured by standard statistical methods. Roughly, supervised ML go under two headings: **regressors**, which treat continuous output/label, and **classifiers**, which treat discrete/categorical output/label. For continuous output, the *R-squared* is used. This is introduced for a regression in Appendix D and we will see it again in Sect. 4.2.6. For discrete output, one first uses *naïve precision*, which is simply the fraction of cases where the predicted category agrees with the actual category. In order to have an idea of false negatives and false positives, one further creates a *confusion matrix*, from which one often computes the *F1-score* and *Matthews' coefficient* as a measure of how close the matrix is to being diagonal. All these quantities deserve a full treatment, and we will define them properly in Sect. 4.2.6. In all cases, these measures of goodness of fit, be they R-squared, F1-score, precision, Matthews' coefficient, etc., are customarily normalized so that they are valued in $[0, 1] \subset \mathbb{R}$, so that 1 means a perfect prediction/validation and 0 means complete uselessness.

Hyper-parameters: The numerical quantities associated with the choice of architecture of NN, such as the number of nodes in a layer, the number of layers, the learning rate, the dropout rates, kernel sizes of CNNs, etc., are called the hyper-parameters. These are chosen before training and are distinguished from the parameters, such as the weights and biases, which are to be optimized during training. Tuning hyper-parameters also can significantly alter performance.

Several methods exist to optimize these hyper-parameters. For the case of a few hyper-parameters, one could search by hand, varying parameters explicitly and training repeatedly until an optimal accuracy is achieved. For the learning rate,

for instance, a commonly used method is the so-called ADAM (adaptive moment estimation) optimizer [257].

A grid search could also be used, where each parameter is scanned through a range of values. However, for a large number of hyper-parameters permitting a large number of values, this quickly becomes an extremely time consuming task. Random searches can often speed up this process, where parameter values are drawn from a random distribution across a sensible range. Finally, random search coupled with a *genetic algorithm* is very much favoured, which effectively begins as a random search but then makes an informed decision on how to *mutate* parameters to increase accuracy.

Regularization : Sometimes the parameters (weights and biases) can become too large in the loss function during optimization. In order to control this, one defines an appropriate norm $|W|$ for a weight tensor W (e.g., sum of squares over all entries), and adds a Lagrange multiplier term $\lambda|W|$ to the loss function.

Data Enhancement : When there is a paucity of data, one can often increase the size by *enhancement*, which means that we add equivalent representations of the same data point multiple times. An example is where the input is a matrix and any row/column permutation thereof represents the same object. We will encounter many such cases later.

Data enhancement is particularly relevant for *imbalanced data* where the number of cases in a classification problem differs significantly across categories. For instance, in a binary classification, suppose we have 10^4 cases of “1” and 10^3 cases of “0”, an ML can obtain great accuracy in predicting all cases to be “1”, which is very misleading. In this case, we throw in equivalent representations for the input for cases corresponding to “0” so that each category has around 10^4 cases. Alternatively, we can *under-sample* the “1” cases by randomly selecting around 10^3 cases for both. Such *balanced* datasets can then be fed to a supervised ML algorithm.

Training Rounds: The training data \mathcal{T} is typically passed over to an ML multiple times; each such a time is called a round or **epoch**. Typically $|\mathcal{T}|$ is large, so it is divided into **batches** (sometimes also called mini-batches) so that with an epoch, we have a number of iterations of passing \mathcal{T} . In particular, therefore,

$$|\mathcal{T}| = (\text{Batch size}) \times (\# \text{ Iterations}).$$

During training, one evaluates the loss function on the validation set as well as the training set (or at least a sample of the validation set) to monitor progress as we go through the batches and the epochs; this loss is then plotted against training rounds/batches. This resulting pair of curves (loss for training and loss for validation) is called the **learning curve** (sometimes also called the training curve), which helps with the visualization of how well the ML algorithm is behaving. It is hoped that they are decreasing functions (up to stochastic fluctuations). If the training curve is decreasing steadily for the training set but struggles to decrease for the validation set, this is often an indication of possible over-fitting.

There are also other possible measures of the learning curve, such as plotting the various measures of goodness of fit against increasing size of \mathcal{T} in a cross-

validation, as we will later see. In this case, it is hoped that the learning curve is an increasing function (up to fluctuations and standard deviation) from 0 to 1.

4.2.5 Other Common Supervised ML Algorithms

Having familiarized ourselves with some basic terms, it is helpful to that the world of ML goes far beyond NNs, which we exemplified with MLPs and CNNs above. In this section, we will introduce a few more which we will use later.

Support Vector Machines

One of the most widely used methods to address high dimensional labeled data is support vector machines (**SVMs**). In contrast to NNs, SVMs take a purely geometric approach and have the advantage of **interpretability**: one can tell the equation (hypersurface) which separates the data into regions. SVM can act as both classifiers and regressors which we shall introduce sequentially.

SVM Classifiers While a neural network classifier essentially fits a large number of parameters (weights and biases) to obtain a desired function $f(\mathbf{v}_{in}) \in [0, 1]$, a SVM tries to establish an optimal hyperplane separating clusters of points in the *feature space*, the n -dimensional Euclidean space to which the n -dimensional input vector belongs. Points lying on one side of the plane are identified with one class, and vice versa for the other.

Thus, a vanilla SVM is only capable of acting as a binary classifier for linearly separable data. This is somewhat restrictive, but the approach can be generalized to non-linearly separable data via the so-called *kernel trick* and likewise can be extended to deal with multiple classes [330]. We illustrate this in Fig. 4.2. We wish

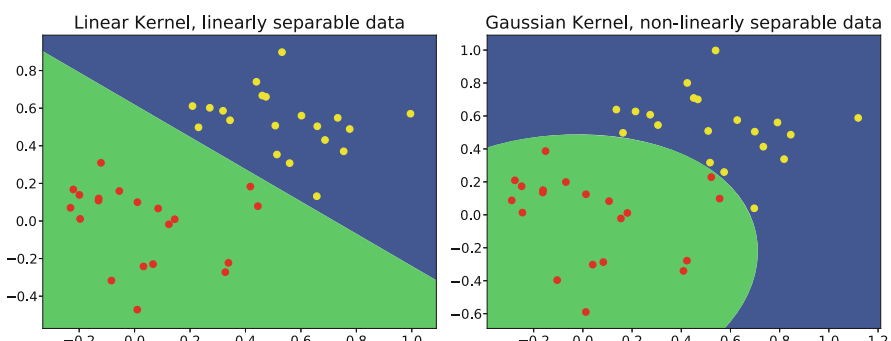


Fig. 4.2 Example SVM separation boundary using different kernels

to separate points \mathbf{x}_i with a hyperplane based on a classification of true/false, which we represent with the labelling $y_i = \pm 1$; this is the so-called binary feature.

First define a hyperplane

$$\{x \in \mathbb{R}^n | f(\mathbf{x}) = \mathbf{w} \cdot \mathbf{x} + b = 0\}, \quad (4.14)$$

where \mathbf{w} is the normal vector to the hyperplane. Then we have that:

Definition 14 **Support vectors** are the points in the feature space lying closest to the hyperplane on either side which we denote as \mathbf{x}_i^\pm .

The **margin** is the distance between these two vectors projected along the normal \mathbf{w} , i.e.,

$$\text{Margin} := \mathbf{w} \cdot (\mathbf{x}_i^+ - \mathbf{x}_i^-) / |\mathbf{w}|. \quad (4.15)$$

There is typically not a unique hyperplane we could choose to separate labeled points in the feature space, but the most optimal hyperplane is one which maximizes the margin. This is because it is more desirable to have points lie as far from the separating plane as possible, as points close to the boundary could be easily misclassified. Note that the condition defining a hyperplane (4.14) is not unique as a re-scaling $\alpha(\mathbf{w} \cdot \mathbf{x} + b) = 0$ describes the same hyperplane. Thus we can re-scale the normal vector such that $f(\mathbf{x}_i^\pm) = \pm 1$ and the margin reduces to

$$\text{Margin} = \frac{2}{|\mathbf{w}|}. \quad (4.16)$$

Moreover, with such a re-scaling, the SVM acts as a classifier on an input \mathbf{x} through the function $\text{sgn}(f(\mathbf{x})) = \pm 1$. In particular, for each point (x_i, y_i) , $y_i = 1$ if $\mathbf{w} \cdot \mathbf{x}_i + b \geq 1$ and $y_i = -1$ if $\mathbf{w} \cdot \mathbf{x}_i + b \leq -1$, so that the product $y_i \times (\mathbf{w} \cdot \mathbf{x}_i + b)$ is always ≥ 1 for each i . Maximizing the margin thus corresponds to minimizing $|\mathbf{w}|$, with the constraint that each point is correctly classified. This wholly defines the problem which can be stated as

$$\text{Min } \frac{1}{2} |\mathbf{w}|^2 \text{ subject to } y_i \times (\mathbf{w} \cdot \mathbf{x}_i + b) \geq 1. \quad (4.17)$$

This is a quadratic programming problem with well-known algorithms to solve it. Reformulating this problem with Lagrange multipliers:

$$\begin{aligned} L &= \frac{1}{2} |\mathbf{w}|^2 - \sum_i \alpha_i (y_i (\mathbf{w} \cdot \mathbf{x}_i + b) - 1) \Rightarrow \\ \frac{\partial L}{\partial \mathbf{w}} &= \mathbf{w} - \sum_i \alpha_i y_i \mathbf{x}_i = 0, \quad \frac{\partial L}{\partial b} = - \sum_i \alpha_i y_i = 0, \end{aligned} \quad (4.18)$$

leads to the *dual problem* upon substitution:

Question 5 Solve the quadratic programming:

$$\begin{aligned} \text{Min } & \frac{1}{2} \sum_{i,j} \alpha_i \alpha_j y_i y_j \mathbf{x}_i \cdot \mathbf{x}_j - \sum_j \alpha_j , \\ \text{subject to } & \alpha_j \geq 0, \quad \sum_j \alpha_j y_j = 0 . \end{aligned} \quad (4.19)$$

With our classifying function now being $\text{sgn}(f(\mathbf{x})) = \text{sgn} \left(\sum_i (\alpha_i y_i \mathbf{x}_i \cdot \mathbf{x}) + b \right)$.

The Python package `Cvxopt` implements a quadratic computing algorithm to solve such problems.

The dual approach is much more illuminating as it turns out the only α_i which are non-zero corresponding to the support vectors [330] (hence the name support vector machine). This makes SVMs rather efficient as unlike a neural network which requires a vast amount of parameters to be tuned; a SVM is fully specified by its support vectors and is ignorant of the rest of the data. Moreover, the quadratic programming optimization implemented via `Cvxopt` ensures the minimum found is a global one.

The dual approach also enables us to generalize to non-linearly separable data rather trivially. In theory, this is achieved by mapping points in the feature space into a higher dimensional feature space where the points are linearly separable, finding the optimal hyperplane and then mapping back into the original feature space. However, in the dual approach, only the dot product between vectors in the feature space is used.

Therefore, in practice we can avoid the mapping procedure as we only need to generalize the dot product in the higher dimensional space, known as a **kernel** (it is unfortunate that the kernel of an SVM, that of a CNN, and that of a matrix, all mean completely different things). Hence, by replacing $\mathbf{x}_i \cdot \mathbf{x}$ with $\text{Ker}(\mathbf{x}_i, \mathbf{x})$ we can deal with non-linearly separable data at almost no extra computational cost. This is known as the *kernel trick* which just replaces the usual dot product to common kernels such as

$$\begin{aligned} \text{Gaussian: } & \text{Ker}(\mathbf{x}_i, \mathbf{x}) = \exp \left(\frac{-|\mathbf{x}_i - \mathbf{x}|^2}{2\sigma} \right) , \\ \text{Polynomial: } & \text{Ker}(\mathbf{x}_i, \mathbf{x}) = (1 + \mathbf{x}_i \cdot \mathbf{x})^n . \end{aligned} \quad (4.20)$$

Indeed, the choice of kernel is another hyper-parameter.

We remark that SVMs reduce to our familiar linear regressor by finding a function $f(\mathbf{x}) = \mathbf{w} \cdot \mathbf{x} + b$ to fit to the data. Analogous to the above discussion, one can frame this as an optimization problem by choosing the flattest line which fits the data within an allowed residue ϵ . Likewise one can make use of Lagrange multipliers and the kernel trick to act as a non-linear regressor as well.

Note in the above discussion we have avoided the concept of slack. In order to avoid over-fitting to the training data, one can allow a few points in the training data to be mis-classified in order to not constrain the hypersurface too much, allowing for better generalization to unseen data. In practice this becomes quantified by replacing the condition $\alpha_i \geq 0$ with

$$0 \leq \alpha_i \leq C , \quad (4.21)$$

where C is the cost variable [330].

SVM Regressors Having discussed SVM as a classifier, its role as a regressor is similar. The optimization problem for a linear SVM regressor follows from finding the flattest possible function $f(\mathbf{x}) = \mathbf{w} \cdot \mathbf{x} + b$ which fits the data within a residue ϵ . As $|\nabla f|^2 = |\mathbf{w}|^2$, this flatness condition reduces to the problem:

$$\text{Min } \frac{1}{2} |\mathbf{w}|^2 \text{ subject to } -\epsilon \leq y_i - (\mathbf{w} \cdot \mathbf{x}_i + b) \leq \epsilon . \quad (4.22)$$

Again, introducing Lagrange multipliers

$$L = \frac{1}{2} |\mathbf{w}|^2 - \sum_i \alpha_i (y_i - (\mathbf{w} \cdot \mathbf{x}_i + b) + \epsilon) + \sum_i \alpha_i^* (y_i - (\mathbf{w} \cdot \mathbf{x}_i + b) - \epsilon) \Rightarrow \\ \frac{\partial L}{\partial \mathbf{w}} = \mathbf{w} - \sum_i (\alpha_i - \alpha_i^*) \mathbf{x}_i = 0, \quad \frac{\partial L}{\partial b} = \sum_i (\alpha_i - \alpha_i^*) = 0 , \quad (4.23)$$

leads to the dual problem:

Question 6 Solve the optimization problem

$$\text{Min } \frac{1}{2} \sum_{i,j} (\alpha_i - \alpha_i^*)(\alpha_j - \alpha_j^*) y_i y_j \mathbf{x}_i \cdot \mathbf{x}_j + \epsilon \sum_i (\alpha_i + \alpha_i^*) + \sum_i y_i (\alpha_i^* - \alpha_i) \\ \text{subject to } \alpha_i, \alpha_i^* \geq 0 , \quad \sum_i (\alpha_i - \alpha_i^*) = 0 . \quad (4.24)$$

Thus, as with the classifier, this optimization problem can be implemented with Cvxopt. As the dual problem again only contains a dot product between two entries in the feature space, we can use the kernel trick to generalize this approach to fit non-linear functions.

Decision Trees

Another widely used classifier is the decision tree. Suppose we have a target variable y and a set of input variables x_i . Typically, y is *discrete*. However, we can treat a

continuous variable as discrete by splitting it into appropriate intervals and taking the average of the interval to be its discretized value. The input, on the other hand, can be arbitrary.

A tree is then built from the input variables as a sequence of if/then/else statements. Starting with x_1 , we create a node and then travel down a “branch” depending on the value of x_1 : if $x_1 \in [a_1, b_1]$ then we proceed to the first branch, if $x_1 \in [b_1, c_1]$, we proceed to a different branch, etc. At the end of each branch we create new node, say for x_2 , from which new branches are created. As before, we then travel down one of these new branches depending on the value of x_2 . Repeating this for all of the input variables gives a set of nodes partially connected by branches, giving a tree structure. The outermost nodes (the leaves) correspond to different predictions for the value of the output variable y . Once the tree structure is established, we can present it with a new input x_i and then follow the tree structure to find the predicted output (the leaf) that it leads to.

As in regression, the optimal parameters ($a_j, b_j, c_j \dots$) are determined by optimizing some goodness-of-fit score, for example, the sum of squares of the error between the actual and predicted target variables. To prevent over-fitting, one often sets a maximum depth for the tree structure or a maximum number of leaves.

In a way, a decision tree can be understood as a highly non-analytic analogue of regression: whereas regression ultimately fits the target into some differentiable function $y = f(x_i)$ by minimizing sum squared errors, a decision tree writes down y from x_i via a sequence of discrete choices. Thus, when the output data y is highly fluctuating with respect to x_i , regression is not so useful since an analytic function f is difficult to find; slotting into a sequence of decisions is much more appropriate.

In order to improve the performance of predictions via decision trees, one can set up an ensemble (or forest) of trees, each with different decision criteria. The overall score of the prediction can be taken to be the sum over all trees. Now, optimizing all parameters in all trees at once could become computationally intractable. Instead, one can take an additive strategy so that the predicted target y is obtained by adding one tree at a time: $y^{(j)} = y^{(j-1)} + g_j(x_i)$ where g_j heuristically represents the function which captures the information about the tree at stage j . The ensemble of trees is thus “boosted” iteratively, and the tree to add at each stage is simply the one which optimizes the overall fitness score.

Naïve Bayes Classifier

Essentially, this classifier is a conditional probability problem. Naïve Bayes is particularly simple but useful for categorical classification, and we now illustrate with a binary case. Suppose our training set is of the form $\mathcal{T} = \{t_i \rightarrow v_i\}$ where each $t_i = t_i^{(a)}$ is a list indexed by a and $v_i \in \{0, 1\}$. First, we recall Bayes’ theorem:

$$P(v|T) = \frac{P(T|v)P(v)}{P(T)}, \quad (4.25)$$

that the probability $P(v|T)$ of v_i occurring contingent on some condition T can be expressed in terms of the reverse $P(T|v)$, and the (marginal) probabilities $P(v)$ and $P(T)$.

Now, v is binary and suppose we are given a new input $T = T^{(a)}$ from the validation set, we wish to compare $P(0|T^{(a)})$ and $P(1|T^{(a)})$, whichever is larger will have the output being 0 or 1 correspondingly. Since the denominators are the same, being some unknown quantity $P(T)$, we luckily do not need to consider it, and simply compare $P(T|0)P(0)$ versus $P(T|1)P(1)$.

Now comes the “naïve” part, which is remarkably powerful. We assume that all entries of t_i are independent, so that

$$P(T|v) = \prod_a P(T^{(a)}|v). \quad (4.26)$$

Therefore, we only need to count in the training set: $P(0)$ is the total percentage of cases with 0 output, and likewise for $P(1)$; $P(T|0) = \prod_a P(T^{(a)}|0)$ is the product over all percentages of components $T^{(a)}$ whose output is 0, and likewise for $P(T|1)$.

The only subtlety that occurs is when a component $T^{(a)}$ has not appeared in the training set, i.e., if $P(T^{(a)}|v) = 0$ for some $T^{(a)}$ and v . This is resolved by so-called *Laplace smoothing*: we add 1 to numerator to any counts c (regardless of whether it is 0 or not), and—to balance it so that the percentage never exceeds 1—add the total number of possible values N_t of $t_i^{(a)}$ to any numerator n . Thus, when we compute any of the percentages above, we always calculate $(c + 1)/(n + N_t)$, instead of c/n . These smoothed percentages are what go into $P(T|0)P(0)$ and $P(T|1)P(1)$ before comparison.

Nearest Neighbours

A very efficient classifier that is quick to implement is the ***k*-nearest-neighbour** algorithm. Take a hyper-parameter k and consider a random sample of k labeled data points from the training set, and suppose these are of the form $\{v_i \rightarrow f_i\}$ where $v_i \in \mathbb{R}^n$ and f_i is some output/label. Fix an appropriate distance d . Suppose the input is a vector of reals, then d could simply be the Euclidean distance in \mathbb{R}^n . If the input were a binary vector, then the Hamming distance (number of positions where the 2 vectors differ) is a good choice. Given a new vector w from the validation set, we simply compute d between w and all k vectors v_i (neighbours) and the label/output for w is that of the nearest by distance.

There are myriad more classifiers and regressors which the readers are encouraged to explore. Hopefully, in this subsection and the previous one, we have familiarized them with some of the most commonly used supervised ML methods, NN and non-NN.

4.2.6 Goodness of Fit

In this final section introducing ML, as promised above, we define some standard measures of accuracies in a prediction, generally called **Goodness of Fit**. Common measures of the goodness of fit include (q.v. [344]).

Definition 15 Let $y_{i=1,\dots,N}$ be the actual output for input x_i in the validation set, and let y_i^{pred} be the values predicted by the machine-learning model on x_i , then

(naive) precision is the percentage agreement of y_i with y_i^{pred}

$$p := \frac{1}{N} |\{y_i = y_i^{pred}\}| \in [0, 1];$$

root mean square error (RMS) $\left(\frac{1}{N} \sum_{i=1}^N (y_i^{pred} - y_i)^2 \right)^{1/2};$

coefficient of determination $R^2 := 1 - \frac{\sum_{i=1}^N (y_i - y_i^{pred})^2}{\sum_{i=1}^N (y_i - \bar{y})^2} \in [0, 1]$

where \bar{y} is the mean over y_i ;

cosine distance Considering y_i and y_i^{pred} as vectors \vec{y} and \vec{y}^{pred} , respectively, compute the cosine of the angle between them so that 1 is complete agreement, -1 , worst fit and 0, random correlation:

$$d_C := \frac{\vec{y} \cdot \vec{y}^{pred}}{|\vec{y}| |\vec{y}^{pred}|} \in [-1, 1];$$

In the cases of categorical data where y_i belong to finite, discrete categories, such as the binary case at hand, there are a few more measures. First, we define:

Definition 16 Let $\{x_i \rightarrow y_i\}$ be categorical data, where $y_i \in \{1, 2, 3, \dots, k\}$ take values in k categories. Then, the $k \times k$ **confusion matrix** has 1 added to its (a, b) -th entry, whenever there is an actual value of $y = a$ but is predicted to $y^{pred} = b$.

Ideally, of course, we want the confusion matrix to be diagonal. In the case of binary y_i as in (4.28), the 2×2 confusion matrix takes the rather familiar form and nomenclature

		Actual		(4.27)
		True (1)	False (0)	
Predicted Classification	True (1)	True Positive(tp)	False Positive(fp)	
	False (0)	False Negative(fn)	True Negative(tn)	

As mentioned above, in categorical classification, we have to be careful about **imbalanced** data. For instance, consider the case where only 0.1% of the data is classified as true. In minimizing its loss function on training, the machine-learning algorithm could naively train a model which just predicts false for *any* input. Such a model would still achieve a 99.9% accuracy as defined by p in Definition 15, but it is useless in finding the special few cases in which we are interested. Thus, naive p is meaningless and we need more discriminatory measures. These measure how diagonal the confusion matrix is.

Definition 17 For binary data, two commonly used measures of goodness of fit, in furtherance to naive accuracy are

F-Score: $F_1 := \frac{2}{\frac{1}{TPR} + \frac{1}{Precision}}$ where [349], using the confusion matrix (4.27),

$$\begin{aligned} TPR &:= \frac{tp}{tp+fn}, & FPR &:= \frac{fp}{fp+tn}, \\ \text{Accuracy } p &:= \frac{tp+tn}{tp+tn+fp+fn}, & \text{Precision} &:= \frac{tp}{tp+fp}. \end{aligned}$$

where TPR (FPR) stands for true (false) positive rate.

Matthews' Correlation Coefficient: Using the confusion matrix (4.27), the Matthew's coefficient is the square root of the normalized chi-squared:

$$\phi := \sqrt{\frac{\chi^2}{N}} = \frac{tp \cdot tn - fp \cdot fn}{\sqrt{(tp + fp)(tp + fn)(tn + fp)(tn + fn)}}.$$

The definition is also generalizable to $k \times k$ confusion matrices [288].

We must guarantee that both F_1 and ϕ are close to 1, in addition to p being close to 1, in order to conclude that the machine-learning model has predicted to satisfaction.

In addition to these measures of accuracy, we have the notion of a confidence interval for the fit.

Definition 18 The Wilson confidence interval is $[\omega, \omega_+]$ where

$$\omega_{\pm} := \frac{p + \frac{z^2}{2n}}{1 + \frac{z^2}{n}} \pm \frac{z}{1 + \frac{z^2}{n}} \left(\frac{p(1-p)}{n} + \frac{z^2}{4n^2} \right)^{1/2}.$$

Here n is the sample size, p is the accuracy or probability of correct prediction within the sample, $z = \sqrt{2}\text{Erf}^{-1}(2P - 1)$ is the probit for a normal distribution.

This is a confidence interval in the sense that with probability P , the Wilson interval contains the mean of the accuracy from the population.

Finally, let us clearly define learning/training curves. To avoid confusion, let us, in this book, call the plot of the loss function during training as the training curve and the plot of appropriate goodness of fit as we increase training size, a learning curve. In other words, we have the following. Let $\{x_i \rightarrow y_i\}_{i=1,\dots,N}$ be N data

points. We choose cross-validation by taking a percentage γN of the data randomly for a chosen $\gamma \in (0, 1]$ as training data \mathcal{T} , the complement $(1 - \gamma)N$ data points will be the validation data \mathcal{C} . Then, we have:

Definition 19 For a fixed γ and hence \mathcal{T} , evaluate the loss function evaluated on \mathcal{T} and \mathcal{C} , against increasing batch size. This produces a pair of curves called the **training curve**;

as well as

Definition 20 Compute a chosen goodness of fit from the above, it is a function $L(\gamma)$ of γ as we increase training size. The **learning curve** is the plot of $L(\gamma)$ against γ .

In practice, γ will be chosen at discrete intervals, for instance in increments of 10% until the full dataset is attained for training. Furthermore, we repeat each random sample γN a number of times, so the learning curve has error bars associated with each of its points.

4.3 Machine-Learning Algebraic Geometry

Armed with an arsenal of technique, we return to the theme of this book, viz., Calabi–Yau data. We have seen in Sect. 4.1 a list of typical problems in computational algebraic geometry, inspired by physical need, all of which can *in principle* be addressed by brute-force methods ranging from Gröbner bases to polytope triangulations, all of which are exponential in complexity.

It is therefore natural to pose the adventurous query:

Question 7 Can AI/ML help with algebraic geometry?

Indeed, can machines help with problems in pure mathematics and theoretical physics, *without* explicit knowledge of the actual methods involved. We know a plethora of cases which *have* been computed by traditional methods and wish to extrapolate to those where computing power hinders us, by essentially bypassing—in a mysterious way, as we shall see—the frontal attacks offered by the likes of Gröbner bases. This is precisely in analogy of the handwritten digit problem: to recognize a new, esoteric written digit is hard, but furnished with tens of thousands of samples already classified by experience, to predict this new digit to good accuracy does not seem impossible. After all, there is inherent pattern, however big the variance, in written digits (or, for that matter, any manuscript).

There are inherent patterns in problems in mathematics; could some of these problems, too, not be amenable to this philosophy?

Of course, this philosophy is not new. It is simply the process of forming a conjecture. There is a long tradition of experimental mathematics from which countless conjectures have been posited, many leading to the most profound consequences. Consider the greatest mind of the eighteenth century, that of K. F. Gauß which can

be considered as the best neural network of the time. By looking at the distribution of primes, supposedly in his teens, Gauß was able to predict that the prime-counting function $\pi(x) \sim x / \log(x)$, a fact which had to wait over a century to be proven by de la Vallée-Poussin and Hadamard, using complex analysis, a method entirely unknown to the eighteenth century.

Minds of the calibre of Gauß are rare, but neural networks of increasing sophistication now abound. Could the combined efforts of AI at least stochastically achieve some correct predictions? In this section, we will see that many, if not most, of the problems discussed in this book could indeed be machine-learned to great accuracy.

4.3.1 Warm-up: Hypersurface in Weighted \mathbb{P}^4

Let us warm-up with the simplest of the input configurations, viz., that of hypersurfaces in $W\mathbb{P}^4$, discussed in Sect. 2.3.1, which is specified by a single 5-vector of co-prime positive integers. To make things even simpler, suppose we wish for a *binary query* of whether $h^{2,1}$ is larger than a certain value, say 50. We know that $h^{2,1} \in [1, 491]$ with the histogram shown in Fig. 2.2; 50 is a reasonable division point. In terms of geometry, we are looking for manifolds which have a relatively large/small number of complex structure deformations, a question of physical interest as well.

Our data, therefore, is of the form $\{x_i \rightarrow y_i\}$:

$$\{1, 1, 1, 1, 1\} \rightarrow 1, \quad \{1, 1, 1, 1, 2\} \rightarrow 1, \quad \dots, \quad \{2, 2, 3, 3, 5\} \rightarrow 0, \dots \quad (4.28)$$

totalling 7555. The first entry, is the quintic Q in regular \mathbb{P}^4 and its $h^{2,1} = 101$ gives a positive hit (denoted as 1) on $h^{2,1} > 50$. Further down the list, the degree 15 hypersurface in $W\mathbb{P}^4[2, 2, 3, 3, 5]$ has $h^{2,1} = 43$, giving us the negative hit (denoted as 0). As mentioned in Sect. 2.3.1, the $h^{2,1}$ values were calculated meticulously by Candelas et al. [77, 78] using Landau–Ginzberg methods (even on **SageMath** (linked to **Macaulay2** or **Singular**), the computation using sequence-chasing is not straight-forward) and the results, though known, quite escape the human eye in any discernible pattern. Again, we note that while the Euler number χ can be expressed in terms of the weights, the individual Hodge/Betti numbers cannot be. This is a generic situation in algebraic geometry and is the story with index-type theorems: individual terms in (co-)homology are difficult to compute, but the index of an exact sequence typically reduces to an integral.

The classification problem in (4.28) constitutes a labeled dataset and lends itself perfectly to supervised ML as a binary classification problem. Of course, this is a somewhat contrived problem, but we will use it, if anything, to present the reader with some **Python TensorFlow** and **Wolfram Mathematica** syntax.

ML $W\mathbb{P}^4$ -Hypersurfaces: Python

Let us take 25% random samples as training data \mathcal{T} , establish a neural network which is a simple MLP with three hidden layers: a linear layer of size 5×50 (i.e., a 5×50 matrix transformation of the 5-vector input), followed by an element-wise sigmoid transformation, and then a linear layer of size 50×10 , before summing up to an integer. This choice of hyper-parameter 50 is purely ad hoc and merely to illustrate. A more serious thing to do would be, as mentioned above, to optimize the network structure and the hyper-parameters such as the sizes of the matrices in the linear layers. To be completely explicit, we will explain the Python [310] code in detail, as we have always done with software throughout the book.

As mentioned, the great thing about SageMath [320] is that its core language is Python-based and we even execute Python from within SageMath (by, for instance, calling sage -ipython as with our early Macaulay2 [163] example in the previous chapters). One could also run a Jupyter notebook from which one can run the ensuing code, after all, WWJD is our guiding question.

We begin with the usual preamble of calling the necessary Python packages: “numpy” for numerical recipes, “scipy” for scientific computing, “matplotlib.pyplot” for plotting, “pandas” for data analysis and “random” for random number generation:

```
import numpy as np
import scipy as sp
import matplotlib.pyplot as plt
import pandas as pd
import random
```

Next, we load the key packages, Tensorflow, the premium Python package for neural networks as well as keras, which is the high-level interface (wrapper) for Tensorflow. From keras, a few standard ones of its layers (most of which we will not use for this example but keep here for illustration) and network structures:

```
import tensorflow as tf
import keras
from keras.models import Sequential,load_mod
from keras.layers import Dense,Activation,Dropout
from keras.layers import Conv1D,Conv2D,MaxPooling1D,MaxPooling2D,Flatten
```

Suppose now we have organized the data in the form (importing from <http://hep.itp.tuwien.ac.at/~kreuzer/CY/> on the “CY/4d” tab, for instance):

```
dataX = [[1, 1, 1, 1, 1], [1, 1, 1, 1, 2], [1, 1, 1, 1, 3],
         [1, 1, 1, 2, 2], [1, 1, 1, 1, 4], ...];
dataY = [1, 1, 1, 1, 1, ...];
```

`dataX` is the *ordered* list of 5-vector weights of $W\mathbb{P}^4$ and `dataY`, whether the corresponding CY3 has $h^{2,1} > 50$. Note that there are 2867 cases of 1 and 4688 of 0, so this is a fairly balanced problem; it so happens in the ordering of the configurations, the first quite a few (the first being the quintic) all have $h^{2,1} > 50$.

From this we split (achieved by the set difference) the data into training \mathcal{T} and validation \mathcal{C} sets as a 25–75% split, and then convert \mathcal{T} and \mathcal{C} into arrays for pre-processing:

```
trainingindex = random.sample([k for k in range(len(dataX))],  
    round(len(dataX)/4)) ;  
validateindex = list(set([k for k in range(len(dataX))]) -  
    set(trainingindex));  
  
trainingX = np.array([dataX[a] for a in trainingindex]);  
trainingY = np.array([dataY[a] for a in trainingindex]);  
  
validateX = np.array([dataX[a] for a in validateindex]);  
validateY = np.array([dataY[a] for a in validateindex]);
```

Finally, we are ready to establish our simple neural network:

```
network = Sequential()  
network.add(Dense(50,activation=None,input_dim=5))  
network.add(Activation('sigmoid'))  
network.add(Dense(10,activation=None))  
network.add(Dense(1))
```

Let us give a few points of explanation here. The `Sequential()` specification indicates that the neural network is an MLP. The first (input) layer, `Dense()`, is a fully connected layer meaning that the input 5-vector will be mapped to 50 nodes in a fully connected way, i.e., the weight matrix will be dotted with the vector, and then, added with a bias, will return a 50-vector. The specification of `activation = None` means it is defaulted to the linear function $f(x) = x$.

The output of the input layer is fed to the first hidden layer, which is an element-wise sigmoid function $\sigma(x)$ defined under Definition 11, which is then sent to the second hidden layer, again a linear, fully connected layer, this time outputting a 10-vector, before finally being sent to the output layer which sums everything into a single number by the `Dense(1)`. Note that only the input layer requires a specification of its input-shape (of dimension 5), and the network will then automatically deal with the subsequent dimensions. We will show a schematic of this shortly.

Having established the network structure, we can train simply by compiling and then fitting

```
network.compile(loss='mean_squared_error', optimizer = 'adam',  
    metrics=['accuracy'])  
network.fit(trainingX,trainingY,batch_size=32,epochs=100,verbose=1,  
    validation_data=(validateX,validateY))
```

In the above, the `batch_size` specifies that the training data is passed in groups of 32 at a time, and the `epochs` means that the data will be passed through the network 100 times to optimize the parameters. The optimizer for the gradient descent is the widely used ADAM, as discussed in Sect. 4.2.4.

Finally, we can use the fitted network to check the validation data by “predicting”:

```
predictY = network.predict(validateX, verbose = 1)[:, 0]
```

where the `[:, 0]` is merely an artefact of the output format of `network.predict()`, which is an array whose every entry is of the form such as `array([1.07], dtype=float32)`, so that we extract only the 0-th entry, viz., the number itself.

This last point is actually rather important: the predicted result is a floating number (real number up to, here, 32 significant digits). Nowhere did we specify in the network structure that the result should be an integer 0 or 1. The optimization performed only finds the best fit over the reals. Therefore, the final answer needs to be rounded. For instance, the error can be obtained by doing

```
error=0;
for a in range(len(train_predict)):
    if(np.round(train_predict[a] - validatey[a]) != 0):
        error+=1;
```

The error turns out to be 375 here.

Let us pause a moment to reflect upon the above calculation. The neural network randomly saw 25% of the 7555 cases of whether $h^{2,1} > 0$, and when optimized, it predicted on the remaining *unseen* 75% of the cases with only 375 errors, i.e., to an accuracy of $1 - 375/(7555 \cdot 75\%) \simeq 93.3\%$, which is rather remarkable, considering the total computation time was less than a minute on an ordinary laptop.¹⁰

ML $W\mathbb{P}^4$ -Hypersurfaces: Mathematica

Before we go on to do more pedantic statistics, it is a comforting fact for the **Mathematica** aficionado that as of version 11.2+ (timely released in 2017), machine-learning has been built into the core operating system, and being such a high-level language, allows the above to be condensed into a few lines of code. Note that, for clarity, we are not using any **Mathematica** shorthand which would even shorten any of the list manipulation commands further.

The reader is highly encouraged to vary all the code below to adapt to his/her own needs, in architecture, hyper-parameters, as well as to explore the multitude of possibilities of which our naive example has touched only the surface. Luckily, by now, **Mathematica** version 12+ has detailed pedagogical documentation on ML, which, back in 2017, was very much lacking.

¹⁰Of course, for this baby example, the actual calculation of over 5600 Hodge numbers for a $W\mathbb{P}^4$ -hypersurface (estimating whether $h^{2,1} > 50$ has no short-cut) would not have been long in any event. Later, we will see how vast reductions in calculation time can be achieved.

We have dataset of the form

```
datah21 = {
  {1, 1, 1, 1, 1} -> 1, {1, 1, 1, 1, 2} -> 1, {1, 1, 1, 1, 3} -> 1,
  {1, 1, 1, 2, 2} -> 1, {1, 1, 1, 1, 4} -> 1, ...
};
```

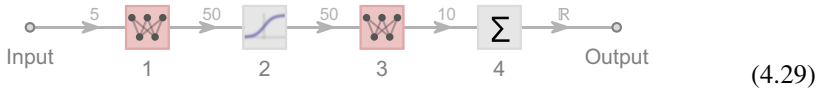
from which we obtain \mathcal{T} and \mathcal{C} as

```
training = RandomSample[datah21, 2000];
validation = Complement[datah21, training];
```

Then, the same neural network as in the previous section, can be specified by:

```
net = NetChain[{LinearLayer[50], ElementwiseLayer[LogisticSigmoid],
  LinearLayer[10], SummationLayer[]}, "Input" -> {5}];
```

This can be visualized by the `Information[net, "SummaryGraphic"]` command:



One can see the input, output, as well as the 3 hidden layers:

1. Input: A vector in \mathbb{R}^5 (for the NN, that the input is in \mathbb{Z}^5 is, in this case, not exploited);
2. A fully connected linear layer that takes the input in \mathbb{R}^5 to \mathbb{R}^{50} (i.e., the most general 5×50 affine transformation).
3. An element-wise logistic sigmoid layer, i.e., $\mathbb{R}^{50} \xrightarrow{\sigma} \mathbb{R}^{50}$.
4. Another fully connected linear layer, an affine transformation $\mathbb{R}^{50} \rightarrow \mathbb{R}^{10}$;
5. Output: A linear layer with no argument is a linear map from \mathbb{R}^{10} to \mathbb{R} ; the output should be a number.

Note that the final output is in \mathbb{R} , so we will need to take integer round-up.

Strictly, what we have done here is a **neural regressor** since we are evaluating the actual value. Of course, it is better to use a **classifier** and in particular to use cross entropy as the loss function. But, this example is purely to illustrate Python and Mathematica implementations, so we chose relatively simple commands.

The training is done by:

```
trainednet = NetTrain[net, training, ValidationSet -> validation,
  Method -> {"ADAM", "LearningRate" -> 1/100}, MaxRounds -> 100];
```

Here, we have used the ADAM optimizer, with learning rate $\eta = 0.01$, as well as 100 iterations of feeding the training set into batches. We have specified to check validation during the training and can see the training curves during the training for the squared-error loss function; this is shown in Fig. 4.3 for both the training set and the validation set. Indeed, they both converge towards 0.

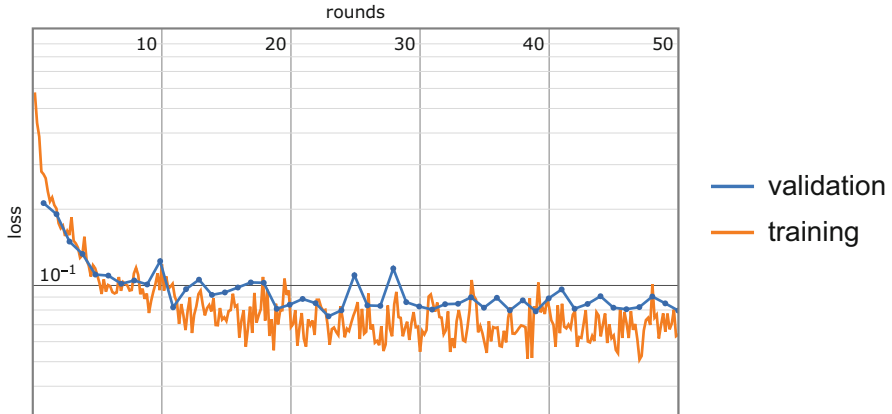


Fig. 4.3 Training curve for NN (4.29) machine-learning whether $h^{2,1} > 50$ for a hypersurface Calabi–Yau threefold in $W\mathbb{P}^4$, for both training and validation sets as we feed batches into the training

We can check the predictions against the validation set by (note the integer round):

```
actual = Table[validation[[i, 2]], {i, 1, Length[validation]}];
predict = Table[Round[net[validation[[i, 1]]]],
{i, 1, Length[validation]}];
```

This gives us a confusion matrix $\begin{pmatrix} 3669 & 361 \\ 83 & 1931 \end{pmatrix}$, giving us naïve precision 0.926, F-score 0.896 and Matthews' $\phi = 0.844$.

In the above, we set the training-validation split at around 20%; as an extra check, we can see how the various goodness of fit behaves as we increase the training size. The learning curve for this problem is presented in Fig. 4.4 (recall that we made, for clarity, a distinction between the learning curve and training curve in Definitions 19 and 20).

We have repeated, at each incremental interval of 5%, the training/prediction 10 times, which gives us the error bars. There is a large error when the seen training data is less than 10%, as expected—the network simply has not seen enough data to make a valid prediction. However, starting at 20%, as discussed above, we are already looking at 96% precision with Matthew's ϕ -coefficient around 0.9. The curve is slowly but steadily climbing to around 97% precision and $\phi \sim 0.92$ at around 80% seen data. All of this is indeed reassuring. The neural network can estimate a solution to our complex structure problem to very high precision and confidence at orders of magnitude less computation time.

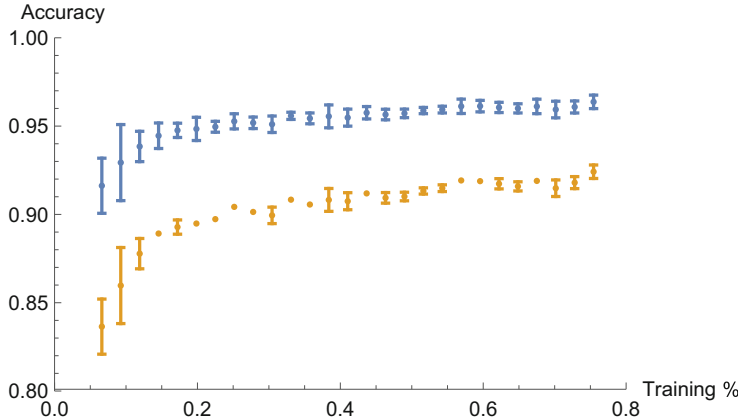


Fig. 4.4 Learning curve for NN (4.29) machine-learning whether $h^{2,1} > 50$ for a hypersurface Calabi–Yau threefold in $W\mathbb{P}^4$. The blue (top curve) is the naïve precision and the orange (bottom curve) is Matthews’ ϕ

Non-NN ML methods

As we mentioned in footnote 10, to treat the present example with ML, especially NNs, is quite an overkill. We have chosen this warm-up not only to illustrate **Python** and **Mathematica** syntax, but also because of the simplicity of the representation of the input: a 5-vector of integers. We close this subsection with some non-NN methods.

First, we can think of the data as a labeled point cloud in \mathbb{R}^5 and apply SVM to see whether there is separation. To this effect, the simple **Mathematica** command (retaining the variables “training” and “validation” from the above)

```
cc = Classify[training, Method -> {"SupportVectorMachine",
    "KernelType" -> "RadialBasisFunction"}];

actual = Table[validation[[i, 2]], {i, 1, Length[validation]}];
predict = Table[cc[ validation[[i, 1]] ], {i, 1, Length[validation]}];
```

In the above, we have specified the SVM kernel (4.20) to be Gaussian (here called “`RadialBasisFunction`”; one could also choose “`Linear`” or “`Polynomial`”). The result is comparable to the NN in (4.29), for example, we obtain naïve precision of around 0.936. Moreover, one could find the parameters in the Gaussian kernel by `Information[cc, "GammaScalingParameter"]`, which gives $\gamma := \frac{1}{2\sigma}$, and `Information[cc, "BiasParameter"]`, which gives $b = 1$. The bias is 1 here because we have labeled our categories as 0 and 1, while in the search for the support hyperplane described in (4.17), they are ± 1 .

Of course, the problem at hand is simple enough that one could even try a straight-forward regression, similar to Appendix D:

$$f(w_i) = \sigma \left(\sum_{i=0}^4 w_i x_i + b \right), \quad (4.30)$$

where x_i are the 5 components of the input and (w_i, b) are coefficients (weights and bias if you will) to be optimized. Note that the sigmoid function σ already has range $[0, 1]$, so it is perfect for binary classifications. Moreover, we are not doing cross-validation here since there are only 6 parameters, and there is no danger of over-fitting some 8000 data points.

The **Mathematica** command is¹¹

```
datah21regress = Table[ Flatten[ {datah21[[i,1]], datah21[[i,2]]}], {i,1,Length[datah21]}];
vars = Table[x[i], {i, 1, 5}];
coefs = Flatten[ {Table[w[i], {i, 1, 5}], b} ];
model = NonlinearModelFit[datah21regress,
    LogisticSigmoid[ Sum[w[i] x[i], {i, 1, 5}] + b ], coefs, vars ],
```

From this, we can extract the R-squared as `model["RSquared"]`, giving us $R^2 \sim 0.843$. Again, we can take integer round to obtain the predicted¹² values:

```
predict = Table[ Round[ model@@(datah21[[i,1]]) ], {i,1,Length[datah21]}];
actual = Table[ datah21[[i, 2]], {i, 1, Length[datah21]} ];
```

This gives us naïve precision 0.919, F-score 0.892 and Matthews' $\phi = 0.827$, which is comparable to the NN and the SVM. As with the SVM, we have interpretability, the coefficients in the model can be explicitly found, using `Normal[model]`, here, we find

$$b \sim 6.901, w_i \sim (2.529, -0.273, -0.060, 0.0079, 0.046). \quad (4.31)$$

4.3.2 Learning CICYs

Emboldened by the success in the warm-up, we can proceed to more sophisticated inputs. A CICY, we recall, is an integer matrix with number of rows ranging from 1 to 12 and number of columns, from 1 to 15, and whose entries are 0 to 5. As far as the computer is concerned, this is a 12 array of arrays (by down-right padding

¹¹The reason we had to restructure the data upfront is esoteric: regression in **Mathematica** is not considered an ML algorithm so it does not like the arrow notation for “input → output”, but rather prefers “(input, output)”.

¹²We use `model@ @` rather than `model[]` because the input is a list and `model` is a function of 5 variables, so we need to “thread” the function over the input list.

with zeros) with 6 discrete entries. In other words, it is a 12×15 pixelated image with 6 shades of grey (or 6 different colours). For instance, this very colourful representation [203] for the CICY which is the complete intersection of 8 equations in $(\mathbb{P}^1)^5 \times (\mathbb{P}^2)^3$ would be

$$\left(\begin{array}{ccccccc|c} 1 & 1 & 0 & 0 & 0 & 0 & 0 & 0 \\ 1 & 0 & 1 & 0 & 0 & 0 & 0 & 0 \\ 0 & 0 & 0 & 1 & 0 & 1 & 0 & 0 \\ 0 & 0 & 0 & 0 & 1 & 0 & 1 & 0 \\ 0 & 0 & 0 & 0 & 0 & 0 & 2 & 0 \\ 0 & 1 & 1 & 0 & 0 & 0 & 0 & 1 \\ 1 & 0 & 0 & 0 & 0 & 1 & 1 & 0 \\ 0 & 0 & 0 & 1 & 1 & 0 & 0 & 1 \\ \hline & & & & & & 0 & \\ & & & & & & 0 & \\ \end{array} \right) \xrightarrow{\sim} \begin{array}{|c} \hline \text{purple} \\ \text{green} \\ \text{red} \\ \hline \end{array} \quad 12 \times 15 \quad (4.32)$$

where purple is 0, green, 1 and red, 2. This is a CY3 with Hodge pair $(h^{1,1}, h^{2,1}) = (8, 22)$ (and thus $\chi = -28$); that $h^{1,1}$ is equal to the number of product projective spaces means it is favourable. For the reader's amusement, the *average* CICY as an image was drawn in *cit. ibid.*

Now, we have shown in Sect. 2.1 how to compute individual $h^{1,1}$ or $h^{2,1}$ from the configuration matrix. Even for the simplest case of the quintic, some substantial machinery such as long exact sequences in cohomology is needed. And, even if one were to do this on a computer using **Macaulay2**, the Grobner basis will render all but the simplest configurations intractable. Yet, at the end of the day, we have an output as succinct as the number 22 (say, if we were interested in $h^{2,1}$). How different indeed is this association "colourful matrix" in (4.32) → 22 any different from (4.4) in recognizing the digit 3? Indeed, it was the similarity that prompted the investigations in [203].

With such an image, one could use a CNN to process it, much like hand-writing recognition. While we will not do so here, the point of presenting the manifold in this way is to emphasize the fact that the computer knows absolutely nothing about the algebraic geometry, or even that the image should correspond to a geometry. We can associate to the image, an integer (such as the topological numbers), much as one associates a value to a handwritten scribble. Yet with enough samples of correct values we can teach the machine how to "guess" the right values. This is feasible because there is an inherent pattern in algebraic geometry, regular enough to be "learnt".

In [203, 204], the analogous NN approach to testing CICY Hodge numbers as the one presented in detail above for $W\mathbb{P}^4$ was performed. A more insightful and

comprehensive analysis¹³ specifically for CICYs was then done in [63, 64]. The input data is a CICY configuration (image) and one can try the following structures to study not just whether one of the Hodge numbers exceeds a value, but the precise value of, say, $h^{1,1}$. This is obviously of great importance as we are actually going to let the machine calculate the exact value of a topological invariant simply by experience:

NN regressor: The output is continuous (i.e., some real number which we will then round-up); optimal neural network hyper-parameters were found with a genetic algorithm, leading to an overall architecture of five hidden layers with 876, 461, 437, 929 and 404 neurons, respectively. The algorithm also found that a ReLU activation layer and dropout layer of dropout probability 0.2072 between each neuron layer give optimal results.

SVM: The output is one of the possible values for $h^{1,1}$, viz., an integer¹⁴ between 0 and 19, inclusive; here the hyper-parameters were found to be a Gaussian kernel with $\sigma = 2.74$, as well as slack $C = 10$ and margin $\epsilon = 0.01$ (recall that these quantities were defined in Sect. 4.2.5, in Eqs. (4.20)–(4.22)).

NN classifier: the output is a 20-channel classifier (like handwritten digits being a 10-channel classifier) with each neuron mapping to 0 or 1. The optimal architecture can be found to be four convolution layers with 57, 56, 55 and 43 feature maps, respectively, all with a kernel size of 3×3 . These layers were followed by two hidden fully connected layers containing 169 and 491 neurons respectively, and finally followed by the output layer. ReLU activations and a dropout of 0.5 were included between every layer, with the last layer using a sigmoid activation.

Importantly, training with a laptop took in the order of 10 minutes and execution on the validation set, seconds. The actual Hodge computation of the CICYs, on the other hand, was a stupendous task.

The performance is again quite satisfactory, for a 25–75% split of training versus validation (the machine has only seen 1/4 of the data!) and we have the various accuracy measures for the 3 above methods as

	Accuracy	RMS	R^2	ω_-	ω_+	
NN Regressor	0.78 ± 0.02	0.46 ± 0.05	0.72 ± 0.06	0.742	0.791	
SVM Reg	0.70 ± 0.02	0.53 ± 0.06	0.78 ± 0.08	0.642	0.697	
NN Classifier	0.88 ± 0.02	—	—	—	$0.847 \quad 0.886$	

(4.33)

¹³Though I am very much an amateur to data science, I must use this opportunity to thank my former Masters student Kieran Bull from Oxford, who was the torch-bearer for [63]. With admiration I joke with him that he eats 2000 lines of Python for breakfast, and, in retrospect, he probably did.

¹⁴An artefact of the CICY dataset is that $h^{1,1} = 0$ is a marker for a trivial CY3, such as the direct product $(T^2)^3$.

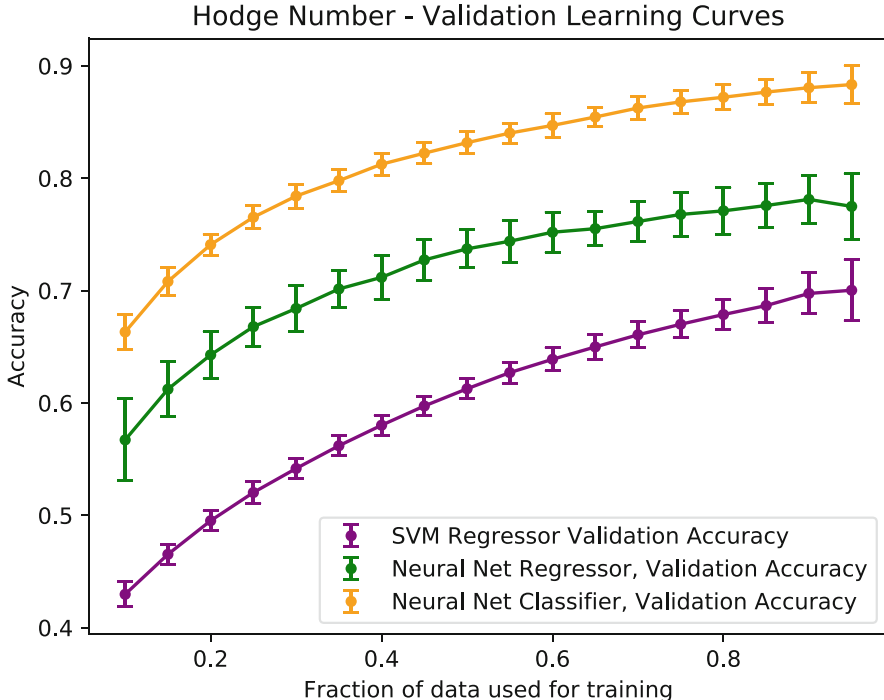
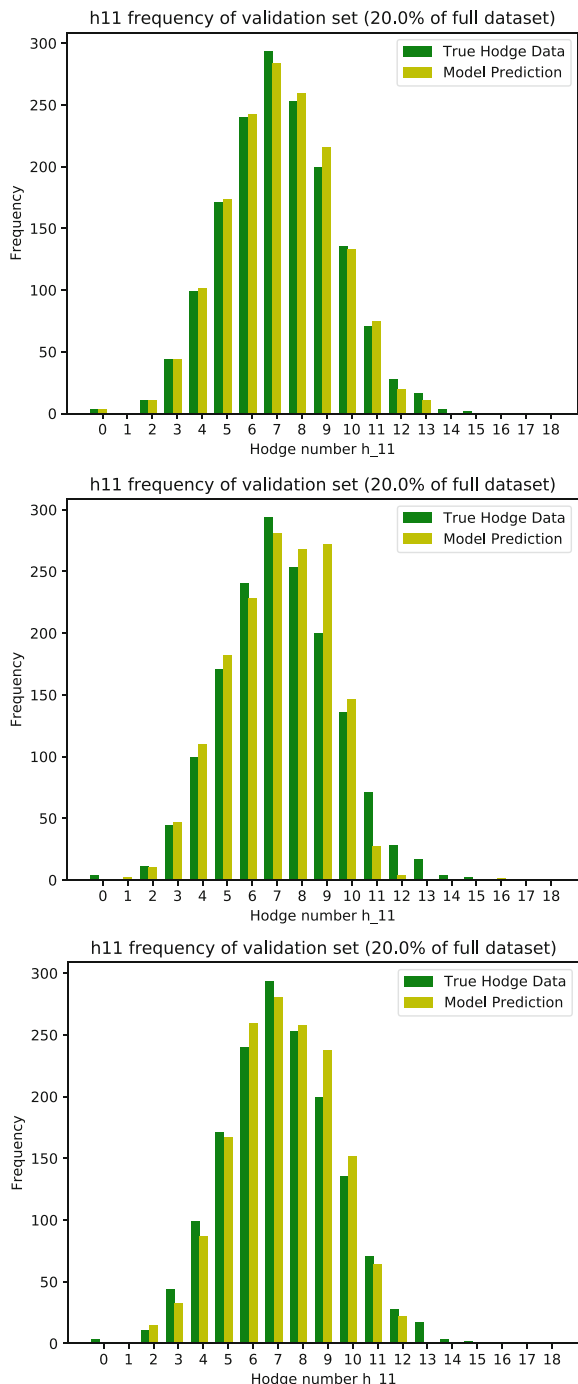


Fig. 4.5 Hodge learning curves generated by averaging over 100 different random cross-validation splits. The accuracy quoted for the 20 channel (since $h^{1,1} \in [0, 19]$) neural network classifier is for complete agreement across all 20 channels

In the above, the error bars come from repetition over 100 random samples, the dashes for the RMS and R^2 are because these are only defined for continuous variables, and ω_{\pm} give the Wilson confidence interval. Moreover, we have put in bold face the best performance. Recently, a systematic study using the so-called Google Inception CNN was carried out [130, 130] on the CICYs and accuracies in the vicinity of 99% have been achieved.

Reassured by the prediction based only on 1/4 of seen data, the learning curves for the above three different methods are presented in Fig. 4.5. We see that interestingly the SVM seems to be the best performer, quite quickly reaching 90% accuracy. For reference, we also demonstrate, in Fig. 4.6, the comparative performance among the 3 methods at 20% seen training data, for each of the 20 values of $h^{1,1}$, checked against the 80% unseen validation data. We recall from Fig. 2.1 that the distribution for $h^{1,1}$ is approximately Gaussian, peaked at 7, for CICYs.

Fig. 4.6 The histogram of predicted versus actual CICY $h^{1,1}$ at 20–80% training-validation split, for (1) the neural network classifier, (2) regressor, and the SVM regressor



4.3.3 More Success Stories in Geometry

Over the last few years, there have been various success stories along the lines of the above in applying ML to problems in algebraic geometry, especially in the context of the CY landscape. We will list some of the main directions below, in line with what we have covered in this book.

The KS Dataset An enormous challenge with the KS dataset is that the half-billion polytopes, each of which gives a certain Hodge pair according to (2.31), but could lead to many topologically inequivalent CY3s with the same $(h^{1,1}, h^{2,1})$. To compute the Chern numbers and the intersection form (q.v. (2.22)) requires full triangulation of the polytope (thus, the KS dataset actually produces several orders of magnitude more than 473,800,776 CY3s!).

While this has been done systematically for the low-lying cases [7, 110, 345], to do so for the full list is many orders of magnitude beyond current computer abilities. Could one train on these known cases in a supervised machine-learning and predict what c_2 and d_{rst} would most likely be and thus complete the topological data for the KS set?¹⁵ On a simpler level, could one predict how many triangulations—and hence different candidate CY₃ manifolds—there should be? Recently, an ML estimate using equation learners was nicely performed for the full KS set in [8] and an astounding 10^{10^5} number of total triangulations was proposed. Recently, in [111], a beautiful upper bound of the number of fine, regular, star triangulations of the set was found to be $\binom{14,111}{494} \simeq 10^{928}$.

The CICY Dataset Other than ML of the CICY threefold Hodge numbers discussed in detail above, it is natural to also consider that of the CY4 version, a dataset of CICY4s which was created in [162]. The Hodge numbers for these also responded well to MLPs and to a branched forward-feed NN [212]. In parallel, elliptic fibrations were classified within the CICY3 set by Anderson et al. [14]; again, with a simple MLP or an SVM, these can be distinguished [211] to high accuracy.

Bundle Cohomology There is, of course, nothing special about configuration matrices; these, as we saw, are degrees of the normal bundle in the embedding into the ambient projective space. Line bundles, or sequences of line bundles, can be likewise represented. Bundle cohomology is subtle and depends on regions in moduli space; these have nevertheless been computed over the years. The novel approach of genetic algorithms was employed to compute bundle cohomologies in [318] and applied to the string landscape. Likewise, cohomology of bundles of

¹⁵If one has the c_2 and d_{rst} , one could pursue many serious phenomenological questions. For example, certainly properties of the d_{rst} (so-called Swiss-cheese [93]) single out manifolds which can be used in cosmology. However, the computation to decide whether a manifold is Swiss-cheese is very computationally intensive [161]. Machine-learning the dataset in distinguishing such manifolds while not being impeded by the expensive steps would be much desired.

CICY and KS manifolds [262, 275] respond well to ML algorithms. Of particular note is [57, 94], where, having obtained 100% accuracy, the authors were able to conjecture new analytic expressions for bundle cohomology, which were then proven using classical algebraic geometry.

Numerical Metrics and Volumes Numerical volume of Sasaki–Einstein bases of affine CYs is an important quantity [65, 127, 223, 287]. ML has been applied to these with success [265]. Likewise, volumes of hyperbolic knots and related Jones polynomials respond well to MLPs [245]. Furthermore, we discussed in Sect. 2.7 the Donaldson algorithm for numerically computing CY metrics, and mentioned its complexity as more and more monomials are required. With a decision tree classifier, one could speed this up by almost two orders of magnitude [17].

Outlook However apparent the power of ML, much of it does remain mysterious: of all the intricate connections among the neurons, or optimization of kernels and hyperplanes, what exactly is doing what? As Yau critiques, “there are no theorems in machine-learning”. Indeed, for a pure mathematician of his calibre, getting a topological invariant correct 99% of the time may not be precise enough. Nevertheless, getting such a quick estimate *entirely bypassing the expensive steps such as polytope triangulation, or finding a Gröbner basis or finding the ranks of all the matrices in an exact sequence* is salient enough for practical purposes that the endeavour is well worth pursuing. One concrete line of attack might be:

Let P be a problem in algebraic geometry with a simple answer (such as an integer); reduce its computation to its constituent parts (typically finding kernels and cokernels of matrix maps¹⁶); test which of these is being out-performed by the likes of a neural network or SVM, and how.

We will address the problem of ML to pure mathematics shortly, but, from an applicability point of view for the physics, the potential is already enormous. As mentioned in the end of the first chapter, Calabi–Yau compactifications with the naturally endowed tangent bundle constitute only a small portion of the heterotic landscape. More sophisticated methods now use stable holomorphic vector bundles on manifolds with non-trivial fundamental groups in obtaining the *exact* standard model. This is a much richer and phenomenologically interesting landscape of geometries which involve the much more intractable task of computing bundle-valued cohomology groups. Initial attempts to find exact standard models from CY constructions using ML are already under way [43, 83, 107, 295, 301, 318]. Indeed, once we have more efficient methods of numerical metrics [17], getting particle masses in realistic string standard models will finally be within reach.

What about beyond Calabi–Yau geometry? We know the string landscape extends far beyond Calabi–Yau manifolds and touches deeply upon G_2 -manifolds, generalized Kähler manifolds and more. The paradigm of machine-learning alge-

¹⁶Even finding the Gröbner basis, in a chosen basis of monomials in the variables, reduces to tensor manipulation. In the case of toric varieties, the problem can be entirely phrased in combinatorics of polytopes whose vertices are extracted from the exponents of monomials [133].

braic geometry is clearly of interest to physicists and mathematicians alike, and applicable to varieties other than Calabi–Yau manifolds. What can they say about computing topological or rational invariants in general? We leave all these tantalizing challenges to the dedicated reader.

4.4 Beyond Algebraic Geometry

Encouraged by our string of successes, one might be led astray by optimism. While there are, by definition, patterns in all fields of mathematics, machine-learning is not some omnipotent magical device, nor an oracle capable of predicting any pattern. Otherwise, we might as well use it to guess the position of the Riemann zeros or similar such questions of profound consequences. Indeed, one would expect problems in number theory to not be particularly amenable to our paradigm.

We therefore finish with a sanity check that machine-learning is not a magic black box predicting all things. A reprobate¹⁷ example which should be doomed to failure is the primes. Indeed, if a neural network could guess some unexpected pattern in the primes, this would be a rather frightening prospect for mathematics. Suppose we have a sequence of labeled data

$$\begin{aligned} \{2\} &\rightarrow 3; \\ \{2, 3\} &\rightarrow 5; \\ \{2, 3, 5\} &\rightarrow 7; \\ \{2, 3, 5, 7\} &\rightarrow 11; \dots \end{aligned} \tag{4.34}$$

One can easily check that even with millions of training data, any neural network or SVM would be useless in prediction and that we are better off with a simple regression against the $n \log(n)$ curve in light of the Prime Number Theorem.

Perhaps the reader is worried about the huge variation in the output, that only some form of highly specialized regressor would do well (this had indeed been the experience from the various cases in Sect. 4.3.3). To re-assure the reader, let us make it as simple as possible. We set up the data as follows:

1. Let $\delta(n) = 0$ or 1 be the prime characteristic function so that it is 1 when an odd number n is prime and 0 otherwise (there is no need to include even numbers);
2. Consider a “sliding window” of size, say, 100 , and consider the list of vectors $\{\delta(2i + 1), \dots, \delta(2(i + 100) + 1)\}_{i=1,\dots,50000}$ in \mathbb{R}^{100} . This is our input;
3. For output, consider the prime characteristic of some distinct number from each window, say, $\delta(2(i + 100 + k) + 1)$ for $k = 10,000$.

¹⁷In Calvinist heresy, a reprobate is a soul doomed for condemnation. I am grateful to my wife Dr. Elizabeth Hunter He, an expert on Reformation history, for teaching me this.

We thus have a binary classification problem of binary vectors, of the form (we have ordered the set with a subscript for reference)

$$\begin{aligned} \{1, 1, 1, 0, 1, 1, \dots, 1, 0, 1, 1, 0, 0\}_1 &\rightarrow 0 ; \\ \{1, 1, 0, 1, 1, 0, \dots, 0, 1, 1, 0, 0, 0\}_2 &\rightarrow 0 ; \\ \dots \\ \{1, 0, 0, 0, 0, 0, \dots, 0, 0, 0, 0, 1, 0\}_{600} &\rightarrow 1 ; \dots \end{aligned} \tag{4.35}$$

Now, the primes are distributed fairly rarely ($\pi(x) \sim x/\log(x)$ among the integers), so we down-sample the 0-hits to around 9000 each of 0 and 1. Applying various classifiers it was found that the k-nearest neighbour (using $k = 50$ and Hamming distance) worked best, at naïve precision around 0.77 and Matthews $\phi \sim 0.60$. While this is perhaps somewhat surprisingly good¹⁸ and deserves further investigation, the performance is visibly not as good as the algebro-geometric experiments in this chapter, with precision in the 0.99 range.

This principle of algebraic geometry being more susceptible to ML than number theory could be approximately understood. At the most basic level, every computation in algebraic geometry, be it a spectral sequence or a Gröbner basis, reduces to finding kernels and cokernels of sets of matrices (over \mathbb{Z} or even over \mathbb{C}), albeit of quickly forbidding dimensions. Matrix/tensor manipulation is exactly the heart of any machine-learning—after all, this why the `TensorFlow` package is called `TensorFlow`—and what ML is good at. Number theory, on the other hand, ultimately involves patterns of prime numbers which, as is well known, remain elusive. Nevertheless, a natural question comes to mind as to

How well do different branches of mathematics respond to ML?

Is the intuitive hierarchy of difficulty, from numerical analysis to Diophantine problems, wherein the former has an abundance of methods, while the latter is provably undecidable by Matiyasevich (Hilbert 10-th), somewhat in line with the performance of ML algorithms? This question is one of the author's current programmes and we shall report some preliminary results here.

Algebra and Representation Theory Trying a sample from the GAP database of finite groups and rings [338], questions such as (1) whether one could distinguish a Cayley multiplication table from a random collection of Latin squares (Sudokus), or (2) whether one could recognize a finite simple group by looking at its Cayley table (admittedly a difficult problem) were fed into the supervised ML paradigm [210]. With SVM classifiers, precision on the order of 0.90 and 0.99 can be achieved

¹⁸This might have something to do with the fact that recognizing whether an integer is prime or not has (only recently!) been unconditionally determined by the AKS algorithm [2] to be $\log(n)^{7.5}$. We remark that the same binary classification experiment, using more erratic functions such as the Liouville lambda-function (which counts even/odd number of prime factors) instead of the prime characteristic δ , gave naïve precision around 0.50 and Matthews $\phi \sim 0.001$, which means that the ML algorithm is doing as well as a random guess.

at 20–80 cross-validation for the 2 problems, respectively. For continuous groups, simple MLPs were applied [85] to some of the most important calculations for Lie groups, viz., tensor product decompositions and branching rules; these also reached accuracies in the 0.90 range.

In representation theory, particularly in relation to quivers, an important concept is *cluster mutation* (in physics, this is Seiberg duality and we alluded to this in Chap. 3), and there has been much work in establishing datasets of equivalence classes under mutation, both in the physics and the mathematics communities. A Naïve Bayes classifier [24] was found to distinguish between various different mutation classes up to the 0.90–1.00 precision range. Closely related is the ML of the plethystic programme [26] of Hilbert series (q.v. Appendix B.2), where 0.90–0.99 accuracies can be achieved in recognition of information such as dimension, degree and complete intersection.

Combinatorics Using the Wolfram database of finite simple graphs [358], experiments were carried out on how many properties can be predicted by ML from the adjacency matrix alone [216]. While the focus was mainly on Ricci-flatness of graphs, a discrete analogue of the CY property and common properties were also tested, primarily with an SVM. It was found that cyclicity and Ricci-flatness can be learned with accuracies in the 0.92–0.95 range, while classical problems such as existence of Euler and Hamiltonian cycles were in the 0.73–0.78 range. It is quite interesting how the Euler problem (which has linear complexity in number of edges by the Hierholzer algorithm) and the Hamiltonian problem (which is extremely hard and in fact NP-complete) have similar responses to an SVM classifier.

Number Theory As mentioned from the outset, problems and patterns in number theory are subtle. A frontal attack on the primes is ineffectual. Likewise, it was found that ML predictions to relevant quantities in the Birch–Swinnerton-Dyer conjecture had very limited accuracies [6]. However, some problems in arithmetic geometry, residing in between algebraic geometry and number theory, have met with surprising success. The classification of degree of Galois extension from examining the permutation structure of *dessins d'enfants* has 0.90–0.93 range of accuracies by simple ReLU MLPs [225]. Classification of properties such as complex-multiplication and Sato–Tate groups for hyper-elliptic curves over the rationals, which ordinarily requires highly refined techniques, can be classified, using Naïve Bayes, to 0.99–1.00 accuracies [226]. Similarly, finding the degree and rank of extensions of number fields over \mathbb{Q} from the zeta coefficients is also in the >0.9 range of accuracies [224].

4.5 Epilogue

We have followed the colourless skein of history throughout the book, keeping track of the discovery of the manifolds and the compilation of the datasets in tune with the contemporaneous developments in mathematics and physics. Though the area

of machine-learning geometry and applying the latest results from data science to treat the landscape is still in its infancy, and much of its inner workings are still perplexing, its power is apparent and its potential, vast. This new paradigm should prove useful as both a *classifier* and *predictor* of geometrical quantities. The ability to rapidly obtain results stochastically, before embarking on to intensively compute from first principles is at once curious and enticing. What we have sacrificed in complete confidence and analytical result, we have gained by improving the computation time by many orders of magnitude. And, for pure mathematics, when 100% accuracies are reached, through unconventional ways, new conjectures and directions can be proposed.

To quote Boris Zilber, Professor of Mathematical Logic at Merton College, Oxford, “you have managed syntax without semantics.” This is an astutely appropriate analogy, not only for our present context but also for AI research for mathematics in general. The prowess of machine-learning is precisely its not taking a reductionist framework where all intermediate quantities are computed analytically from first principles—much like our earlier comment of trying to recognize hand-writing by setting up Morse functions—but by gathering large quantities of data to probabilistically find latent patterns.

Nevertheless, the “AI mathematician” and the “AI physicist” are already being devised, not only from the automated theorem-proving point of view [298, 352], but from the ML perspective over the last year or so. In physics, the NN *SciNet* has been employed to discover Newtonian mechanics from motion data [243], while AI Feymann [346] has led to symbolic regression analysis of data leading to fundamental laws. In mathematics, ML of symbolic algebra [274] and the so-called *Ramanujan machine* in generating new (continued-fraction) identities [311] have already met with success. Indeed, the linguistic structure of ArXiv, from its titles alone, upon using the NN *Word2Vec*, already tells us a lot about the field of study [222].

It is interesting to see that in the first decades of the twentieth century, theoretical physicists had to learn algebraic geometry, and in its last decades, many mathematicians turned to learn some theoretical physics; now, in the dawn of the twenty-first, it is AI which can be put to “learn” some tricks of the trade. We are reminded of many species of primates who have learned to effectively use herbal medicine by trial and error without any idea of chemical composition. Perhaps confronting the vast landscape of mathematics and theoretical physics, the human mind is still learning by tentation.

Chapter 5

Postscriptum



Thus concludes our excursion into the *terra sancta* of Calabi–Yau manifolds. From the compact landscape of CICYs and KS hypersurfaces to the non-compact vista of quiver representations and Sasaki–Einstein cones, from the computational algebraic geometry of topological invariants to the combinatorics of convex polytopes and rational cones, and from the plethora of data compiled into readily accessible webpages to the *terra incognita* of machine-learning algebraic geometry, I hope the reader has beheld the richness of the grounds, fertile with mathematics, physics and data science.

Though from these alluring terrains we now pause to return to our mundanities, our orisons shall continue to drift to this lofty pursuit that transcends disciplines, and so it is only fitting to close with an excerpt¹ from the master himself, the “Ode to Time and Space” by Prof. S.-T.Yau:

...

大哉大哉，宇宙之謎。美哉美哉，真理之源。
時空量化，智者無何。管測大塊，學也洋洋。

丘成桐先生：時空頌

¹ The Chinese poem is written in the antique style (1 millennium BC), rather than more familiar classical style (the height of which is the seventh–eighth centuries AD); I will attempt a translation here. “The mysteries of the Cosmos, how grand thou art; the font of Truth, how beauteous thou art. To quantize time and space, the Wise knows not the ways; the world though the dioptra, endless study fills the days.”

Appendix A

Some Rudiments of Complex Geometry

In this appendix, we give a lightning recapitulation of the key concepts from complex geometry which we use throughout the text. Other than the canonical texts [169, 194], the reader is also referred to brief, self-contained expositions in [47, 71], both of which do a wonderful job in rapid initiation.

A.1 (Co-)Homology

First, let us recall some standard facts on homology and cohomology of real manifolds. For a compact, smooth, differential manifold M of dimension n , we can define differential p -forms $\eta^{(p)}$ as elements of $\Omega^p := \bigwedge^p T_M^\vee$, the p -th antisymmetric power of the cotangent bundle T_M^\vee , as well as a differential operator $d : \Omega^p \rightarrow \Omega^{p+1}$ satisfying $d^2 = 0$. Whence, we have the (de Rham) *cohomology* group $H_{dR}^p(M; K) = \ker(d)/\text{Im}(d)$ for $p = 0, \dots, n$, where K is the set, typically \mathbb{Z} or \mathbb{R} , wherein the coefficients for the linear combination of the elements take value.

We can take the dual to the above to define an appropriate *homology*, for instance, simplicial homology, where one approximates the cycles C_q of M of each dimension $q = 0, \dots, n$ by the Abelian group freely generated by the (standard) simplices at dimension q . Here we have a boundary operator $\partial : C_q \rightarrow C_{q-1}$, satisfying $\partial^2 = 0$, giving us the *homology* group $H_q(M; K) = \ker(\partial)/\text{Im}(\partial)$ for $q = 0, \dots, n$. The duality is furnished by the inner product $H^p \times H_p \rightarrow K$, integrating a p -form over a p -cycle. The non-degenerate, positive-definiteness of this inner product renders H^p isomorphic to H_p . The rank of H^p (and thus also of H_p) is the p -th Betti number b_p from which we obtain the Euler number of M as $\chi = \sum_{p=0}^n (-1)^p b_p$. Though we mentioned in passing, in the Prologue, bundle-valued cohomology groups,

throughout this book we will not actually make use of them in any substantial way. Hence, we will not introduce Čech cohomology here.

Our running example of T^2 , a manifold of (real) dimension 2, will serve to illustrate the above points. We have 3 homology groups $H_{q=0,1,2}$, where H_0 is the class of the point (the torus is connected), and H_2 , that of the entire T^2 . Thus $b_0 = b_2 = 1$. Moreover, H_1 has two inequivalent generators: the 2 circles, since $S^1 \times S^1 = T^2$. Thus, $b_1 = 2$. The dual is to think of forms: let x, y be the coordinates on T^2 (or of the plane of which T^2 is the quotient by a lattice), H^0 is just the constant function; H^2 is generated by $dx \wedge dy$; and H^1 is generated by dx and dy . Thus again, $b^0 = b^2 = 1$ and $b^1 = 2$. Importantly, $b_0 - b_1 + b_2 = 0$, which is the Euler number of T^2 , consistent, via Gauß-Bonnet, with the fact that T^2 is Ricci-flat.

A.2 From Real to Complex to Kähler

Next, we recall the following sequence of specializations by imposing incremental structures to [manifolds](#)

Riemannian M is endowed with a positive-definite symmetric metric g ; With this metric, we can define the Hodge star operator $\star : \Omega^p \rightarrow \Omega^{n-p}$ as $\star(dx^{\mu_1} \wedge \dots \wedge dx^{\mu_p}) := \frac{\epsilon^{\mu_1 \dots \mu_n}}{\sqrt{|g|}} g_{\mu_{p+1} \nu_{p+1}} \dots g_{\mu_n \nu_n} dx^{\nu_{p+1}} \wedge \dots \wedge dx^{\nu_n}$ so that a Laplacian Δ can be defined:

$$\Delta_p = dd^\dagger + d^\dagger d = (d + d^\dagger)^2, \quad d^\dagger := (-1)^{np+n+1} \star d \star .$$

Importantly, Harmonic p -forms can be put into 1-1 correspondence with elements of cohomology, that is, $\Delta_p \eta^p = 0 \longleftrightarrow \eta \in H_{dR}^p(M)$. This allows us to solve for the zero-modes of the Laplacian to find representatives in (co-)homology, rather than to compute the often more involved quotient \ker/im .

Complex M is further endowed with a complex structure $J : T_M \rightarrow T_M$, inducing the split $\Omega^p = \bigoplus_{r+s=p} \Omega^{r,s}$ so that we have (p,q) -forms with p -holomorphic and q -antiholomorphic indices. Clearly, n needs to be even at this point. Subsequently, the operator d also splits to $d = \partial + \bar{\partial}$, together with $\partial^2 = \bar{\partial}^2 = \{\partial, \bar{\partial}\} = 0$.

Hermitian The Riemannian metric on M further obeys $g(J_, J_) = g(_, _)$, so that in local coordinates $g_{\mu\nu} = g_{\bar{\mu}\bar{\nu}} = 0$ and we only have the mixed components $g_{\mu\bar{\nu}}$. This is the Hermitian metric. At this point we can define **Dolbeault Cohomology** $H_{\bar{\partial}}^{p,q}(X)$ as the cohomology of $\bar{\partial}$ (we could equivalently use ∂) with Laplacian $\Delta_\partial := \partial\partial^\dagger + \partial^\dagger\partial$ and similarly $\Delta_{\bar{\partial}}$.

Kähler

With the Hermitian metric one can define a Kähler form $\omega := ig_{\mu\bar{\nu}}dz^\mu \wedge d\bar{z}^\nu$ such that $d\omega = 0$. This, in particular, implies that $\partial_\mu g_{\nu\bar{\lambda}} = \partial_\nu g_{\mu\bar{\lambda}}$ so that $g_{\mu\bar{\nu}} = \partial\bar{\partial}K(z, \bar{z})$ for some scalar function (the Kähler potential) $K(z, \bar{z})$. Now, the Laplacian becomes $\Delta = 2\Delta_{\bar{\partial}} = 2\Delta_{\bar{\partial}}$, and we have the **Hodge decomposition**

$$H^i(M; \mathbb{C}) \simeq \bigoplus_{p+q=i} H^{p,q}(M) = \bigoplus_{p+q=i} H^q(M, \bigwedge^p T_M^\vee), \quad i = 0, 1, \dots, n. \quad (\text{A.1})$$

In the above, we have written ordinary complex-valued cohomology in terms of Dolbeault cohomology in the first equality and in terms of bundle-valued cohomology in the second, where T_M^\vee is the cotangent bundle of M , dual to the tangent bundle T_M , and \wedge^p gives its p -th wedge (antisymmetric tensor) power.

A.3 Bundles and Sequences

The only bundles we use in the book are the tangent, the cotangent and line bundles over a projective space A , their restrictions to an algebraic variety M living in A , as well as the normal bundle of M . Thus, instead of boring the reader with standard definitions, let us simply illustrate with the case of [Complex projective space](#) as well as a variety of degree d therein.

Let us begin with \mathbb{CP}^1 . This is just S^2 as a real manifold. To see this, we notice that \mathbb{CP}^1 has 2 local patches by definition. The homogeneous coordinates are $[z_0 : z_1]$, so patch U_0 is where $z_0 \neq 0$ and the local affine coordinates are $(1, z_1/z_0)$. Similarly, patch U_1 is where $z_1 \neq 0$ and the local coordinates are $(1, z_0/z_1)$. Clearly, each patch is homeomorphic to \mathbb{C} , parametrized by a single complex coordinate, respectively, $w_0 := z_1/z_0$ and $w_1 := z_0/z_1$. The transition function between the two patches is thus $w_1 = 1/w_0$ on the intersection $U_0 \cap U_1 = \mathbb{C}^* = \mathbb{CP}^1 \setminus \{0, \infty\}$.

On the other hand, S^2 has 2 famous local patches, the north and south. Embed S^2 , with unit radius and centre at the origin, into \mathbb{R}^3 , with Cartesian coordinates (x, y, z) . The two patches are the upper and lower hemispheres. Projection from the north pole at $(0, 0, 1)$ puts the upper hemisphere in bijection with the plane $z = 0$ through the equator, giving stereographic coordinates $(X_N, Y_N) := (\frac{x}{1-z}, \frac{y}{1-z})$. Similarly, projection from the south pole at $(0, 0, -1)$ puts the lower hemisphere in bijection with the $z = 0$ plane with stereographic coordinates $(X_S, Y_S) := (\frac{x}{1+z}, -\frac{y}{1+z})$. The complexification $Z := X_N + iY_N$ and $W := X_S + iY_S$ then furnishes coordinates Z and W , respectively, for the 2 patches, with transition function $W = \frac{x-iy}{1+z} = \frac{1-z}{1+z}(X_N - iY_N) = \frac{X_N - iY_N}{X_N^2 + Y_N^2} = 1/Z$.

Thus, we see the same two patches, with the same transition functions between \mathbb{CP}^1 and S^2 , whereby identifying them as (real) manifolds. Unfortunately, the above

algebra does not work for any of the higher even-dimensional spheres, and S^2 is the only sphere which is complex (and in fact also Kähler: being complex dimension 1, the differential of the Kähler 2-form trivially vanishes).

Let us proceed to *bundles* on \mathbb{CP}^1 . Of course, there is the tangent bundle $T_{\mathbb{CP}^1}$, which is locally a 1 complex dimensional vector space, with coordinate $\frac{\partial}{\partial w_i}$ for $i = 0, 1$ for each of the 2 patches. Dual thereto is the cotangent bundle $T_{\mathbb{CP}^1}^\vee$, a dual 1 complex dimensional vector space (locally), with coordinate $d w_i$.

The final important example of a vector bundle we will use is the bundle $\mathcal{O}_{\mathbb{CP}^1}(k)$ called the *line bundle of degree k*, which, when without ambiguity, is often just written as $\mathcal{O}(k)$. The construction, adhering to the 2 aforementioned patches with coordinates w_0 and w_1 , is as follows. Consider $U_{i=0,1} \times \mathbb{C}$ with coordinates (w_i, ξ_i) so that locally each is $\mathbb{C} \times \mathbb{C}$. Glue them by the transition function $w_0 = 1/w_1$ and $\xi_0 = \xi_1/(w_1)^k$ for some $k \in \mathbb{Z}$ at the intersection. This is the vector bundle of rank 1 (meaning that the local vector space is of complex dimension 1) and is denoted as the line bundle $\mathcal{O}_{\mathbb{CP}^1}(k)$.

All these above discussions are readily generalized to \mathbb{CP}^n , with $n + 1$ local patches. Some relevant properties of $\mathcal{O}_{\mathbb{CP}^n}(k)$ are

- The case of $k = 0$, i.e., $\mathcal{O}_{\mathbb{CP}^n}$, is the trivial bundle over \mathbb{CP}^n ;
- The global sections (i.e., globally defined continuous maps from the base \mathbb{CP}^n to the bundle) for $k > 0$ are the homogeneous degree k polynomials in the projective coordinates w_0, w_1, \dots, w_n , i.e., with monomials $w_0^{k_0} \dots w_n^{k_n}$ as the basis; the trivial bundle $k = 0$ has only constant section and $\mathcal{O}_{\mathbb{CP}^n}(k)$ has no sections for $k < 0$; The space of global sections is written as the bundle-valued cohomology group $H^0(\mathbb{CP}^n, \mathcal{O}_{\mathbb{CP}^n}(k))$;
- The *dual* bundle to $\mathcal{O}_{\mathbb{CP}^n}(k)$ is $\mathcal{O}_{\mathbb{CP}^n}(-k)$;
- The canonical bundle $K := \wedge^n T_{\mathbb{CP}^n}^\vee$ is simply the line bundle $\mathcal{O}_{\mathbb{CP}^n}(-n - 1)$. We see that \mathbb{CP}^n is Fano in that the anti-canonical bundle K^\vee is positive degree.
- As degree k polynomials are obtained by multiplication of the variables, we have that $\mathcal{O}(k) = \mathcal{O}(1)^{\otimes k}$, the tensor product over the degree 1 line bundle;
- Line bundles are rank 1, we can also form rank m bundles by direct sum (Whitney sum) $\mathcal{O}(k_1) \oplus \mathcal{O}(k_2) \oplus \dots \oplus \mathcal{O}(k_m)$.

Everything we have said so far is on \mathbb{CP}^n . The entire field of algebraic geometry is about realizing manifolds as polynomials in an appropriate ambient space. In this book, we are only concerned with Kähler manifolds M embedded into projective space (i.e., realized as projective varieties) or into toric varieties,¹ we can obtain bundles on M by restriction. For example, the CY₁ as an elliptic curve \mathcal{E} in \mathbb{CP}^2 is a cubic hypersurface. We can restrict the bundle $\mathcal{O}_{\mathbb{CP}^2}(k)$ on \mathcal{E} . Care must be taken in general to ensure that this restriction remains a bundle (rather than a sheaf). The most important fact we will need here is that the *normal bundle* which defines \mathcal{E} is

¹Note that though infinite numbers of toric varieties are projective varieties, not all are.

the bundle prescribed by the degree of the embedding hypersurface, in other words, $N_{\mathcal{E}} = \mathcal{O}_{\mathbb{CP}^2}(3)$.

We mentioned above that one can obtain higher rank bundles from the Whitney sum, which locally is just the direct sum of the vector spaces. Another non-trivial way is to build them from *Exact sequence*. Instead of launching into the vast subject of homological algebra, it suffices to review some generalities. Suppose we have objects (be they vector spaces, bundles, groups, etc.) A_i as well as maps $f_i : A_i \rightarrow A_{i+1}$ so that a sequence can be written as

$$\dots \xrightarrow{f_{i-1}} A_i \xrightarrow{f_i} A_{i+1} \xrightarrow{f_{i+1}} \dots . \quad (\text{A.2})$$

If $\ker(f_{i+1}) = \text{Im}(f_i)$ for each i , then the sequence is called **exact**. The most important case is when we have 3 objects A, B, C , maps $f : A \rightarrow B, g : B \rightarrow C$, and

$$0 \hookrightarrow A \xrightarrow{f} B \xrightarrow{g} C \rightarrow 0 \quad \ker(g) = \text{Im}(f) . \quad (\text{A.3})$$

Here the first map from 0 is the trivial inclusion and the last map to 0 is the trivial map. Such a case² is called a *short exact sequence*.

The most important sequence of bundles we will use in this book is the Euler sequence for \mathbb{CP}^n :

$$0 \rightarrow \mathcal{O}_{\mathbb{CP}^n} \rightarrow \mathcal{O}_{\mathbb{CP}^n}(1)^{\oplus(n+1)} \rightarrow T_{\mathbb{CP}^n} \rightarrow 0 , \quad (\text{A.4})$$

from which we have the useful corollary that for a projective variety $M \subset \mathbb{CP}^n$,

$$0 \rightarrow T_M \rightarrow T_{\mathbb{P}^n}|_M \rightarrow N_{M/\mathbb{P}^n} \rightarrow 0 . \quad (\text{A.5})$$

This states that the tangent bundle of the ambient space \mathbb{CP}^n , when restricted to M , is composed of the tangent bundle and the normal bundle of M inside the ambient space. Note that locally, the middle term is just the direct sum,³ but the structure of the bundle dictates that globally this “splitting” does not hold and we need the short exact sequence.

Of course, not all sequences are exact. When it is not so but nevertheless $\text{Im}(f_i) \subset \ker(f_{i+1})$ in (A.2), we can do something interesting. Note that this subset condition, written in a more familiar way, is simply $f^2 = 0$. Hence, we can define

²The prototypical example is $0 \xrightarrow{i} \mathbb{Z} \xrightarrow{f} \mathbb{Z} \xrightarrow{g} \mathbb{Z}/(2\mathbb{Z}) \xrightarrow{p} 0$ where f is multiplication by 2 and g is integer modulo 2. We see that (a) $\text{Im}(i) = \{0\}$ and $\ker(f) = \{0\}$; (b) $\text{Im}(f) = 2\mathbb{Z}$ since f is multiplication by 2 and $\ker(g) = 2\mathbb{Z}$ since only even numbers reduce to 0 modulo 2; and (c) $\text{Im}(g) = \{0, 1\} = \mathbb{Z}/(2\mathbb{Z})$ and $\ker(p) = \mathbb{Z}/(2\mathbb{Z})$ since p is the zero map so its kernel is the full pre-image. Hence, the sequence is exact at every stage and we have a short exact sequence.

³Think of embedding S^2 into \mathbb{R}^3 , the direct sum of tangent space at a point and the normal vector together composes \mathbb{R}^3 .

the homology of a sequence as $H_i := \ker(f_{i+1})/\text{Im}(f_i)$. With this we are familiar. When A_i are the (vector) spaces of i -forms and f_i are the differentiation operators d_i , H_i is (de Rham) cohomology. When A_i are the freely generated Abelian groups of i -simplices and f_i are the boundary operators ∂_i , H_i is (simplicial) homology.

The final fact on bundles and sequences we need in this book is the following. Given a short exact sequence of bundles $0 \rightarrow V_1 \rightarrow V_2 \rightarrow V_3 \rightarrow 0$ on a manifold M , this induces a long exact sequence in bundle-valued cohomology $H(M, V)$:

$$\begin{aligned} 0 \rightarrow H^0(M, V_1) &\rightarrow H^0(M, V_2) \rightarrow H^0(M, V_3) \rightarrow \\ &\rightarrow H^1(M, V_1) \rightarrow H^1(M, V_2) \rightarrow H^1(M, V_3) \rightarrow \end{aligned} \quad (\text{A.6})$$

The fancier way of saying this is that the cohomological functor $H^*(M, \bullet)$ is covariant and left exact on short exact sequences.

A.4 Chern Classes

One of the most distinguishing properties of vector bundles on manifolds is their characteristic classes, especially the [Chern class](#), which we use in this book. In this section, we will begin with the differential-geometric definition, before proceeding to the algebro-geometric.

The Ricci curvature 2-form also assumes a particularly simple form for M Kähler, which in local coordinates, is

$$R = -i\partial_\mu\bar{\partial}_{\bar{\nu}} \log \det(g) dz^\mu \wedge d\bar{z}^{\bar{\nu}}. \quad (\text{A.7})$$

This is a $(1, 1)$ -form which as a real 2-form is closed. Hence, we can define the **Chern classes** $c_k(M) = c_k(T_M) \in H^{2k}(M)$ as

$$\det\left(\mathbb{I}_{n \times n} + \frac{it}{2\pi} R\right) = \sum_{k=0}^{n/2} c_k(M) t^k. \quad (\text{A.8})$$

As we will always take a more algebraic rather than differential approach, we can think of the Chern classes more axiomatically [194]. In the above we defined the Chern classes of M , understood as those of the tangent bundle T_M ; they can be defined for arbitrary bundles.

Definition 21 Let E be a complex vector bundle of rank r over our manifold M (i.e., locally, $E \simeq M \times \mathbb{C}^r$). Then the Chern classes $c_k(E) \in H^{2k}(M; \mathbb{Z})$, together with their associated formal sum (the total Chern class)

$$c(E) := c_0(E) + c_1(E) + \dots + c_r(E),$$

obey the axiomata

- Leading term: $c_0(E) = 1$ for any E ;
- Naturality: if $f : N \rightarrow M$ is a continuous morphism from manifold N to M and $f^*(E) \rightarrow N$ is the pull-back vector bundle, then

$$c_k(f^*E) = f^*c_k(E) ;$$

- Whitney sum: If $F \rightarrow X$ is another complex bundle on M , then

$$c(E \oplus F) = c(E) \wedge c(F) \quad \rightsquigarrow \quad c_k(E \oplus F) = \sum_{i=0}^k c_i(E) \wedge c_{k-i}(F) ;$$

- Normalization: For complex projective space \mathbb{CP}^n , let H be the Poincaré dual to the hyperplane class $\mathbb{CP}^{n-1} \subset \mathbb{CP}^n$. Then for the degree 1 bundle $\mathcal{O}_{\mathbb{P}^n}(1)$ whose transition functions are linear (the dual $\mathcal{O}_{\mathbb{P}^n}(-1)$ is the tautological bundle),

$$c(\mathcal{O}_{\mathbb{P}^n}(1)) = 1 + H .$$

We remark that the Whitney sum generalized to a short exact sequence of bundles (*a splitting principle* due to Grothendieck) gives

$$0 \rightarrow E \rightarrow G \rightarrow F \rightarrow 0 \quad \Rightarrow \quad c(G) = c(E) \wedge c(F) . \quad (\text{A.9})$$

Furthermore, for the *dual bundle* E^\vee , we have that

$$c_i(E^\vee) = (-1)^i c_i(E) . \quad (\text{A.10})$$

We can reorganize the Chern class into a *character* from $(\oplus, \otimes) \rightarrow (+, \wedge)$ called the *Chern character* $\text{Ch}()$.

$$\text{Ch}(E \oplus F) = \text{Ch}(E) + \text{Ch}(F) , \quad \text{Ch}(E \otimes F) = \text{Ch}(E) \wedge \text{Ch}(F) . \quad (\text{A.11})$$

The total Chern class does not enjoy this nice property, For a line bundle (i.e., rank 1) L , the Chern character is $\text{Ch}(L) := \exp(c_1(L))$, and more generally for a rank r bundle E , using the splitting principle into line bundles, $E = \bigoplus_{i=1}^r L_i$, we have that

$$\text{Ch}(E) := \sum_{i=1}^r \exp(c_1(L_i)) = \sum_{m=0}^{\infty} \frac{1}{m!} \sum_{i=1}^r c_1(L_i)^m = \text{Ch}_0(E) + \text{Ch}_1(E) + \dots$$

where

$$\begin{aligned}\text{Ch}_0(E) &= \text{rk}(E), \\ \text{Ch}_1(E) &= c_1(E), \\ \text{Ch}_2(E) &= \frac{1}{2}(c_1(E)^2 - 2c_2(E)), \\ \text{Ch}_3(E) &= \frac{1}{6}(c_1(E)^3 - 3c_1(E)c_2(E) + 3c_3(E)), \dots\end{aligned}\tag{A.12}$$

The recasting of Ch_i in terms of the c_i is an exercise in Newton symmetric polynomials. The Chern character of more sophisticated combinations such as antisymmetric products, crucial in physics, can be similarly obtained (cf. Appendix A of [116]).

Finally, we will also be making use of the Todd class. It is yet another combination of the Chern classes, here multiplicative over \oplus , i.e.,

$$\text{Td}(E \oplus F) = \text{Td}(E) \wedge \text{Td}(F).\tag{A.13}$$

Much like the Chern class, we have the expansion:

$$\begin{aligned}\text{Td}(E) &= 1 + \text{Td}_1(E) + \text{Td}_2(E) + \text{Td}_3(E) + \dots, \text{ where} \\ \text{Td}_1(E) &= \frac{1}{2}c_1(E), \\ \text{Td}_2(E) &= \frac{1}{12}(c_2(E) + c_1(E)^2), \\ \text{Td}_3(E) &= \frac{1}{24}(c_1(E)c_2(E)), \dots\end{aligned}\tag{A.14}$$

In general, the above are obtained from the series expansion of $x(1 - e^{-x})^{-1}$. One can invert the above to obtain, for instance, the top Chern class, from an identity of Borel-Serre (cf. 3.2.5 of [146])

$$\sum_{i=0}^r (-1)^i \text{Ch}(\bigwedge^i E^\vee) = c_r(E) \text{Td}(E)^{-1}.\tag{A.15}$$

A.5 Covariantly Constant Spinor

We discussed in the Prologue that physicists first came across Ricci-flat, Kähler manifolds by considering heterotic string compactifications. While we refer the reader to the excellent pedagogical material in Vol. 2 of [165], especially the chapters on algebraic geometry, it is helpful to summarize the key arguments here.

In brief, the authors of [74] take the effective 10-dimensional action

$$S \sim \int d^{10}x \sqrt{g} e^{-2\Phi} \left[R + 4\partial_\mu \Phi \partial^\mu \Phi - \frac{1}{2}|H'_3|^2 - \frac{1}{g_s^2} \text{Tr}|F_2|^2 \right] + SUSY \quad (\text{A.16})$$

of the heterotic string (where we write only the bosonic part and $+SUSY$ is understood to be the supersymmetric completion) and consider ⁴ the supersymmetric variation δ on the various fields:

gravitino	$\delta_\epsilon \Psi_{m'=1,\dots,10} = \nabla_{m'} \epsilon - \frac{1}{4} H_{m'}^{(3)} \epsilon$
dilatino	$\delta_\epsilon \lambda = -\frac{1}{2} \Gamma^{m'} \partial_{m'} \Phi \epsilon + \frac{1}{4} H_{m'}^{(3)} \epsilon$
adjoint Yang-Mills	$\delta_\epsilon \chi = -\frac{1}{2} F^{(2)} \epsilon$
Bianchi	$dH^{(3)} = \frac{\alpha'}{4} [\text{Tr}(R \wedge R) - \text{Tr}(F \wedge F)]$

(A.17)

and demand that these all vanish so that supersymmetry is preserved. Assume that the 3-form field $H^{(3)} = 0$ (this is a strong assumption and can be generalized, for which there has been much recent work, cf., e.g., [105]), we have that upon dimensional reduction $\mathbb{R}^{1,9} \simeq \mathbb{R}^{1,3} \times M$ for some compact (internal) 6-manifold M ,

$$0 = \delta_\epsilon \Psi_{m'=1,\dots,10} = \nabla_{m'} \epsilon = \nabla_{m'} \xi(x^{\mu=1,\dots,4}) \eta(y^{m=1,\dots,6}), \quad (\text{A.18})$$

giving us the Killing spinor equation on M .

Now, the external space, being Minkowski, is flat so that $[\nabla_\mu, \nabla_\nu] \xi(x) = 0$. Thus, the internal space M is also Ricci-flat and admits not only a spinor (and is thus a spin manifold), but in fact a covariant constant spinor

$$\nabla_m \eta = 0. \quad (\text{A.19})$$

Defining $\eta_+^* = \eta_-$ to split chirality to the original 10-dimensional spinor as $\epsilon(x^{1,\dots,4}, y^{1,\dots,6}) = \xi_+ \otimes \eta_+(y) + \xi_- \otimes \eta_-(y)$, we have the following set of definitions which sequentially specialize M :

- Define $J_m^n = i\eta_+^\dagger \gamma_m^n \eta_+ = -i\eta_-^\dagger \gamma_m^n \eta_-$, one can check that $J_m^n J_n^p = -\delta_m^n$ for Clifford Gamma matrix γ_m^n . Therefore, (M, J) is **almost-complex**;
- However, η covariantly constant $\rightsquigarrow \nabla_m J_n^p = 0 \rightsquigarrow \nabla N_{mn}^p = 0$ so that the Nijenhuis tensor $N_{mn}^p := J_m^q \partial_{[q} J_{n]}^p - (m \leftrightarrow n)$. Therefore, (M, J) is **complex** (in

⁴One way to think of supersymmetry, regardless of experimental results and from a philosophical point of view, is to ask “are complex numbers part of reality?” We know that the complex numbers complete the reals in a canonical way and have become indispensable even to engineers. Supersymmetry completes QFTs in a canonical way and should likewise be thought of as the natural realm in which to study elementary physics.

- particular, one can choose coordinates (z, \bar{z}) so that $J_m^n = i\delta_m^n$, $J_{\bar{m}}^{\bar{n}} = i\delta_{\bar{m}}^{\bar{n}}$, $J_{\bar{m}}^n = J_m^{\bar{n}} = 0$, rendering the transition functions holomorphic);
- Define $J = \frac{1}{2}J_{mn}dx^m \wedge dx^n$ with $J_{mn} := J_m^k g_{kn}$. One can check that $dJ = (\partial + \bar{\partial})J = 0$, so that (M, J) is **Kähler**.

Now, for a spin 6-manifold, the holonomy group is generically $SO(6) \simeq SU(4)$. The existence of the covariantly constantly spinor implies that the holonomy is reduced: in the decomposition $\mathbf{4} \rightarrow \mathbf{3} \oplus \mathbf{1}$ of $SU(4) \rightarrow SU(3)$, this covariantly constant spinor corresponds to the $\mathbf{1}$. Thus, in summary, our internal manifold M is Kähler, $\dim_{\mathbb{C}} = 3$, and with $SU(3)$ holonomy.

A.6 A Lightning Refresher on Toric Varieties

This section, as mentioned in the main text, is not meant to be a review on toric geometry, of which there are many excellent sources in the literature [47, 89, 99, 133, 145]. We will use the quadric hypersurface, the “conifold”,

$$\{ab = cd\} \in \mathbb{C}_{(a,b,c,d)}^4, \quad (\text{A.20})$$

to illustrate the three equivalent definitions of an affine [toric variety](#). As in the standard case for manifolds, these affine patches, with the appropriate transition functions, can be glued to a compact toric variety.

(i) Combinatorics of Lattice Cones The most standard definition of an affine toric variety is via

Definition 22 A convex polyhedral cone is the set $\sigma := \{r_1v_1 + \dots + r_sv_s \in V : r_i \in \mathbb{R}_{\geq 0}\}$ for $v_i \in V$. Here $V = N_{\mathbb{R}} = N \otimes_{\mathbb{Z}} \mathbb{R}$ is a vector space obtained from a lattice $N \simeq \mathbb{Z}^n$.

In other words, σ is the cone with tip at the origin and whose edges are rays determined by lattice vectors. The lattice N has its dual lattice $M = \text{hom}(N, \mathbb{Z})$ by the inner product $\langle M, N \rangle$, as well as its own associated vector space $M_{\mathbb{R}} = M \otimes_{\mathbb{Z}} \mathbb{R}$.

The **dual cone** σ^{\vee} is the set of vectors in $M_{\mathbb{R}}$ whose inner product with all vectors in σ are non-negative. The affine toric variety U_{σ} for σ is then

$$U_{\sigma} := \text{Spec}(\mathbb{C}[\sigma^{\vee} \cap M]), \quad \sigma^{\vee} \cap M := \{u \in M : \langle u, v \rangle \geq 0 \ \forall v \in \sigma\}. \quad (\text{A.21})$$

In the physics literature, the set of end-points of the integer vector generators of $\sigma^{\vee} \cap M$ is called the **toric diagram**.

A.6.1 Digressions on Spec and All That

Since we have made repeated use of the symbol “[Spec](#)” in this book so it might be worth to explain it a little and here is as good a place as any other. We first recall that in a commutative (in this book we almost exclusively consider commutative polynomial rings) ring $(R, +, \times)$, an ideal I is a subgroup under $+$ closed under \times . That is, $(I, +)$ is a subgroup of $(R, +)$ such that for every $r \in R$ and every $x \in I$, we have that $rx \in I$. A maximal ideal is, as the name suggests, a proper ideal such that no other proper ideal contains it.

For instance, in the polynomial ring $\mathbb{C}[x]$, (i.e., set of polynomials in a single variable x with complex coefficients that constitute a ring by ordinary $+$ and \times), the set of polynomials which are of the form $(x - 1)f(x)$ (i.e., polynomials with $(x - 1)$ as a factor) is an ideal which is maximal. This ideal is denoted as $\langle x - 1 \rangle$. The set of polynomials of the form $(x - 1)(x - 2)f(x)$ is also an ideal, denoted as $\langle (x - 1)(x - 2) \rangle$. But it is not maximal because $\langle (x - 1)(x - 2) \rangle \subset \langle (x - 1) \rangle$.

Now, we get to the heart of the matter by defining⁵

Definition 23 $\text{Spec}(R) := \{\text{maximal ideals in } R\}$, called the (maximal) spectrum of the ring R .

While this may seem like an artificially constructed set, the geometric meaning is profound. Returning to our example of $R = \mathbb{C}[x]$, it is clear that every maximal ideal is of the form $\langle (x - a) \rangle$ for an arbitrary $a \in \mathbb{C}$. In other words, because we have complete factorization of polynomials over \mathbb{C} , any polynomial can be uniquely factorized into linear factors—the fundamental theorem of algebra helps us here and this is, again, the reason we work over \mathbb{C} , rather than over \mathbb{R} , say. Hence, $\text{Spec}(\mathbb{C}[x]) \simeq \mathbb{C}$. In general, we have that, for the polynomial ring in n variables,

$$\text{Spec}(\mathbb{C}[x_1, x_2, \dots, x_n]) \simeq \mathbb{C}^n . \quad (\text{A.22})$$

The key point is that we now have a purely algebraic way of describing the geometrically familiar object: the affine space \mathbb{C}^n .

As this book is about polynomial systems in complex variables defining manifolds as varieties, it is natural to ask how to extend (A.22) to a [variety](#) $X \subset \mathbb{C}^n$. First, as mentioned in the main text, a polynomial system S itself constitutes an ideal: its vanishing locus which defines the manifold remains so by any multiplication by an element of the polynomial ring. It is standard to denote this ideal as $I(X) \in \mathbb{C}[x_1, x_2, \dots, x_n]$.

As groups can quotient normal subgroups, so too can rings quotient ideals. Consider, therefore, the quotient ring $R_X = \mathbb{C}[x_1, x_2, \dots, x_n]/I(X)$. In this ring, polynomial $+$ and $-$ proceed as normal, but modulo the defining polynomial system

⁵Sometimes this is written explicitly as $\text{Spec}_M(R)$ to show that we are dealing with the set of maximal ideals. Another commonly used concept is $\text{Spec}_P(R)$, the set of *prime ideals* in R . Since we are not going into prime ideals here, our *Spec* will merely refer to Spec_M .

S. For example, suppose we have a hypersurface in \mathbb{C}^2 defined by $y = x^2$, then whenever we see an x^2 , we can substitute y for x^2 . This quotient ring R_X thus captures the property of the variety X and is called the **coordinate ring** of X . The set of maximal ideals on R_X are likewise those on $\mathbb{C}[x_1, x_2, \dots, x_n]$, but modulo the defining polynomials.⁶ Thus, in a similar fashion, we have a correspondence between points on the variety X and $\text{Spec}(R_X)$.

Everything said above was for affine (non-compact) varieties, there is a graded analogue for Spec , which is ‘‘Proj’’, which should be applied to projective (compact) varieties. For example, the projective space itself, is

$$\text{Proj}(\mathbb{C}[x_0, x_1, \dots, x_n]) \simeq \mathbb{CP}^n. \quad (\text{A.23})$$

This is the starting point for playing with varieties in software such as **Macaulay2** [163].

A.6.2 Example: The Conifold

The diagrams in Fig. A.1 will reify the above concepts. In part (a), the cone is spanned by the four vectors

$$\{(0, -1, 1), (-1, 0, 1), (0, 1, 0), (1, 0, 0)\} \quad (\text{A.24})$$

in \mathbb{Z}^3 (so the resulting variety is complex dimension 3). One can readily check that the dual cone is spanned by the four vectors

$$\{(0, 0, 1), (1, 1, 1), (0, 1, 1), (1, 0, 1)\}, \quad (\text{A.25})$$

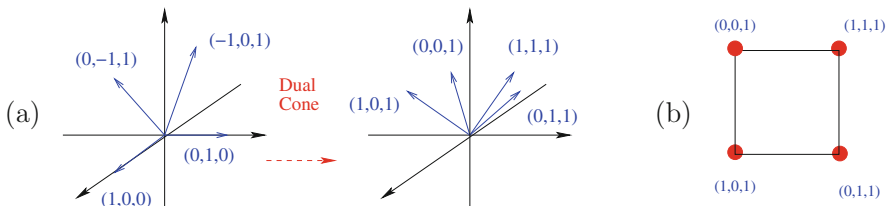


Fig. A.1 (a) The cone and dual cone; (b) the toric diagram, for the conifold

⁶Note that in order to simplify discussions, we have glossed over technicalities of ideals defined, for example, by powers of the polynomial system, which obviously give the same geometry. In other words, we have bypassed the discussions on radicals of ideals and the Nullstellensatz as well as distinctions between varieties and schemes.

so that all pair-wise inner products of the generators of σ^\vee and σ are non-negative. In part (b), the end-points of the generators of σ and σ^\vee are coplanar, as is in congruence with the fact that our hypersurface is Calabi–Yau. The diagram is a square of unit area and the last coordinate is 1 (of course, any $GL(3; \mathbb{Z})$ transformation on the diagram gives the same variety). In fact, dropping the last coordinate gives the convex polygon, here the square, which is the diagram used in the main text.

We treat the coordinates of these generators of the dual cone as exponents of three complex variables (x, y, z) , giving us

$$S_\sigma = \langle a = z, c = yz, b = xyz, d = xz \rangle. \quad (\text{A.26})$$

Finally, computing the maximal spectrum of the polynomial ring $\mathbb{C}[S_\sigma]$ means that we need to compute $\text{Spec} \mathbb{C}[a = z, c = yz, b = xyz, d = xz]$. In other words, as introduced in Sect. A.6.1, we need to find any basic relations among (a, b, c, d) . Clearly, there is one quadratic relation: $(z)(xyz) = (yz)(xz)$, this gives the hypersurface (A.20), the **Conifold** as desired.

(ii) Kähler Quotients The second definition of a toric variety is a direct generalization of projective space \mathbb{P}^n , which we recall to be \mathbb{C}^{n+1} (with coordinates $x_{i=0, \dots, n}$) quotiented by a $\lambda \in \mathbb{C}^*$ action $x_i \mapsto \lambda x_i$. Now, consider \mathbb{C}^q with homogeneous (also called Cox) coordinates $x_{i=0, \dots, q}$ and a $(\mathbb{C}^*)^{q-d}$ action

$$x_i \mapsto \sum_a \lambda_a^{Q_{i=1 \dots q}^{a=1 \dots q-d}} x_i, \quad \lambda_a \in \mathbb{C}^*, Q_i^a \in \mathbb{Z}, \quad (\text{A.27})$$

where Q is called a charge matrix, the integer kernel of which is given by

$$\sum_{i=1}^d Q_i^a v_i = 0, \quad (\text{A.28})$$

and the generator v_i is the toric diagram.

For our running example, take $Q = [-1, -1, 1, 1]$, as a \mathbb{C}^* action on \mathbb{C}^4 , so that $\ker(Q) = \begin{pmatrix} 1 & 0 & 0 & 1 \\ 1 & 0 & 1 & 0 \\ 1 & 1 & 1 & 1 \end{pmatrix}$ and the four columns are precisely (A.25).

(iii) Computational Definition This is the simplest definition of a toric variety. The defining equation $ab = cd$ for the conifold is known as a *binomial ideal*, i.e., every defining equation is of the form of “monomial = monomial”. It turns out that [133] every such polynomial ideal defines a toric variety. Interestingly, this condition is crucial to the bipartite interpretation of quiver representation variety for toric CY3, as in Theorem 10.

A.6.3 From Cones to Fans

Everything said so far about toric varieties has been about *affine* ones, where a single (convex, polyhedral, lattice) cone gives a monomial ideal from (A.21). From the point of view of local Calabi–Yau space, this is sufficient. Indeed, as mentioned in the main text, so long as the end-points of the generators of the cone are co-hyperplanar, the result is affine CY. However, this condition, as we will see shortly, immediately rules out compact toric CY:

Theorem 14 *There are no compact toric Calabi–Yau manifolds.*

Note that it is certainly fine for the *ambient* variety to be toric, such as \mathbb{CP}^4 for the quintic as discussed in detail in Sect. 2.1.

As one forms a (compact) manifold out of affine patches by gluing, so too can one construct a compact toric variety by gluing affine ones. Let us take \mathbb{CP}^2 as a simple example. We recall from Sect. A.3 that \mathbb{CP}^2 has 3 patches: using the homogeneous coordinates $[z_0 : z_1 : z_2]$, they are $U_{i=0,1,2} \simeq \mathbb{C}^2$ with coordinates $w_j^{(i)} = z_j/z_i$ for $i \neq 0$. The transition function from U_{i_1} to U_{i_2} at their intersection where $z_{i_1}, z_{i_2} \neq 0$ is $w_j^{(i_1)} = w_j^{(i_2)} z_{i_2}/z_{i_1}$.

All of this information can be phrased torically. Let us look back to Fig. 2.4. There are three cones $\sigma_{0,1,2}$. The cone σ_0 has generators $(0, 1)$ and $(-1, -1)$; its dual cone has generators $(-1, 0)$ and $(-1, 1)$, so the coordinate ring is $\mathbb{C}[1/x, y/x]$. The cone σ_1 has generators $(1, 0)$ and $(-1, -1)$; its dual cone has generators $(0, -1)$ and $(1, -1)$, so the coordinate ring is $\mathbb{C}[1/y, x/y]$. The cone σ_2 has generators $(0, 1)$ and $(1, 0)$; its dual cone has generators $(1, 0)$ and $(0, 1)$, so the coordinate ring is $\mathbb{C}[x, y]$. Thus, taking the maximal spectrum, each is just \mathbb{C}^2 . The three cones together form a **fan**. Thus, if we defined $x := z_1/z_0$ and $y := z_2/z_0$, the cones $\sigma_{0,1,2}$ can be identified with the above ordinary patches $U_{1,2,0}$, respectively.

We have therefore given a toric description of \mathbb{CP}^2 as a compact variety. The fan can be re-packaged into a convex lattice polytope by the face-fan construction discussed near Fig. 2.4. Some important results (q.v. [99, 145]) are the following (note that since our expositions here are informal, we have not used the standard but technical terms such as the M and N lattices).

Theorem 15 *The complex n -dimensional toric variety is compact iff the fan is complete, in the sense that the collection of cones covers all of \mathbb{R}^n .*

For example, we can see the three cones of \mathbb{CP}^2 covering the plane. Thus, the co-hyperplanar condition already renders a compact toric CY impossible.

Theorem 16 *The toric variety is smooth iff each cone is regular, in the sense that the determinant of the matrix, formed by generators as lattice vectors, is ± 1 .*

A.7 Dramatis Personae

Recall the trichotomy of $g = 0$, $g = 1$ and $g > 1$ from Fig. 1.1. As Riemann surfaces/complex manifolds, these are, respectively, $S^2 \simeq \mathbb{P}^1$ (positive curvature), $CY_1 \simeq T^2$ (zero curvature) and hyperbolic (negative curvature). This trichotomy [194] in complex dimension 1 persists to general Kähler manifolds and are referred to as (1) **Fano**; (2) **Calabi–Yau** and (3) **general type**, the first two falling into some classifiable families while the third usually proliferates untamably. More strictly, for a (complete) complex manifold M consider its anti-canonical sheaf $K_M^\vee := (\wedge^n T_M^\vee)^\vee$. If it is trivial, M is Calabi–Yau and if it is ample, then M is Fano.

In complex dimension two, the Calabi–Yau case consists of T^4 and K3, while the Fano family also enjoys a wealth of structure. Clearly, \mathbb{P}^2 and $\mathbb{P}^1 \times \mathbb{P}^1$ are Fano, the first since $K_{\mathbb{P}^n}^\vee = \mathcal{O}_{\mathbb{P}^n}(n+1)$, and the second, essentially by Künneth. Interestingly, there are 8 more. To introduce these, we need the concept of a **blow-up**.

In brief, a blow-up of a point in an n -fold is to replace the point with a \mathbb{P}^{n-1} . The general definition is rather abstruse (cf. §7, circa Prop 7.11 of [194] but locally the definition is straight-forward. Consider a codimension k subvariety $Z \subset \mathbb{C}^n$ with affine coordinates $x_{i=1,\dots,n}$, defined, for simplicity, by $x_1 = x_2 = \dots = x_k = 0$. Let y_i be the homogeneous coordinates of \mathbb{P}^{k-1} , then the blow-up $\widetilde{\mathbb{C}^n}$ of \mathbb{C}^n along Z is defined by the equations

$$\{x_i y_j = x_j y_i\}_{i,j=1,\dots,k} \subset \mathbb{C}^n \times \mathbb{P}^{k-1}. \quad (\text{A.29})$$

Thus defined, away from Z , $\widetilde{\mathbb{C}^n}$ is just \mathbb{C}^n as the non-identical-vanishing of x_i fixes y_i to be a single point on \mathbb{P}^{k-1} (i.e., we project back to \mathbb{C}^n), but along Z , where x_i vanish, we have arbitrary y_i , parametrizing \mathbb{P}^{k-1} . Thus, we have “replaced” Z by \mathbb{P}^{k-1} .

del Pezzo Surfaces We apply the aforementioned to $\mathbb{P}_{[X_0:X_1:X_2]}^2$. Take the point $P = [0 : 0 : 1]$ without loss of generality, and work on the affine patch $X_2 \neq 0$ so that $(x, y) = (X_0/X_2, X_1/X_2) \in \mathbb{C}^2$. We blow the point P up by “replacing” it with a $\mathbb{P}_{[z:w]}^1$. Then the blow-up of \mathbb{P}^2 at P is given by

$$\{(x, y); [z:w]\} : xz + yw = 0\} \subset \mathbb{C}^2 \times \mathbb{P}^1. \quad (\text{A.30})$$

At points away from P where (x, y) are not simultaneously 0, we can fix a value of $[z:w]$ but at P where $(x, y) = (0, 0)$, $[z:w]$ are arbitrary and parametrizes a full \mathbb{P}^1 . The result is a smooth complex surface, denoted dP_1 , which is \mathbb{P}^2 blown up at a point.

Now, take r generic points ⁷ on \mathbb{P}^2 , and perform successive blow-up. We denote the result as dP_r , the r -th **del Pezzo surface** (with $r = 0$ understood to be \mathbb{P}^2 itself). Letting ℓ be the hyperplane class of \mathbb{P}^1 in \mathbb{P}^2 and $E_{i=1,\dots,r}$ be the **exceptional divisors** corresponding to the various \mathbb{P}^1 blow-ups, the intersection numbers are

$$\ell \cdot \ell = 1, \quad \ell \cdot E_i = 0, \quad E_i \cdot E_j = -\delta_{ij}, \quad (\text{A.31})$$

and the Chern classes are given by

$$c_1(dP_r) = 3\ell - \sum_{i=1}^r E_i, \quad c_2(dP_r) = 3 + r. \quad (\text{A.32})$$

The canonical class K_{dP_r} is $c_1(dP_r)$ and its self-intersection is the **degree**: using (A.31), we see that the degree is $c_1(dP_r)^2 = 9 - r$. For instance, a smooth degree 3 surface in \mathbb{P}^2 , on which there are the famous 27 lines, corresponds to $r = 6$ blow-ups.

From the degree, we see the $r \leq 8$, thus there are only $8 + 1$ del Pezzo surfaces ($r = 0, \dots, 8$) which are Fano.⁸ It is remarkable that they correspond to the exceptional simply-laced series in semi-simple Lie algebras, viz., $E_{r=8,7,6,\dots,1}$ with the convention that

$$E_{5,4,3,2,1} := (D_5, D_4, A_2 \times A_1, A_2, A_1), \quad (\text{A.33})$$

in the precise sense that the matrix of intersection forms in (A.31) is the adjacency matrix of the Dynkin diagram for affine E_r (with the extra affine node corresponding to ℓ). Finally, we remark that $dP_{r=0,1,2,3}$ are toric varieties.

Hirzebruch Surfaces The other of the two basic Fano surfaces, $\mathbb{P}^1 \times \mathbb{P}^1$, also belongs to a notable family. Consider surfaces which are \mathbb{P}^1 -fibrations over \mathbb{P}^1 . It turns out that such surfaces are classified by a single integer, viz, the number of self-intersections of the class of the base [145], a positive integer r , and the surface is called the r -th **Hirzebruch surface**, denoted \mathbb{F}_r .

The simplest case is when the fibration is trivial and the surface is $\mathbb{F}_0 := \mathbb{P}^1 \times \mathbb{P}^1$. In general, let f be the class of the fibre \mathbb{P}^1 and b , the class of the base \mathbb{P}^1 , then the intersection numbers are

$$f \cdot f = 0, \quad f \cdot b = 1, \quad b \cdot b = -r. \quad (\text{A.34})$$

⁷Generic means that no 3 points are colinear, no 4 points are co-planar, etc., so that the points are in general position, i.e., their projective coordinates can be taken as n random triples $[x_i : y_i : z_i]$.

⁸When $r = 9$, we have $c_1(dP_9)^2 = 0$ so that dP_9 is not Fano. It has been jocundly called half-K3 because while the first Chern class is not zero, it “squares” to zero. In the mathematics literature, del Pezzo surfaces and Fano surfaces are synonymous in that Fano varieties in complex dimension 2 are called del Pezzo, but in the physics literature, dP_9 has been added to the list of del Pezzo surfaces.

The Chern classes are

$$c_1(\mathbb{F}_r) = 2b + (r+2)f, \quad c_2(\mathbb{F}_r) = 4. \quad (\text{A.35})$$

All members of the Hirzebruch family are toric (q.v. §1.1 of [145]).

Of the family \mathbb{F}_r , it turns out that only $r=0$ is Fano. Clearly, we could perform successive one-point blow-ups on $\mathbb{P}^1 \times \mathbb{P}^1$. However, \mathbb{F}_0 blown up at 1 point is just dP_2 (this can be seen from the toric diagrams). Therefore, in all we have 10 Fano surfaces, organizing themselves in a curious fashion:

$$\begin{array}{c} \mathbb{F}_0 \\ \downarrow \\ dP_0 = \mathbb{P}^2 \rightarrow dP_1 \rightarrow dP_2 \rightarrow \dots \rightarrow dP_7 \rightarrow dP_8 \end{array} \quad (\text{A.36})$$

where “ \rightarrow ” means blow-up by one point. Finally, we remark that of this sequence, $dP_{0,1,2,3}$ and \mathbb{F}_0 are toric varieties but not the others. The toric diagrams for these are given in Fig. 3.1 in the text. Incidentally, it was noticed in [241] that this is exactly the structure of M-theory/string theory compactifications on successive circles, a mysterious duality indeed!

Thus, in analogy with the trichotomy of Riemann surfaces/complex curves of Fig. 1.1, the situation in complex dimension 2 is

10 Fano surfaces in (A.36)	$CY_2 =$	Surfaces of general type
$dP_{n=0,\dots,8}, \mathbb{P}^1 \times \mathbb{P}^1$	$T^4, K3$	
+ curvature	0 curvature	- curvature

(A.37)

The complex dimension 3 case is, on the other hand, much more complicated and this book is devoted to the middle column of CY3s, of which there already is a superabundance.

A.8 The Kodaira Classification of Elliptic Fibrations

We mentioned elliptically fibred CYs in the text and stated that this can be achieved by promoting the coefficients in the Weierstraß equation to functions. In this appendix, let us illustrate this explicitly with elliptically fibred surfaces, especially as an invitation to Kodaira’s beautiful classification [261], which is yet another emergence of the ADE meta-pattern (q.v. Sect. 3.2.1).

Let us consider a complex surface S which is an elliptic fibration over a \mathbb{P}^1 base whose projective coordinate is w . This means that we can write the equation of S in Weierstraß form (2.26) as (at least in the $z=1$ patch):

$$y^2 = 4x^3 - g_2(w)x - g_3(w), \quad (\text{A.38})$$

where g_2 and g_3 are arbitrary polynomials in w . Globally, we really should think of the complex coordinates (x, y, z) as being sections of the bundles $(L^{\oplus 2}, L^{\oplus 3}, L)$ where $L = \mathcal{O}_{\mathbb{P}^1}(2)$ is the anti-canonical bundle of \mathbb{P}^1 , but we will work in the $z = 1$ affine patch for simplicity.

Now, every isomorphism class of an elliptic curve $y^2 = 4x^3 - g_2x - g_3$ is determined by the famous j -invariant (into which this book sadly does not have the space to go) $j := g_2^3/(g_2^3 - 27g_3^2)$. Thus, for an elliptic surface, the j -invariant becomes a meromorphic function in w , as a map from \mathbb{P}^1 to \mathbb{P}^1 :

$$j(w) := \frac{g_2(w)^3}{g_2(w)^3 - 27g_3(w)^2}, \quad \Delta(w) := g_2(w)^3 - 27g_3(w)^2. \quad (\text{A.39})$$

It is a fascinating fact that this is a clean, trivalent Belyi map (q.v. Sect. C.1 and [225]). When the denominator Δ vanishes the curve (elliptic fibre) becomes singular. This can be easily checked: consider the RHS $f = 4x^3 - g_2x - g_3 = 0$ and $f' = 12x^2 - g_2$. the elliptic curve becomes singular when $f = f' = 0$, which upon eliminating x , gives the condition $\Delta = 0$.

Kodaira then proceeded to classify all possible singularity types by considering what happens to g_2 and g_3 on the singular locus $\Delta(w) = 0$. To give a trivial example, suppose $y^2 = 4x^3 - wx$ so that $g_2 = w$, $g_3 = 0$, and $\Delta = w^3$. The discriminant Δ vanishes at 0, so the singular locus is the point $\{w = 0\}$, where the order of vanishing of g_2 is 1, that of g_3 is infinity, and that of Δ , 3. A simple transformation renders the equation to be $(y/2)^2 = x(x^2 - w/4)$, which, upon redefining $y/2 = s$, $u = x$ and $v = x^2 - w/4$ gives the equation $s^2 = uv$, which is the surface singularity A_1 (q.v. (3.12)).

In general, massaging the Weierstrass form into surface singularity types is highly non-trivial and requires the so-called Tate-Nagell algorithm. The insight of Kodaira is the classification of the complete singularity types of the elliptic fibration. Defining $\text{Ord}(f(w))$ as the order of vanishing of a function $f(w)$ at w_0 , i.e., the Taylor series of $f(w)$ starts with $\mathcal{O}(w - w_0)^{\text{Ord}(f(w))}$, we have

Theorem 17 (Kodaira) *The elliptic fibration types are determined by the order of vanishing of g_2 , g_3 , Δ at the singular locus $\Delta = 0$, and are the following*

$\text{Ord}(g_2)$	$\text{Ord}(g_3)$	$\text{Ord}(\Delta)$	<i>Kodaira Notation</i>	<i>Singularity type</i>
≥ 0	≥ 0	0	<i>smooth</i>	—
0	0	n	I_n	A_{n-1}
≥ 1	1	2	II	<i>none</i>
≥ 1	≥ 2	3	III	A_1
≥ 2	2	4	IV	A_2
2	≥ 3	$n + 6$	I_n^*	D_{n+4}
≥ 2	3	$n + 6$	I_n^*	D_{n+4}
≥ 3	4	8	IV^*	E_6
3	≥ 5	9	III^*	E_7
≥ 4	5	10	II^*	E_8

Beautifully, we see another emergence of the ADE meta-pattern (q.v. Sect. 3.2.1).

In the above, we illustrated with an elliptic surface as a fibration over \mathbb{P}^1 . For 3-folds, the Weierstrass coefficients will depend on more base variables. In the text in Sect. 2.3.2, the base types are enumerated into 4 families of surfaces. Suppose their coordinates are (w_1, w_2) , then g_2, g_2, Δ will be polynomials in these.

Appendix B

Gröbner Bases: The Heart of Computational Algebraic Geometry

As much as almost any problem in linear algebra begins with Gaussian elimination, when encountering a system of polynomials—to which almost any query in algebraic geometry can be reduced—one begins with the [Gröbner basis](#). This analogy is actually strict: for a system of polynomials all of degree 1 (i.e., back to a linear system), the Gröbner basis (in elimination ordering) is Gaussian elimination to triangular form.

As promised in the text, we cannot possibly not go into a brief digression into Gröbner bases, which lies at the root of all the algorithms used in this book. The reader is referred to [98] for a marvellous account of the subject of computational geometry. For diehards in [Mathematica](#), a package has been written [160] to link it with [Singular](#) so that much of the algorithms can be performed with a more familiar front-end.

As always, we exclusively work over the polynomial ring $\mathbb{C}[x_i]$, and with $x_i \in \mathbb{C}$, which greatly simplifies things. First, we need to define an ordering of the monomials, denoted as $\mathbf{x}^\alpha \prec \mathbf{x}^\beta$ where \mathbf{x}^α is the standard vector exponent notation understood to be the monomial $x_1^{\alpha_1} x_2^{\alpha_2} \dots x_n^{\alpha_n}$. This is a *total order* in the sense that if $u \preceq v$ and w is any other monomial, then $uw \preceq vw$ (it is in fact furthermore well-ordered in that $1 \preceq u$ for any u). There are many ways to define such an ordering and indeed the Gröbner basis is dependent on such a choice. The final conclusions in the geometry must, of course, be independent of any ordering choice. The most common choices of ordering are (we will use the four monomials $\{x_1 x_2^2 x_3, x_3^2, x_1^3, x_1^2 x_2^2\}$ to illustrate each case):

- | | |
|--------------|--|
| lex | or Lexicographic ordering, which, like a dictionary, compares the exponent of x_1 , and if equal, proceeds to x_2 , etc., so that the power of $x_{i < j}$ dominates over x_j ; e.g., $x_1^3 \succ x_1^2 x_3^2 \succ x_1 x_2^2 x_3 \succ x_3^2$; |
| grlex | or Graded (or degree)-lexicographic ordering, which compares <i>total degree</i> first and in the case of ties, proceeds to lex; e.g., $x_1^2 x_3^2 \succ x_1 x_2^2 x_3 \succ x_1^3 \succ x_3^2$ (tie on highest degree, 4, in the first two, and proceeded to lex so that x_1 dominated); |

- grevlex** or Graded (or degree) reversed lexicographic ordering, which compares total degree first and then uses the reversed order of lex for ties; e.g., $x_1x_2^2x_3 > x_1^2x_3^2 > x_1^3 > x_3^2$;
- lexdeg** or Elimination (or block) ordering, which divides the variables into ordered blocks, each of which has a chosen ordering, usually grevlex; e.g., suppose we wish to eliminate x_1 , we create two blocks: $\{x_1\}$ and $\{x_2, x_3\}$ so that lex ordering is considered for $\{x_1\}$ before $\{x_2, x_3\}$; e.g., $x_1^3 > x_1^2x_3^2 > x_1x_2^2x_3 > x_3^2$.

With a monomial ordering fixed, we have a definite *leading term* of any polynomial f , denoted $LT(f)$, which is the monomial, together with its coefficients, maximal according to $>$. Suppose we are given $F = \{f_i\}$, a system of multivariate polynomials. The Gröbner basis G of F is obtained by the **Buchberger Algorithm** as follows.

1. Set $G := F$ to initialize;
2. For every pair $f_i, f_j \in G$, find the leading terms $LT(f_i)$ and $LT(f_j)$, as well as their least common multiple¹ $a_{ij} := LCM(LT(f_i), LT(f_j))$;
3. Compute the S-polynomial $S_{ij} := \frac{a_{ij}}{LT(f_i)} f_i - \frac{a_{ij}}{LT(f_j)} f_j$ so that the leading terms cancel by construction;
4. Divide S_{ij} by every element of G to see if there is a remainder, i.e., write $S_{ij} = \sum_{g \in G} p_g g + r$. This is called reduction of S_{ij} over the set G . The remainder r is so that none of its terms divides any of the leading terms from p_g , in analogy to arithmetic division.
5. If there is non-trivial remainder: $r \neq 0$, then add r to G ;
6. Repeat until all pairs are considered in the augmented G (i.e., including the generated remainders included into G as we go along) and until no new remainders are generated.

The final list of polynomials G (which in general will have more elements than F) is the Gröbner basis.

There are many implementations of the Buchberger Algorithm, exemplified by the `GroebnerBasis[]` command in **Mathematica**, the `gb()` command in **Macaulay2**, the `groebner()` command in **Singular**. Let us illustrate with a very simple example, step by step:

1. INPUT: $G = F = \{-12xy+3y^2, 4x-6y\}$, with lex ordering $x > y$, the leading terms are $LT(F_1) = -12xy$ and $LT(F_2) = 4x$;
2. There is one S-polynomial between the 2 elements of I . First, $a_{12} = LCM(xy, x) = xy$ (where the polynomial LCM is done without the coefficient, but this a mere convention and including the coefficient will just give an overall

¹While finding the LCM of two polynomials involves a generalization of the Euclidean division algorithm, since we are only finding the LCM of two monomials, this is easily done by comparing exponents.

numerical factor), so $S_{12} = \frac{a_{12}}{LT(F_1)}F_1 - \frac{a_{12}}{LT(F_2)}F_2 = \frac{5y^2}{4}$. Note that here, by design, the leading terms cancelled; Reducing S_{12} by the 2 elements of G gives non-trivial remainder for both, so S_{12} should be kept.

3. At this point G is augmented to $G = \{-12xy + 3y^2, 4x - 6y, \frac{5y^2}{4}\}$, with leading terms $LT(G_{1,2}) = LT(F_{1,2}), LT(G_3) = G_3$. We now have 2 new S-polynomials to compute: $a_{13} = xy^2 \rightsquigarrow G_{13} = -\frac{y^3}{4}$ and $a_{23} = xy^2 \rightsquigarrow G_{23} = -\frac{3y^3}{2}$. Both G_{13} and G_{23} , when reduced on G have zero remainder because $a_{13} = -\frac{1}{5}yG_3$ and $a_{23} = -\frac{6}{5}G_3$. Thus nothing new can be added and G is the final Gröbner basis.

B.1 An Elimination Problem

Of the many wonders of the Gröbner basis, let us only illustrate one, viz., elimination, on our favourite quintic from (2.12) (note that we have for convenience included a factor of 5 in front of the complex structure parameter ψ)

$$Q := \sum_{i=0}^4 z_i^5 - 5\psi \prod_{i=0}^4 z_i , \quad \psi \in \mathbb{C} . \quad (\text{B.1})$$

Suppose we wish to check the conditions on ψ for which Q is non-singular. To do this, we compute the Jacobian of Q and form an ideal \mathcal{I} together with Q :

$$\mathcal{I} = \left\{ \sum_{i=0}^4 z_i^5 - 5\psi \prod_{i=0}^4 z_i , \left(5z_j^4 - 5\psi \prod_{k=0, k \neq j}^4 z_k \right)_{j=0, \dots, 4} \right\} . \quad (\text{B.2})$$

We now consider lexdeg ordering by having two blocks: variables $z_{1, \dots, 4}$ and $\{z_0\}$, leaving ψ as a free complex parameter, and establish the Gröbner basis $G(\mathcal{I})$ for the ideal \mathcal{I} , which we then intersect with $\mathbb{C}[z_0]$. That is, we eliminate the variables $z_{0, \dots, 4}$. We find that:

$$G(\mathcal{I}) \cap \mathbb{C}[z_0] = (\psi^5 - 1)z_0^{16} . \quad (\text{B.3})$$

Suppose we are at a generic point $z_0 \neq 0$, this means that if ψ is not a 5-th root of unity, then the above is not zero, meaning that there are no simultaneous solutions to Q and its Jacobian vanishing. In summary then, Q is smooth so long as $\psi^5 \neq 1$.

B.2 Hilbert Series

The [Hilbert Series](#) is an important quantity that characterizes an algebraic variety. It is not a topological invariant in that it depends on the embedding under consideration [98, 322]. For a complex variety M in $\mathbb{C}[x_1, \dots, x_k]$, the Hilbert series is the generating function for the dimensions of the graded pieces:

$$H(t; M) = \sum_{i=0}^{\infty} (\dim_{\mathbb{C}} M_i) t^i , \quad (\text{B.4})$$

where M_i , the i -th graded piece of M can be thought of as the number of independent degree i polynomials on the variety M . Again, we are being slightly loose in using the variety M and its coordinate ring $S = \mathbb{C}[x_1, \dots, x_k]/I$, where I is the defining ideal of M , interchangeably. The coefficients $\dim_{\mathbb{C}} M_i$ (as a function of i) constitute the so-called **Hilbert function**. We remark that ordinarily, the Hilbert series is defined for *projective* varieties, especially for varieties defined in weighted projective space. Since much of the calculations performed in the physics literature is for *affine* varieties, we “decompactify” by considering the affine cone over the projective variety for which we compute the Hilbert series, but retain the grading (weights).

An important computational fact about the Hilbert series is a classic result due to Macaulay (q.v. [33]):

Theorem 18 *The Hilbert series of the initial ideal $\text{in}(I)$, the ideal generated by leading terms $\langle LT(f_i) \rangle$, is the same as that of the ideal $I = \langle f_i \rangle$ itself.*

Thus a Gröbner basis provides a practical method to calculate the Hilbert series for any algebraic variety.

Let us turn to some examples. Consider the simplest case of $M = \mathbb{C}$ (as a cone over a point if you wish), given as the maximal spectrum $\mathbb{C} = \text{Spec}(\mathbb{C}[x])$, i.e., \mathbb{C} being parametrized by a single complex number x . Clearly, at degree i , there is only a single monomial x^i . Thus, $\dim_{\mathbb{C}} M_i = 1$ for all $i \in \mathbb{Z}_{\geq 0}$ so that the Hilbert series becomes $H(t; \mathbb{C}) = (1 - t)^{-1}$. In general, we have that

$$H(t; \mathbb{C}^n) = (1 - t)^{-n} . \quad (\text{B.5})$$

For multi-graded rings with pieces $X_{\vec{i}}$ and grading $\vec{i} = (i_1, \dots, i_k)$, the Hilbert series takes the form $H(t_1, \dots, t_k; M) = \sum_{\vec{i}=0}^{\infty} \dim_{\mathbb{C}}(X_{\vec{i}}) t_1^{i_1} \dots t_k^{i_k}$ and becomes multivariate. This is sometimes called refinement [39] and one could “unrefine” it to a univariate Hilbert series by, for instance, setting all $t_k = t$.

A useful property of $H(t)$ is that for algebraic varieties it is always a rational function in t and can be written in two ways:

$$H(t; M) = \begin{cases} \frac{Q(t)}{(1-t)^k}, & \text{Hilbert series of the first kind;} \\ \frac{P(t)}{(1-t)^{\dim(M)}} , & \text{Hilbert series of the second kind.} \end{cases} \quad (\text{B.6})$$

Importantly, both $P(t)$ and $Q(t)$ are polynomials with *integer* coefficients. The powers of the denominators are such that the leading pole captures the dimension of the embedding space and the manifold, respectively.

For a Hilbert series in the second form,

$$H(t; M) = \frac{P(1)}{(1-t)^{\dim(M)}} + \dots, \quad P(1) = \text{degree}(M). \quad (\text{B.7})$$

In particular, $P(1)$ always equals the degree of the variety. We recall that when an ideal is described by a single polynomial, the degree of the variety is simply the degree of the polynomial. In the case of multiple polynomials, the degree is a generalization of this notion: it is the number of points at which a generic linear space of complementary dimension intersects the variety.

In the context of Sect. 3.3.2 in the text, one of the important expansions of the Hilbert series is a Laurent expansion about 1. When M is a non-compact Calabi–Yau 3-fold, as a cone over a Sasaki–Einstein base Y . The coefficient of the leading pole in the Laurent expansion can be interpreted as the volume of Y . This volume is in turn related to the central charges of supersymmetric gauge theory (*cf.* [136, 223, 287]).

Molien Series When M is an orbifold (not necessarily Calabi–Yau), of the form \mathbb{C}^n/G for some finite group G acting on the n coordinates, the Hilbert series is the Molien [335] series for G :

$$H(t; \mathbb{C}^n/G) = \frac{1}{|G|} \sum_{g \in G} \frac{1}{\det(\mathbb{I} - tg)}, \quad (\text{B.8})$$

where all group elements g are $n \times n$ matrices denoting the action on the coordinates. We can immediately check that for $G = \mathbb{I}$, the trivial group, we have $|G| = 1$, and that $\det(\mathbb{I} - tg) = \det((1-t)\mathbb{I}_{n \times n}) = (1-t)^n$ and the Molien series agrees with the Hilbert series for \mathbb{C}^n in (B.5).

For reference, we tabulate the Hilbert series for the ADE subgroups of $SU(2)$, with $\omega_n := e^{\frac{2\pi i}{n}}$ and

$$\begin{aligned} S &:= \frac{1}{2} \begin{pmatrix} -1+i & -1+i \\ 1+i & -1-i \end{pmatrix}, & T &:= \begin{pmatrix} i & 0 \\ 0 & -i \end{pmatrix}, \\ U &:= \frac{1}{\sqrt{2}} \begin{pmatrix} 1+i & 0 \\ 0 & 1-i \end{pmatrix}, & V &:= \begin{pmatrix} \frac{i}{2} & \frac{1-\sqrt{5}}{4} - i \frac{1+\sqrt{5}}{4} \\ -\frac{1-\sqrt{5}}{4} - i \frac{1+\sqrt{5}}{4} & -\frac{i}{2} \end{pmatrix}, \end{aligned} \quad (\text{B.9})$$

as follows:

G	$ G $	Generators	Equation	Molien/Hilbert $HS(t; G)$
\hat{A}_{n-1}	n	$\langle \begin{pmatrix} \omega_n & 0 \\ 0 & \omega_n^{-1} \end{pmatrix} \rangle$	$uv = w^n$	$\frac{(1+t^n)}{(1-t^2)(1-t^n)}$
\hat{D}_{n+2}	$4n$	$\langle \begin{pmatrix} \omega_{2n} & 0 \\ 0 & \omega_{2n}^{-1} \end{pmatrix}, \begin{pmatrix} 0 & i \\ i & 0 \end{pmatrix} \rangle$	$u^2 + v^2 w = w^{n+1}$	$\frac{(1+t^{2n+2})}{(1-t^4)(1-t^{2n})}$
\hat{E}_6	24	$\langle S, T \rangle$	$u^2 + v^3 + w^4 = 0$	$\frac{1-t^4+t^8}{1-t^4-t^6+t^{10}}$
\hat{E}_7	48	$\langle S, U \rangle$	$u^2 + v^3 + vw^3 = 0$	$\frac{1-t^6+t^{12}}{1-t^6-t^8+t^{14}}$
\hat{E}_8	120	$\langle S, T, V \rangle$	$u^2 + v^3 + w^5 = 0$	$\frac{1+t^2-t^6-t^8-t^{10}+t^{14}+t^{16}}{1+t^2-t^6-t^8-t^{10}-t^{12}+t^{16}+t^{18}}$

(B.10)

Toric Hilbert Series When M is a toric Calabi–Yau n -fold as prescribed by a toric diagram which is a convex lattice polyhedron Δ_{n-1} , its Hilbert series is also easy to compute [287]. The fully refined (multi-graded) version is succinctly obtained from the triangulation of Δ_{n-1} as follows

$$H(t_1, \dots, t_n; M(\Delta_{n-1})) = \sum_{i=1}^r \prod_{j=1}^n (1 - \vec{t}^{\vec{u}_{i,j}})^{-1}, \quad (\text{B.11})$$

Here, the index $i = 1, \dots, r$ runs over the $n - 1$ -dimensional simplices in the (fine, regular, stellar) triangulation and $j = 1, \dots, n$ runs over the faces of each such simplex. Each $\vec{u}_{i,j}$ is an integer n -vector, being the outer normal to the j -th face of the fan associated with i -th simplex. $\vec{t}^{\vec{u}_{i,j}} := \prod_{a=1}^n t_a^{u_{i,j}(a)}$ multiplied over the a -th component of \vec{u} .

General Case For a general variety, defined by a polynomial ideal, one first finds the Gröbner basis. Then, the Hilbert function $\dim_{\mathbb{C}} M_i$ is the number of monomials of degree i that are not a multiple of any leading monomial in the Gröbner basis.

The Plethystic Programme As discussed in the very beginning of Chap. 2, there is an intimate relation between the geometry of representation variety of the quiver and the gauge invariants of the quantum field theory. A so-called plethystic programme [39] was established to harness the Hilbert series of $\mathcal{M}(\mathcal{Q})$ which gave some intriguing properties of the Hilbert series of algebraic varieties in general. We will present some key points as observations since a rigorous treatment is yet to be fully administered. We begin with a few definitions:

Definition 24 Given a smooth function $f(t)$, its plethystic exponential [147] is the formal series

$$PE[f(t)] = \exp\left(\sum_{n=1}^{\infty} \frac{f(t^n) - f(0)}{n}\right).$$

One can readily check from this definition by direct manipulation of the series expansions (assuming reasonable regions of convergence), that

Proposition 8 If $f(t)$ has Taylor series $f(t) = \sum_{n=0}^{\infty} a_n t^n$, then

- There is a Euler-type product formula

$$g(t) = PE[f(t)] = \prod_{n=1}^{\infty} (1 - t^n)^{-a_n};$$

- There is explicit inverse (called plethystic logarithm) such that

$$f(t) = PE^{-1}(g(t)) = \sum_{k=1}^{\infty} \frac{\mu(k)}{k} \log(g(t^k)).$$

In the above, $\mu(k)$ is the standard Möbius function for $k \in \mathbb{Z}_+$ which is 0 if k has repeated prime factors and is $(-1)^n$ if k factorizes into n distinct primes (also with the convention that $\mu(1) = 1$). From the physical perspective, the plethystic exponential relates single-trace to multi-trace operators in the gauge theory, as mentioned in the dictionary between quiver representation and supersymmetric gauge theory in Sect. 3.1.1.

Now, let us apply this formalism to a Hilbert series $H(t; M)$ (whose Taylor coefficients are by definition non-negative integers):

Observation 1 Given the Hilbert series $H(t; M)$ of an algebraic variety M , the plethystic logarithm is of the form

$$PE^{-1}[H(t; M)] = b_1 t + b_2 t^2 + b_3 t^3 + \dots$$

where all $b_n \in \mathbb{Z}$ and a positive b_n corresponds to a generator in the coordinate ring of M and a negative b_n , a relation. In particular, if M is a complete intersection, then $PE^{-1}[H(t; M)]$ is a finite polynomial.

For example, our quadric hypersurface \mathcal{C} in \mathbb{C}^4 from (3.28) has Hilbert series

$$H(t; \mathcal{C}) = (1 - t^2)/(1 - t)^4 = \sum_{n=0}^{\infty} (n+1)^2 t^n, \quad (\text{B.12})$$

which can be obtained from (B.11) because \mathcal{C} is a toric variety. One checks that

$$PE^{-1}[H(t; \mathcal{C})] = 4t - t^2, \quad (\text{B.13})$$

meaning that there are four generators in degree 1 (corresponding to the 4 complex coordinates of \mathbb{C}^4) with 1 relation at degree 2 (meaning that \mathcal{C} is a single quadratic hypersurface, and hence complete intersection, in \mathbb{C}^4). Thus, one could have retrieved this Hilbert series by simply writing down $4t - t^2$ and taking the plethystic exponential.

On the other hand, for $\text{Cone}(dP_0) = \mathbb{C}^3/(\mathbb{Z}/3\mathbb{Z})$, the Hilbert series is the Molien series

$$H(t; \mathbb{C}^3/(\mathbb{Z}/3\mathbb{Z})) = \frac{1 + 7t + t^2}{(1-t)^3} = \sum_{n=0}^{\infty} \frac{1}{2} (2 + 9n + 9n^2) t^n, \quad (\text{B.14})$$

and its plethystic logarithm is

$$PE^{-1}[H(t; \mathbb{C}^3/(\mathbb{Z}/3\mathbb{Z}))] = 1 + 10t + 28t^2 + 55t^3 + 91t^4 + 136t^5 + 190t^6 + \dots \quad (\text{B.15})$$

which is non-terminating, in congruence with the fact that the variety, as discussed in Sect. 3.3.1, is not a complete intersection. For these examples, it seems PE^{-1} only terminates for complete intersections, but how one might disentangle positive and negative contributions to each b_n is, as far as we are aware, not known in general.

Appendix C

Brane Tilings

In this brief appendix, we give a summary diagram of some of the inter-connections in the quiver-bipartite tiling-toric Calabi–Yau correspondence. In Fig. C.1, we present the quiver with superpotential for $\mathcal{N} = 4$ super-Yang–Mills theory, whose moduli space of representations is trivially the non-compact toric Calabi–Yau 3-fold \mathbb{C}^3 . This can be encoded into a single periodic quiver with the plus/minus term of the superpotential captured by the anti-clockwise/clockwise 3-cycles and identifying the 4 nodes into 1. Subsequently, this can be graph-dualized to a trivalent bipartite graph on T^2 as the dimer model/brane-tiling. The perfect matchings of a dimer model can be found by the Kasteleyn matrix whose determinant, as a bivariate polynomial, is exactly the Newton polynomial for the toric diagram for \mathbb{C}^3 .

Likewise in Fig. C.2, we present the same for the conifold, the quadric hypersurface in \mathbb{C}^4 , which is also a local toric Calabi–Yau 3-fold. We have also added the two projections of the Newton polynomial, the so-called amoeba and alga (co-amoeba) projections. The reader is referred to the brief lecture [202] as well as the excellent monographs [253, 359] for further details.

C.1 Dessins d’Enfants

It is impossible to resist, when speaking of bipartite graphs on Riemann surfaces, to at least introduce Grothendieck’s **dessin d’enfant**, one of the most profound pieces of modern mathematics [324], residing in the intersections between number theory, geometry and combinatorics. Indeed, in his own immortal words,

This discovery, which is technically so simple, made a very strong impression on me, and it represents a decisive turning point in the course of my reflections, a shift, in particular, of my centre of interest in mathematics, which suddenly found itself strongly focused. *I do not believe that a mathematical fact has ever struck me quite so strongly as this one, nor had a comparable psychological impact.*

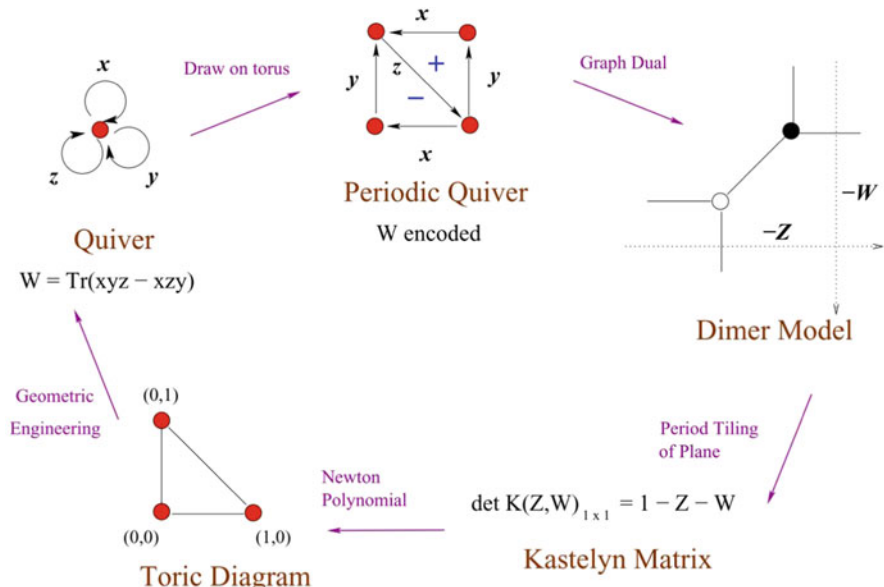


Fig. C.1 The web of correspondences of the quiver, bipartite graph and toric Calabi–Yau moduli space for \mathbb{C}^3

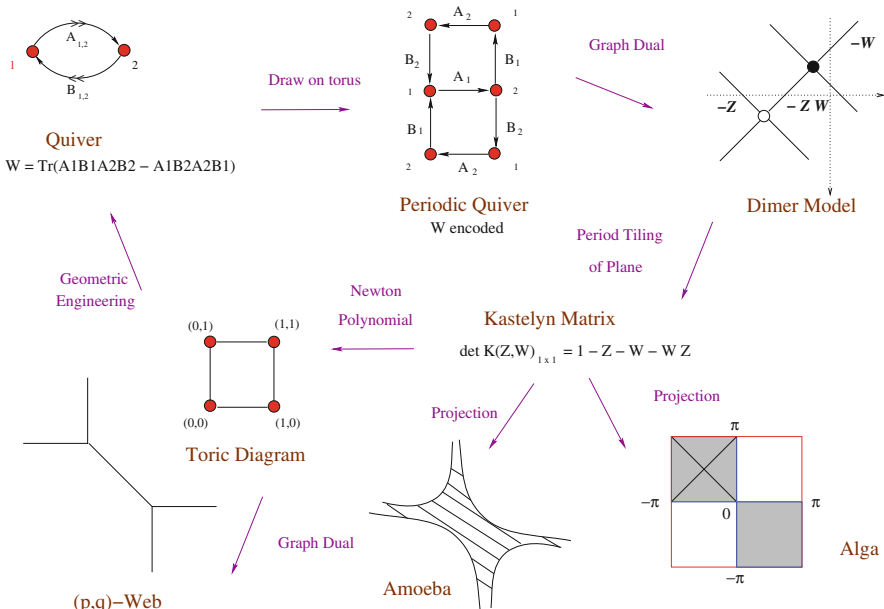


Fig. C.2 The web of correspondences of the quiver, bipartite graph and toric Calabi–Yau moduli space for \mathcal{C}

This is surely because of the very familiar, non-technical nature of the objects considered, of which any child's drawing scrawled on a bit of paper (at least if the drawing is made without lifting the pencil) gives a perfectly explicit example. To such a dessin we find associated subtle arithmetic invariants, which are completely turned topsy-turvy as soon as we add one more stroke.

A. Grothendieck

First, there is the extraordinary theorem of Belyi [38]:

Theorem 19 *Let Σ be a smooth compact Riemann surface, then Σ has an algebraic model over $\overline{\mathbb{Q}}$ IFF there is surjective map $\beta : \Sigma \rightarrow \mathbb{P}^1$ ramified at exactly 3 points.*

There are several points of note about this theorem. First, the IFF translates the analytic property of ramification (i.e., in local coordinates the Taylor series of β starts from order 2) to the number-theoretical property of the algebraic closure of \mathbb{Q} . Second, the proof, which uses classical methods essentially known to Riemann, arose as late as 1980.

Using $SL(2; \mathbb{C})$ on \mathbb{P}^1 , we can take the three branch points to be $(0, 1, \infty)$. Then the theorem states that Σ , defined as a polynomial in $\mathbb{C}[x, y]$ (say, as a hyper-elliptic curve $y^2 = p(x)$), has coefficients as algebraic numbers IFF one can find a rational function $f(x, y) : \Sigma \rightarrow \mathbb{P}^1$ whose Taylor series has no linear term at $0, 1, \infty$.

Grothendieck's insight was to realize that the Belyi map gives an embedded graph on Σ as follows:

Definition 25 Consider $\beta^{-1}(0)$, which is a set of points on Σ that can be coloured as black, and likewise $\beta^{-1}(1)$, white. The pre-image of any simple curve with endpoints 0 and 1 on \mathbb{P}^1 is a bipartite graph embedded in Σ whose valency at a point is given by the ramification index (i.e., order of vanishing of Taylor series) on β . This is the **dessin d'enfant**.

Restricted by Riemann-Hurwitz, $\beta^{-1}(\infty)$ is not an independent degree of freedom, but is rather taken 1-to-1 to the faces in the bipartite graph, with the number of sides of the polygonal face being twice the ramification index. One can succinctly record the valencies as

$$[r_0(1), r_0(2), \dots, r_0(B) \mid r_1(1), r_1(2), \dots, r_1(W) \mid r_\infty(1), r_\infty(2), \dots, r_\infty(I)],$$

where $r_0(j)$ is the valency (ramification index) of the j -th black node, likewise $r_1(j)$, that for the j -th white node, and $r_\infty(j)$, half the number of sides to the j -th face. This nomenclature is called the *passport* of the dessin; it does not uniquely determine it since one further needs the connectivity between the white/black nodes, but it is nevertheless an important quantity. The *degree* of the Belyi map is the row-sum $d = \sum_j r_0(j) = \sum_j r_1(j) = \sum_j r_\infty(j)$ and is the degree of β as a rational function. Finally, Riemann-Hurwitz demands that

$$2g - 2 = d - (B + W + I), \tag{C.1}$$

where g is the genus of Σ and B, W, I are, respectively, the number of pre-images of $0, 1, \infty$. Of course, our focus will be on $g = 1$, balanced (i.e., $B = W$) dessins, for which the total number of pre-images of $0, 1, \infty$ is equal to the degree. We emphasize that the dessin is *completely rigid*, fixing the coefficients in the defining polynomial of Σ to be specific—and oftentimes horrendous—algebraic numbers with no room for complex parameters. That is, given a bipartite graph on a Riemann surface, there is, up to coordinate change (birational transformation), a unique algebraic model and associated Belyi map which gives the graph as a dessin; even the slight change in the numerical coefficients in either will result in an utterly different graph.

In passing we mention that there is a purely combinatorial way to encode dessins—though, of course, in bypassing the analytics of Belyi maps, the algebro-number-theoretic information is somewhat lost. Nevertheless, the ramification structure is captured completely, unlike the rather coarse encoding by passports. One simply labels all edges, say $1, 2, \dots, d$, of the graph on Σ , and work within the symmetric group \mathfrak{S}_n using the standard cycle notation for the elements. Choose a *single* orientation, say clockwise, and for each black node, write the cycle $(e_1 e_2 \dots e_i)$ going clockwise where e_j is the integer label for the said edge. Then form an element $\sigma_B \in \mathfrak{S}_d$ which is the product over all cycles for all black nodes. Similarly, do this for the white nodes (also going clockwise for the edges), forming $\sigma_W \in \mathfrak{S}_d$. Finally, define $\sigma_\infty \in \mathfrak{S}_d$ such that

$$\sigma_B \sigma_W \sigma_\infty = Id ; \quad (C.2)$$

this so-called **permutation triple** captures the structure (valency and connectivity) of the dessin. Indeed, when σ_∞ is itself expressed in terms of product of cycles—as every element of a symmetric group ultimately must—each cycle is associated with a face of the dessin, with its length being half the number of sides of the polygon.

Let us re-consider the hexagon example of (3.35). Observe the Belyi pair of elliptic curve Σ and Belyi map β

$$y^2 = x^3 + 1 , \quad \beta = \frac{1}{2}(1 + y) . \quad (C.3)$$

We see that the pre-image of 0 has $y = -1$, whence $(x, y) = \beta^{-1}(0) = (0, -1)$ on the elliptic curve $y^2 = x^3 + 1$. Choosing local coordinates $(x, y) = (0 + \epsilon, -1 + \delta)$ for infinitesimals (ϵ, δ) , we have that $-2\delta = \epsilon^3$. Therefore locally the map is $\beta = \frac{\delta}{2} \sim -\frac{\epsilon^3}{4}$ and thus the ramification index for this single pre-image of 0 is 3 . Similarly, the pre-image of 1 has $y = +1$, i.e., $(x, y) = (0, 1)$ is the single pre-image of 1 , where local coordinates can be chosen as $(0 + \epsilon, 1 + \delta)$, so that $\beta \sim \frac{\epsilon^3}{2}$. Hence, the ramification index is also 3 for this single pre-image of 1 . Finally, (∞, ∞) is the pre-image of ∞ where the local coordinates $(\epsilon^{-1}, \delta^{-1})$ can

be chosen so that $(x, y) \sim (\epsilon^{-2}, \epsilon^{-3})$. Hence, the ramification index at ∞ is also 3. Thus, the passport is $[3|3|3]$ and the maps is degree 3. In summary

$\mathbb{T}^2 : y^2 = x^3 + 1$	$\xrightarrow{\beta=\frac{1}{2}(1+y)}$	\mathbb{P}^1	Local Coordinates on \mathbb{T}^2	Ram. Index(β)
$(0, -1)$	$\sim -\frac{1}{4}\epsilon^3$	0	$(x, y) \sim (\epsilon, -1 - \frac{1}{2}\epsilon^3)$	3
$(0, 1)$	$\sim \frac{1}{4}\epsilon^3$	1	$(x, y) \sim (\epsilon, 1 + \frac{1}{2}\epsilon^3)$	3
(∞, ∞)	$\sim \frac{1}{2}\epsilon^{-3}$	∞	$(x, y) \sim (\epsilon^{-2}, \epsilon^{-3})$	3

Therefore, what we have is a bipartite graph on T^2 specified by the elliptic curve in (C.3), with a single pair of black/white nodes, each trivalent.

Appendix D

Remembering Logistic Regression

It is expedient to recollect some elements of non-linear regression, especially with the logistic sigmoid function $\sigma(z) = (1 + \exp(-z))^{-1}$. We will phrase this problem from an introductory statistics course in as much ML language as possible.

First, let us take some actual data. As it is rather topical, let us take some COVID19 data from the Johns Hopkins University COVID resource centre <https://coronavirus.jhu.edu/>. In Fig. D.1a, we plot the (cumulative) number of infections I in the UK since the beginning of records (Jan 22nd, 2020) by the day t . Thus, we have a labeled dataset $\mathcal{D} = \{t \rightarrow I\}$, a total of 157 points. Inspecting the curve, a logistic sigmoid function seems a good fit. We introduce weights and biases

$$\sigma_{a,b,c,d}(t) = a(1 + b \exp(-ct))^{-1} + d , \quad (a, b, c, d) \in \mathbb{R} . \quad (\text{D.1})$$

Ordinarily, we would try to fit the curve to the entire set of points; since there are only four parameters (a, b, c, d) , there is no danger of over-fitting here. In a more complicated supervised ML situation, there might be thousands of parameters, and we thus adopt the strategy of cross-validation. It is, of course, an overkill in the present example, but let us thus proceed for illustrative purposes.

We split \mathcal{D} into a training set \mathcal{T} , a random sample of, say, 20% of the data. Then we minimize a cost-function, which here can be taken to be the sum squared:

$$F(a, b, c, d) := \sum_{(t \rightarrow I) \in \mathcal{T}} \left[(a(1 + b \exp(-ct))^{-1} + d) - I \right]^2 , \quad (\text{D.2})$$

in order to find (a, b, c, d) . For example, we find (on one random 20% sample), $(a, b, c, d) = (288681.0, 241.259, 0.0666724, -7933.96)$. In part (b) of the figure, we plot the fitted curve against the complement validation set $\mathcal{C} = \mathcal{D} - \mathcal{T}$. The missing points in the (blue) scatter plot are precisely the ones which we used for the training set.

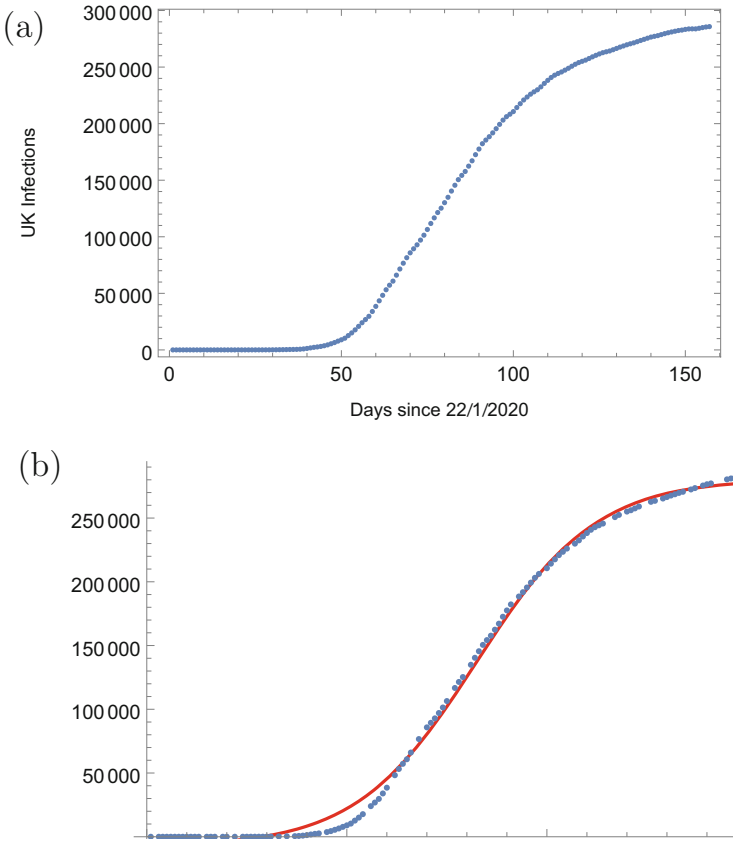


Fig. D.1 (a) UK daily cumulative infection of COVID19 since Jan 22nd, 2020; (b) a fit by a logistic sigmoid

While we see that the fit is fairly reasonable, we need to quantify a measure of “goodness of fit”. For continuous variables, such as I here, a commonly used one is the **coefficient of determination**, otherwise known as “R-squared”, defined as

$$R^2 := 1 - \frac{\sum_i (y_i - f_i)^2}{\sum_i (y_i - \bar{y})^2}, \quad (\text{D.3})$$

where y_i are the outputs (in the above, the list of I values), \bar{y} is the mean over y_i and f_i are the fitted values (in the above, the list of $\sigma(t)$). The numerator $\sum(y_i - f_i)^2$ is thus, for the above example, our list of $F(a, b, c, d)$ at the optimized values of (a, b, c, d) . A value of $R^2 = 1$ would be a perfect fit, and a value of $R^2 = 0$ is the baseline where the model always predicts the mean. In our example above, we find that $R^2 \sim 0.999$. We remark that in ML, such measures are ordinarily only computed for the validation set.

What we have done in this example is to phrase a simple non-linear regression in the terminologies of ML. In fact, where there is a single neuron, with a sigmoid activation function, this problem is exactly what supervised ML is for a neural “network” with a single node.

Appendix E

A Computational Compendium: Homage to SageMath

As promised in the text, we demonstrate in this appendix some of the powers of **SageMath**, an over-arching, open-source software which takes full advantage of the various software we have mentioned throughout the book. As always, we illustrate with explicit examples, paying attention to how it links to the software.

The dedicated are encouraged to download the latest version of **SageMath** onto their laptops from

<https://www.sagemath.org/>

Those who wish for a more casual acquaintance and immediate calculation can go to the Cloud version at

<https://cocalc.com/>

One creates a free account, hits the “Create Project” tab, followed by the “New” tab, within which one then chooses the option to create a “Sage worksheet”. This brings us to the worksheet interface immediately.

E.1 Algebraic Varieties

We begin with some problems in standard algebraic geometry, and our go-to programme [163] is **Macaulay2**, which we can easily call within **SageMath**:

```
1. macaulay2('R = ZZ/101[x,y,z]');
2. macaulay2('testid = ideal(z*y^2 - x^3 - 4*x*z^2 - z^3)');
3. macaulay2('ell = Proj( R / testid )');
```

In line 1, we first create a polynomial ring R in 3 complex variables (x, y, z) , with coefficients in $\mathbb{Z}/(101\mathbb{Z})$. In **Macaulay2** it is customary to work with coefficients modulo some prime, here 101, to avoid rapid growth of the size of coefficients. In other words, we use $\mathbb{Z}/(101\mathbb{Z})[x, y, z]$ to model $\mathbb{C}[x, y, z]$. In case

we hit bad primes, we could always redo the computation over a few different coefficient fields to make sure all geometric quantities stabilize. That is, we could try $\text{ZZ}/101[x, y, z]$, $\text{ZZ}/541[x, y, z]$, etc. and repeat the calculation to make sure that we obtain the same answer.

In line 2, we create an ideal, called `testid`, defined by a single (homogeneous) cubic in the 3 variables. In line 3, the projective algebraic variety `e11` is created from the coordinate ring `R/testid` by taking `Proj`. If one wished to create an affine algebraic variety, one would have used `macaulay2.Spec(R/testid)`. To create an ideal defined by multiple polynomials, we simply list these polynomials separated by comma, e.g.,

```
4. macaulay2('testid2 = ideal(z*y^2 - x^3 - 4*x*z^2 - z^3, x+y+z)');
5. macaulay2('pt = Proj(R/testid2)');
```

Indeed, `e11` is now an elliptic curve as a hypersurface in \mathbb{CP}^2 with homogeneous coordinates $[x : y : z]$. If one wished to play with \mathbb{CP}^2 itself, one would execute `Proj(R)` directly without going to the quotient (coordinate) ring. To quickly check that the dimensions are correct, we execute

```
6. macaulay2.dim(e11)
7. macaulay2.dim(pt)
```

which return 1 and 0, respectively (these are understood to be the complex dimensions).

Let us check that the elliptic curve is smooth with

```
8. macaulay2('singularLocus(e11)');
```

which returns `Proj (R / 1)`, meaning that the corresponding ideal is $(1) \in R$ which is clearly never vanishing. In other words, the singular locus is the null set.

We can further check that `e11` is Calabi–Yau explicitly. First, we construct the canonical bundle

```
9. macaulay2('cb = cotangentSheaf(e11)');
10. macaulay2('can = exteriorPower(1, cb)');
11. macaulay2('rank(can)'),
```

where we check that the canonical bundle $\wedge^1 T^*$, the top wedge product of the cotangent bundle T^* , is rank 1. Of course, here in dimension 1, this is an overkill. In dimension n , we do need to compute $\wedge^n T^*$ using `exteriorPower(n, _)`.

In particular, line 10 returns, for the canonical bundle K_{ell} as \mathcal{O}_{ell} , which is one of the equivalent definitions of Calabi–Yau-ness. In any event, we can go to compute all the requisite cohomology groups

```
11. macaulay2('HH^0(can)');
12. macaulay2('HH^1(can)');
```

giving, as expected, 1 and 1.

Finally, we can compute the Hilbert series of this variety, embedded in \mathbb{P}^2 :

```
13. macaulay2('hilbertSeries ideal(ell)');
```

which returns $(1 - T^3)/(1 - T)^3$, being that of a single cubic in 3 (projective) variables with the same grading 1.

We make some parenthetical remarks here. In the above we had all computations done *within Macaulay2*. One can actually pass variables freely *between SageMath* and an external software, in which case, we can redo the above with (note the Python syntax in commands such as `macaulay2.ideal()`):

```
R = macaulay2('ZZ/101[x,y,z]');
x = macaulay2('x'); y = macaulay2('y'); z = macaulay2('z');
testid = macaulay2.ideal(z*y^2 - x^3 - 4*x*z^2 - z^3);
ell = macaulay2.Proj(R/testid);
cot = macaulay2.cotangentSheaf(ell);
can = macaulay2.exteriorPower(1, cot);
macaulay2.cohomology(0, cot); macaulay2.cohomology(1, cot)
```

The advantage of this approach, of course, would be the flexibility to manipulate these objects within *SageMath*.

Second, we could just as easily go to *Singular* as the preferential computational geometry software [108], in which case the syntax for creating the variety and testing its dimension would be something like:

```
r = singular.ring(101, '(x,y,z)', 'lp');
testid = singular.ideal(z*y^2 - x^3 - 4*x*z^2 - z^3, x+y+z);
singular.dim(testid)
```

The reader is referred to [160] for linking *Singular* to *Mathematica*.

E.2 Combinatorics and Toric Varieties

Luckily, manipulations of polytopes and related toric varieties have been built into *SageMath* so there is no need to even call external software. In fact, all reflexive polytopes for dimension $n = 2, 3$ are also built in (the half billion $n = 4$ cases are, unfortunately, too large a set). Let us try \mathbb{P}^2 as a toric variety. There are three equivalent ways to define it:

```
1. p2dual = ReflexivePolytope(2,0);
2. p2 = p2dual.polar();
3. V1 = ToricVariety( NormalFan(p2) );
4. V2 = ToricVariety( Fan(
    Cone([(1,0), (0,1)]),
    Cone([(1,0), (-1,-1)]),
    Cone([(0,1), (-1,-1)]) ) );
5. V3 = toric_varieties.P2();
```

In lines 1 and 2, we pull up the 2-dimensional reflexive polytope in **SageMath**'s database, number 0 (there are 16 reflexive polygons, so the index goes from 0 to 15; for `ReflexivePolytope(2, n)`, n ranges from 0 to 4318). This happens to be the polar dual polytope to that for \mathbb{P}^2 , thus we take the dual back in line 2. Next, in line 3, we construct the normal fan to this polygon and construct the toric variety `V1`. Alternatively, we can be explicit and write down the list of cones, and the subsequent fan, to obtain `V2` in line 4. Finally, \mathbb{P}^2 is standard enough that it is in the small built-in database of `toric_varieties`. One can readily check, e.g., by `V1.fan().rays()`, or `V3.fan().cones()`, that the 3 definition do coincide.

We could further visualize the fan (line 6) and the polygon (line 7) by

```
6. V1.fan().plot()
7. LatticePolytope(p2).polyhedron().plot()
```

Moreover, we can check the dimension of the variety with `dimesion(V1)`, giving 2 as required.

Next, we can start experimenting in algebraic geometry. One extracts (co-)homology classes by

```
8. hh = V1.cohomology_ring()
9. hh.gens()
```

Line 8 produces the cohomology ring $H^*(\mathbb{P}^2; \mathbb{Z})$. We know this to be $\mathbb{Z}[x]/\langle x^3 \rangle$, with generator x corresponding to the class $H^2(\mathbb{P}^2; \mathbb{Z})$; indeed, \mathbb{CP}^2 is a 4-manifold, with $H^p(\mathbb{P}^2; \mathbb{Z}) = 0$ for $p = 1, 3$ and \mathbb{Z} for $p = 0, 2, 4$. One sees that line 9 produces a single generator.

From the above, one can proceed to intersection theory, and hence integration:

```
10. D = V1.divisor(0);
11. V1.integrate( hh(D)^2 );
```

We create a divisor (codimension 1 sub-manifold) D , which for the toric variety, corresponds to the 3 rays. In line 10, we take the first of them and then take the corresponding element in the cohomology ring hh , a real 2-form. The square (wedge product) gives a 4-form, which can then be integrated over the whole manifold, here returning the (normalized) value of 1.

E.3 Representation Theory

The go-to program in finite group theory, another subject extensively discussed in this book, is perhaps **GAP** [338]. Again, **SageMath** readily incorporates the functionalities thereof. We begin by creating a finite group. To be concrete, let us take the \widehat{E}_8 example from (B.10):

```
1. GG = gap('Group(
1/2*[[-1+E(4), -1+E(4)], [[1+E(4), -1-E(4)]], [[E(4), 0], [0, -E(4)]],
```

```

[[E(4)/2, (1-ER(5))/4-E(4)*(1+ER(5))/4],
 [- (1-ER(5))/4-E(4)*(1+ER(5))/4, -E(4)/2]] ]); ');
2. gap.IdGroup(GG);
3. gap.StructureDescription(GG);

```

In line 1, we have called **GAP** from within **SageMath** and the command to create a finite group is simply `Group()`. The 3 matrix generators are $\langle S, T, V \rangle$ as given in (B.10). Note that in **GAP**, $E(n)$ means the primitive n -th root of unity (hence $E(4)$ is their notation for i) and $ER(n)$ means \sqrt{n} . In line 2, we use the command `IdGroup()` which identifies **GAP**'s internal database of small groups.

As mentioned in the text, this is a database of *all* finite groups up to order 2000, except that of order 1024, a staggering total of 423,164,062 groups (there are, in addition, few more families). The command returns `[120, 5]`, which is number 5 (in their internal library) of the groups of order 120; the order is certainly correct. We further identify the group using line 3, which returns `SL(2, 5)`, which is the finite group $SL(2; \mathbb{F}_5)$, the special linear group defined on the finite field of 5 elements. This is indeed an equivalent description for the binary icosahedral group. Matrix groups are only one of the many ways to encode groups. **SageMath** and **GAP** can as easily handle explicit presentation from free groups, or permutations in terms of cycle notation.

We could obtain standard group theoretic properties, such as

```

4. tt = gap.CharacterTable(GG);
5. gap.Display(tt);
6. gap.IsSimple(GG);

```

where lines 4 and 5 display the ordinary character table of the group and line 6 checks whether it is a simple finite group.

To obtain the Molien series (Hilbert series) from the action by a particular representation, we execute:

```

7. irr = gap.Irr( tt );
8. gap.MolienSeries( irr[2] );

```

where line 7 gives the list of all irreducible representations and line 8 takes the second (the defining 2-dimensional irrep) and computes the Molien series according to (B.8).

E.4 Number Theory and More

Of course, of all the branches of pure mathematics and of the tens of thousands of commands, we have only given a glimpse of **SageMath**'s power and versatility, but hopefully enough to get the non-experts started with explorations and sufficient elements to allow them to experiment with the concepts presented in this book. With the growing importance of the interactions between number theory and physics, as well as the beginnings of machine-learning in number theory [6, 226], we end

our homage to **SageMath** with some of its abilities therein to whet the reader's appetite.

The important LMFdB (L-functions and modular forms database), to which we alluded several times in the book [341], has much of its contents also incorporated into **SageMath**. For instance,

```
1. E = EllipticCurve('37a')
```

returns the elliptic curve number '`37a`' which is the so-called Cremona label. We can see explicitly that this is the elliptic curve $y^2 + y = x^3 - x$ in Tate form. One can extract many of our favourite quantities such as

```
2. E.analytic_rank()  
3. E.lseries()  
4. E.j_invariant()  
5. E.conductor()  
6. E.short_weierstrass_model()
```

which are, respectively, the analytic rank, L-series, j-invariant, conductor and Weierstraß model.

Glossary

n -Fold Complex manifold of complex dimension n 1, 5

n -Manifold Real manifold of real dimension n 1, 5

$\mathcal{O}_{\mathbb{CP}^n}(k)$ Line bundle of degree k over \mathbb{CP}^n . It is the k -th tensor product $\mathcal{O}_{\mathbb{CP}^n}(1)^{\otimes k}$.

The global sections have, as a basis, degree k monomials in the $n + 1$ homogeneous coordinates. One can restrict this to a variety $X \subset \mathbb{CP}^n$ and write $\mathcal{O}_X(k)$ 1, 136

ADE The simply laced Lie algebras, i.e., complex Lie algebras whose Dynkin diagrams only have single bonds. By the McKay Correspondence, these are intimately related to the discrete finite subgroups of $SU(2)$ 1, 67, 157

Betti number b_i of a manifold is the rank of the i -th (co-)homology group (suitably defined), e.g., de Rham cohomology. It counts the number of independent algebraic cycles in dimension i . Importantly, the Euler number χ is the alternating sum of b_i 1, 4

Canonical bundle K_M , the top wedge power of the cotangent bundle of a manifold, e.g., for M a complex n -fold, $K_M := \wedge^n T_M^\vee$. This is a line bundle whose degree determines whether the variety is Fano, Calabi-Yau or general-type; e.g., degree 0 means CY, degree negative (i.e., the dual bundle, or, anti-canonical bundle, has positive degree) means Fano 1, 16, 20, 27, 68

Chern class A topological invariant of a manifold M , one of the most commonly used characteristic classes. The i -th Chern class c_i takes value in $H^{2i}(M; \mathbb{Z})$, as a real cohomology class. It has an analytic definition in terms of curvature as well as an algebraic definition in terms of Grothendieck's axioms 1, 21, 138

Complete intersection A algebraic variety whose co-dimension is equal to the number of its defining equations. A hypersurface is trivially a complete

intersection. This is very important in algebraic geometry: k equations in n variables do not necessarily define a variety of dimension $n - k$; when it does, it is complete intersection. Complete intersection Calabi-Yau manifolds embedded in products of (weighted) projective spaces are historically denoted as CICYs 1,

Complex projective space Denoted \mathbb{CP}^n , or simply \mathbb{P}^n , is the set of directions in \mathbb{C}^{n+1} . It has homogeneous coordinates $[x_0 : \dots : x_n]$ inherited from the affine coordinates (x_0, x_1, \dots, x_n) of \mathbb{C}^{n+1} by quotienting $\lambda : (x_0, x_1, \dots, x_n) \mapsto \lambda(x_0, x_1, \dots, x_n)$ for $\lambda \in \mathbb{C}^\times$. One can weight the λ -action to give weighted projective space $W\mathbb{P}^n$ 1, 20, 135

Conifold In physics, the conifold refers to the affine CY₃ defined by the hypersurface $uv = wz$ in \mathbb{C}^4 with affine coordinates (x, y, z, w) . In the mathematics literature, it is simply called the quadric hypersurface 1, 77, 145

Convex polytope Δ_n is the convex hull of k vertices in \mathbb{R}^n . It is also the solution of a set of linear inequalities. In this book we only consider convex lattice polytopes, whose vertices are lattice points. Furthermore, we primarily consider reflexive polytopes, which are convex lattice polytopes with a single interior lattice point and such that all bounding hyperplanes (facets) are distance 1 away therefrom 1, 38

CY_n Calabi-Yau (Kähler, Ricci-flat) manifold of complex dimension n 1, 7

D-branes Solitonic objects in type II string theory. A D p -brane has space-times dimension $p + 1$. In type IIA, there are D p -branes for $p = 0, 2, 4, 5, 8$ and in type IIB, $p = -1, 1, 3, 5, 7, 9$. These provide the sub-varieties of $\mathbb{R}^{9,1}$ on which open strings can end 1, 60

del Pezzo surface Complex surfaces (real dimension 4) with positive curvature, i.e., Fano varieties in dimension 2. These are \mathbb{P}^2 blown up at $n = 0, \dots, 8$ generic points (denoted dP_n), as well as $\mathbb{P}^1 \times \mathbb{P}^1$ 1, 148

Euler number χ , also called Euler characteristic, a topological invariant of a manifold, being the alternating sum of Betti numbers. It is also the integral of the top Chern class. The equivalence between the combinatorial/topological notion and the integral/analytic notion is a sequence of the index theorem 1, 3, 23

Exact sequence A chain of objects (vector space, groups, etc.,) A_i and maps $f_i : A_i \rightarrow A_{i+1}$ such that $\ker(f_{i+1}) = \text{Im}(f_i)$. If there are 3 terms, it is called short exact. For a sequence which is not exact, (co-)homology measures the extent of non-exactness: $H^i := \ker(f_{i+1})/\text{Im}(f_i)$ 1, 24, 137

Fano A Fano variety is a complex manifold of positive curvature, such as \mathbb{CP}^n . In general, complex algebraic varieties can be (birational to) varieties which

are Fano (positive curvature), Calabi-Yau (zero curvature) and general-type (negative curvature) 1, 41, 147

Genus The genus g of a Riemann surface is the number of “holes”, it is related to the Euler number as $\chi = 2 - 2g$ 1, 3

Goodness of Fit Measures for accuracies in a model. Some commonly used ones are tabulated in Sect. 4.2.6. We also distinguish between **training curve** (Definition 19) and **learning curve** (Definition 20) in this book (purely the author’s convention) 1, 110

Gröbner basis A generalization of Gaussian elimination (multi-variate linear system) for multi-variate polynomials; also called standard basis. This is the heart of computational algebraic geometry, any given ideal (system of polynomials) which defines a variety is first put into an appropriate (well-defined monomial ordering) Gröbner basis 1, 153

Heterotic string A (duality-equivalent) formalism of super-string theory, which has an naturally endowed E_8 or $SO(32)$ gauge group. It was the first direction from string theory which required Calabi-Yau manifolds from the point of view of compactification 1, 8, 50

Hilbert Series One of the most important property of an algebraic variety is its Hilbert series, which counts the number of independent monomials at each degree on the variety. For a variety coming from an orbifold by a finite group, this reduces to the Molien series of group invariants. There is a plethystic programme of using the plethystic exponential/logarithm functions to study operators in a quantum field theory 1, 156

Hirzebruch surface A complex surface which is a \mathbb{P}^1 fibration over \mathbb{P}^1 . These are classified by a single integer $r \geq 0$, called the r -th Hirzebruch surface, denoted \mathbb{F}_r . They are all toric varieties 1, 148

Hodge numbers $h^{p,q}$, the complex, double-indexed, version of the Betti number for complex manifolds. By Poincaré duality and complex conjugation, they can be organized into a diamond-shaped diagram with explicit symmetries, called **Hodge diamond** 1, 16, 33, 36, 45

Hypersurface An algebraic variety defined by a single polynomial in an ambient space (typically \mathbb{P}^n). Its (complex) codimension is therefore 1. A degree 1 hypersurface is a hyperplane, e.g., \mathbb{P}^n is a hyperplane in \mathbb{P}^{n+1} , defined by any linear equation in the $n + 1$ variables 1, 20

Ideal The subset of a ring closed under $+$, \times . In this book, we only consider ideals I of a polynomial ring $R = \mathbb{C}[x_1, \dots, x_n]$. Specially, these are generated by a list of multi-variable polynomials $f_{i=1, \dots, k}$ in the n variables. We write $I = \langle f_1, \dots, f_k \rangle$. We also write $X(I)$ as the vanishing locus of the polynomials,

i.e., the (affine) variety defined by I . The quotient R/I is a ring, called the coordinate ring of $X(I)$ 1, 25

Landscape While in string theory, the landscape has become a more technical term, we use it loosely to mean the plethora of geometrical data 1, 13, 49, 84

Loss Function A measure of error during training and validation. There are many choices; typically for continuous data, the sum of squares error is preferred and for discrete data, cross-entropy is preferred 1, 96

Manifolds Topological spaces which are locally \mathbb{R}^n (a real n -manifold) or \mathbb{C}^n (a complex n -fold). An important sequence of specializations: manifolds \supset Riemannian \supset complex/Hermitian \supset **Kähler** \supset **Calabi-Yau** 1, 134

McKay Correspondence A remarkable correspondence between the finite discrete subgroups of $SU(2)$ and the simply-laced Lie algebras, viz., types A_n , D_n and $E_{6,7,8}$. This is part of a wider story where the ADE pattern appears in many seemingly unrelated branches of mathematics 1, 69

ML Machine-Learning. Roughly divided into unsupervised and supervised ML. The former does not label the data-points and algorithms are designed to find inherent patterns in the data. The latter has each data-point labeled according to some output and an algorithm has to find an optimal way of finding the pattern input \rightarrow output. When the output is continuous, the ML algorithm is typically called a **regressor**; when the output is discrete or categorical, the algorithm is called a **classifier**. Some common supervised ML techniques are given in Sects. 4.2.2, 4.2.3, and 4.2.5 1, 94

MLP Multi-layer Perceptron, nowadays more referred to as forward-feeding **Neural Networks**. A connected, directed graph, whose nodes are neurons/perceptrons and whose arrows are input/outputs. The MLP can be organized into a layered structure when one proceeds through (1) the input, (2) the hidden layers and (3) the output. Various technical terms to an NN is summarized in Sect. 4.2.4 1, 97

Neural Network A connected, directed graph of neurons/perceptrons/activation-functions. Using the complexity in connectivity, it is widely used in ML. The Universal Approximation Theorems 12 and 13, dictate that given sufficient depth and/or width of the NN, arbitrary input-output can be approximated. Common NNs are MLPs (Sect. 4.2.2), CNNs (Sect. 4.2.3), etc. 1, 98

Orbifolds singular, non-compact, complex manifolds obtained by the quotient of an action by a finite group with fixed point. For example, \mathbb{C}^2/Γ is an orbifold of \mathbb{C}^2 by some finite group Γ which fixes the origin $(0, 0)$, e.g., $\Gamma \ni g : (x, y) \mapsto (-x, -y)$ 1, 66

Perceptron or Neuron. A function (called **activation function**), typically differentiable, with some multi-indexed input z and output $f(w \cdot z + b)$, where w are the weights and b , the bias. 1, 95

Quintic Degree 5 hypersurface in \mathbb{P}^4 is the most famous CY₃ 1, 21, 25, 56
quiver a (finite) directed graph, whose vertices are associated to vector spaces \mathbb{C}^m and arrows are maps (matrices) from \mathbb{C}^m to \mathbb{C}^n . There could be formal relations amongst the arrow prescribed by (the Jacobian) of a super-potential. In physics, such relations are called **F-terms** and the adjacency information of the graph, **D-terms**. These both contribute to the Lagrangian of a gauge theory which the quiver encodes 1, 61

Regression Given a labeled set $\{\mathbf{x}_i \rightarrow y_i\}$, one finds a differentiable function $f(\mathbf{x}_i)$ which is the “best fit” by minimizing error (such as sum of squares error) 1, 167

Riemann surfaces Σ , these are surfaces as real-dimension 2 manifolds and can be complexified to complex curves, of complex dimension 1 1, 5

Spec The spectrum of a ring. In this book, we only consider the maximal spectrum, or the set of maximal ideals, of a polynomial ring $R = \mathbb{C}[x_1, \dots, x_n]$. $\text{Spec}(R)$ is a purely algebraic way to define \mathbb{C}^n , as $\text{Spec}(R/I)$ is a purely algebraic way to define an affine variety given by a polynomial system (ideal) I . The analogue for a projective variety is “Proj”. 1, 143

Standard Model The standard model of particle physics is a gauge theory with fundamental particles being connections and sections of an $SU(3) \times SU(2) \times U(1)$ bundle over spacetime $\mathbb{R}^{3,1}$. The minimal supersymmetric extension therofe is usually denoted the **MSSM** 1, 8, 11

SVM Support vector machine is a common geometric method in supervised ML. It is not a NN and use a hyperplane to separate labeled data-points. 1, 104

Topological types For (compact, smooth) Riemann surfaces (without boundary or punctures), the topological type is distinguished by a single non-zero integer, the genus (or equivalently, the Euler number). For CY₃, this is the data of Hodge numbers, second Chern class, and the triple intersection numbers. 1, 3, 50

Toric variety A complex manifold which has $(\mathbb{C}^*)^n$ as a dense subset, and whose action extends to the whole manifold. It can be described purely combinatorially in terms of lattice cones and polyhedra 1, 41, 72, 142

Variety or, algebraic variety, is the locus of points defined by the vanishing of a system of polynomials. In \mathbb{C}^n , it is called an affine variety and in \mathbb{CP}^n ,

a projective variety. In this book we only consider such complex algebraic varieties. Purely algebraically, we work in a polynomial ring $R = \mathbb{C}[x_1, \dots, x_n]$ and the polynomial system can be considered as an ideal in R

[1](#), [25](#), [143](#)

VMS Vacuum Moduli Space of a quantum field theory is the manifold parametrized by the vacuum expectation values of the scalars in the theory. In a supersymmetric gauge theory, this is the set of solutions to the D-terms and F-terms, and defines a complex algebraic variety

[1](#), [63](#)

References

1. D. Adams, *The Hitchhiker's Guide to the Galaxy* (Arthur Barker, London, 1979)
2. M. Agrawal, N. Kayal, N. Saxena, PRIMES is in P. Ann. Math. **160**(2), 781–793 (2002)
3. L.F. Alday, G. Aldazabal, In quest of just the standard model on D-branes at a singularity. J. High Energy Phys. **0205**, 022 (2002) [hep-th/0203129]
4. G. Aldazabal, L.E. Ibanez, F. Quevedo, A.M. Uranga, D-branes at singularities: a bottom-up approach to the string embedding of the standard model. J. High Energy Phys. **0008**, 002 (2000) [hep-th/0005067]
5. G. Aldazabal, S. Franco, L.E. Ibanez, R. Rabadan, A.M. Uranga, Intersecting brane worlds. J. High Energy Phys. **0102**, 047 (2001) [hep-ph/0011132]
6. L. Alessandretti, A. Baronchelli, Y.H. He, Machine learning meets number theory: the data science of Birch–Swinnerton-Dyer (2019) [arXiv:1911.02008 [math.NT]]
7. R. Altman, J. Gray, Y.H. He, V. Jejjala, B.D. Nelson, A Calabi-Yau database: threefolds constructed from the Kreuzer-Skarke list. J. High Energy Phys. **1502**, 158 (2015) [arXiv:1411.1418 [hep-th]]
8. R. Altman, J. Carifio, J. Halverson, B.D. Nelson, Estimating Calabi-Yau hypersurface and triangulation counts with equation learners. J. High Energy Phys. **03**, 186 (2019) [arXiv:1811.06490 [hep-th]]
9. L.B. Anderson, Y.H. He, A. Lukas, Heterotic compactification, an algorithmic approach. J. High Energy Phys. **0707**, 049 (2007) [hep-th/0702210]
10. L.B. Anderson, Y.H. He, A. Lukas, Monad bundles in heterotic string compactifications. J. High Energy Phys. **0807**, 104 (2008). [arXiv:0805.2875]
11. L.B. Anderson, V. Braun, R.L. Karp, B.A. Ovrut, Numerical Hermitian Yang-Mills connections and vector bundle stability in heterotic theories. J. High Energy Phys. **06**, 107 (2010) [arXiv:1004.4399 [hep-th]]
12. L.B. Anderson, J. Gray, A. Lukas, E. Palti, Two hundred heterotic standard models on smooth Calabi-Yau threefolds. Phys. Rev. D **84**, 106005 (2011) [arXiv:1106.4804 [hep-th]]; L.B. Anderson, J. Gray, A. Lukas, E. Palti, Heterotic line bundle standard models. J. High Energy Phys. **1206**, 113 (2012) [arXiv:1202.1757 [hep-th]]; L.B. Anderson, J. Gray, A. Lukas, E. Palti, Heterotic standard models from smooth Calabi-Yau three-folds. PoS CORFU **2011**, 096 (2011); A. Constantin, A. Lukas, Formulae for line bundle cohomology on Calabi-Yau threefolds (2019). arXiv:1808.09992 [hep-th]
13. L.B. Anderson, F. Apruzzi, X. Gao, J. Gray, S.J. Lee, A new construction of Calabi–Yau manifolds: generalized CICYs. Nucl. Phys. B **906**, 441–496 (2016) [arXiv:1507.03235 [hep-th]]

14. L.B. Anderson, X. Gao, J. Gray, S.J. Lee, Fibrations in CICY threefolds. *J. High Energy Phys.* **1710**, 077 (2017) [arXiv:1708.07907 [hep-th]]; L.B. Anderson, J. Gray, B. Hammack, Fibrations in non-simply connected Calabi-Yau quotients. *J. High Energy Phys.* **1808**, 128 (2018) [arXiv:1805.05497 [hep-th]]
15. L.B. Anderson, M. Gerdes, J. Gray, S. Krippendorf, N. Raghuram, F. Ruehle, Moduli-dependent Calabi-Yau and $SU(3)$ -structure metrics from machine learning (2020) [arXiv:2012.04656 [hep-th]]
16. M. Artin, *Algebra* (Pearson Education, Boston, 2011)
17. A. Ashmore, Y.H. He, B.A. Ovrut, Machine learning Calabi-Yau metrics. *Fortsch. Phys.* **68**(9), 2000068 (2020) [arXiv:1910.08605 [hep-th]]
18. P.S. Aspinwall, K3 surfaces and string duality, in *Differential Geometry Inspired by String Theory*, ed. by S.T. Yau (1996), pp. 1–95 [hep-th/9611137]
19. M.F. Atiyah, Vector bundles over an elliptic curve. *Proc. LMS (3)* **7**, 414–452 (1957)
20. M. Atiyah, E. Witten, M theory dynamics on a manifold of $G(2)$ holonomy. *Adv. Theor. Math. Phys.* **6**, 1 (2003) [hep-th/0107177]
21. A.C. Avram, M. Kreuzer, M. Mandelberg, H. Skarke, The web of Calabi-Yau hypersurfaces in toric varieties. *Nucl. Phys. B* **505**, 625 (1997) [hep-th/9703003]
22. D. Bailin, G.V. Kraniotis, A. Love, Supersymmetric standard models on D-branes. *Phys. Lett. B* **502**, 209 (2001) [hep-th/0011289]
23. E. Ballico, E. Gasparim, B. Suzuki, Infinite dimensional families of Calabi–Yau threefolds and moduli of vector bundles. *J. Pure Appl. Algebra* **225**, 4 (2021)
24. J. Bao, S. Franco, Y.H. He, E. Hirst, G. Musiker, Y. Xiao, Quiver mutations, seiberg duality and machine learning (2020) [arXiv:2006.10783 [hep-th]]
25. J. Bao, Y.H. He, E. Hirst, S. Pietromonaco, Lectures on the Calabi-Yau landscape (2020) [arXiv:2001.01212 [hep-th]]
26. J. Bao, Y.H. He, E. Hirst, J. Hofscheier, A. Kasprzyk, S. Majumder, Hilbert Series, Machine Learning, and Applications to Physics [arXiv:2103.13436 [hep-th]]
27. V. V. Batyrev, Canonical models of toric hypersurfaces [arXiv:2008.05814 [math.AG]]
28. V.V. Batyrev, Dual polyhedra and mirror symmetry for Calabi-Yau hypersurfaces in toric varieties. *J. Alg. Geom.* **3**, 493 (1994). [alg-geom/9310003]
29. V.V. Batyrev, L.A. Borisov, On Calabi-Yau complete intersections in toric varieties (1994). arXiv:alg-geom/9412017; V.V. Batyrev, Dual polyhedra and mirror symmetry for Calabi-Yau hypersurfaces in toric varieties. *J. Alg. Geom.* **3**, 493–545 (1994) [arXiv:alg-geom/9310003]
30. V.V. Batyrev, L.A. Borisov, On Calabi-Yau complete intersections in toric varieties (1994) arXiv:alg-geom/9412017
31. V. Batyrev, I. Ciocan-Fontanine, B. Kim, D. van Straten, Conifold transitions and mirror symmetry for Calabi-Yau complete intersections in Grassmannians. *Nucl. Phys. B* **514**(3), 640–666 (1998); Mirror symmetry and toric degenerations of partial flag manifolds. *Acta Math.* **184**(1), 1–39 (2000); M.I. Qureshi, B. Szendroi, Calabi-Yau threefolds in weighted flag varieties. *Adv. High Energy Phys.* **2012**, 547317 (2012), 14pp. arXiv:1105.4282 [math.AG]
32. K. Baur, A. King, R. Marsh, Dimer models and cluster categories of Grassmannians (2016). arXiv:1309.6524
33. D. Bayer, M. Stillman, Computation of Hilbert functions. *J. Symbol. Computat.* **14**(1), 31–50 (1992)
34. A. Beauville, *Complex Alg. Surfaces*. LMS. Texts, vol. 34 (Cambridge University Press, Cambridge, 1996)
35. K. Becker, M. Becker, J.H. Schwarz, *String Theory and M-Theory: A Modern Introduction* (Cambridge University Press, Cambridge, 2007)
36. C. Beil, The geometry of noncommutative singularity resolutions (2011). arXiv:1102.5741
37. A. Belinson, Coherent sheaves on P_n and problems in linear algebra. *Funktional. Anal. i Prilozhen.* **12**(3), 6869 (1978)
38. G. Belyi, (Trans. N. Koblitz), Galois extensions of a maximal cyclotomic field. *Math. USSR Izv.* **14**(2), 247–256 (1980)
39. S. Benvenuti, B. Feng, A. Hanany, Y.H. He, Counting BPS operators in gauge theories: quivers, syzygies and plethystics. *J. High Energy Phys.* **0711**, 050 (2007) [hep-th/0608050];

- B. Feng, A. Hanany, Y.H. He, Counting gauge invariants: the Plethystic program. *J. High Energy Phys.* **0703**, 090 (2007) [hep-th/0701063]
40. D. Berenstein, V. Jejjala, R.G. Leigh, The standard model on a D-brane. *Phys. Rev. Lett.* **88**, 071602 (2002) [hep-ph/0105042]
41. M. Berger, Sur les groupes d'holonomie homogènes des variétés à connexion affines et des variétés riemanniennes. *Bull. Soc. Math. France* **83**, 279–330 (1953)
42. P. Berglund, T. Hübsch, On Calabi-Yau generalized complete intersections from Hirzebruch varieties and novel $K3$ -fibrations. *Adv. Theor. Math. Phys.* **22**, 261–303 (2018). [arXiv:1606.07420 [hep-th]]; A. Garbagnati, B. van Geemen, A remark on generalized complete intersections. *Nucl. Phys. B* **925**, 135–143 (2017). [arXiv:1708.00517 [math.AG]]; P. Berglund, T. Hübsch, A generalized construction of Calabi-Yau models and mirror symmetry. *SciPost Phys.* **4**(2), 009 (2018). [arXiv:1611.10300 [hep-th]]
43. M. Bies, M. Cvetič, R. Donagi, L. Lin, M. Liu, F. Ruehle, Machine learning and algebraic approaches towards complete matter spectra in 4d F-theory (2020) [arXiv:2007.00009 [hep-th]]
44. R. Bocklandt, Graded Calabi-Yau algebras of dimension 3. *J. Pure Appl. Alg.* **212**(1), 14–32 (2008); R. Bocklandt, Consistency conditions for dimer models. *Glasgow Math. J.* **54**(02), 429–447 (2012); R. Bocklandt, Generating toric noncommutative Crepant resolutions. *J. Algebra* **364**, 119–147 (2012)
45. R. Bocklandt, A. Craw, A. Quintero-Vélez, Geometric Reid's recipe for dimer models. *Math. Ann.* **361**(3–4), 689–723 (2015)
46. H.F. Blichfeldt, *Finite Collineation Groups* (University of Chicago Press, Chicago, IL, 1917)
47. V. Bouchard, Lectures on complex geometry, Calabi-Yau manifolds and toric geometry (2007). hep-th/0702063 [HEP-TH]
48. J.L. Bourjaily, Y.H. He, A.J. McLeod, M. Von Hippel, M. Wilhelm, Traintracks through Calabi-Yaus: amplitudes beyond elliptic polylogarithms (2018). arXiv:1805.09326 [hep-th]
49. J.L. Bourjaily, A.J. McLeod, M. von Hippel, M. Wilhelm, A (bounded) bestiary of Feynman integral Calabi-Yau geometries (2018). arXiv:1810.07689 [hep-th]
50. R. Bousso, J. Polchinski, Quantization of four form fluxes and dynamical neutralization of the cosmological constant. *J. High Energy Phys.* **06**, 006 (2000) [arXiv:hep-th/0004134 [hep-th]]; S. Kachru, R. Kallosh, A.D. Linde, S.P. Trivedi, De Sitter vacua in string theory. *Phys. Rev. D* **68**, 046005 (2003) [arXiv:hep-th/0301240 [hep-th]]
51. V. Braun, On free quotients of complete intersection Calabi-Yau manifolds. *J. High Energy Phys.* **1104**, 005 (2011) [arXiv:1003.3235 [hep-th]]
52. A.P. Braun, N.O. Walliser, A New offspring of PALP (2011). arXiv:1106.4529 [math.AG]; A.P. Braun, J. Knapp, E. Scheidegger, H. Skarke, N.O. Walliser, PALP - a user manual (2012). arXiv:1205.4147 [math.AG]
53. V. Braun, Y.H. He, B.A. Ovrut, T. Pantev, A heterotic standard model. *Phys. Lett. B* **618**, 252 (2005) [hep-th/0501070]; V. Braun, Y.H. He, B.A. Ovrut, T. Pantev, The exact MSSM spectrum from string theory. *J. High Energy Phys.* **0605**, 043 (2006) [hep-th/0512177]; V. Bouchard, R. Donagi, An SU(5) heterotic standard model, *Phys. Lett. B* **633**, 783 (2006) [hep-th/0512149]
54. V. Braun, T. Breidiz, M.R. Douglas, B.A. Ovrut, Calabi-Yau metrics for quotients and complete intersections. *J. High Energy Phys.* **05**, 080 (2008). [arXiv:0712.3563 [hep-th]]; V. Braun, T. Breidiz, M.R. Douglas, B.A. Ovrut, Eigenvalues and eigenfunctions of the scalar Laplace operator on Calabi-Yau manifolds. *J. High Energy Phys.* **07**, 120 (2008). [arXiv:0805.3689 [hep-th]]
55. V. Braun, P. Candelas, R. Davies, A three-generation Calabi-Yau manifold with small Hodge numbers. *Fortsch. Phys.* **58**, 467 (2010) [arXiv:0910.5464 [hep-th]]; L.B. Anderson, J. Gray, Y.H. He, A. Lukas, Exploring positive monad bundles and a new heterotic standard model. *J. High Energy Phys.* **1002**, 054 (2010) [arXiv:0911.1569 [hep-th]]; V. Braun, P. Candelas, R. Davies, R. Donagi, The MSSM spectrum from (0,2)-deformations of the heterotic standard embedding. *J. High Energy Phys.* **1205**, 127 (2012) [arXiv:1112.1097 [hep-th]]

56. A.P. Braun, J. Knapp, E. Scheidegger, H. Skarke, N.O. Walliser, PALP - a user manual (2012). arXiv:1205.4147 [math.AG]
57. C.R. Brodie, A. Constantin, R. Deen, A. Lukas, Machine learning line bundle cohomology. *Fortsch. Phys.* **68**(1), 1900087 (2020) [arXiv:1906.08730 [hep-th]]
58. N. Broomhead, Dimer models and CY algebras (2010). arXiv:0901.4662
59. N. Broomhead, S. Franco, Y.-H. He, G. Musiker, *Toric Geometry, Dimers and String Theory* (to appear)
60. G. Brown, A database of polarized K3 surfaces. *Exp. Math.* **16**(1), 7–20 (2007)
61. I. Brunner, M. Lynker, R. Schimmrigk, Unification of M theory and F theory Calabi-Yau fourfold vacua. *Nucl. Phys. B* **498**, 156 (1997) [hep-th/9610195]; A. Klemm, B. Lian, S.S. Roan, S.T. Yau, Calabi-Yau fourfolds for M theory and F theory compactifications. *Nucl. Phys. B* **518**, 515 (1998) [hep-th/9701023]
62. F. Buccella, J.P. Derendinger, S. Ferrara, C.A. Savoy, Patterns of symmetry breaking in supersymmetric gauge theories. *Phys. Lett. B* **115**, 375 (1982); R. Gatto, G. Sartori, Consequences of the complex character of the internal symmetry in supersymmetric theories. *Commun. Math. Phys.* **109**, 327 (1987); C. Procesi, G.W. Schwarz, The geometry of orbit spaces and gauge symmetry breaking in supersymmetric gauge theories. *Phys. Lett. B* **161**, 117 (1985)
63. K. Bull, Y.H. He, V. Jejjala, C. Mishra, Machine learning CICY threefolds. *Phys. Lett. B* **785**, 65–72 (2018). [arXiv:1806.03121 [hep-th]]
64. K. Bull, Y.H. He, V. Jejjala, C. Mishra, Getting CICY high. *Phys. Lett. B* **795**, 700–706 (2019) [arXiv:1903.03113 [hep-th]]
65. A. Butti, A. Zaffaroni, R-charges from toric diagrams and the equivalence of a-maximization and Z-minimization. *J. High Energy Phys.* **0511**, 019 (2005) [hep-th/0506232]
66. K. Buzzard, The future of Mathematics. CRNS-Imperial Lecture <https://www.youtube.com/watch?v=aZHbnQIFOn4>
67. E. Calabi, The space of Kähler metrics. *Proc. Int. Congress Math. Amsterdam* **2**, 206–207 (1954); E. Calabi, On Kähler manifolds with vanishing canonical class, in *Algebraic Geometry and Topology. A Symposium in Honor of S. Lefschetz*, ed. by Fox, Spencer, Tucker. Princeton Mathematical Series, vol. 12 (PUP, Princeton, 1957), pp. 78–89
68. E. Calabi, Métriques Kähleriennes et brés holomorphes. *Ann. Sci. de ENS* **12**, 268–294 (1979)
69. Calabi-Yau Manifold Explorer. <https://benjaminjurke.com/academia-and-research/calabi-yau-explorer/>
70. P. Cameron, P.-D. Dechant, Y.-H. He, J. McKay, *ADE* (to appear)
71. P. Candelas, Lectures on complex manifolds, in *Trieste 1987, Proceedings, Superstrings '87*, pp. 1–88
72. P. Candelas, R. Davies, New Calabi-Yau manifolds with small Hodge numbers. *Fortsch. Phys.* **58**, 383 (2010) [arXiv:0809.4681 [hep-th]]; V. Braun, P. Candelas, R. Davies, A three-generation Calabi-Yau manifold with small Hodge numbers. *Fortsch. Phys.* **58**, 467 (2010) [arXiv:0910.5464 [hep-th]]
73. P. Candelas, X. C. de la Ossa, Comments on conifolds. *Nucl. Phys. B* **342**, 246 (1990)
74. P. Candelas, G.T. Horowitz, A. Strominger, E. Witten, Vacuum configurations for superstrings. *Nucl. Phys. B* **258**, 46 (1985)
75. P. Candelas, A.M. Dale, C.A. Lutken, R. Schimmrigk, Complete intersection Calabi-Yau manifolds. *Nucl. Phys. B* **298**, 493 (1988)
76. P. Candelas, C.A. Lutken, R. Schimmrigk, Complete intersection Calabi-Yau manifolds. 2. Three generation manifolds. *Nucl. Phys. B* **306**, 113 (1988)
77. P. Candelas, M. Lynker, R. Schimmrigk, Calabi-Yau Manifolds in weighted P(4). *Nucl. Phys. B* **341**, 383 (1990)
78. P. Candelas, X. de la Ossa, S.H. Katz, Mirror symmetry for Calabi-Yau hypersurfaces in weighted P**4 and extensions of Landau-Ginzburg theory. *Nucl. Phys. B* **450**, 267 (1995) [hep-th/9412117]

79. P. Candelas, X. de la Ossa, Y.H. He, B. Szendroi, Triadophilia: a special corner in the landscape. *Adv. Theor. Math. Phys.* **12**, 429 (2008) [arXiv:0706.3134 [hep-th]]
80. P. Candelas, A. Constantin, H. Skarke, An abundance of K3 fibrations from polyhedra with interchangeable parts. *Commun. Math. Phys.* **324**, 937 (2013) [arXiv:1207.4792 [hep-th]]
81. P. Candelas, X. de la Ossa, F. Rodriguez-Villegas, Calabi-Yau manifolds over finite fields. 1 & 2. hep-th/0012233; *Fields Inst. Commun.* **38**, 121 (2013) [hep-th/0402133]
82. P. Candelas, A. Constantin, C. Mishra, Calabi-Yau threefolds with small Hodge numbers. *Fortsch. Phys.* **66**(6), 1800029 (2018) [arXiv:1602.06303 [hep-th]]
83. J. Carifio, J. Halverson, D. Krioukov, B.D. Nelson, Machine learning in the string landscape. *J. High Energy Phys.* **1709**, 157 (2017) [arXiv:1707.00655 [hep-th]]
84. CERN knowledge transfer. <https://kt.cern/competences/machine-learning-and-deep-learning>
85. H.Y. Chen, Y.H. He, S. Lal, S. Majumder, Machine learning lie structures & applications to physics (2020) [arXiv:2011.00871 [hep-th]]
86. H.Y. Chen, Y.H. He, S. Lal, M.Z. Zaz, Machine learning Etudes in conformal field theories (2020) [arXiv:2006.16114 [hep-th]]
87. M. Cicoli, S. Krippendorf, C. Mayrhofer, F. Quevedo, R. Valandro, The web of D-branes at singularities in compact Calabi-Yau manifolds. *J. High Energy Phys.* **1305**, 114 (2013) [arXiv:1304.2771 [hep-th]]
88. M. Cirafici, Persistent homology and string vacua. *J. High Energy Phys.* **03**, 045 (2016) [arXiv:1512.01170 [hep-th]]; M. Cirafici, BPS spectra, barcodes and walls. *SIGMA* **15**, 052 (2019) [arXiv:1511.01421 [hep-th]]
89. C. Closset, Toric geometry and local Calabi-Yau varieties: an introduction to toric geometry (for physicists). arXiv:0901.3695 [hep-th]
90. A. Cole, G. Shiu, Topological data analysis for the string landscape. *J. High Energy Phys.* **03**, 054 (2019) [arXiv:1812.06960 [hep-th]]
91. A. Cole, A. Schachner, G. Shiu, Searching the landscape of flux vacua with genetic algorithms. *J. High Energy Phys.* **11**, 045 (2019) [arXiv:1907.10072 [hep-th]]
92. J. Conlon, *Why String Theory* (CRC, Boca Raton, FL, 2015). ISBN: 978-1-4822-4247-8
93. J.P. Conlon, F. Quevedo, K. Suruliz, Large-volume flux compactifications: moduli spectrum and D3/D7 soft supersymmetry breaking. *J. High Energy Phys.* **0508**, 007 (2005) [hep-th/0505076]
94. A. Constantin, A. Lukas, Formulae for line bundle cohomology on Calabi-Yau threefolds. *Fortsch. Phys.* **67**(12), 1900084 (2019) [arXiv:1808.09992 [hep-th]]
95. A. Constantin, Y.H. He, A. Lukas, Counting string theory standard models (2018). arXiv:1810.00444 [hep-th]
96. J. Conway et al., *ATLAS of Finite Groups* (OUP, Oxford, 2003). ISBN: 978-0-19-853199-9; R. Wilson et al., ATLAS of finite group representations (Queen Mary University, London). <http://brauer.maths.qmul.ac.uk/Atlas/v3/>
97. S. Coughlan, L. Golebiowski, G. Kapustka, M. Kapustka, Arithmetically Gorenstein Calabi-Yau threefolds in P7. arXiv:1609.01195 [math.AG]
98. D. Cox, J. Little, D. O’Shea, *Ideals, Varieties, and Algorithms, An Introduction to Computational Algebraic Geometry and Commutative Algebra* (Springer, New York, 2007). ISBN: 978-0-387-35651-8; D. Cox, J. Little, D. O’Shea, *Using Algebraic Geo.* GTM, vol. 185 (Springer, New York, 2007). ISBN: 978-0-387-20706-3
99. D.A. Cox, H.K. Schenck, J. Little, *Toric Varieties* (AMS, Providence, 2011). ISBN-13: 978-0-8218-4819-7
100. S. Cremonesi, A. Hanany, R.K. Seong, Double handled brane tilings. *J. High Energy Phys.* **1310**, 001 (2013) [arXiv:1305.3607 [hep-th]]
101. G. Cybenko, Approximation by superpositions of a sigmoidal function. *Math. Control Sign. Syst.* **2**(4), 303–314 (1989); K. Hornik, Approximation capabilities of multilayer feedforward networks. *Neural Netw.* **4**(2), 251–257 (1991)
102. J. Davenport et al., Machine-assisted proofs (ICM 2018 Panel). arXiv:1809.08062 [math.HO]
103. J. Davey, A. Hanany, J. Pasukonis, On the classification of Brane tilings. *J. High Energy Phys.* **1001**, 078 (2010) [arXiv:0909.2868 [hep-th]]

104. B. Davison, Consistency conditions for brane tilings. *J. Algebra* **338**(1), 1–23 (2011)
105. X. de la Ossa, M. Larfors, E.E. Svanes, Exploring $SU(3)$ structure moduli spaces with integrable G_2 structures. *Adv. Theor. Math. Phys.* **19**, 837 (2015) [arXiv:1409.7539 [hep-th]]
106. B. de Mont Sion, Prologus (sive Descriptiones) Terraes Sanctae (1283), in *Rudimentum Noviciorum* (Lübeck, Brandis, 1475)
107. R. Deen, Y.H. He, S.J. Lee, A. Lukas, Machine learning string standard models (2020) [arXiv:2003.13339 [hep-th]]
108. W. Decker, G.-M. Greuel, G. Pfister, H. Schönemann, Singular 4-1-1 — a computer algebra system for polynomial computations (2018). <http://www.singular.uni-kl.de>
109. A. Degeratu, K. Wendland, Friendly giant meets pointlike instantons? On a new conjecture by John McKay, in *Moonshine: The First Quarter Century and Beyond*. LMS Lecture Note Series, vol. 372 (Cambridge University Press, Cambridge, 2010), pp. 55–127
110. M. Demirtas, C. Long, L. McAllister, M. Stillman, The Kreuzer-Skarke axiverse (2018). arXiv:1808.01282 [hep-th]
111. M. Demirtas, L. McAllister, A. Rios-Tascon, Bounding the Kreuzer-Skarke landscape (2020) [arXiv:2008.01730 [hep-th]]
112. F. Denef, M.R. Douglas, Computational complexity of the landscape. I. *Ann. Phys.* **322**, 1096–1142 (2007) [arXiv:hep-th/0602072 [hep-th]]
113. M. Dine, *Supersymmetry and String Theory: Beyond the Standard Model* (Cambridge University Press, Cambridge, 2007)
114. I. Dolgachev, M. Gross, Elliptic Three-folds I: Ogg-Shafarevich theory (1993). arXiv:alg-geom/9210009
115. R. Donagi, B.A. Ovrut, T. Pantev, D. Waldram, Standard models from heterotic M theory. *Adv. Theor. Math. Phys.* **5**, 93 (2002) [hep-th/9912208]; R. Donagi, B.A. Ovrut, T. Pantev, D. Waldram, Standard model bundles on nonsimply connected Calabi-Yau threefolds. *J. High Energy Phys.* **0108**, 053 (2001) [hep-th/0008008]; R. Donagi, B.A. Ovrut, T. Pantev, D. Waldram, Standard model bundles. *Adv. Theor. Math. Phys.* **5**, 563 (2002) [math/0008010 [math-ag]]; E. Buchbinder, R. Donagi, B.A. Ovrut, Vector bundle moduli and small instanton transitions. *J. High Energy Phys.* **0206**, 054 (2002) [hep-th/0202084]; R. Donagi, B.A. Ovrut, T. Pantev, R. Reinbacher, SU(4) instantons on Calabi-Yau threefolds with $Z(2) \times Z(2)$ fundamental group. *J. High Energy Phys.* **0401**, 022 (2004) [hep-th/0307273]
116. R. Donagi, Y.H. He, B.A. Ovrut, R. Reinbacher, Particle spectrum of heterotic compactifications. *J. High Energy Phys.* **0412**, 054 (2004) [hep-th/0405014]
117. R.Y. Donagi, Principal bundles on elliptic fibrations. *Asian J. Math.* **1**, 214 (1997) [alg-geom/9702002]
118. S. Donaldson, Scalar curvature and projective embeddings, I. *J. Different. Geom.* **59**(3), 479–522 (2001)
119. S. Donaldson, Some numerical results in complex differential geometry (2005). arXiv:math/0512625
120. C.F. Doran, U.A. Whitcher, From polygons to string theory. *Math. Mag.* **85**(5), 343–359
121. M.R. Douglas, The Statistics of string/M theory vacua. *J. High Energy Phys.* **0305**, 046 (2003) [hep-th/0303194]; K.R. Dienes, M. Lennek, D. Senechal, V. Wasnik, Supersymmetry versus gauge symmetry on the heterotic landscape. *Phys. Rev. D* **75**, 126005 (2007) [arXiv:0704.1320 [hep-th]]; K.R. Dienes, Statistics on the heterotic landscape: Gauge groups and cosmological constants of four-dimensional heterotic strings. *Phys. Rev. D* **73**, 106010 (2006) [hep-th/0602286]; D. Lust, The landscape of string theory (orientifolds and their statistics, D-brane instantons, AdS(4) domain walls and black holes). *Fortsch. Phys.* **56**, 694 (2008); J.J. Heckman, Statistical inference and string theory. *Int. J. Mod. Phys. A* **30**(26), 1550160 (2015) [arXiv:1305.3621 [hep-th]]
122. M.R. Douglas, G.W. Moore, D-branes, quivers, and ALE instantons (1996). hep-th/9603167
123. M.R. Douglas, R.L. Karp, S. Lukic, R. Reinbacher, Numerical Calabi-Yau metrics. *J. Math. Phys.* **49**, 032302 (2008) [arXiv:hep-th/0612075 [hep-th]]; M.R. Douglas, R.L. Karp, S. Lukic, R. Reinbacher, Numerical solution to the Hermitian Yang-Mills equation on the Fermat quintic. *J. High Energy Phys.* **12**, 083 (2007) [arXiv:hep-th/0606261 [hep-th]]

124. M.R. Douglas, S. Lakshminarasimhan, Y. Qi, Numerical Calabi-Yau metrics from holomorphic networks (2020) [arXiv:2012.04797 [hep-th]]
125. P. du Val, On isolated singularities of surfaces which do not affect the conditions of adjunction. I,II,III. Proc. Cambridge Philos. Soc. **30**(4), 453–459, 460–465, 483–491; cf. M. Reid, The Du Val Singularities. <http://homepages.warwick.ac.uk/~masda/surf/more/DuVal.pdf> for a pedagogical account
126. T.W. Dubé, The structure of polynomial ideals and Gröbner bases. SIAM J. Comput. **19**(4), 750–773 (1990)
127. R. Eager, Equivalence of A-maximization and volume minimization. J. High Energy Phys. **01**, 089 (2014) [arXiv:1011.1809 [hep-th]]; R. Eager, M. Gary, M.M. Roberts, Can you hear the shape of dual geometries? J. High Energy Phys. **10**, 209 (2013) [arXiv:1011.5231 [hep-th]]
128. T. Eguchi, A. Hanson, Self-dual solutions to Euclidean gravity. Ann. Phys. **120**(1), 82–106 (1979); T. Eguchi, A. Hanson, Gravitational instantons. Gener. Relat. Gravitat. **11**(5), 315–320 (1979)
129. H. Erbin, R. Finotello, Machine learning for complete intersection Calabi-Yau manifolds: a methodological study (2020) [arXiv:2007.15706 [hep-th]]
130. H. Erbin, R. Finotello, Inception neural network for complete intersection Calabi-Yau 3-folds (2020) [arXiv:2007.13379 [hep-th]]
131. Elliptically fibred Calabi-Yau manifolds. <http://ctp.lns.mit.edu/wati/data.html>
132. G. Ewald, On the classification of toric fano varieties. Discr. Comput. Geom. **3**, 49–54 (1988). K. Watanabe, M. Watanabe, The classification of fano 3-folds with torus embeddings. Tokyo J. Math. **05**, 37–48 (1982); V.V. Batyrev, Toroidal fano 3-folds. Maths USSR-Izvestiya **19**, 13 (1982)
133. G. Ewald, *Combinatorial Convexity and Algebraic Geometry* (Springer, New York, 1996). ISBN: 978-0-387-94755-6; B. Sturmfels, *Gröbner Bases and Convex Polytopes* (AMS, Providence, 1996). ISBN: 978-0-8218-0487-2
134. B. Feng, A. Hanany, Y.H. He, D-brane gauge theories from toric singularities and toric duality. Nucl. Phys. B **595**, 165 (2001) [hep-th/0003085]
135. B. Feng, Y.H. He, K.D. Kennaway, C. Vafa, Adv. Theor. Math. Phys. **12**(3), 489 (2008) [hep-th/0511287]
136. D. Forcella, A. Hanany, Y.H. He, A. Zaffaroni, The master space of N=1 gauge theories. J. High Energy Phys. **0808**, 012 (2008) [arXiv:0801.1585]
137. S. Franco, Bipartite field theories: From D-Brane probes to scattering amplitudes. J. High Energy Phys. **1211**, 141 (2012) [arXiv:1207.0807 [hep-th]]
138. S. Franco, A. Uranga, Bipartite field theories from D-Branes. J. High Energy Phys. **1404**, 161 (2014) [arXiv:1306.6331 [hep-th]]
139. S. Franco, A. Hanany, K.D. Kennaway, D. Vegh, B. Wecht, Brane dimers and quiver gauge theories. J. High Energy Phys. **0601**, 096 (2006) [hep-th/0504110]; S. Franco, A. Hanany, D. Martelli, J. Sparks, D. Vegh, B. Wecht, Gauge theories from toric geometry and brane tilings. J. High Energy Phys. **0601**, 128 (2006) [hep-th/0505211]
140. S. Franco, D. Rodriguez-Gomez, H. Verlinde, N-ification of forces: a holographic perspective on D-brane model building. J. High Energy Phys. **0906**, 030 (2009) [arXiv:0804.1125 [hep-th]]
141. S. Franco, D. Galloni, A. Mariotti, Bipartite field theories, cluster algebras and the Grassmannian. J. Phys. A **47**(47), 474004 (2014) [arXiv:1404.3752 [hep-th]]
142. S. Franco, Y.H. He, C. Sun, Y. Xiao, A comprehensive survey of brane tilings. Int. J. Mod. Phys. A **32**(23 and 24), 1750142 (2017) [arXiv:1702.03958 [hep-th]]
143. R. Friedman, J.W. Morgan, E. Witten, Vector bundles over elliptic fibrations (1997). alg-geom/9709029
144. R. Friedman, J. Morgan, E. Witten, Vector bundles and F theory. Commun. Math. Phys. **187**, 679 (1997) [hep-th/9701162]
145. W. Fulton, *Introduction to Toric Varieties*. AM-131 (PUP, Princeton, 1993). ISBN: 978-1-4008-8252-6
146. W. Fulton, *Intersection Theory*. (Springer, New York, 1998). ISBN: 978-1-4612-1700-8

147. W. Fulton, J. Harris, *Representation Theory. A First Course*, GTM, vol. 129 (Springer, New York, 1991). ISBN: 978-0-387-97495-8
148. A. Futaki, Complete Ricci-flat Kahler metrics on the canonical bundles of toric Fano manifolds (2009). arXiv:math/0703138; A. Futaki, H. Ono, G. Wang, Transverse Kahler geometry of Sasaki manifolds and toric Sasaki-Einstein manifolds (2006). arXiv:math.DG/0607586. A. Futaki, H. Ono, Y. Sano, Hilbert series and obstructions to asymptotic semistability. *Adv. Math.* **226**, 254–284 (2011) [arXiv:0811.1315]
149. M. Gabella, Y.H. He, A. Lukas, An abundance of heterotic vacua. *J. High Energy Phys.* **0812**, 027 (2008) [arXiv:0808.2142 [hep-th]]
150. P. Gabriel, Unzerlegbare Darstellungen. I. *Manuscr. Math.* **6**, 71–103 (1972)
151. M. Gagnon, Q. Ho-Kim, An exhaustive list of complete intersection Calabi-Yau manifolds. *Mod. Phys. Lett. A* **9**, 2235 (1994)
152. T. Gannon, Monstrous moonshine and the classification of CFT (1999). arXiv:math/9906167 [math.QA]
153. E.G. Gimon, J. Polchinski, Consistency conditions for orientifolds and d manifolds. *Phys. Rev. D* **54**, 1667 (1996) [hep-th/9601038]; S. Kachru, E. Silverstein, 4D conformal field theories and strings on orbifolds (1998). hep-th/9802183; W. Lerche, P. Mayr, J. Walcher, A new kind of McKay correspondence from non-Abelian gauge theories (2001). hep-th/0103114
154. V. Ginzburg, Calabi-Yau algebras (2007). arXiv:math/0612139
155. F. Gmeiner, R. Blumenhagen, G. Honecker, D. Lust, T. Weigand, One in a billion: MSSM-like D-brane statistics. *J. High Energy Phys.* **0601**, 004 (2006) [hep-th/0510170]
156. I. Goodfellow, Y. Bengio, A. Courville, *Deep Learning* (MIT Press, Cambridge, 2016). ISBN: 978-0-2620-3561-3
157. G. Gonzalez-Sprinberg, J.-L. Verdier, Construction géométrique de la correspondance de McKay. *Ann. Sci. ENS* (4) **16**(3), 409–449 (1984); L. Dixon, J.A. Harvey, C. Vafa, E. Witten, Strings on orbifolds. *Nucl. Phys. B* **261**(4), 678–686 (1985); A. Degeratu, Flops on Crepant resolutions. *Turk. J. Math.* **28**, 23–40 (2004)
158. A. Grassi, Minimal models of elliptic threefolds. Duke PhD Thesis. 1990; *Math. Ann.* **290**, 287–301 (1991)
159. A. Grassi, D.R. Morrison, Group representations and the Euler characteristic of elliptically fibered Calabi-Yau threefolds. math/0005196 [math-ag]; W. Taylor, On the Hodge structure of elliptically fibered Calabi-Yau threefolds. *JHEP* **1208**, 032 (2012). [arXiv:1205.0952 [hep-th]]
160. J. Gray, Y.H. He, A. Ilderton, A. Lukas, STRINGVACUA: a mathematica package for studying vacuum configurations in string phenomenology. *Comput. Phys. Commun.* **180**, 107 (2009) [arXiv:0801.1508 [hep-th]]. <http://www-thphys.physics.ox.ac.uk/projects/Stringvacua/>
161. J. Gray, Y.H. He, V. Jejjala, B. Jurke, B.D. Nelson, J. Simon, Calabi-Yau manifolds with large volume vacua. *Phys. Rev. D* **86**, 101901 (2012) [arXiv:1207.5801 [hep-th]]
162. J. Gray, A.S. Haupt, A. Lukas, All complete intersection Calabi-Yau four-folds. *J. High Energy Phys.* **07**, 070 (2013) [arXiv:1303.1832 [hep-th]]
163. D. Grayson, M. Stillman, Macaulay2, a software system for research in algebraic geometry. Available at <https://faculty.math.illinois.edu/Macaulay2/>
164. D.J. Gross, J.A. Harvey, E.J. Martinec, R. Rohm, The heterotic string. *Phys. Rev. Lett.* **54**, 502 (1985)
165. M.B. Green, J.H. Schwarz, E. Witten, *Superstring Theory*. Cambridge Monographs on Mathematical Physics, vol. 1 & 2 (Cambridge University Press, Cambridge, 1987)
166. P.S. Green, T. Hubsch, C.A. Lutken, All Hodge numbers of all CICY manifolds. *Class. Quant. Grav.* **6**, 105 (1989)
167. B. Greene, *The Elegant Universe: Superstrings, Hidden Dimensions, and the Quest for the Ultimate Theory* (Norton & Company, New York, 2003). ISBN: 0-393-05858-1
168. B.R. Greene, K.H. Kirklin, P.J. Miron, G.G. Ross, A superstring inspired standard model. *Phys. Lett. B* **180**, 69 (1986)

169. P. Griffiths, J. Harris, *Principles of Algebraic Geometry* (Wiley, New York, 1978). ISBN 04-713-2792-1
170. M. Gross, A finiteness theorem for elliptic Calabi-Yau threefolds. *Duke Math. J.* **74**(2), 271–299 (1994)
171. M. Gross, D. Huybrechts, D. Joyce, *Calabi-Yau Manifolds and Related Geometries*. Universitext (Springer,2003). ISBN: 978-3-642-19004-9
172. J. Gray, Y.H. He, V. Jejjala, B. Jurke, B.D. Nelson, J. Simon, Calabi-Yau manifolds with large volume vacua. *Phys. Rev. D* **86**, 101901 (2012) [arXiv:1207.5801 [hep-th]]
173. T.W. Grimm, F. Ruehle, D. van de Heisteeg, Classifying Calabi-Yau threefolds using infinite distance limits (2019) [arXiv:1910.02963 [hep-th]]
174. S.S. Gubser, Einstein manifolds and conformal field theories. *Phys. Rev. D* **59**, 025006 (1999) [hep-th/9807164]; K.A. Intriligator, B. Wecht, The Exact superconformal R symmetry maximizes a. *Nucl. Phys. B* **667**, 183 (2003) [hep-th/0304128]; M. Henningson, K. Skenderis, The Holographic Weyl anomaly. *J. High Energy Phys.* **9807**, 023 (1998) [hep-th/9806087]; S. Benvenuti, S. Franco, A. Hanany, D. Martelli, J. Sparks, An infinite family of superconformal quiver gauge theories with Sasaki-Einstein duals. *J. High Energy Phys.* **0506**, 064 (2005) [hep-th/0411264]
175. D.R. Gulotta, Properly ordered dimers, r-charges, and an efficient inverse algorithm. *J. High Energy Phys.* **2008**(10), 014 (2008)
176. J. Halverson, P. Langacker, TASI lectures on Remnants from the string landscape. PoS TASI **2017**, 019 (2018) [arXiv:1801.03503]
177. J. Halverson, C. Long, Statistical predictions in string theory and deep generative models. *Fortsch. Phys.* **68**(5), 2000005 (2020) [arXiv:2001.00555 [hep-th]]
178. J. Halverson, F. Ruehle, Computational complexity of vacua and near-vacua in field and string theory. *Phys. Rev. D* **99**(4), 046015 (2019) [arXiv:1809.08279 [hep-th]]
179. J. Halverson, C. Long, B. Sung, Algorithmic universality in F-theory compactifications. *Phys. Rev. D* **96**(12), 126006 (2017) [arXiv:1706.02299 [hep-th]]; J. Carifio, W.J. Cunningham, J. Halverson, D. Krioukov, C. Long, B.D. Nelson, Vacuum selection from cosmology on networks of string geometries. *Phys. Rev. Lett.* **121**(10), 101602 (2018) [arXiv:1711.06685 [hep-th]]; J. Halverson, F. Ruehle, Computational complexity of vacua and near-vacua in field and string theory (2019). arXiv:1809.08279 [hep-th]
180. J. Halverson, B. Nelson, F. Ruehle, Branes with brains: exploring string vacua with deep reinforcement learning. *J. High Energy Phys.* **06**, 003 (2019) [arXiv:1903.11616 [hep-th]]
181. J. Halverson, A. Maiti, K. Stoner, Neural networks and quantum field theory (2020) [arXiv:2008.08601 [cs.LG]]
182. A. Hanany, Y.H. He, NonAbelian finite gauge theories. *J. High Energy Phys.* **9902**, 013 (1999) [hep-th/9811183]
183. A. Hanany, Y.H. He, A monograph on the classification of the discrete subgroups of SU(4). *J. High Energy Phys.* **0102**, 027 (2001) [hep-th/9905212]
184. A. Hanany, K.D. Kennaway, Dimer models and toric diagrams (2005). hep-th/0503149
185. A. Hanany, R.K. Seong, Brane tilings and reflexive polygons. *Fortsch. Phys.* **60**, 695 (2012) [arXiv:1201.2614 [hep-th]]
186. A. Hanany, R.K. Seong, Brane tilings and specular duality. *J. High Energy Phys.* **1208**, 107 (2012) [arXiv:1206.2386 [hep-th]]
187. A. Hanany, G. Torri, Brane tilings and SUSY gauge theories. *Nucl. Phys. Proc. Suppl.* **216**, 270 (2011) [arXiv:1102.3611 [hep-th]]
188. A. Hanany, A.M. Uranga, Brane boxes and branes on singularities. *J. High Energy Phys.* **9805**, 013 (1998) [hep-th/9805139]; A. Hanany, A. Zaffaroni, On the realization of chiral four-dimensional gauge theories using branes. *J. High Energy Phys.* **9805**, 001 (1998) [hep-th/9801134]
189. A. Hanany, D. Vegh, Quivers, tilings, branes and rhombi. *J. High Energy Phys.* **0710**, 029 (2007) [hep-th/0511063]
190. A. Hanany, C.P. Herzog, D. Vegh, Brane tilings and exceptional collections. *J. High Energy Phys.* **0607**, 001 (2006) [hep-th/0602041]

191. A. Hanany, Y.H. He, V. Jejjala, J. Pasukonis, S. Ramgoolam, D. Rodriguez-Gomez, The beta ansatz: a tale of two complex structures. *J. High Energy Phys.* **1106**, 056 (2011) [arXiv:1104.5490 [hep-th]]
192. A. Hanany, V. Jejjala, S. Ramgoolam, R.K. Seong, Consistency and derangements in Brane tilings. *J. Phys. A* **49**(35), 355401 (2016) [arXiv:1512.09013 [hep-th]]
193. B. Hanin, Approximating continuous functions by ReLU nets of minimal width (2018). arXiv:1710.11278
194. R. Hartshorne, *Algebraic Geometry*. GTM (Springer, New York, 1997). ISBN-13: 978-0-3879-0244-9
195. K. Hashimoto, AdS/CFT correspondence as a deep Boltzmann machine. *Phys. Rev. D* **99**(10), 106017 (2019) [arXiv:1903.04951 [hep-th]]
196. K. Hashimoto, S. Sugishita, A. Tanaka, A. Tomiya, Deep learning and the AdS/CFT correspondence. *Phys. Rev. D* **98**(4), 046019 (2018) [arXiv:1802.08313 [hep-th]]
197. J. Hauenstein, A. Sommese, C. Wampler, Bertini: software for numerical algebraic geometry. www.nd.edu/~sommese/bertini
198. J. Hauenstein, Y.H. He, D. Mehta, Numerical elimination & moduli space of vacua. *J. High Energy Phys.* **1309**, 083 (2013) [arXiv:1210.6038 [hep-th]]
199. Y.H. He, An algorithmic approach to heterotic string phenomenology. *Mod. Phys. Lett. A* **25**, 79–90 (2010) [arXiv:1001.2419 [hep-th]]
200. Y.H. He, An algorithmic approach to heterotic string phenomenology. *Mod. Phys. Lett. A* **25**, 79 (2010) [arXiv:1001.2419 [hep-th]]
201. Y.H. He, Calabi-Yau geometries: Algorithms, databases, & physics. *Int. J. Mod. Phys. A* **28**, 1330032 (2013) [arXiv:1308.0186]
202. Y.H. He, Calabi-Yau varieties: from Quiver representations to Dessins d’Enfants (2016). arXiv:1611.09398 [math.AG]
203. Y.H. He, Deep-learning the landscape (2017). arXiv:1706.02714 [hep-th]; q.v. *Science* **365**(6452) (2019)
204. Y.H. He, Machine-learning the string landscape. *Phys. Lett. B* **774**, 564 (2017)
205. Y.H. He, *From Geometry, to Physics, to Machine Learning Mathematical Structures*. Oxford ML Meets Physics Series 2019, <https://www.youtube.com/watch?v=nMP2f14gYzc>; String-Math 2020, <https://www.youtube.com/watch?v=GqoqxFsaogY>
206. Y.-H. He, The Calabi-Yau landscape, in *Quantum Geometry & Moduli Spaces* (I’Institute Confucius, Geneva & Sonderburg, 2018). www.qgm.au.dk/fileadmin/www.qgm.au.dk/Events/2018/CYlandscape.pdf
207. Y.-H. He, Universes as Bigdata, or Machine-Learning Mathematical Structures. Oxford ML&Physics Seminar. <https://www.youtube.com/watch?v=nMP2f14gYzc>. StringMaths 2020, <https://www.youtube.com/watch?v=GqoqxFsaogY>
208. Y.H. He, Calabi-Yau spaces in the string landscape, in *Oxford Research Encyclopaedia of Physics* (OUP, Oxford, 2020) [arXiv:2006.16623 [hep-th]]
209. Y.-H. He, Universes as big data (2020) [arXiv:2011.14442 [hep-th]]; Y.-H. He, ML mathematical structures (2021) [arXiv:2101.06317 [cs.LG]]
210. Y.H. He, M. Kim, Learning algebraic structures: preliminary investigations (2019) [arXiv:1905.02263 [cs.LG]]
211. Y.H. He, S.J. Lee, Distinguishing elliptic fibrations with AI. *Phys. Lett. B* **798**, 134889 (2019) [arXiv:1904.08530 [hep-th]]
212. Y.H. He, A. Lukas, Machine learning Calabi-Yau four-folds (2020) [arXiv:2009.02544 [hep-th]]
213. Y.H. He, J. McKay, Sporadic & exceptional (2015). arXiv:1505.06742
214. Y.H. He, J. McKay, Moonshine and the meaning of life, in *Contemporary Mathematics*, vol. 694, ed. by M. Bhargava et al. (2017) [arXiv:1408.2083 [math.NT]]
215. Y.-H. He, D. Mehta (Organizers), Applications of computational and numerical algebraic geometry to theoretical physics, in *SIAM Conference on Applied Algebraic Geometry*, Colorado, 2013; Y.-H. He, R.-K. Seong, M. Stillman, *Applications of Computational Algebraic Geometry to Theoretical Physics* (SIAM AG, Daejeon, 2015)

216. Y.H. He, S.T. Yau, Graph Laplacians, Riemannian manifolds and their machine-learning (2020) [arXiv:2006.16619 [math.CO]]
217. Y.H. He, S.J. Lee, A. Lukas, Heterotic models from vector bundles on toric Calabi-Yau manifolds. *J. High Energy Phys.* **1005**, 071 (2010) [arXiv:0911.0865 [hep-th]]
218. Y.H. He, M. Kreuzer, S.J. Lee, A. Lukas, Heterotic bundles on Calabi-Yau manifolds with small Picard number. *J. High Energy Phys.* **1112**, 039 (2011) [arXiv:1108.1031 [hep-th]]
219. Y.-H. He, P. Candelas, A. Hanany, A. Lukas, B. Ovrut (eds.) *Computational Algebraic Geometry in String and Gauge Theory*, Hindawi, Special Volume (2012). ISBN: 1687-7357
220. Y.H. He, V. Jejjala, C. Matti, B.D. Nelson, M. Stillman, The geometry of generations. *Commun. Math. Phys.* **339**(1), 149 (2015) [arXiv:1408.6841 [hep-th]]
221. Y.H. He, V. Jejjala, L. Pontiggia, Patterns in Calabi-Yau distributions. *Commun. Math. Phys.* **354**(2), 477 (2017) [arXiv:1512.01579 [hep-th]]
222. Y.H. He, V. Jejjala, B.D. Nelson, High energy physics - theory hep-th (2018). [arXiv:1807.00735 [cs.CL]]
223. Y.-H. He, R.-K. Seong, S.-T. Yau, Calabi-Yau volumes and reflexive polytopes. *Commun. Math. Phys.* **361**(1), 155 (2018) [arXiv:1704.03462 [hep-th]]
224. Y.H. He, K.H. Lee, T. Oliver, Machine-learning number fields (2020) [arXiv:2011.08958 [math.NT]]
225. Y.H. He, E. Hirst, T. Peterken, Machine-learning Dessins d'Enfants: explorations via modular and Seiberg-Witten curves (2020) [arXiv:2004.05218 [hep-th]]
226. Y.H. He, K.H. Lee, T. Oliver, Machine-Learning the Sato-Tate conjecture (2020) [arXiv:2010.01213 [math.NT]]
227. M. Headrick, A. Nassar, Energy functionals for Calabi-Yau metrics. *Adv. Theor. Math. Phys.* **17**(5), 867–902 (2013) [arXiv:0908.2635 [hep-th]]
228. M. Headrick, T. Wiseman, Numerical Ricci-flat metrics on K3. *Class. Quant. Grav.* **22**, 4931–4960 (2005) [arXiv:hep-th/0506129 [hep-th]]
229. J.J. Heckman, C. Vafa, D. Xie, M. Yamazaki, String theory origin of bipartite SCFTs. *J. High Energy Phys.* **1305**, 148 (2013) [arXiv:1211.4587 [hep-th]]
230. J. Herz, A. Krough, R.G. Palmer, *Introduction to the Theory of Neural Computation* (Addison-Wesley, Redwood City, 1991); M.H. Hassoun, *Fundamentals of Artificial Neural Networks* (MIT Press, Cambridge, 1995); S. Haykin, *Neural Networks: A Comprehensive Foundation*, 2nd edn. (Macmillan, New York, 1999); C. Bishop, *Pattern Recognition and Machine Learning* (Springer, New York, 2006)
231. Heterotic Compactification Database. <http://www-thphys.physics.ox.ac.uk/projects/CalabiYau/>
232. C.F. Higham, D.J. Higham, Deep learning: an introduction for applied mathematicians (2019). arXiv:1801.05894; P. Mehta, M. Bukov, C.-H. Wang, A.G.R. Day, C. Richardson, C.K. Fisher, D.J. Schwab, A high-bias, low-variance introduction to Machine Learning for physicists (2018). arXiv:1803.08823; E. Weinan, *Machine Learning: Mathematical Theory and Scientific Applications*. Notices of AMS, Dec 2019, pp. 1813–1821
233. L. Hille, Moduli of representations, Quiver Grassmannians, and Hilbert schemes (2015). arXiv:1505.06008 [math.RT]
234. H. Hopf, Differentialgeometry und topologische Gestalt. Jahresbericht der Deutschen Mathematiker-Vereinigung **41**, 209–228 (1932); S.-S. Chern, On curvature and characteristic classes of a Riemann manifold. Abhandlungen aus dem Mathematischen Seminar der Universität Hamburg. **20**, 117–126 (1966)
235. K. Hori, S. Katz, A. Klemm, R. Pandharipande, R. Thomas, C. Vafa, R. Vakil, E. Zaslow, *Mirror Symmetry* (AMS, Providence, 2000). ISBN: 0-8218-2955-6
236. Y.C. Huang, W. Taylor, On the prevalence of elliptic and genus one fibrations among toric hypersurface Calabi-Yau threefolds. arXiv:1809.05160 [hep-th]; Comparing elliptic and toric hypersurface Calabi-Yau threefolds at large Hodge numbers. arXiv:1805.05907 [hep-th]; W. Taylor, Y.N. Wang, Non-toric bases for elliptic Calabi-Yau threefolds and 6D F-theory vacua. *Adv. Theor. Math. Phys.* **21**, 1063 (2017). [arXiv:1504.07689 [hep-th]]

237. T. Hubsch, *Calabi-Yau Manifolds: A Bestiary for Physicists* (World Scientific, Singapore, 1994). ISBN: 981-0-20662-3
238. B. Huisgen-Zimmermann, The geometry of uniserial representations of finite dim. algebra. I. J. Pure Appl. Alg. **127**(1), 3972 (1998)
239. C. Hull, Superstring compactifications with torsion and space-time supersymmetry, in *Turin 1985 Proceedings. Superunification and Extra Dimensions*, vol. 347(375) (World Scientific Publishers, Singapore, 1986)
240. L.E. Ibáñez, A.M. Uranga, *String Theory and Particle Physics: An Introduction to String Phenomenology* (Cambridge University Press, Cambridge, 2012)
241. A. Iqbal, A. Neitzke, C. Vafa, A Mysterious duality. Adv. Theor. Math. Phys. **5**, 769 (2002) [hep-th/0111068]
242. A. Ishii, K. Ueda, On moduli spaces of quiver representations associated with dimer models (2008). arXiv:0710.1898
243. R. Iten, T. Metger, H. Wilming, L. del Rio, R. Renner, Discovering physical concepts with neural networks. Phys. Rev. Lett. **124**, 010508 (2020)
244. Y. Ito, M. Reid, The McKay correspondence for finite subgroups of $SL(3;C)$ (1994). alg-geo/9411010; S.-S. Roan, Minimal resolutions of Gorenstein orbifolds in dimension three. Topology **35**, 489–508 (1996); Y. Ito, Gorenstein quotient singularities of monomial type in dimension three. J. Math. Sci. Univ. Tokyo **2**, 419 (1995). alg-geom/9406001
245. V. Jejjala, A. Kar, O. Parrikar, Deep learning the hyperbolic volume of a knot. Phys. Lett. B **799**, 135033 (2019) [arXiv:1902.05547 [hep-th]]
246. C.V. Johnson, R.C. Myers, Aspects of type IIB theory on ALE spaces. Phys. Rev. D **55**, 6382 (1997) [hep-th/9610140]
247. S.B. Johnson, W. Taylor, Calabi-Yau threefolds with large $h^{2,1}$. J. High Energy Phys. **1410**, 23 (2014) [arXiv:1406.0514 [hep-th]]
248. Jupyter Dev. Team, Jupyter Notebooks – a publishing format for reproducible computational workflows (2016). 10.3233/978-1-61499-649-1-87
249. S. Kachru, R. Kallosh, A.D. Linde, S.P. Trivedi, De Sitter vacua in string theory. Phys. Rev. D **68**, 046005 (2003) [hep-th/0301240]
250. S. Katz, Enumerative geometry and string theory, in *SML*, vol. 32 (AMS, Providence, 2006). ISBN: 978-0-8218-3687-3
251. S.H. Katz, A. Klemm, C. Vafa, Geometric engineering of quantum field theories. Nucl. Phys. B **497**, 173 (1997)
252. B. Keller, S. Scherotzke, Desingularizations of quiver Grassmannians via graded quiver varieties (2013). arXiv:1305.7502
253. K.D. Kennaway, Brane tilings. Int. J. Mod. Phys. A **22**, 2977 (2007) [arXiv:0706.1660 [hep-th]]
254. P. Kidger, T. Lyons, Universal approximation with deep narrow networks, in *Conference on Learning Theory* (2019) [arXiv:1905.08539]
255. J.K. Kim, C.J. Park, Y. Yoon, Calabi-Yau manifolds from complete intersections in products of weighted complex projective spaces. Phys. Lett. B **224**, 108–114 (1989)
256. A. King, Moduli of representations of finite-dimensional algebras. Quart. J. Math. **45**(180), 515–530
257. D.P. Kingma, J. Ba, Adam: a method for stochastic optimization, in *3rd Int. Conf. for Learning Representations*, San Diego, 2015. arXiv:1412.6980 [cs.LG]
258. E. Kiritsis, D-branes in standard model building, gravity and cosmology. Phys. Rept. **421**, 105 (2005) Erratum: [Phys. Rept. **429**, 121 (2006)] [hep-th/0310001]
259. E. Kiritsis, *String Theory in a Nutshell*, 2nd edn. (PUP, Princeton, 2019)
260. E.D. Koch, R. de Mello Koch, L. Cheng, Is deep learning a renormalization group flow? (2019) [arXiv:1906.05212 [cs.LG]]
261. K. Kodaira, On the structure of compact complex analytic surfaces. I. Am. J. Math. **86**, 751–798 (1964). Part II, Am. J. Math. **88**, 682–721 (1966)
262. D. Klaewer, L. Schlechter, Machine learning line bundle cohomologies of hypersurfaces in toric varieties (2018). [arXiv:1809.02547 [hep-th]]

263. I.R. Klebanov, E. Witten, Superconformal field theory on three-branes at a Calabi-Yau singularity. *Nucl. Phys. B* **536**, 199 (1998) [hep-th/9807080]
264. F. Klein, Vorlesungen über das Ikosaeder und die Auflösung der Gleichungen vom fünften Grade". <https://archive.org/details/lecturesonikosa00kleigoog/page/n10>
265. D. Krefl, R.K. Seong, Machine learning of Calabi-Yau volumes. *Phys. Rev. D* **96**(6), 066014 (2017). [arXiv:1706.03346 [hep-th]]
266. M. Kreuzer, B. Nill, Classification of toric fano 5-folds. arXiv:math/0702890.; M. Oebro, An algorithm for the classification of smooth Fano polytopes. arXiv:0704.0049; T. Bogart, C. Haase, M. Hering, B. Lorenz, B. Nill, A. Paffenholz, G. Rote, F. Santos, H. Schenck, Few smooth d-polytopes with n lattice points. *Israel J. Math.* **207**(1), 301–329 (2015). arXiv:1010.3887
267. M. Kreuzer, H. Skarke, On the classification of reflexive polyhedra. *Commun. Math. Phys.* **185**, 495 (1997) [hep-th/9512204]. M. Kreuzer, H. Skarke, Reflexive polyhedra, weights and toric Calabi-Yau fibrations. *Rev. Math. Phys.* **14**, 343 (2002) [math/0001106 [math-ag]]
268. M. Kreuzer, H. Skarke, Classification of reflexive polyhedra in three-dimensions. *Adv. Theor. Math. Phys.* **2**, 853 (1998) [hep-th/9805190]
269. M. Kreuzer, H. Skarke, Complete classification of reflexive polyhedra in four-dimensions. *Adv. Theor. Math. Phys.* **4**, 1209 (2002) [hep-th/0002240]
270. M. Kreuzer, H. Skarke, PALP: a package for analyzing lattice polytopes with applications to toric geometry. *Comput. Phys. Commun.* **157**, 87 (2004) [math/0204356 [math.NA]]
271. S. Krippendorf, M. Syvaeri, Detecting symmetries with neural networks (2020) [arXiv:2003.13679 [physics.comp-ph]]
272. P.B. Kronheimer, The construction of ALE spaces as hyper-Kahler quotients. *J. Differ. Geom.* **29**(3), 665–683 (1989)
273. T. Lai, G. Musiker, Beyond Aztec castles: toric cascades in the dp_3 quiver (2017). arXiv:1512.00507
274. G. Lample, F. Charton, Deep learning for symbolic mathematics (2019). arXiv:1912.01412 [cs.SC]
275. M. Larfors, R. Schneider, Explore and exploit with heterotic line bundle models. *Fortsch. Phys.* **68**(5), 2000034 (2020) [arXiv:2003.04817 [hep-th]]
276. A.E. Lawrence, N. Nekrasov, C. Vafa, On conformal field theories in four-dimensions. *Nucl. Phys. B* **533**, 199 (1998) [hep-th/9803015]
277. R. Laza, M. Schütt, N. Yui, *Calabi-Yau Varieties: Arithmetic, Geometry and Physics* (Springer, New York, 2015), ISBN: 978-1-4939-2830-9
278. N. Lei, K. Su, L. Cui, S.-T. Yau, D. X. Gu, A geometric view of optimal transportation and generative model. arXiv:1710.05488
279. K.J.C. Leney [ATLAS Collaboration], A neural-network clusterisation algorithm for the ATLAS silicon pixel detector. *J. Phys. Conf. Ser.* **523**, 012023 (2014); C.P. Novaes, A. Bernui, I.S. Ferreira, C.A. Wuensche, A neural-network based estimator to search for primordial non-Gaussianity in Planck CMB maps. *JCAP* 1509 (09), 064 (2015) [arXiv:1409.3876 [astro-ph.CO]]; A.J. Ballard, R. Das, S. Martiniani, D. Mehta, L. Sagun, J. Stevenson, D. Wales, Perspective: energy landscapes for machine learning (2017). arXiv:1703.07915; W.C. Gan, F.W. Shu, Holography as deep-learning (2017). arXiv:1705.05750 [gr-qc]; Deep-Learning and Physics Conference: http://kabuto.phys.sci.osaka-u.ac.jp/~koji/workshop/tsrp/Deep_Lerning.html
280. W. Lerche, D. Lust, A.N. Schellekens, Ten-dimensional heterotic strings from Niemeier lattices. *Phys. Lett. B* **181**, 71 (1986). A.N. Schellekens, The Landscape ‘avant la lettre’. physics/0604134
281. J. Li, S.-T. Yau, The existence of supersymmetric String theory with torsion. *J. Differ. Geom.* **70**(1), 143–181 (2005)
282. Links to CICY, Monads, and StringVacua Package: http://www-thphys.physics.ox.ac.uk/people/AndreLukas/Site/Andre_Lukas.html
283. J. Liu, Artificial neural network in cosmic landscape. *J. High Energy Phys.* **12**, 149 (2017) [arXiv:1707.02800 [hep-th]]; J. Carifio, W.J. Cunningham, J. Halverson, D. Krioukov,

- C. Long, B.D. Nelson, Vacuum selection from cosmology on networks of string geometries. Phys. Rev. Lett. **121**(10), 101602 (2018) [arXiv:1711.06685 [hep-th]]
284. M.A. Luty, W.I. Taylor, Varieties of vacua in classical supersymmetric gauge theories. Phys. Rev. D **53**, 3399 (1996) [hep-th/9506098]
285. Magma Comp. Algebra System (2021). <http://magma.maths.usyd.edu.au/>
286. J.M. Maldacena, The large N limit of superconformal field theories and supergravity. Int. J. Theor. Phys. **38**, 1113 (1999) [Adv. Theor. Math. Phys. **2**, 231 (1998) [hep-th/9711200]
287. D. Martelli, J. Sparks, S.T. Yau, The geometric dual of a-maximisation for toric Sasaki-Einstein manifolds. Commun. Math. Phys. **268**, 39 (2006) [hep-th/0503183]; D. Martelli, J. Sparks, S.T. Yau, Sasaki-Einstein manifolds and volume minimisation. Commun. Math. Phys. **280**, 611 (2008) [hep-th/0603021]; J.P. Gauntlett, D. Martelli, J. Sparks, S.T. Yau, Obstructions to the existence of Sasaki-Einstein metrics. Commun. Math. Phys. **273**, 803 (2007) [hep-th/0607080]
288. B. Matthews, Comparison of the predicted and observed secondary structure of T4 phage lysozyme. Biochim. Biophys. Acta (BBA) Prot. Struct. **405**(2), 442–451 (1975); J. Gorodkin, Comparing two K-category assignments by a K-category correlation coefficient. Comp. Biol. Chem. Elsevier **28**(5), 367–374 (2004)
289. J. McKay, Graphs, singularities, and finite groups. Proc. Symp. Pure Math. **37**, 183–186 (1980)
290. D. Mehta, Y.H. He, J.D. Hauenstein, Numerical algebraic geometry: a new perspective on string and gauge theories. J. High Energy Phys. **1207**, 018 (2012) [arXiv:1203.4235 [hep-th]]
291. J.W. Milnor, On simply-connected 4-manifolds, in *Symposium International de Topologia Algebraica*, Mexico (1958), pp. 122–128
292. D.R. Morrison, M.R. Plesser, Nonspherical horizons. 1. Adv. Theor. Math. Phys. **3**, 1 (1999) [hep-th/9810201]; A.M. Uranga, Brane configurations for branes at conifolds. J. High Energy Phys. **9901**, 022 (1999) [hep-th/9811004]; C. Beasley, B.R. Greene, C.I. Lazaroiu, M.R. Plesser, D3-branes on partial resolutions of Abelian quotient singularities of Calabi-Yau threefolds. Nucl. Phys. B **566**, 599 (2000) [hep-th/9907186]
293. D.R. Morrison, C. Vafa, Compactifications of F theory on Calabi-Yau threefolds. 1 & 2. Nucl. Phys. B **473**, 74 & **476**, 437 (1996) [hep-th/9602114], [hep-th/9603161]
294. S. Mozgovoy, M. Reineke, On the NC Donaldson–Thomas invariants arising from brane tilings. Adv. Math. **223**(5), 1521–1544 (2010)
295. A. Mütter, E. Parr, P.K.S. Vaudrevange, Deep learning in the heterotic orbifold landscape. Nucl. Phys. B **940**, 113–129 (2019) [arXiv:1811.05993 [hep-th]]
296. M. Nakahara, *Geometry, Topology and Physics* (Taylor & Francis, Boca Raton, 2018). ISBN: 978-1-4200-5694-5
297. H. Nakajima, Instantons on ALE spaces, quiver varieties, and Kac-Moody algebras. Duke Math. J. **76**, 365–416 (1994)
298. M. Newborn, *Automated Theorem Proving: Theory and Practice* (Springer, New York). ISBN: 0-387-95075-3
299. B. Nill, Gorenstein toric Fano varieties (2004) [math/0405448]
300. C. Okonek, A. Teleman, Master spaces and the coupling principle: from geometric invariant theory to gauge theory. Commun. Math. Phys. **205**, 437–458 (1999)
301. H. Otsuka, K. Takemoto, J. High Energy Phys. **05**, 047 (2020) [arXiv:2003.11880 [hep-th]]
302. N. Otter, M.A. Porter, U. Tillmann, P. Grindrod, H.A. Harrington, A roadmap for the computation of persistent homology. EPJ Data Sci. **6**(1), 17 (2017). arXiv:1506.08903 [math.AT]
303. A. Paffenholz, polyDB: A Database for Polytopes and Related Objects. arXiv:1711.02936
304. E. Parr, P.K.S. Vaudrevange, Contrast data mining for the MSSM from strings. Nucl. Phys. B **952**, 114922 (2020) [arXiv:1910.13473 [hep-th]]
305. E. Parr, P.K.S. Vaudrevange, M. Wimmer, Predicting the orbifold origin of the MSSM. Fortsch. Phys. **68**(5), 2000032 (2020) [arXiv:2003.01732 [hep-th]]
306. D. Peifer, M. Stillman, D. Halpern-Leistner, Learning selection strategies in Buchberger’s algorithm (2020) [arXiv:2005.01917]

307. J. Polchinski, Dirichlet Branes and Ramond-Ramond charges. Phys. Rev. Lett. **75**, 4724 (1995) [[hep-th/9510017](#)]
308. J. Polchinski, *String Theory*, vols. 1& 2 (CUP, Cambridge, 1998)
309. B. Poonen, F. Rodriguez-Villegas, Lattice polygons and the number 12. Am. Math. Monthly **107**(3), 238–250 (2000)
310. Python Software Foundation. Python Language Reference, <http://www.python.org>; G. van Rossum, Python tutorial, Technical Report CS-R9526, Centrum voor Wiskunde en Informatica (CWI), Amsterdam, May 1995
311. G. Raayoni, S. Gottlieb, G. Pisha, Y. Harris, Y. Manor, U. Mendlovic, D. Haviv, Y. Hadad, I. Kaminer, The Ramanujan machine: automatically generated conjectures on fundamental constants (2019). arXiv:1907.00205 [cs.LG]
312. L. Randall, R. Sundrum, An alternative to compactification. Phys. Rev. Lett. **83**, 4690 (1999) [[hep-th/9906064](#)]
313. M. Reid, The moduli space of 3-folds with $K = 0$ may nevertheless be irreducible. Math. Ann. **278**, 329–334 (1987)
314. M. Reid, *Undergraduate Algebraic Geometry*. LMS Student Texts, vol. 12 (Cambridge University Press, Cambridge, 1989)
315. M. Reineke, Every projective variety is a quiver Grassmannian (2012). arXiv:1204.5730; M. Reineke, Moduli of representations of quivers (2008). arXiv:0802.2147
316. D. Rickles, *A Brief History of String Theory: From Dual Models to M-Theory* (Springer, New York, 2014). ISBN-13: 978-3642451270
317. F. Rosenblatt, The Perceptron—a perceiving and recognizing automaton. Report 85-460-1, Cornell Aeronautical Laboratory (1957)
318. F. Ruehle, Evolving NNs with genetic algorithms to study the string landscape. J. High Energy Phys. **08**, 038 (2017) [[arXiv:1706.07024 \[hep-th\]](#)]
319. F. Ruehle, Data science applications to string theory. Phys. Rept. **839**, 1–117 (2020)
320. SageMath, *The Sage Mathematics Software System* (The Sage Developers, Thousand Oaks, CA). <http://www.sagemath.org>
321. I. Satake, On a generalization of the notion of manifold. Proc. Natl. Acad. Sci. U. S. A. **42**, 359–363 (1956)
322. H. Schenck, *Computational Algebraic Geometry* (Cambridge University Press, Cambridge, 2003). ISBN: 978-0-5215-3650-9
323. H. Schenck, M. Stillman, B. Yuan, Calabi-Yau threefolds in P^n and Gorenstein rings (2020). arXiv:2011.10871
324. L. Schneps, *The Grothendieck Theory of Dessins d’Enfants*. LMS Lecture Note Series (Cambridge University Press, Cambridge, 1994)
325. C. Schoen, On fiber products of rational elliptic surfaces with section. Math. Z. **197**, 177–199 (1988)
326. F. Schöller, H. Skarke, All weight systems for Calabi-Yau fourfolds from reflexive polyhedra (2018). arXiv:1808.02422 [hep-th]; cf. also M. Kreuzer, On the statistics of lattice polytopes, in *Proceedings of the “Information Theory and Statistical Learning”, WORLDCOMP’08*, Las Vegas, July 14–15, 2008 [arXiv:0809.1188 [math.AG]]
327. M. Schuett, Arithmetic of K3 surfaces (2008). arXiv:0808.1061
328. L.R. Silverstein, Probability and machine learning in combinatorial commutative algebra. University of California, Davis. Thesis (2019). https://www.math.ucdavis.edu/~tdenena/dissertations/201903_Silverstein_dissertation.pdf
329. P. Slodowy, Platonic solids, Kleinian singularities, and Lie groups, in *Algebraic Geometry, Proceedings of the Ann Arbor, 1981*, ed. by I. Dolgachev; M. Reid, McKay correspondence. alg-geom/9702016; M. Reid, Algebraic surfaces, in *Complex Algebraic Geometry*. IAS/Park City Mathematics Series, vol. 3 (AMS, Providence, 1997), pp. 3–159
330. A.J. Smola, B. Scholkopf, A tutorial on support vector regression. Tech. Rep. Statistics and Computing, 2003
331. N. Srivastava, G. Hinton, A. Krizhevsky, I. Sutskever, R. Salakhutdinov, Dropout: a simple way to prevent neural networks from overfitting. J. Mach. Learn. Res. **15**, 1929–1958 (2014)

332. R.P. Stanley, Hilbert functions of graded algebras. *Adv. Math.* **28**, 57–83 (1978)
333. String Data Repository. <https://github.com/stringdata>
334. A. Strominger, Superstrings with Torsion. *Nucl. Phys. B* **274**, 253 (1986)
335. B. Sturmfels, *Algorithms in Invariant Theory* (Springer, New York, 1993). ISBN: 0-387-82445-6
336. B. Szendroi, Non-commutative Donaldson-Thomas theory and the conifold. *Geom. Topol.* **12**, 1171–1202 (2008). arXiv:0705.3419
337. “The Calabi-Yau Operator Database” for Picard-Fuchs PDEs. <http://cydb.mathematik.uni-mainz.de/>
338. The GAP Group, GAP – Groups, Algorithms, and Programming, version 4.9.2 (2018). <https://www.gap-system.org>
339. The Graded Ring Database. <http://www.grdb.co.uk/>; The C^3 NG collaboration: <http://geometry.ma.ic.ac.uk/3CinG/index.php/team-members-and-collaborators/>. Data at: <http://geometry.ma.ic.ac.uk/3CinG/index.php/data/>. <http://coates.ma.ic.ac.uk/fanosearch/>
340. The Knots Atlas (2015). http://katlas.org/wiki/Main_Page
341. The L-functions & Modular Forms Database. <http://www.lmfdb.org/>
342. The MNIST database of handwritten digits (2010). <http://yann.lecun.com/exdb/mnist/>
343. The Particle Data Group (2010). cf. <http://pdg.lbl.gov/>
344. K.-M. Ting, Encyclopedia of Machine Learning (Springer, New York, 2011). ISBN: 978-0-387-30164-8
345. Toric Calabi-Yau Database. <http://www.rossealtman.com/>
346. S.M. Udrescu, M. Tegmark, AI Feynman: a physics-inspired method for symbolic regression (2019) [arXiv:1905.11481 [physics.comp-ph]]
347. K. Ueda, M. Yamazaki, A note on dimer models and McKay quivers. *Commun. Math. Phys.* **301**, 723–747 (2011). arXiv:math/0605780
348. A.M. Uranga, The standard model in string theory from D-branes. *Nucl. Phys. Proc. Suppl.* **171**, 119 (2007)
349. C. Van Rijsbergen, *Information Retrieval* (2nd edn.) (Butterworth-Heinemann, Newton, 1979); D. Powers, Evaluation: from precision, recall and F-measure to ROC, informedness, markedness & correlation. *J. Mach. Learn. Technol.* **2**(1), 37–63 (2011)
350. H. Verlinde, M. Wijnholt, Building the standard model on a D3-brane. *J. High Energy Phys.* **0701**, 106 (2007) [hep-th/0508089]
351. R. Vidunas, Y.H. He, Composite genus one Belyi maps. *Indag. Math.* **29**, 3 (2018) arXiv:1610.08075 [math.AG]
352. V. Voevodsky, Univalent Foundations of Mathematics. Heidelberg Laureate Forum (2013)
353. C.T.C. Wall, Classification problems in differential topology, V: on certain 6-manifolds. *Invent. Math.* **1**, 355 (1966)
354. Y.N. Wang, Z. Zhang, Learning non-Higgsable gauge groups in 4D F-theory. *J. High Energy Phys.* **08**, 009 (2018) [arXiv:1804.07296 [hep-th]]
355. T. Weigand, TASI Lectures on F-theory. arXiv:1806.01854 [hep-th]
356. M. Wijnholt, Large volume perspective on branes at singularities. *Adv. Theor. Math. Phys.* **7**(6), 1117 (2003) [hep-th/0212021]; C.P. Herzog, J. Walcher, Dibaryons from exceptional collections. *J. High Energy Phys.* **0309**, 060 (2003) [hep-th/0306298]; C.P. Herzog, Exceptional collections and del Pezzo gauge theories. *J. High Energy Phys.* **0404**, 069 (2004) [hep-th/0310262]
357. P.M.H. Wilson, Boundedness questions for Calabi-Yau threefolds (2017). arXiv:1706.01268 [math.AG]; P.M.H. Wilson, Calabi-Yau threefolds with Picard number three (2020). arXiv:2011.12876 [math.AG]
358. Wolfram Research, Inc. *Mathematica* (Wolfram Research, Inc., Champaign, IL, 2018). www.wolfram.com
359. M. Yamazaki, Brane tilings and their applications. *Fortsch. Phys.* **56**, 555 (2008) [arXiv:0803.4474 [hep-th]]
360. C.N. Yang, M.L. Ge, Y.H. He (eds.) *Topology and Physics*, with contributions from Atiyah, Penrose, Witten, et al. WS, 2019. ISBN: 978-981-3278-49-3 <https://doi.org/10.1142/11217>

361. S.-T. Yau, Calabi's conjecture and some new results in algebraic geometry. Proc. Natl. Acad. U. S. A. **74**(5), 1798–1799 (1977). S.-T. Yau, On the Ricci curvature of a compact Kähler manifold and the complex Monge-Ampère equation I. Commun. Pure Appl. Maths **31**(3), 339–411 (1978)
362. S.-T. Yau, A survey of Calabi–Yau manifolds, in *Geometry, Analysis, and Algebraic Geometry: Forty Years of the Journal of Differential Geometry*. Surveys in Differential Geometry, vol. 13 (International Press, Somerville, MA, 2009), pp. 277–318
363. S.-T. Yau, S. Nadis, *Shape of Inner Space: String Theory and the Geometry of the Universe's Hidden Dimension* (Basic Books, Perseus, New York, 2012). ISBN-13: 978-0465028375
364. B. Zwiebach, *A First Course in String Theory* (Cambridge University Press, Cambridge, 2004). ISBN: 978-0-5118-4168-2

Index

A

- ADE, 67, 69–72, 84, 85, 149, 151, 157, 177, 180
Adjacency matrix, 69, 74, 81, 89, 91, 129
Adjunction formula, 29
Algebraic variety, viii, 19, 26, 38, 65, 135, 156–159, 171–173
Ambient space, 20, 22, 25, 29, 30, 35, 38, 42, 45, 46, 49, 56, 136, 137
Architecture (NN), 100, 102, 116, 122
Artificial intelligence (AI), viii, ix, x, 2, 30, 79, 87, 88, 91, 93, 112, 113, 130, 137, 138, 178

B

- Back-propagation (NN), 100
Belyi map, 150, 163, 164
Betti number, 4, 16, 18, 79, 113, 133
Bipartite graph, 80–82, 91, 161–165
Blow-up, 68, 71, 73, 78, 83, 147–149
Brane tiling/dimer model, 80–82, 91, 161–165

C

- Calabi conjecture, 6, 7, 53
Calabi-Yau, 2, 19, 59, 87, 131, 145, 157, 172
Canonical bundle, 16, 18, 20, 27, 68, 76, 136, 150, 172
Character table, 72, 80, 175
Chern class, 6, 7, 21, 22, 29–31, 37, 45, 46, 72, 90, 138–140, 148, 149
Cohomology, ix, 12, 18, 22, 24, 25, 28, 31, 51, 88–90, 121, 125, 126, 133–136, 138, 172–174

- Compactification, vii, viii, 9, 11, 13–15, 51, 52, 60, 126, 140, 149
Complete intersection, 2, 28–33, 76, 121, 129, 159, 160
Complex affine space (C^n), 143
Complex manifold, 19, 22, 147
Complex projective space (CP^n), 6, 20, 135, 139
Complex structure, 16, 17, 23, 27, 41, 68, 78, 79, 113, 118, 134, 155
Conifold, 77, 80, 82, 83, 85, 142, 144, 145, 161
Convolutional neural network (CNN), 98–99, 106, 121, 123
Cotangent bundle, 16, 18, 27, 69, 77, 133, 135, 136, 172

D

- D-brane, 13, 14, 49, 60, 68, 80–82
Decision tree, 107–108, 126
del Pezzo surface, 37, 43, 73, 74, 82, 147, 148
Depth (NN), 35, 97–99, 108
Desingularization, 45, 68
Dessin d’Enfant, 161, 163
Donaldson algorithm, 53, 58, 126
D-term, 62, 63
Dual (polar) polytope, 174

E

- Elliptic curve, 7, 19, 20, 36, 43, 95, 129, 136, 150, 164, 165, 172, 176
Elliptic fibration, 14, 33, 36–37, 47, 50, 52, 88, 125, 149–151

Euler characteristic (number), 3, 4, 12, 13, 18, 22–24, 28, 29, 31, 33–36, 113, 133, 134
 Euler sequence, 21, 24, 29
 Exact sequence, x, 21–24, 28, 52, 121, 126, 137–139

F

Fano, 6, 38, 40–43, 45, 47, 49, 82, 83, 136, 147–149
 F-score (ML), 111, 118, 120
 F-term, 61–65

G

GAP (software), viii, 3, 38, 72, 128, 174, 175
 Gauss-Bonnet, 4–6, 134
 Genus, 3, 4, 6, 31, 50, 164
 Gorenstein, 40, 42, 47, 83, 84
 Gröbner basis, 25, 67, 84, 126, 128, 153–156, 158
 GUT, 9, 12, 33, 51

H

Hilbert series, 83, 84, 129, 156–160, 173, 175
 Hirzebruch surface, 37, 43, 148
 Hodge decomposition, 16, 18, 23, 28, 135
 Hodge number (diamond), ix, 16, 18, 22, 28, 29, 31, 33–37, 45–48, 79, 90, 91, 116, 121, 122, 125
 Holonomy, 10, 12, 14, 16, 66, 142
 Homology, ix, 4, 5, 12, 16, 18, 22, 24, 25, 28, 31, 51, 88–90, 92, 113, 121, 125, 126, 133–136, 138, 172–174
 Homotopy, 90
 Hypersurface, viii, 14, 20, 21, 28, 32, 34–37, 41–43, 45, 46, 49, 50, 67, 68, 71, 77, 80, 85, 90, 104, 107, 113–120, 131, 136, 137, 142, 144, 145, 159, 160, 172

I

Ideal, 25–27, 33, 38, 64–66, 76, 80, 81, 143, 145, 155–158, 171–173
 Index theorem, 4, 22, 23
 Irreducible representations (Irreps), 69, 70, 72, 74, 175

J

J-invariant, 150, 176

K

Kähler manifold, 6, 7, 10, 18, 126, 136, 147
 Kähler structure, 68
 Kodaira classification, 149–151
 Kreuzer-Skarke data, vii, 3, 38–49, 88
 K3 surface, 7, 8, 37, 43, 50, 68, 71, 77, 85, 149

L

Lattice cone, 38, 142, 146
 Lattice fan, ix, 7, 8, 14, 38–44, 46, 52, 72, 73, 77, 80, 82, 84, 85, 90, 91, 134, 142, 146, 158, 174
 Lattice polytope, ix, 39, 85, 146
 Learning curve, 103, 104, 112, 118, 119, 123
 Learning rate, 100–102, 117
 Line bundle ($O_{CP1}(k)$ of degree k), 21, 52, 76, 83, 90, 125, 135, 136, 139
 Loss function, 96, 100, 103, 111, 112, 117

M

Macaulay2, viii, 3, 25–28, 41, 75, 76, 90, 113, 114, 121, 144, 154, 171–173
 Machine Learning (ML), xi, ix, 57, 87–130, 175
 Matthews correlation coefficient (ML), 111
 McKay Correspondence, 69–71
 Metric, 4–7, 9, 16, 52–58, 60, 65, 68, 69, 77–79, 94, 134, 135
 Mirror symmetry, vii, 14, 15, 33–35, 47, 78
 Moduli space, 63, 64, 71, 78, 79, 85, 125, 161, 162
 Molien series, 84, 157, 175
 Monomial basis, 57
 Multi-layer perceptron (MLP), 97, 98, 114, 115, 125

N

Naive Bayes, 108–109, 129
 Neural network (NN), 88, 97–104, 106, 109, 113–127, 130
 n-fold, 6, 7, 16, 40, 52, 59, 78, 147, 158
 n-manifold, 5
 Normal bundle, 20–22, 125, 135–137

O

Orbifold, 14, 66–73, 76, 77, 80, 82–85, 88, 157

P

Perceptron, 95–98
 Polynomial ring, 19, 25, 76, 143, 145, 153, 171
 Proj, 26, 27, 144, 171–173
 Python, 41, 91, 106, 113–117, 119, 128, 173

Q

Quintic, 20–29, 33, 34, 41, 49, 52, 56–59, 78, 84, 113, 114, 121, 146, 155
 Quiver, 14, 60–66, 70–71, 73–75, 79–82, 85, 89–91, 131, 145, 158, 159, 161, 162

R

Reflexive polytope, 39–41, 174
 Regression, 95–97, 101, 102, 108, 120, 127, 130, 167–169
 Reid’s fantasy, 50, 78
 ReLu, 38, 96, 101, 122, 129
 Ricci curvature, 4, 7, 10, 16, 50, 138
 Riemannian manifold, vii, 5, 10
 Riemann surface, 4, 5, 7, 31, 149, 161, 163, 164

S

SageMath, 3, 25, 41, 42, 46, 77, 89–91, 113, 114, 171–176
 Sasaki-Einstein, 78, 79, 83, 126, 131, 157
 Schoen manifold, 52
 Serre duality, 18
 Sigmoid, 95, 96, 101, 114, 115, 117, 120, 122, 167–169
 Singular (Software), viii, 3, 26, 27, 35, 41, 60, 66, 68, 77, 78, 83, 113, 150, 153–155, 172, 173
 Spec, 26, 35, 63, 64, 142–144, 156, 172
 Sphere, 3, 59, 136
 Standard model (SM), vii, 2, 8, 9, 11–15, 51, 52, 60, 72, 88, 89, 91
 String landscape, 13, 14, 51, 125, 126

String phenomenology, 8, 9, 11, 33, 88

String Theory, vii, viii, x, xi, 2, 8–10, 13, 36, 47, 51, 60, 61, 65, 66, 71, 88, 91, 149

Superpotential, 14, 61–65, 73, 75, 79–82, 91, 161

Support vector machine (SVM), 104–107, 119, 120, 122–129

T

Tangent bundle, 10, 12, 13, 16, 18, 20–22, 27, 51, 69, 77, 126, 133, 135–138, 172
 Tian-Yau manifold, 33
 Topology, vii, xi, 3–5, 7, 31, 49, 50
 Toric variety, 38, 40, 41, 45, 72, 73, 81, 84, 142, 145, 146, 159, 173, 174
 Torus, 3, 4, 7, 14, 19, 20, 50, 79, 80, 134, 162
 Training curve, 103, 111, 112, 118
 Training set, 101, 103, 108, 109, 117, 167
 Triangulation, 46, 90, 125, 126, 158

V

Validation set, 103, 109, 110, 117, 118, 122, 167, 168
 Variety of general type, 6, 50, 147, 149
 Vector bundle, 9, 10, 13, 18, 21, 51, 52, 126, 136, 138, 139
 Volume form, 16, 56

W

Weierstrass form, 150
 Weighted projective space (CPn), 14, 35, 37, 38
 Width (NN), 97–99, 101
 Wolfram Mathematica, 113

Y

Yau’s conjecture, vii, 7, 8, 31, 49, 50, 78

Editors in Chief: J.-M. Morel, B. Teissier;

Editorial Policy

1. Lecture Notes aim to report new developments in all areas of mathematics and their applications – quickly, informally and at a high level. Mathematical texts analysing new developments in modelling and numerical simulation are welcome.

Manuscripts should be reasonably self-contained and rounded off. Thus they may, and often will, present not only results of the author but also related work by other people. They may be based on specialised lecture courses. Furthermore, the manuscripts should provide sufficient motivation, examples and applications. This clearly distinguishes Lecture Notes from journal articles or technical reports which normally are very concise. Articles intended for a journal but too long to be accepted by most journals, usually do not have this “lecture notes” character. For similar reasons it is unusual for doctoral theses to be accepted for the Lecture Notes series, though habilitation theses may be appropriate.

2. Besides monographs, multi-author manuscripts resulting from SUMMER SCHOOLS or similar INTENSIVE COURSES are welcome, provided their objective was held to present an active mathematical topic to an audience at the beginning or intermediate graduate level (a list of participants should be provided).

The resulting manuscript should not be just a collection of course notes, but should require advance planning and coordination among the main lecturers. The subject matter should dictate the structure of the book. This structure should be motivated and explained in a scientific introduction, and the notation, references, index and formulation of results should be, if possible, unified by the editors. Each contribution should have an abstract and an introduction referring to the other contributions. In other words, more preparatory work must go into a multi-authored volume than simply assembling a disparate collection of papers, communicated at the event.

3. Manuscripts should be submitted either online at [www.editorialmanager.com/lm](http://www.editorialmanager.com/lnm) to Springer’s mathematics editorial in Heidelberg, or electronically to one of the series editors. Authors should be aware that incomplete or insufficiently close-to-final manuscripts almost always result in longer refereeing times and nevertheless unclear referees’ recommendations, making further refereeing of a final draft necessary. The strict minimum amount of material that will be considered should include a detailed outline describing the planned contents of each chapter, a bibliography and several sample chapters. Parallel submission of a manuscript to another publisher while under consideration for LNM is not acceptable and can lead to rejection.

4. In general, **monographs** will be sent out to at least 2 external referees for evaluation.

A final decision to publish can be made only on the basis of the complete manuscript, however a refereeing process leading to a preliminary decision can be based on a pre-final or incomplete manuscript.

Volume Editors of **multi-author works** are expected to arrange for the refereeing, to the usual scientific standards, of the individual contributions. If the resulting reports can be

forwarded to the LNM Editorial Board, this is very helpful. If no reports are forwarded or if other questions remain unclear in respect of homogeneity etc, the series editors may wish to consult external referees for an overall evaluation of the volume.

5. Manuscripts should in general be submitted in English. Final manuscripts should contain at least 100 pages of mathematical text and should always include
 - a table of contents;
 - an informative introduction, with adequate motivation and perhaps some historical remarks: it should be accessible to a reader not intimately familiar with the topic treated;
 - a subject index: as a rule this is genuinely helpful for the reader.
 - For evaluation purposes, manuscripts should be submitted as pdf files.
6. Careful preparation of the manuscripts will help keep production time short besides ensuring satisfactory appearance of the finished book in print and online. After acceptance of the manuscript authors will be asked to prepare the final LaTeX source files (see LaTeX templates online: <https://www.springer.com/gb/authors-editors/book-authors-editors/manuscriptpreparation/5636>) plus the corresponding pdf- or zipped ps-file. The LaTeX source files are essential for producing the full-text online version of the book, see <http://link.springer.com/bookseries/304> for the existing online volumes of LNM). The technical production of a Lecture Notes volume takes approximately 12 weeks. Additional instructions, if necessary, are available on request from lnm@springer.com.
7. Authors receive a total of 30 free copies of their volume and free access to their book on SpringerLink, but no royalties. They are entitled to a discount of 33.3 % on the price of Springer books purchased for their personal use, if ordering directly from Springer.
8. Commitment to publish is made by a *Publishing Agreement*; contributing authors of multiauthor books are requested to sign a *Consent to Publish form*. Springer-Verlag registers the copyright for each volume. Authors are free to reuse material contained in their LNM volumes in later publications: a brief written (or e-mail) request for formal permission is sufficient.

Addresses:

Professor Jean-Michel Morel, CMLA, École Normale Supérieure de Cachan, France
E-mail: moreljeanmichel@gmail.com

Professor Bernard Teissier, Equipe Géométrie et Dynamique,
Institut de Mathématiques de Jussieu – Paris Rive Gauche, Paris, France
E-mail: bernard.teissier@imj-prg.fr

Springer: Ute McCrory, Mathematics, Heidelberg, Germany,
E-mail: lnm@springer.com